

Induction Healing of Porous Asphalt Concrete

The photo in the cover was shot by Álvaro García.

Induction Healing of Porous Asphalt Concrete

Proefschrift

ter verkrijging van de graad van doctor
aan de Technische Universiteit Delft,
op gezag van de Rector Magnificus prof. ir. K.C.A.M. Luyben,
voorzitter van het College voor Promoties,
in het openbaar te verdedigen op dinsdag 2 oktober 2012 om 10.00 uur

door

Quantao LIU

Master of Science in Materials Science
Wuhan University of Technology, P.R. China
geboren te Xihua, Henan, P.R. China

Dit proefschrift is goedgekeurd door de promotor:
Prof.dr.ir. E. Schlangen

Copromotor:
Ir. M.F.C van de Ven

Samenstelling promotiecommissie:

Rector Magnificus	Technische Universiteit Delft, voorzitter
Prof. dr. ir. E. Schlangen	Technische Universiteit Delft, promotor
Ir. M.F.C. van de Ven	Technische Universiteit Delft, copromotor
Prof. S.P. Wu, BSc, MSc, PhD	Wuhan University of Technology, China
Prof. dr. ir. S. van der Zwaag	Technische Universiteit Delft
Prof. dr. ir. A.A.A. Molenaar	Technische Universiteit Delft
Dr. Z. Su, BSc., MSc	ESHA Group bv, R&D
Dr. A. García, BSc, MSc	EMPA, Switzerland

Prof.dr.ir. K. van Breugel Technische Universiteit Delft, reservelid

ISBN: 978-94-6186-050-7

Key words: Induction heating; Healing; Porous asphalt concrete

Printed by Haveka BV, the Netherlands

Copyright ©2012 by Quantao Liu

All rights reserved. No part of the material protected by this copyright notice may be reproduced or utilized in any form or by any means, electronic or mechanical, including photocopying, recording or by any information storage and retrieval system, without the written permission from the author.

Acknowledgements

This thesis presents the research that I have done in the past four years as a PhD candidate at Delft University of Technology (TU delft). First of all, I would like to acknowledge China Scholarship Council for sponsoring me during my study in the Netherlands. The first development of this research was sponsored by a grant from Agentschap NL. In the initial development Breijn-Heijmans, SGS-Intron and Altravie also had contributions. The final research on the road trial section was sponsored by Rijkswaterstaat-DVS through Infraquest. I am very grateful to these sponsors.

I would like to express my sincere gratitude to my supervisor Prof. dr. ir. E. Schlangen and my co-supervisor Assoc. prof. Martin van de Ven, who supervised me together. I am grateful to their guidance, directions, advices and encouragements. I learnt a lot from the invaluable discussions with them. I thank them for their review work on my thesis.

I am most grateful to Prof. dr. ir. K. van Breugel, who gave me the opportunity to study in Microlab. I am grateful to him for all his support during the past four years.

I would like to acknowledge Dr. Álvaro García for his help and suggestions during my study. His guidance at the beginning of my PhD was very important to me. He revised each journal paper of mine, which is also appreciated.

I thank Assoc. prof. Ye Guang. He is not only a teacher, but also a friend and a family to all Chinese students in Microlab. I am grateful to him for everything he did for us.

I would like to express my appreciation to my master supervisor Prof. Shaopeng Wu, who treated me very well during my master and encouraged me to do a PhD abroad. He even paid the IELTS test fees for me. Without him, I would not have the chance to study abroad.

The majority of my PhD thesis work was done in the laboratory of Road and Railway Engineering. I am grateful to Prof. dr. ir. A.A.A. Molenaar for his support.

I would like to thank Marco Poot for all his advice and help both in arranging the experiments and in setting up the laboratory equipments. I benefited a lot from his practical experience. I am also grateful to Jan Moraal, Jan-Willem Bientjes and Jacqueline Barnhoorn for their help.

I am grateful to the Microlab technicians Gerrit Nagtegaal and Arjan Thijssen for their help in the experiments. I thank all the colleagues in Microlab. I enjoy working with you. Special thanks go to Iris Batterham, Claudia Baltussen, Nynke Verhulst and Melanie Holtzapffel for their help in all kinds of documents.

I also wish to thank Ms. Franca Post of the central liaison office at TU Delft (CICAT) for her support and help.

Especially, I would like to thank all the Chinese students in Microlab for the lunch talks, parties, barbecues with you.

I am very grateful to my dearest friends from Wuhan University of Technology: Yue Xiao, Jian Qiu, Liantong Mo, Ning Li, Zhuqing Yu, Dongxing Xuan, Gang Liu, Yuan Zhang, and Jingang Wang. Thank you all for your companionship and help during these years in Delft.

Finally, I would like to thank my mother and my sisters for their continuous love and support. The final appreciation goes to my wife Nannan Li for her love, understanding and tolerance since our high school. No words can express my thanks to her.

Quantao Liu

April 2012, Delft

Summary

Porous asphalt shows excellent performance in both noise reduction and water drainage. Although porous asphalt has these great qualities, its service life is much shorter (sometimes only half) compared to dense graded asphalt roads. Ravelling, which is the loss of aggregate particles from the surface layer, is the main damage mechanism of porous asphalt surface wearing courses. In this research, an induction healing approach (namely, activating the healing process of asphalt concrete through induction heating) was developed to enhance the durability of the porous asphalt roads. Steel fibers are added to a porous asphalt mixture to make it electrically conductive and suitable for induction heating. When micro cracks are expected to occur in the asphalt mastic of the pavement, the temperature of the mastic can be increased locally by induction heating of the steel fibers so that porous asphalt concrete can repair itself and close the cracks through the high temperature healing of the bitumen (diffusion and flow). The closure of micro cracks will prevent the formation of macro cracks. In such a way, ravelling can be avoided or delayed in the end.

To make asphalt mastic and porous asphalt concrete electrically conductive and suitable for induction heating, steel (wool) fibers were incorporated into them. The electrical conductivity and induction heating speed of asphalt mastic and porous asphalt concrete were first studied in this research. Asphalt mastic and porous asphalt concrete with steel fibers can be heated with induction energy. There is an optimal volume content of steel fiber in asphalt mastic or porous asphalt concrete to obtain the highest induction heating speed. Adding more steel fiber above this optimal volume content does not increase the induction heating speed anymore. Furthermore, the highest induction heating speed corresponds to the minimum electrical resistivity. However, porous asphalt concrete does not need to be fully conductive for induction heating. Every single steel wool is a heating unit. Nonconductive samples with steel fiber can still be heated with induction heating, but at a low heating speed. The diameter, length and content of steel wool fiber are important for the conductivity and heating speed of asphalt concrete matrix. It is proven that induction heating does not cause extra ageing to bitumen. Addition of steel wool also reduces the binder drainage problem in porous asphalt concrete.

The mechanical properties of porous asphalt concrete with steel wool fiber were studied in this research. Adding moderate percentage steel wool to porous asphalt concrete reinforce it by increasing its particle loss resistance, indirect tensile strength and fracture energy, water damage resistance, stiffness and fatigue resistance. The steel wool was optimized to obtain the best particle loss resistance in porous asphalt concrete. 8% steel wool type 00 (volume fraction of bitumen) was considered as the optimal content.

The healing potential of porous asphalt concrete with steel wool fiber was also evaluated in this research with both cylinder and beam samples.

Damaged porous asphalt concrete with steel wool fiber can greatly restore its stiffness, strength and fatigue life with induction heating, which proves that the healing capacity of porous asphalt concrete with steel wool fiber is enhanced by induction heating. The optimal induction heating temperature is 85 °C for porous asphalt concrete to obtain the best healing rate. Reheating does not decrease the healing rate of porous asphalt concrete, which means that heating can be repeated when cracks appear again.

To apply the induction healing technology in real porous asphalt road, a trial section was constructed on Dutch motorway A58 in December 2010. This trial section survived the past two winters perfectly. Experiments were done on the cores drilled from the trial section and the results coincided with those on the laboratory made samples. The field cores showed good particle loss resistance, high strength, good fatigue resistance and high induction healing capacity. Based on the laboratory experiments and field experiences, induction healing can be a very good approach to enhance the durability of porous asphalt pavement.

Finally, some recommendations are given for further research. Steel fiber, mixing technology and induction generator need to be optimized. Modeling work is necessary to fully understand the mechanisms involved in induction healing.

Samenvatting

ZOAB heeft uitstekende prestaties in zowel geluidsreductie als waterafvoer. Ondanks deze goede eigenschappen, is de levensduur van ZOAB veel korter (soms slechts de helft) in vergelijking tot dichtasfaltbetonwegen. Rafeling, het verlies van steenslag uit de topklaag, is het belangrijkste schademechanisme van poreuze asfaltdeklagen. In dit onderzoek werd een inductieherstelling benadering (namelijk het activeren van het herstellingsproces van asfaltbeton door middel van inductieverwarming) ontwikkeld om de duurzaamheid van de ZOAB wegen te verbeteren. Het idee van deze benadering is om staalvezels aan een poreus asfaltmengsel toe te voegen. Wanneer microscheuren in het asfaltmestiek van wegen ontstaan, kan de temperatuur van het mestiek plaatselijk worden verhoogd door inductieverwarming van de staalvezels, zodat poreus asfaltbeton zichzelf kan herstellen en de scheuren kunnen sluiten door de hoge temperatuurherstelling van de bitumen (diffusie en stroming). Het sluiten van microscheuren voorkomt de vorming van macroscheuren. Op deze wijze kan op het eind rafeling worden voorkomen of vertraagd.

Om asfaltmestiek en zeer open asfaltbeton elektrisch geleidend en daarmee geschikt voor inductieverwarming te maken, werden er staal(wol)vezels in verwerkt. De elektrische geleidbaarheid en de opwarmingssnelheid d.m.v. inductie van asfaltmestiek en zeer open asfalt beton werden voor het eerst bestudeerd in dit onderzoek. Asfaltmestiek en zeer open asfalt beton met staalvezels kunnen worden verwarmd met inductie. Er is ook een optimale hoeveelheid van staalvezels in asfaltmestiek of poreuze asfaltbeton om de hoogste inductieverwarmingssnelheid te verkrijgen. Het toevoegen van meer staalvezels boven dit optimale volumepercentage leidt niet meer tot verhoging van de inductieverwarmingssnelheid. Bovendien is de hoogste snelheid van de inductieverwarming overeenkomstig met de minimale elektrische weerstand. Echter, zeer open asfaltbeton hoeft niet volledig geleidend te zijn voor inductieverwarming. Elke staalwolvezel is een verwarmingsunit. Niet-geleidende monsters met staalvezels kunnen toch verwarmd worden met inductieverwarming, maar alleen met een lage verwarmingssnelheid. De diameter, lengte en volumepercentage van staalwolvezels zijn belangrijk voor de geleiding en verwarmingssnelheid van asfaltmatrix. Het is bewezen dat de inductieverwarming niet extra veroudering van bitumen veroorzaakt. Toevoeging van staalwol vermindert ook het afdruipe van bindmiddel in poreus asfaltbeton.

De mechanische eigenschappen van zeer open asfaltbeton met daarin staalwolvezels zijn bestudeerd in dit onderzoek. Het toevoegen van matige hoeveelheid staalwol versterkt zeer open asfaltbeton door verhoging van, de weerstand tegen steenslag, de indirecte treksterkte en breuk energie, weerstand tegen waterschade, stijfheid en vermoeiings weerstand. De staalwol is geoptimaliseerd om de meeste weerstand tegen steenverlies te krijgen in poreus

asfaltbeton. 8% staalwol type 00 (volumepercentage van bitumen) werd beschouwd als het optimale volumepercentage.

Het herstellend potentieel van zeer open asfaltbeton met staalwolvezels is ook onderzocht met zowel cilindervormige als blokvormige monsters. Van beschadigde poreus asfaltbeton met staalwolvezels kan de stijfheid, sterkte en levensduur sterk herstellen met inductieverwarming, waaruit blijkt dat de helende capaciteit van zeer open asfaltbeton met staalwolvezels worden versterkt door middel van inductieverwarming. De optimale temperatuur is 85°C voor zeer open asfaltbeton om het grootste herstel te krijgen. Herverwarmen van poreus asfaltbeton verlaagd het herstellend vermogen niet negatief, dit betekent dat verwarming kan worden herhaald wanneer scheuren terugkeren.

Om de inductiehersteltechnologie in poreus asfaltwegen toe te passen, werd een proefvak aangelegd op de Nederlandse snelweg A58 in december 2010. Deze testsectie heeft de afgelopen twee winters perfect doorstaan. Experimenten zijn uitgevoerd op de boorkernen van de testsectie en de resultaten zijn gelijk aan de in het laboratorium gemaakte monsters. De boorkernen toonden een goede weersstand tegen het verlies van stenen, een hoge sterkte, een goede weerstand tegen vermoeiing en een hoog herstellend vermogen d.m.v. inductie. Op basis van de laboratoriumexperimenten en ervaringen, kan inductieheling een zeer goede aanpak zijn voor verbetering van de duurzaamheid van ZOAB wegdekken.

Tot slot worden enkele aanbevelingen gegeven voor verder onderzoek. Staalvezels, de mengtechniek en inductiegenerator moeten worden geoptimaliseerd. Modelleren is nodig om de mechanismen van inductieheling volledig te begrijpen.

Abbreviations

CT	Computed Tomography
DSR	Dynamic Shear Rheometer
FTIR	Fourier Transform Infrared Spectroscopy
GH IA	GH Induction Atmospheres
GIL	Gilsonite
GPC	Gel Permeation Chromatography
ITS	Indirect tensile strength
ITSR	Indirect tensile strength ratio
LVDT	Linear variable differential transformer
PA	Porous asphalt
PG	Penetration grade
RSAT	Rotating surface abrasion test
SBR	Styrene Butadiene Rubber
SBS	Styrene Butadiene Styrene
SMA	Stone matrix asphalt
UTM	Universal testing machine
VA	Volume of air voids
VFA	Voids filled with bitumen
VMA	Voids in mineral aggregate

Table of Contents

Chapter 1 Introduction.....	1 -
1.1 Ravelling on Dutch highways	1 -
1.2 Potential cause of ravelling	2 -
1.3 Objectives and approach of this research	3 -
1.4 Organization of the thesis	4 -
Chapter 2 Literature Review	7 -
2.1 Application of porous asphalt concrete in the Netherlands	7 -
2.2 Advantages and disadvantages of porous asphalt wearing course	9 -
2.2.1 Advantages of porous asphalt wearing courses	9 -
2.2.2 Disadvantages of porous asphalt.....	11 -
2.3 Ravelling on porous asphalt wearing course	13 -
2.4 Self healing of asphalt concrete	13 -
2.4.1. Concept of self healing	13 -
2.4.2. Self healing of asphalt concrete	15 -
2.4.3. Explanation of self healing of bitumen and asphalt mixes	16 -
2.4.4. Factors influencing self healing of asphalt concrete.....	17 -
2.4.4.1 Bitumen properties.....	17 -
2.4.4.2 Asphalt mixture composition.....	21 -
2.4.4.3 Environments	23 -
2.5 Induction healing of porous asphalt concrete	26 -
2.5.1 Induction heating technology.....	26 -
2.5.2 Conductive asphalt concrete	27 -
2.6 Summary of the literature review	29 -
Chapter 3 Materials and Sample Preparation	31 -
3.1 Raw materials.....	31 -
3.2 Mastic beams.....	33 -
3.3 Porous asphalt concrete cylinders.....	36 -
3.4 Porous asphalt concrete beams	43 -
Chapter 4 Electrical Conductivity and Induction Heating Speed of Asphalt Mastic and Porous Asphalt Concrete with Steel Fiber	45 -
4.1 Introduction	45 -
4.2 Electrical resistivity of asphalt mastic and porous asphalt concrete with steel fiber.....	46 -
4.2.1 Experiments	46 -
4.2.2 Results and discussion	49 -
4.2.2.1 Effect of the sand-bitumen volume ratio on the electrical conductivity of asphalt mastic	49 -
4.2.2.2 Effect of the volume content of steel fiber on the electrical conductivity of asphalt mastic	51 -

4.2.2.3 Effect of the volume content of steel fiber on the electrical conductivity of porous asphalt concrete	- 52 -
4.2.2.4 Effect of the length of steel fiber on the electrical resistivity of porous asphalt concrete	- 55 -
4.2.2.5 Analysis and discussion	- 56 -
4.3 Induction heating of asphalt mastic and porous asphalt concrete with steel fiber	- 58 -
4.3.1 Induction heating principles	- 58 -
4.3.2 Induction heating equipment and setup	- 60 -
4.3.3 Results and discussion	- 61 -
4.3.3.1 Temperature distribution in the sample	- 61 -
4.3.3.2 Ageing potential of bitumen during induction heating	- 65 -
4.3.3.3 Effect of the volume content of steel fiber on the induction heating speed of asphalt mastic	- 66 -
4.3.3.4 Effect of the volume content of steel fiber on the induction heating speed of porous asphalt concrete	- 67 -
4.3.3.5 Effect of the initial length of steel fibers on the induction heating speed of porous asphalt concrete	- 71 -
4.3.3.6 Effect of the distance between the coil of the induction generator and the top surface of heated sample on the induction heating speed of porous asphalt concrete	- 72 -
4.3.3.7 Temperature profile in porous asphalt concrete after induction heating	- 74 -
4.4 Summary and Conclusions	- 75 -

Chapter 5 Mechanical Properties of Porous Asphalt Concrete with Steel

Fiber	- 77 -
5.1 Introduction	- 77 -
5.2 Cantabro test	- 79 -
5.2.1 Test description	- 79 -
5.2.2 Particle loss resistance of porous asphalt concrete with steel (wool) fiber	- 80 -
5.3 Indirect tensile strength test	- 83 -
5.3.1 Test description	- 83 -
5.3.2 Indirect tensile strength of porous asphalt concrete with steel (wool) fiber	- 84 -
5.4 Retained indirect tensile strength test	- 88 -
5.4.1 Test description	- 88 -
5.4.2 Water sensitivity of porous asphalt concrete with steel fiber 00 ..	- 89 -
5.5 Stiffness modulus test	- 89 -
5.5.1 Test description	- 89 -
5.5.2 Stiffness of porous asphalt concrete with steel fiber type 00	- 90 -
5.6 Indirect tensile fatigue test	- 94 -
5.6.1 Test description	- 94 -
5.6.2 Fatigue life of porous asphalt concrete with 8% steel fiber 00	- 95 -
5.7 Nano indentation test	- 97 -

5.7.1 Test description	97 -
5.7.2 Indentation modulus and hardness of the mortar in porous asphalt concrete with steel fiber 00	100 -
5.8 Summary and Conclusions	101 -
Chapter 6 Induction-Healing of Asphalt Mastic and Porous Asphalt Concrete with Steel Fiber	103 -
6.1 Induction healing of asphalt concrete	103 -
6.2 Healing of asphalt mastic beams in three point bending test.....	105 -
6.2.1 Test description	105 -
6.2.2 Test result	106 -
6.3 Healing of porous asphalt concrete cylinders in indirect tensile fatigue test	107 -
6.3.1 Test description	107 -
6.3.2 Test results	110 -
6.4 Healing of porous asphalt concrete beams on elastic foundation setup	113 -
6.4.1 Background of beam on elastic foundation test.....	113 -
6.4.2 Beam on Elastic Foundation Setup	114 -
6.4.3 Test procedure for beam on elastic foundation test	115 -
6.4.4 Test results	116 -
6.5 Healing of porous asphalt concrete beams in four point bending fatigue test	119 -
6.5.1 Fatigue resistance of porous asphalt concrete beams with steel wool	119 -
6.5.2 Natural healing and induction healing of porous asphalt concrete beams.....	121 -
6.5.3 Healing of porous asphalt concrete beams at different temperatures.....	124 -
6.5.4 Healing of porous asphalt beams with different damage degree	125 -
6.5.5 Flexural stiffness recovery of damaged porous asphalt concrete beam	127 -
6.5.6 Application of multiple times induction heating on porous asphalt concrete beams	128 -
6.5.7 Induction healing of aged porous asphalt concrete beams	129 -
6.6 Summary and Conclusions	130 -
Chapter 7 Application of Induction Healing on the Trial section.....	133 -
7.1 Assessment of the porous asphalt mixture with steel wool in the laboratory of Heijmans-Breijn in Rosmalen	134 -
7.2 Trial production of porous asphalt mixture with steel wool in the asphalt plant of Heijmans-Breijn in Zwijndrecht	139 -
7.3 Construction of the induction healing trial section.....	141 -
7.4 Characterization of the material from the field trial section with laboratory experiments.....	143 -
7.4.1 Heating test	143 -

7.4.2. Cantabro test	- 145 -
7.4.3 Indirect tensile strength test	- 146 -
7.4.4 Indirect tensile stiffness test.....	- 148 -
7.4.5 Indirect tensile fatigue test.....	- 150 -
7.4.6 Nano indentation test	- 152 -
7.4.7 Nano CT scanning test.....	- 153 -
7.4.8 Stiffness recovery test.....	- 154 -
7.4.9 Fatigue life extension test	- 155 -
7.5 Modeling of the thermal transfer in the field trial section after induction heating.....	- 156 -
7.5.1 Thermal properties of an asphalt pavement.....	- 156 -
7.5.2 Introduction to the model program FEMMASSE HEAT-MLS	- 158 -
7.5.3 Results and analysis	- 160 -
7.6 Summary and Conclusions	- 166 -
Chapter 8 Conclusions and Recommendations.....	- 169 -
8.1 Introduction.....	- 169 -
8.2 Conclusions.....	- 169 -
8.3 Recommendations.....	- 171 -
References	- 173 -
Appendix	- 182 -

Chapter 1 Introduction

1.1 Ravelling on Dutch highways

In the Netherlands, porous asphalt concrete (PA) surface wearing courses are used very commonly on highways to reduce traffic noise. They were first used in the Netherlands in 1972 [van der Zwan et al 1990]. In 1987, it was decided to start applying porous asphalt surface wearing courses on a larger scale [Swart 1997]. Until now, about 90% of the highways in the Netherlands are surfaced with porous asphalt concrete [Mo 2010]. In most cases, porous asphalt 0/16 is used in a thickness of 50 mm and a minimum air voids content of 20%. Unlike traditional dense-graded asphalt concrete, porous asphalt is an open graded asphalt concrete. This open nature of porous asphalt brings significant benefits. The first important advantage of porous asphalt is that the traffic noise will be reduced by 3-4 dB compared to the typical dense-graded asphalt concrete roads [McDaniel and Thornton 2005, Larsen and Bendtsen 2002]. Another important advantage of porous asphalt is the drainage of water. During rainfall events, water drains through the porous asphalt to the side of the road. This prevents spray and splash as can be observed on dense graded asphalt concrete wearing courses, which strongly improves the visibility and driving safety during rainy weather [Kandhal 2002].



Figure 1.1: Ravelling in porous asphalt surface layer

However, the attractive features of a porous asphalt surface wearing course do not last long because of clogging, stripping, and accelerated aging [Kim et al 2009]. The largest defect in porous asphalt concrete is the poor performance in terms of ravelling, as shown in Figure 1.1. Porous asphalt is very susceptible to ravelling, which is defined as the loss of aggregate particles from the road surface. As shown in Figure 1.2, ravelling occurs due to both climatic influences and traffic loading. According to Hagos, ravelling is caused by an increase of stiffness, reduction of relaxation capacity and formation of micro-cracks in the binder due to ageing [Hagos 2008]. Chemical spills from vehicles can also advance ravelling. Traffic will finally remove the particles from the surface. Ravelling usually occurs at large scale 7 years after paving, but sometimes it may appear as early as 2 or 3 years after paving. Ravelling is the start of more serious defects like potholes, because once a stone is lost, more stones will follow due to lacking support in at least one direction [Kneepkens et al 2004].

Ravelling of a porous asphalt surface layer is most frequently reported as the cause of failure of surface wearing courses [Voskuilen and Verhoef 2003, Padmos 2002]. Ravelling has a negative influence on the noise reduction capacity and skid resistance of porous asphalt wearing course and requires early maintenance, otherwise it can disintegrate the layer within a few months or even a few weeks in some extreme cases [Huber 2000]. In fact, this phenomenon is the main cause for maintenance or replacement of the top layer in the Netherlands [Padmos 2002]. Maintenance intervention is usually performed when the ravelled area of the porous asphalt pavement reaches 40%. Due to ravelling, the service life of porous asphalt on the heavy trafficked lanes of Dutch motorways is much shorter (10-12 years) than dense graded asphalt roads (18 years) [Mo 2010]. In some cases, the lifetime of porous asphalt wearing course can be as low as 4 years.

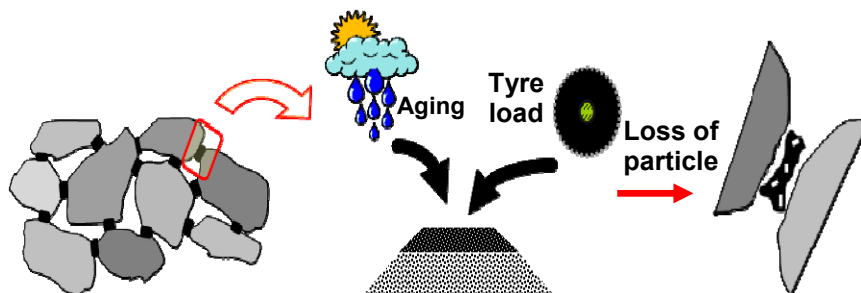


Figure 1.2: The concept of ravelling in porous asphalt surface

1.2 Potential cause of ravelling

Ravelling in a porous asphalt surface wearing course usually starts slowly, but after 7-9 years it develops very quickly because of the domino-like effect of gap growing: When the first stone is removed by a car wheel, the remaining stones around the gap lack support from at least one direction. It is easier to remove the adjacent stones in the gap. Therefore, after the first stones are removed, more stones will follow at a higher rate [Kneepkens et al 2004].

Factors involved in ravelling are very complex. Molenaar et al stated that short term ravelling is assumed to be caused by intense shearing force in the tyre/pavement contact area [Molenaar et al 2000]. According to Voskuilen and Verhoef, short term ravelling (premature ravelling) was largely determined by the quality of the construction materials especially that of the crushed rock and the manufacturing and laying process. They concluded that ravelling was caused by the presence of too high amount of weak rock material which was not detected by the test methods used, too high or too low mixing temperature (causing segregation or poor mixing and crushing of rock respectively), and lower percentages of lime in the filler (causing increased aging) [Voskuilen and Verhoef 2003]. In the Netherlands, fillers, which have at least 25% hydrated lime, are used for porous asphalt. Ravelling was also associated with inadequate compaction [California Department of Transportation 2006].

However, long term ravelling is most often associated with aging of the binder (oxidation and hardening). Hagos defined the ravelling failure as the damage caused by high levels of stress and/or strain in the system due to traffic and environmental actions [Hagos 2008]. Molenaar believes that aging of the binder is the major contributor to poor performance of porous asphalt. Because of the high rate of aging of the bitumen in porous asphalt pavement layers, loss of cohesive bonds in the binder and/or adhesive bonds between the binder and the aggregates occur, resulting in ravelling [Molenaar and Molenaar 2000]. According to Nicholls and Carswell, progressive binder hardening due to oxidative aging produces a material that cannot accommodate the strain from traffic loading and results in brittle failure at lower temperatures [Nicholls and Carswell 2001]. Gravity segregation of the mastic, especially during construction and the first months after paving, also accelerates the ravelling failure process, because the binder drains to the lower part resulting in less binder in the upper half of the porous asphalt layer, which is more susceptible to ageing followed by stripping at the pavement surface [Kneepkens et al 2004, Molenaar and Molenaar 2000].

1.3 Objectives and approach of this research

As the skid resistance and noise reduction functions of a porous asphalt surface wearing course can be decreased by ravelling, maintenance is required. In the Netherlands, ravelling is the main cause for maintenance or renewing of the top layer of porous asphalt pavement. To improve the durability of a porous asphalt surface wearing course, ravelling has to be avoided. If the problem of ravelling can be prevented or delayed, the service life of porous asphalt will be greatly extended. So, the objective of this project is to prevent ravelling on porous asphalt surface wearing course.

To achieve this goal, an induction healing approach (namely, activating the healing process of asphalt concrete through induction heating) will be used. The schematic diagram of induction healing can be illustrated in Figure 1.3. Steel fibers are added to a porous asphalt mixture. When micro cracks are expected to occur in the asphalt mastic (or between mastic and stones) of the

porous asphalt pavement, the temperature of the mastic can be increased locally by induction heating of the steel fibers via an external source so that porous asphalt concrete can repair itself and close the cracks through the high temperature healing of the bitumen (diffusion and flow). The closure of micro cracks will prevent the formation of macro cracks. In such a way, ravelling can be avoided or delayed eventually. The heating process on the porous asphalt wearing course can be repeated if cracks appear again.

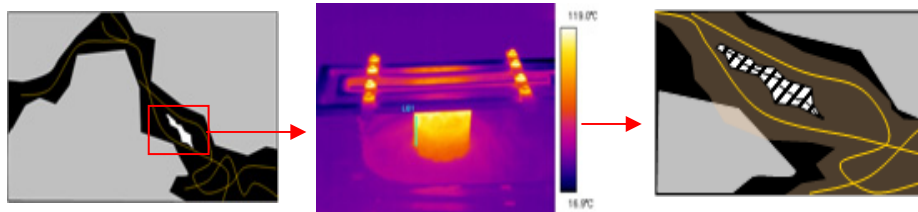


Figure 1.3: The schematic diagram of induction heating in porous asphalt concrete

The major healing mechanism of induction heating is the capillary flow and diffusion of the binder at high temperatures. This healing mechanism has been verified by García with capillary flow tests of bitumen [García 2012].

As asphalt concrete has already shown better self-healing rates at higher temperatures during rest periods [Uchida 2002, Kim and Roque 2006], the future for the application of induction heating of porous asphalt concrete looks very promising. The addition of steel fiber will also reinforce the mastic (bitumen, filler and sand) of porous asphalt concrete, which will delay ravelling. Another important advantage is that the addition of steel fibers will prevent drainage of bitumen from the top of the layer. In this way, better bridges between the stones will be available after construction.

The direct effect of this application will be less maintenance activities on the road and a better net present value of the road construction. According to Dutch Ministry of Transport, Public Works and Water Management (Rijkswaterstaat), even the price of the induction heating porous asphalt is twice of standard porous asphalt, about 90 million euros can be saved annually by investing in induction heating asphalt concrete with a 50% extended life span compared to traditional porous asphalt concrete [NL Agency 2011]. The increase of the lifetime of the pavement by applying induction heating asphalt will also lead to a decrease in CO₂ emission and less energy consumption for production and paving.

1.4 Organization of the thesis

This thesis consists of eight chapters describing the research of using induction heating to heal porous asphalt concrete. A summary of the content of each chapter is given in Figure 1.4.

Chapter 1 gives a brief introduction to this thesis, including the main problem with a porous asphalt layer and the objectives and approach of this research.

After this introductory chapter, a detailed literature review on the following aspects is given in Chapter 2: usage of porous asphalt wearing course in the Netherlands, the advantages and disadvantages of porous asphalt, the self-healing property and conductivity of asphalt concrete, and electromagnetic induction heating.

Chapter 3 introduces the raw materials and samples used in this study including stone, fine sand, filler, bitumen, steel wool/fiber, asphalt mastic and porous asphalt concrete.

Chapter 4 discusses the electrical conductivity and induction heating speed of asphalt mastic and porous asphalt concrete with steel fiber.

Chapter 5 provides the mechanical properties of asphalt mastic and porous asphalt concrete with steel fiber.

Chapter 6 studies the healing efficiency of asphalt mastic and porous asphalt concrete induced by induction heating.

Chapter 7 describes the application of the induction healing approach on the field trial section, the characterization of the material from trial section and the simulation of induction heating on the trial section.

Finally, conclusions and recommendations are given in Chapter 8.

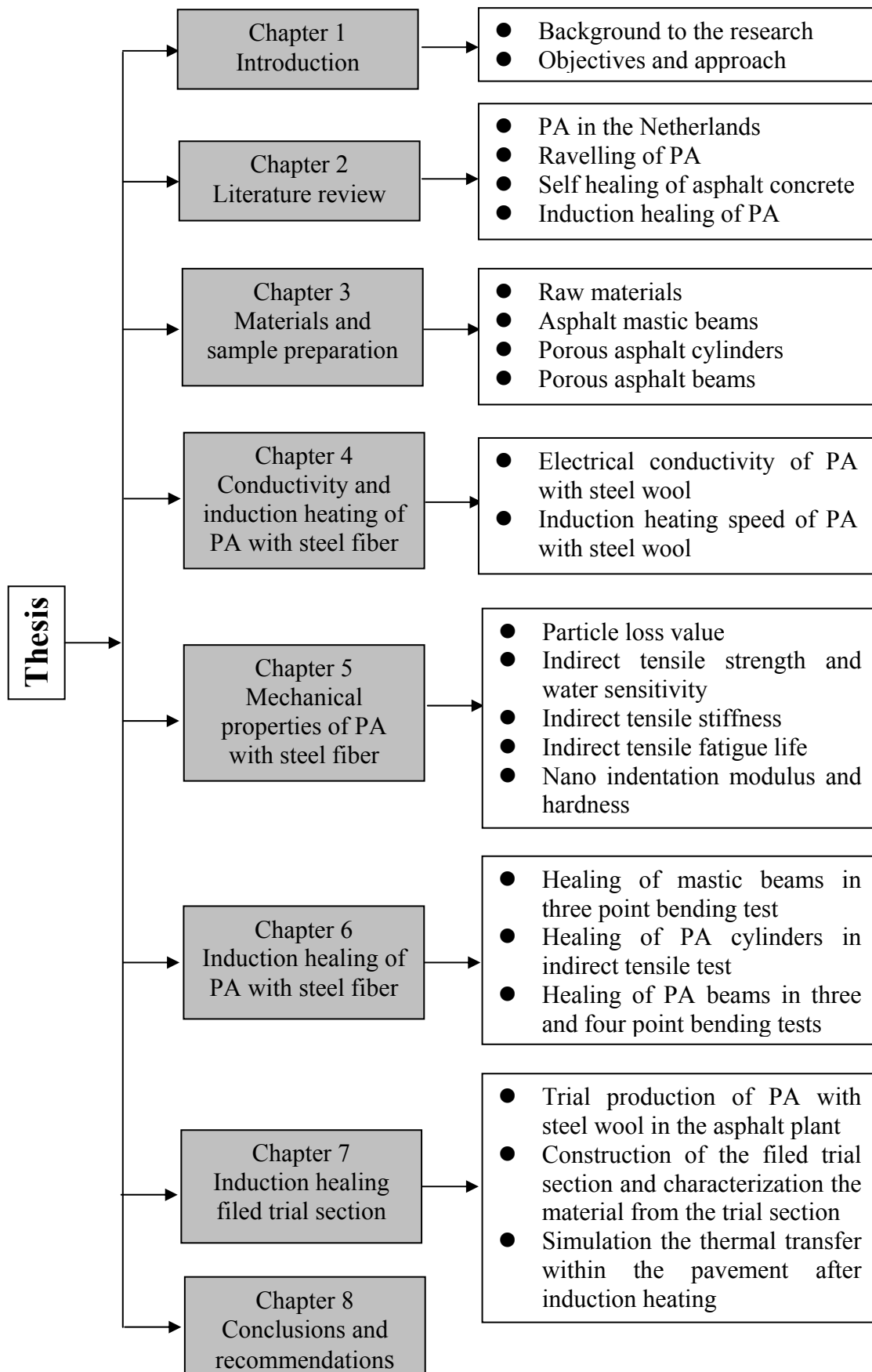


Figure 1.4: Outline of the thesis

Chapter 2 Literature Review

This chapter contains a comprehensive literature review on porous asphalt wearing course dealing with the following aspects: application of porous asphalt concrete in the Netherlands; advantages and disadvantages of porous asphalt concrete; self healing potentials of asphalt concrete; electromagnetic induction heating and electrically conductive asphalt concrete.

2.1 Application of porous asphalt concrete in the Netherlands

Porous asphalt surface wearing course (Open Graded Friction Course) was originally developed to prevent skidding on wet pavements in the 1930s in the US and was generally applied on highways and airports in 1970s. It was first used in the Netherlands in 1972 [van der Zwan et al 1990]. Since then, more and more Dutch highways are surfaced with porous asphalt concrete to reduce traffic noise, which is a very important environmental issue in the Netherlands with many urban areas close to the major highways.

In 1987, the government decided to start applying porous asphalt wearing courses on a larger scale, and three years later the decision was made that the entire main highway network (3.200 km) was qualified for porous asphalt [Swart 1997]. Porous asphalt is now used very extensively on highways in the Netherlands.

Figure 2.1 presents the growth of porous asphalt surface layers on the main roads in the Netherlands. As shown in Figure 2.1, 64.56% of the top layers of highways in the Netherlands were laid with porous asphalt concrete until 2005. At the moment, this percentage is increased to around 90% [Mo 2010]. Figure 2.2 shows the distribution of porous asphalt highways in the Netherlands [Hagos 2008].

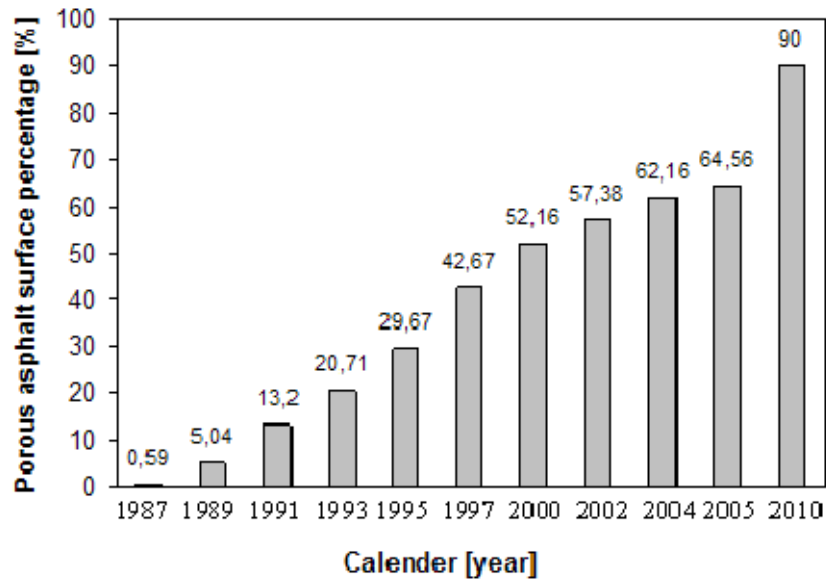


Figure 2.1: Growth of porous asphalt surfaces on the highways in the Netherlands



Figure 2.2: Distribution of porous asphalt highways in the Netherlands [Hagos 2008]

The design and composition of porous asphalt has not really changed since 1990 [Padmos 2002]. The design of porous asphalt in the Netherlands is based on the compaction of samples using 50 blows per face with the Marshall hammer and checking the voids content after Marshall Compaction. The voids content has to be no less than 20%. No further testing was required till 2008, from then on new European Specifications have been introduced. Porous asphalt gradations have maximum aggregate sizes of 11 and 16 mm with a

requirement for crushed aggregates and penetration-graded asphalt binders that are used. Porous asphalt 0/16 (as shown in Figure 2.3) is mostly used in a thickness of 50 mm and with a minimum air voids content of 20%. According to Rijkswaterstaat, Dutch motorways have an area of 87 km², 85% or 74 km² of which are paved with standard porous asphalt concrete PA 0/16. Table 2.1 presents the Dutch specification for porous asphalt concrete PA 0/16.



Figure 2.3: Standard porous asphalt 0/16 used as surface wearing course on a Dutch motorway

Table 2.1 Dutch specification for porous asphalt concrete 0/16(RAW2005)

Sieve size (mm)	RAW Spec. % retained
22.4 - 16.0	0-7
16.0 - 11.2	15-30
11.2 - 8.0	50-65
8.0 - 5.6	70-85
5.6 - 2.0	85
2.0 - 0.063	95.5
< 0.063	100
Bitumen70/100	4.5% by wt.

2.2 Advantages and disadvantages of porous asphalt wearing course

Porous asphalt wearing course is used so commonly, because it has many benefits. This section mainly presents the advantages of porous asphalt wearing course. The disadvantages of porous asphalt wearing course are also discussed here.

2.2.1 Advantages of porous asphalt wearing courses

A porous asphalt mixture is an open graded mixture with a gap at 2/7,

resulting in a high void content (20%). This open nature brings significant benefits. The benefits can be categorized into three aspects of improvement: environment, safety and economy.

Porous asphalt wearing course brings environmental benefit in terms of noise reduction. Porous asphalt can reduce noise both outside and within the vehicle. It is noted by many researchers that the average noise level resulting from traffic on porous asphalt layers is 3 or 5 dB lower than on dense graded pavement layers [van der Zwan 1990, Lefebvre 1993, Huber 2000, Larsen 2002, McDaniel and Thornton 2005]. 3 dB(A) lower noise represents a significant difference, because it is equivalent to halving the sound energy [McDaniel et al 2009]. This noise reduction benefit comes from its texture combined with the voids content and thickness, which play an important role in noise generation and propagation. Porous asphalt reduces the noise generated by air forced out between the rubber blocks of the tire and the road surface (air pumping effect) and reduces propagation of noise from the engine and transmission system of the vehicle (sound is not reflected but absorbed by the porous layer).

Porous asphalt also improves the driving safety, especially under wet conditions [Lefebvre 1993, Watson 1998, Bolzan 2001, Poulidakos 2003, Bennert 2009, Frick 2005, Lane 2005, CDR 2006, Alvarez 2006]. This safety improvement benefit is related to hydroplaning, skid resistance, splash and spray, light reflection and driving speed. Hydroplaning is a serious problem for dense asphalt layer. Hydroplaning occurs when a layer of water builds up between a tire and the pavement surface. This layer of water limits and/or eliminates the contact between the tire and the pavement, which is especially hazardous because it results in loss of control for braking and steering. According to Lefebvre, there are two aspects of porous asphalt that help prevent the occurrence of hydroplaning. First, water drains through porous asphalt into the stone bed and infiltrates into the soil, the film of water is not available to break the bond between the tire and pavement surface. The second aspect is the macro texture provided by porous asphalt, which provides small channels for water to be dissipated as a tire crosses over the pavement [Lefebvre 1993]. Therefore, in wet driving conditions, the skid resistance of porous asphalt wearing layers is generally very good. The use of porous asphalt also strongly reduces splash and spray during rainy conditions [Cooley et al 2000, Huber 2000, Spillemaeker 2000, Bolzan 2001, Bendtsen 2002, Kandhal 2002, Cooper 2004, Punith and Suresha 2004]. On dense-graded pavement, rolling wheels will throw water into the air from pools on the pavement surface, which reduce driver visibility. Through the infiltration of water into a porous asphalt layer, the pools of water will not be available to create splash and spray under rolling wheels. Figure 2.4 compares the surfaces of a porous asphalt and a dense graded asphalt under wet condition. The snow and water on the dense graded asphalt surface will result in hydroplaning and splash/spray, which will be absent on the porous asphalt surface. Another benefit of porous asphalt related to safety is glare reduction, particularly at night. Porous asphalt will diffuse the reflection of light due to the high macrotecture, which increases driver visibility of pavement surface markings [Alderson 1996]. Improvements

are obtained in wet conditions, since less water at the surface is associated with less reflection of incident light [Khalid 1996]. Replacing the dense asphalt wearing courses with porous asphalt has been shown to reduce crashes, injuries and fatalities on highways. What makes the difference is probably the improvement in visibility related to the reduction in splash and spray. During rain events, the absence of hydroplaning and splash/spray on porous asphalt pavement gives drivers increased confidence that results in increased speeds. This is also a benefit of porous asphalt wearing course. However, the increased speeds can again reduce the safety aspect of porous asphalt pavement.



Figure 2.4: Comparison of a porous asphalt surface (left, clean surface) and a dense graded asphalt surface (right, wet surface with ice and water) under wet condition

Finally, porous asphalt brings economic benefit. This benefit is related to pavement smoothness. Lefebvre indicates that porous asphalt layers are typically constructed smoother than dense-graded asphalt layers. Under certain conditions, this has resulted in a 1% to 2% reduction in fuel consumption due to enhanced smoothness [Lefebvre 1993]. In addition, reduction in the rate of tire wear on porous asphalt was suggested based on a decrease in tire stresses generated by the improved macrotexture of porous mixture [Khalid 1996].

2.2.2 Disadvantages of porous asphalt

Porous asphalt wearing course is not perfect. Shorter service life, higher construction costs, extra winter maintenance, and lower structural contribution are the main disadvantages related to the use of porous asphalt.

Relative shorter service life is the first disadvantage of porous asphalt. The performance of porous asphalt wearing courses can be evaluated in terms of both durability and functionality (permeability and noise reduction). Durability issues in porous asphalt are mainly associated with ravelling, which progresses rapidly and needs maintenance [Rogge 2002 and Huber 2000]. In the Netherlands, the lifetime of a porous asphalt pavement is around 11 years, much shorter than that of a dense graded pavement of 18-20 years. As regards functionality, accelerated loss of permeability and noise reduction capacity due to clogging of pores is a main concern for porous asphalt mixtures. In Spain, porous asphalt (voids content lower than 20 percent) kept its drainage capacity

for periods of 9 years when subjected to medium traffic; whereas, after 2 years, clogging was reported in mixtures operating under heavy traffic [Khalid 1996]. In Britain, the reduction in the suppression of noise capacity and permeability and some increases in spray levels are recognized, but the material still retains its noise reduction capacity and similar performance in terms of spray generation compared to thin surfacing [The Highways Agency et al 1999].

Construction costs are usually considered higher for porous asphalt mixtures when compared with dense graded asphalt mixtures [Khalid 1996 and Huber G 2000]. This is a result of the required high quality polish resistant aggregates and polymer modified asphalt binders. Also, pavement markings have to be adapted for porous asphalt. Special impervious layers specifically placed below porous asphalt also increase construction costs. For example, in Germany usually a 20mm dense graded asphalt layers is placed below the porous asphalt layer.

Winter maintenance is considered a significant disadvantage of porous asphalt. Since porous asphalt mixtures have a tendency to cool faster than adjacent dense graded asphalt mixture, porous asphalt can exhibit earlier frost and ice formation than dense graded asphalt mixture, and these conditions may persist for longer periods. Due to the porosity, most of the salt is not staying at the surface. Therefore, larger amounts and more frequent application of deicer agents and higher care in the homogeneity of the application are required. These requirements generate higher maintenance costs for porous asphalt.

Finally, porous asphalt layers typically have no or minimal structural contributions for pavement structural design [Khalid 1996].

Based on the literature survey, the advantages and disadvantages of porous asphalt can be summarized in Table 2.2:

Table 2.2: Advantages and disadvantages of porous asphalt

Characteristic	Porous asphalt wearing course
Advantages	<ul style="list-style-type: none"> • Lower pavement noise levels • Reduced splash and spray • Avoid the phenomena of aquaplaning and water • Minimization of hydroplaning • Improved vehicle adherence and visibility • Reduced water contamination • Improved skid resistance • Improved night visibility(less glare) • Reduced fuel consumption due to enhanced smoothness • Less tire wear
Disadvantages	<ul style="list-style-type: none"> • Relative shorter service life • Higher construction costs • Extra winter maintenance • Lower structural contribution

2.3 Ravelling on porous asphalt wearing course

The durability of a porous asphalt wearing course has been a matter of concern, because the attractive features of porous asphalt do not last very long due to clogging, ravelling, and accelerated aging. Ravelling, which is the loss of aggregates from the road surface (as shown in Figure 2.5), is the main defect on porous asphalt surface wearing course [Padmos 2002, Voskuilen and Huurman 2009].

Ravelling is a failure at the surface of the pavement occurring within the stone-to-stone contact regions. It is caused by the increase of stiffness, reduction of relaxation capacity and formation of micro-cracks in the binder due to traffic and environmental loadings. Traffic will finally remove the particles from the surface. When ravelling occurs, the acoustical benefits and skid resistance of porous asphalt are diminished. Moreover, ravelling requires early maintenance. It is reported that ravelling, in about 76% of the cases, is the cause for maintenance or replacing of the top layer [Padmos 2002]. Due to ravelling, the service life of porous asphalt is much shorter (sometimes only half) than that of a dense graded asphalt road. To extend the lifetime of porous asphalt, ravelling should be prevented.



Figure 2.5: Serious ravelling on highways Amsterdam A1 (top) and The Hague A4 (bottom)

2.4 Self healing of asphalt concrete

2.4.1. Concept of self healing

Self healing can be defined as the built-in ability of a material to automatically heal (repair) the damage occurring during its service life [White et al 2001]. The properties of a material degrade over time due to damage (such

as microcracks) at microscopic scale. These cracks can grow and ultimately lead to full scale failure. Usually, cracks are mended by hand, which is difficult because micro cracks are often hard to detect. In the field of materials science researchers are now trying to introduce self healing components to normal materials to obtain a self healing system to improve the service life of materials. A material that can intrinsically correct damage caused by normal usage could lower production costs of a number of different industrial processes through longer part lifetime, reduction of inefficiency over time caused by degradation, as well as prevent costs incurred by material failure [Wikipedia 2010].

The dominant research on self healing materials is done in the field of polymers. The first patent of a polymer with intentional self healing characteristics dates back to 1966. Craven developed reversible cross-linked polymers from condensation polymers with pendant furan groups cross-linked with maleimides [Craven 1966]. These polymers could reverse to their cross linked state after cracking. Unfortunately, the potential of this route was not appreciated.

In 1994, Dry developed an active and a passive cracking repair method by smart timed release of polymerizable chemicals from porous and brittle hollow fibers into cement matrices [Dry 1994]. As shown in Figure 2.6 (left), the active cracking repair system contains porous fibers coated with wax and filled with methyl methacrylate. When a crack occurs, low heat is applied to the cement matrix, wax is melted and the methyl methacrylate is released into the matrix. Subsequent heating make the methyl methacrylate polymerize to close the crack. In the passive crack filling method, loading, which causes microcracking in the cement matrix, breaks the brittle hollow glass fibers to release the chemicals (Figure 2.6 right).

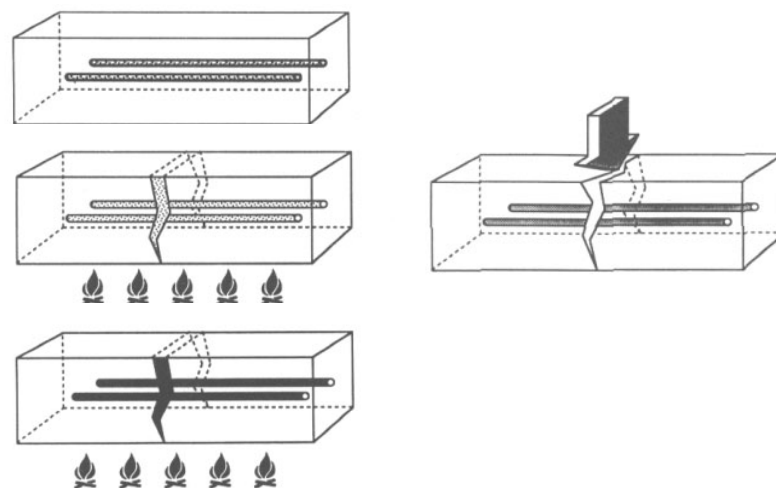


Figure 2.6: Design for timed release of polymerizable chemicals to repair cracks and fill cracks: (left) by melting of the coating on porous fibers, (right) the brittle fiber breaks under load [Dry 1994]

The first completely autonomous synthetic self-healing material was reported by White et al with an example of a polymer composite with

microcapsules [White 2001]. This healing concept is illustrated in Figure 2.7. A microencapsulated healing agent is embedded in a structural composite matrix with a catalyst capable of polymerizing the healing agent. An approaching crack breaks the embedded microcapsules, releasing the healing agent into the crack plane through capillary action. Polymerization of the healing agent is triggered by contact with the embedded catalyst, closing the crack faces.

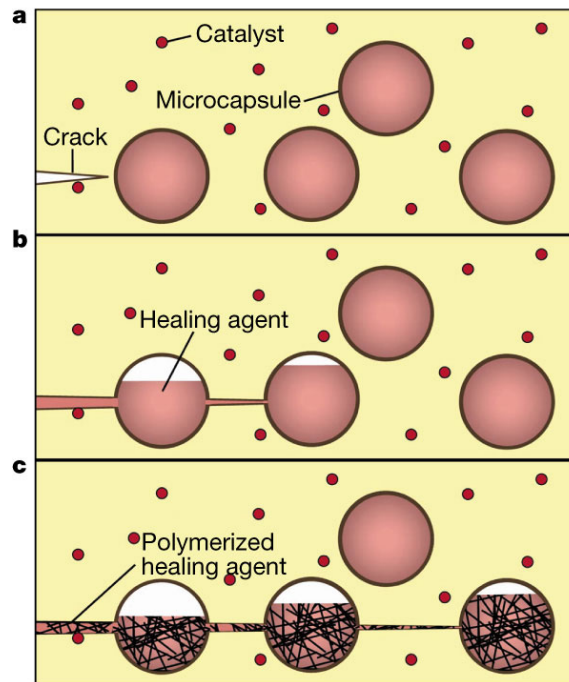


Figure 2.7: The self healing concept with microcapsules [White et al 2001]

Since then, more and more research on creating self healing materials was conducted successfully. These self healing materials consist of concrete [Li and Yang 2007, www.selfhealingconcrete.blogspot.com 2012], asphalt [Little and Bhasin 2007], polymer and composites [Andersson et al 2007], coatings [van Benthem et al 2007], metals and alloys [Lumley 2007], etc.

2.4.2. Self healing of asphalt concrete

Similar to other self healing materials, asphalt concrete can repair the damage autonomously. Asphalt concrete has a potential to restore its stiffness and strength, when subjected to rest periods. This self healing capability of asphalt concrete has been shown both with laboratory tests and in the field since the 1960s [Bazin and Saunier 1967, van Dijk et al 1972, Francken 1979]: Bazin and Saunier found that asphalt concrete beams, tested until failure under uniaxial tensile loads could recover 90% of their original resistance when they were left to rest under pressure at a temperature of 25 °C [Bazin and Saunier 1967]. Meanwhile, they found that fatigue damaged beam samples could regain over a half of the original fatigue life after introducing a one day rest period to the failed samples and pressing the crack faces together with a small pressure during this rest period. The recovery of both strength and fatigue life were

evidence of healing caused by rest periods. After that, more laboratory experiments were done to study the strength recovery and the fatigue life extension of an asphalt mixture when rest periods were introduced in between the loadings. Laboratory experiments done by Castro and Little demonstrated that the fatigue life of an asphalt mixture could be extended when rest periods were introduced in the normally continuous loading test [Castro and Sánchez 2006, Little and Bhasin 2007]. Healing of asphalt concrete was also shown with field experiments: Williams et al used surface wave measurements to assess the stiffness of a pavement before, immediately after, and 24 h after loading passes. The stiffness recovered completely after 24 hours of rest [Williams et al 2001]. It was also reported by many researchers that cracks observed in winter time disappeared in summer time. As a consequence, healing plays an important role in the shift factor required to translate the laboratory fatigue life into the in-situ fatigue life [Lytton et al 1993].

2.4.3. Explanation of self healing of bitumen and asphalt mixes

Healing of an asphalt mixture is the recovery of its stiffness and strength due to closure of the cracks inside. The healing mechanisms of asphalt concrete have been reported by many researchers.

Healing is usually believed to be related to the sol-gel properties of bitumen. Bitumen is traditionally regarded as a colloidal system consisting of high molecular weight asphaltene micelles dispersed or dissolved in the lower molecular weight oily maltenes [Shell 1995]. Within the sol-gel system of bitumen, the transformation from sol to gel or from gel to sol happens reversibly due to the change of temperature, stress, etc. The colloidal properties of bitumen system change from gel-like type at low temperature to sol-like type at high temperature. When the temperature goes down, the colloidal property of bitumen will return from sol-like to gel-like. Loading causes bitumen to behave sol-like, just like water. When the loading is ended, the properties of bitumen immediately turn to gel-like. Castro and Sánchez explained the healing of asphalt mixes during rest periods by the sol gel theories. At high temperature, healing takes place due to a conversion from a sol to a gel structure of bitumen. If the rest time is sufficient, this would be almost complete. At low temperature, rest periods don't allow the healing of the structural damage created by the loading cycles and recovery would only be partial [Castro and Sánchez 2006].

Phillips [1998] proposed a three steps diffusion model to explain the healing of bitumen: (1) surface approach due to consolidating stresses and bitumen flow, (2) wetting (adhesion of two cracked surfaces to each other driven by surface energy density), and (3) diffusion and randomization of asphaltene structures. The first two steps cause the recovery of the modulus (stiffness) and the third step causes the recovery of the strength.

Little and Bhasin (2007) proposed a similar 3 steps model to describe the healing process of asphalt materials: (1) wetting of the two faces of a nanocrack, (2) diffusion of the molecules from one face to the other, and (3) randomization of the diffused molecules to attempt to reach the original

strength of the material. Wetting is determined by the mechanical and viscoelastic properties and material constant of the bitumen (tensile strength, work of cohesion and surface free energy). The subsequent recovery of strength is determined by the surface free energy of the asphalt binder and the self-diffusion of asphalt cement molecules across the crack interface [Bhasin et al 2008].

Little et al separated the healing during rest periods into a short-term healing rate (healing rate occurs during the first 10 s of the rest period) and a long-term healing rate (healing rate occurs after the first 10 s of the rest period) [Little et al 2001]. Short-term healing and long-term healing was distinguished based on their relations with the Lifshitz van der Waals surface energy component and the acid-base surface energy component of the material, respectively. The short term healing was inversely proportional to the Lifshitz van der Waals component of surface energy, while the long term healing was directly proportional to the acid-base component.

Kringos et al used a chemo-mechanical model to simulate healing of bitumen. Bitumen has the tendency to phase separation under mechanical or environmental loadings and the resultant interfaces of the phases will attract high stresses and are prone to cracking. By increasing the temperature or inserting mechanical energy, the phases would rearrange themselves in either a new configuration or mix themselves into a more homogenous state, giving the appearance of the existence of a single phase. The material would thus close the micro cracks, and this will result into a recovery of the mechanical properties [Kringos et al 2009].

2.4.4. Factors influencing self healing of asphalt concrete

Many factors can influence the self healing rate of asphalt concrete. These factors can be divided into three categories: bitumen properties, asphalt mixture compositions and environments.

2.4.4.1 Bitumen properties

Considering the fact that asphalt concrete can restore itself because of the healing potential of the bitumen inside, there is no denying that bitumen properties play a significant role in the self healing potentials of asphalt concrete. Many researchers reported how the bitumen properties influence its healing potentials.

Bitumen type

Van Gooswiligen et al (1994) studied the effect of the bitumen content and the viscosity of the bitumen on the healing of a dense asphalt concrete for a ratio of rest period over load duration equal to 25. As shown in Figure 2.8, the healing rate of the asphalt concrete increased with the increase of the bitumen content and the healing capacity of soft bitumen 80/100 pen was higher than that of hard bitumen 50/60 pen.

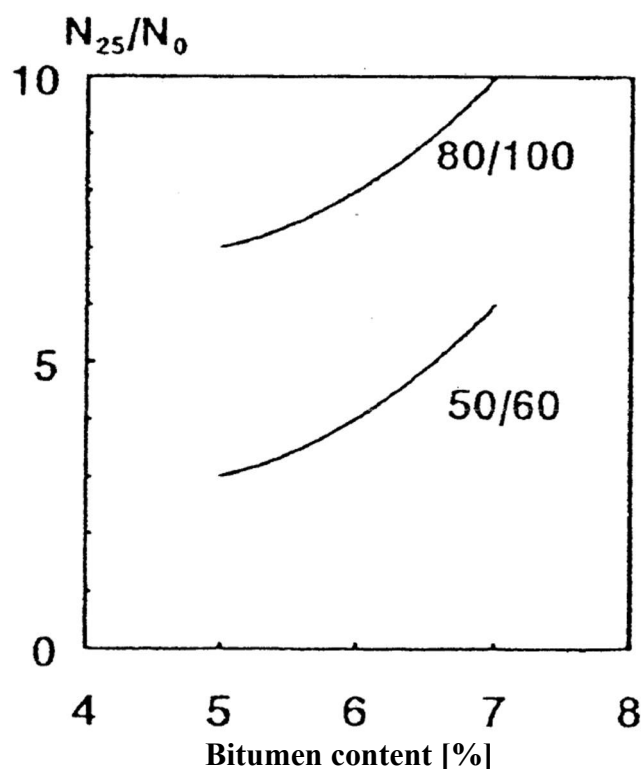


Figure 2.8: Effect of the bitumen content and the penetration grade of the bitumen on the healing of a dense graded asphalt concrete [van Gooswiligen et al 1994]

Viscoelastic properties

As sol-gel theory is often used to explain the self healing of bitumen, the sol-gel nature of bitumen affects its self healing rate. It is a common consensus that the viscoelastic properties, which reflect the sol-gel nature of bitumen, influence the self healing rate of bitumen. Many researchers prove that a sol like bitumen with a lower stiffness and a higher phase angle shows a higher self healing capacity [van Gooswiligen et al 1994].

Surface energy density

Lytton et al (2001) studied the microdamage healing of bitumen and asphalt concrete and established a healing model for asphalt concrete. In his model, the short term healing rate is inversely proportional to the Lifshitz-van de Waals component of surface energy density and the long term healing rate is directly proportional to the acid-base component of surface energy density.

Williams et al linked the healing rate of asphalt concrete (in terms of pseudo-strain energy recovery ratio) with its surface energy density. As shown in Figure 2.9, the inverse relationship between Lifshitz-van de Waals component of surface energy density and short term healing rate (healing occurs in the first 10 seconds of the rest periods) of asphalt concrete was reported. It is evident that Lifshitz-van de Waals behaviors is not favorable to healing of the binder. They also found that the acid-base component of surface energy density promoted the healing rate of asphalt concrete.

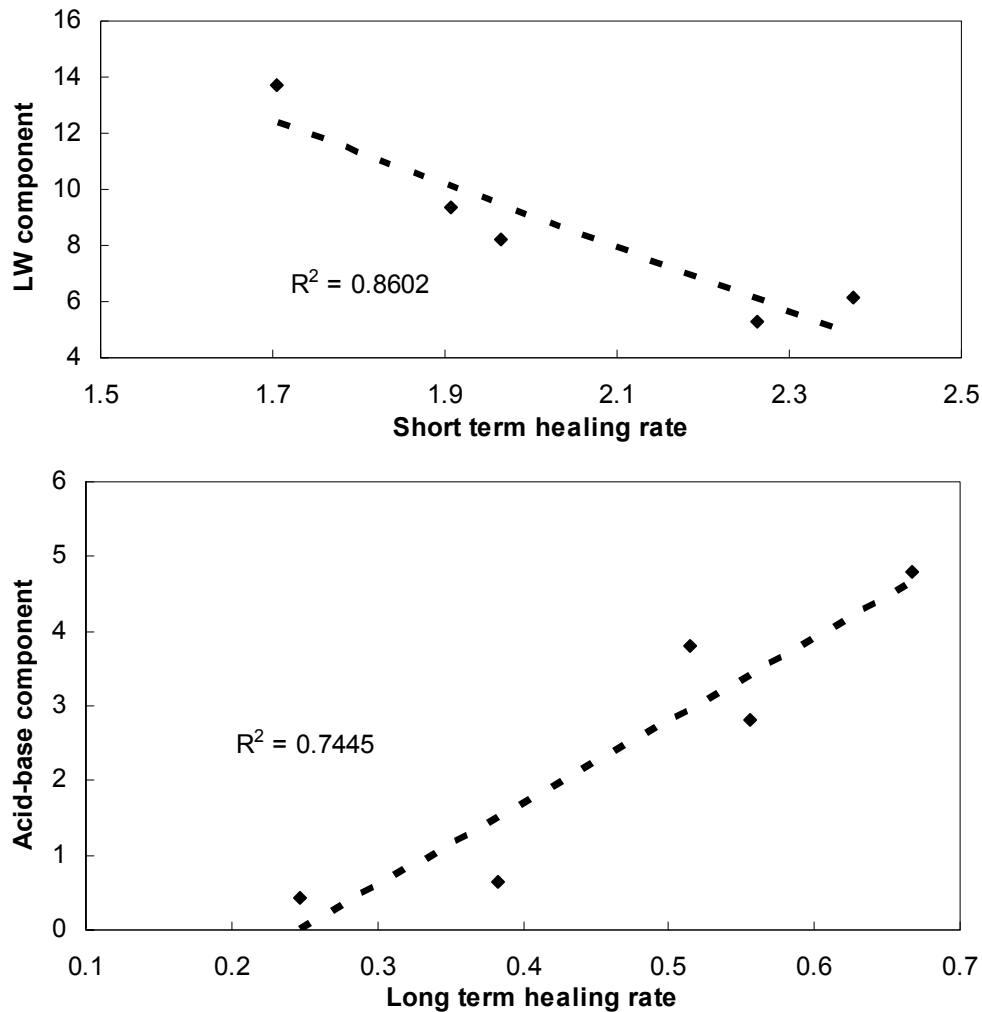


Figure 2.9: The relationship between the Lifshitz-van de Waals/acid-base components of surface energy and the healing rate of asphalt concrete (pseudo-strain energy recovery ratio) [Williams et al 2001]

Bitumen compositions

Williams et al (2001) investigated the effects of the chemical composition of bitumen on its self healing. They concluded that aromatics promote healing for the pi-pi interaction of the aromatic rings. Amphoterics are also important for healing, which could promote healing for the polar-polar bonds. The wax content is also helpful to healing because of the Van der Waals force of the interactions between long chains of hydrocarbons and aliphatic molecules within the wax. In addition, the heteroatom content promotes healing because sulfur, oxygen and nitrogen promote the polarity of bitumen [William et al 2001, Qiu 2008].

Diffusion

Diffusion is one of the key factors affecting healing of asphalt concrete. One of the mechanisms of healing is the self-diffusion of the molecules across the crack surface [Bhasin et al 2011]. So, the healing rate is determined by the

diffusion speed. Philips also concluded that diffusion limited built-up of asphaltene structure controlled the strength recovery in healing [Philips 1998].

Ageing

Edward found that the Lifshitz-van de Waals component of surface energy density increased with ageing, whereas the acid-base component of surface energy density decreased with ageing [Edward 2006]. The Lifshitz-van de Waals component of the surface energy density is related inversely to the short term healing rate and the acid-base component of surface energy density is related to the long term healing rate. As a result, the magnitude of both short term healing and long term healing would decrease with aging. So, the total capacity of healing was decreased by aging.

Modifiers

An asphalt pavement with modified bitumen often has very good fatigue and rutting resistance. However, the effect of modifier on the self healing rate of bitumen during rest periods is far from clear, different researchers reported different effects of modifiers on self healing of bitumen.

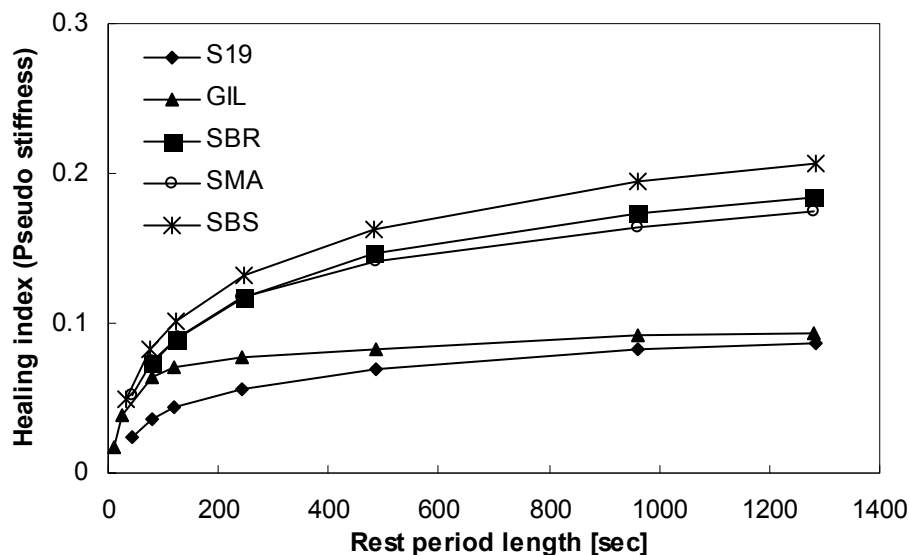


Figure 2.10: Increase of pseudo stiffness during rest periods [Lee et al 2000]

Lee et al (2000) concluded that modifiers positively affect the self healing rate of asphalt concrete. He tested the increase of the pseudo stiffness of five surface course mixtures to compare their healing potentials. The pseudo stiffness was defined as the slope of the stress-pseudo strain loop. As shown in Figure 2.10, Gilsonite (GIL), Styrene Butadiene Rubber (SBR) and Styrene Butadiene Styrene (SBS) modified mixtures and SMA showed a better potential for healing than the unmodified conventional dense graded mixture S19. It was also observed from this figure that the SBS showed the highest increase in pseudo stiffness during rest periods among five mixtures. Besides, the GIL mixture shows a large gain in pseudo stiffness in the short term, but levels out and longer rest periods have little beneficial effect. The SBS mixture,

on the other hand, has a slower initial rate of healing, but continues to gain strength with time, indicating a better healing potential over time.

Carpenter and Shen used the Ratio of Dissipated Energy Approach in Dynamic Shear Rheometer (DSR) test to study the role of healing in fatigue behavior of asphalt binders. They found that the healing rate of polymer modified binders PG 70-22 is significantly greater than that of neat binder PG 64-22 [Carpenter and Shen 2006]. Besides, Shen et al (2010) also reported that polymer modified binder PG 70-28 has a higher healing rate than neat binder PG 64-28 in DSR fatigue test: with the inclusion of 6 seconds rest periods between loadings, the fatigue life was extended about 7 times for the PG 64-28 binder but 17 times for the PG 70-28 binder (25 °C, 60 KPa, 10 Hz).

However, Kim and Roque reported a different result for the effect of styrene-butadiene-styrene (SBS) modifier on the healing rate of asphalt mixture: although SBS polymer modification reduced the rate of damage accumulation, it had relatively little effect on the normalized healing rate of the mixtures tested [Kim and Roque 2006].

Little et al even reported an inverse result: SBS polymer slightly reduced the healing rate of bitumen but retarded the crack growth of an asphalt mixture. They hypothesized that the addition of SBS acts as a filler system that interrupts the ability of pure bitumen to reestablish contact and heal [Little et al 1999]. An explanation of the negative impact of the polymer additives on healing may rest in the effect of the polymer on the compositional make-up of the bitumen. Polymer networks in bitumen are swollen by the bitumen as the more compatible components of the bitumen are partially absorbed into the polymer causing it to swell. The rest of the bitumen is left with a higher asphaltene (highly interactive) component. Bitumen with a higher asphaltene concentration is less likely to flow and heal [Qiu 2008]. Qiu also concluded that the elastic polymer networks can act as confinements to accelerate healing, but they will limit healing once broken [Qiu 2012].

2.4.4.2 Asphalt mixture composition

The asphalt mixture composition, including bitumen content, aggregate structure characteristics and gradation, also influences the self healing rate of asphalt concrete.

Bitumen content

Asphalt concrete can heal itself because the bitumen inside is self healing. So, the bitumen content plays an important role in healing of asphalt concrete. As shown in 2.4.4.1, the experiments of van Gooswiligen et al (1994) showed that an asphalt concrete with higher bitumen contents exhibited higher healing rates.

Mixture gradation

ABO-Qudais and Suleiman monitored fatigue damage and crack healing of asphalt concrete by ultrasound wave velocity. The ultrasound pulse velocity

was measured on the cylinder asphalt sample before and after fatigue test, and after rest periods. The increase of the ultrasound pulse velocity caused by rest periods was used to predict cracking and healing. The sample prepared with higher sizes of aggregates showed a higher healing rate, because the coarse gradation with less surface area has thicker asphalt film thickness and less transition zones between aggregate and asphalt, which improves the asphalt tendency towards cracks healing [ABO-Qudais and Suleiman 2005].

Structural characteristics

Kim and Roque [2006] concluded in their papers that the healing properties of asphalt mixes are more affected by the aggregate structure characteristics (which affects the aggregate interlock, the film thickness and the voids in aggregate) than by polymer modification. As shown in Figure 2.11, the healing rate of asphalt mixture (recovered dissipated creep strain energy per unit time) increases with the increase of $VFA/(VMA*VA)$, where VMA is voids in mineral aggregate, VFA is the voids filled with bitumen and VA is volume of air voids.

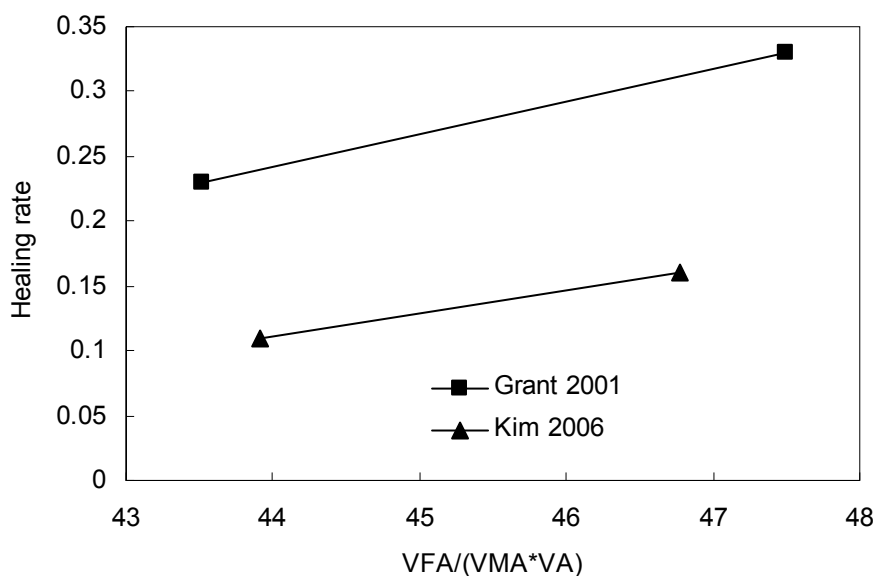


Figure 2.11: The relationship between healing rate (15 °C) and $VFA/(VMA*VA)$

Asphalt layer thickness

The thickness of an asphalt layer is also very important for healing. Figure 2.12 illustrates the shift factor required to convert the crack initiation life to the total fatigue life after surface cracks appear on the road surface [Theyse et al 1996]. He indicated that the shift factor is determined by the thickness of asphalt layer. A thicker asphalt layer is favorable for healing: the shift factor increases with the increase of asphalt layer thickness.

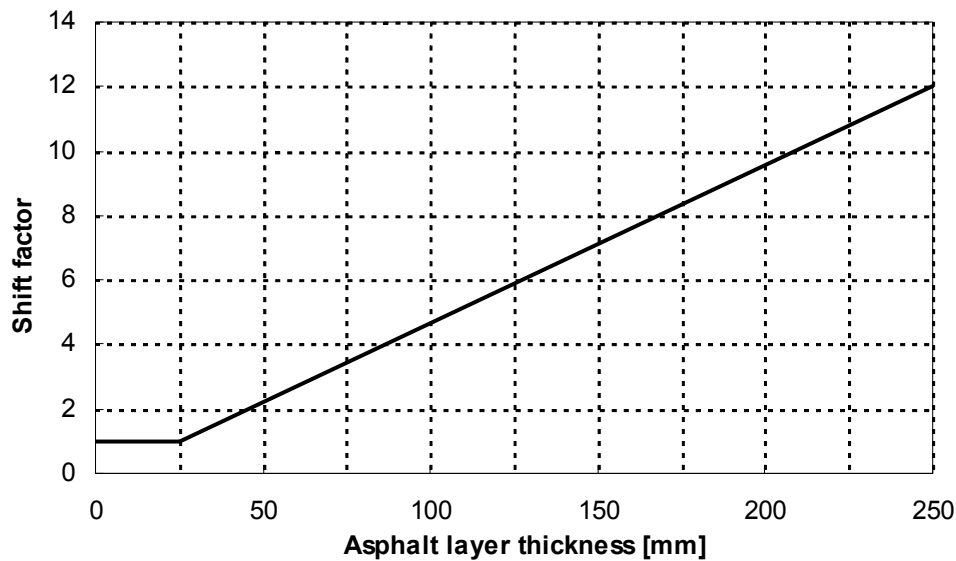


Figure 2.12: Fatigue shift factor for asphalt layer [Theyse et al 1996]

2.4.4.3 Environments

Temperature

Self healing of asphalt concrete is a temperature dependent phenomenon. As shown in Figure 2.13, Williams et al reported in their paper that the increase of the temperature causes a significant increase in the healing rate of asphalt concrete [Williams et al 2001].

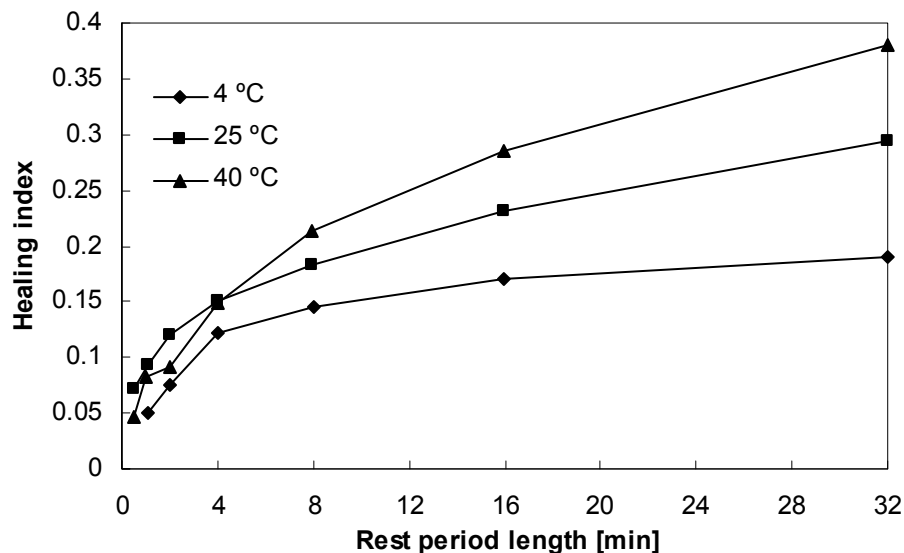


Figure 2.13: Effect of rest period length and temperature on the healing index (recovered dissipated creep strain energy per unit time) [Williams et al 2001]

Grant concluded that the increase of the temperature increases the healing rate (recovered dissipated creep strain energy per unit time) and shortens the time needed to full healing for both coarse and fine mixtures (In Figure 2.14). He implied that, the healing is immediate above a certain temperature [Grant 2001].

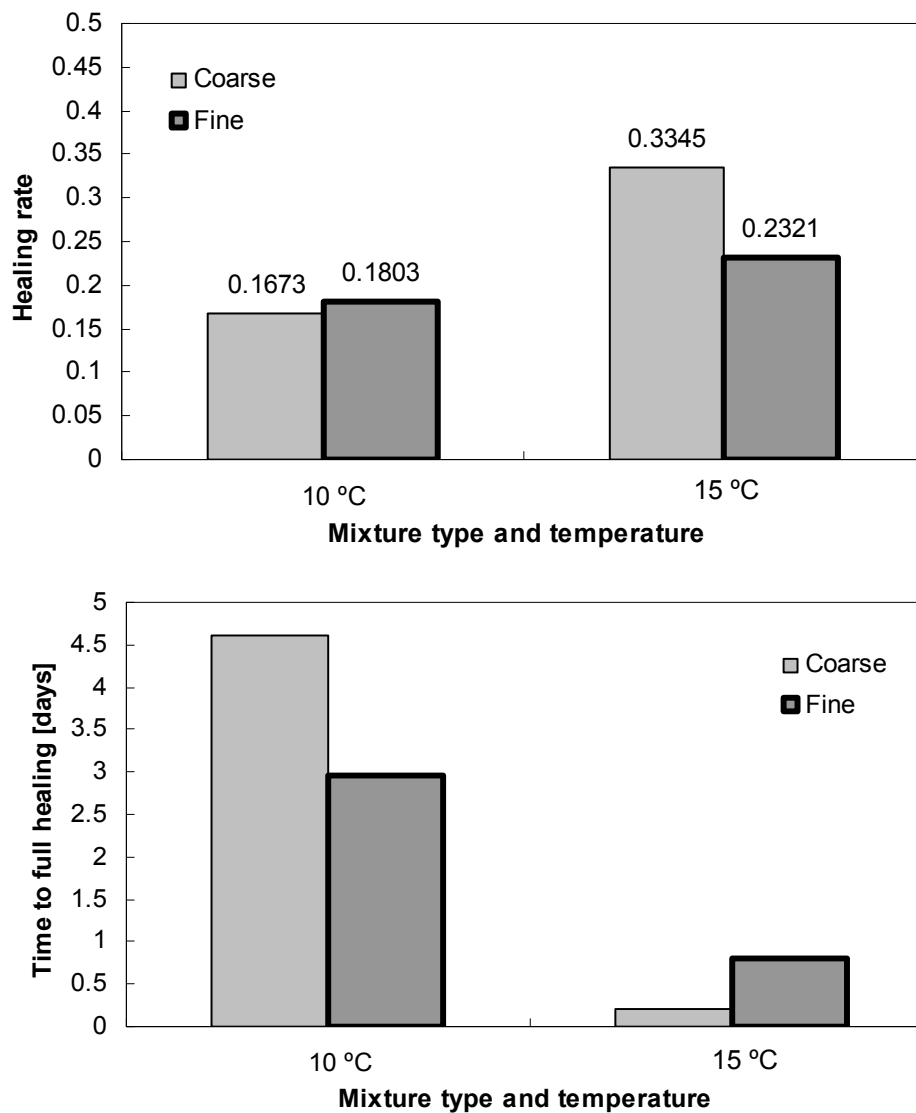


Figure 2.14: Healing of two asphalt mixes (coarse and fine mixtures in terms of gradation) against the mixture type and temperature [Grant 2001]

Kim and Roque also showed with their work that the temperature sensitivity of the self healing rate is highly non-linear and healing increases with the increase of temperature [Kim and Roque 2006].

Loading history

The loading history is one of the major factors affecting healing in asphalt concrete [Seo and Kim 2008]. Kim and Little conducted different types of cyclic loading test with varying rest periods on notched asphalt concrete beams to identify the healing potential. It was shown that the loading history had influence on healing of asphalt beams [Kim and Little 1990, 1991]. Lytton et al developed a constitutive model to predict the damage growth and healing in asphalt concrete. This model successfully predicts damage growth and healing due to complex loading histories, in both controlled-stress and

controlled-strain modes, composed of randomly applied multilevel loading with different loading rates and varying durations of rest periods [Lytton et al 2001].

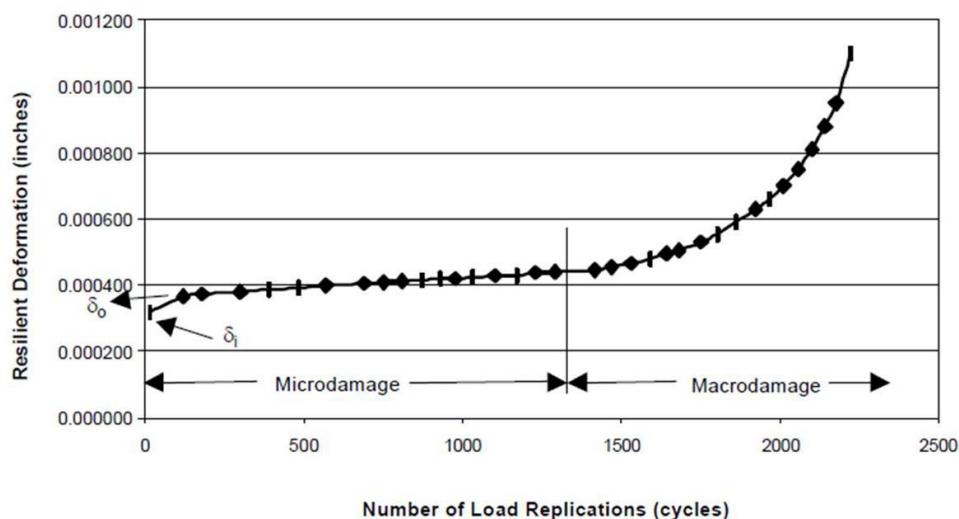


Figure 2.15: The boundary between microdamage and macrodamage during crack growth in indirect tensile fatigue test [Grant 2001]

Figure 2.15 shows an example on the boundary between microdamage and macrodamage during crack growth [Grant 2001]. Zhang et al proposed that no macrocrack would form if a certain threshold was not exceeded. The microdamage could heal themselves with the help of temperature and/or rest periods. They proved with their experiment that if the loading on a sample was stopped before the threshold, full healing occurred with rest and temperature increases [Zhang et al 2001]. Once macro cracks developed, no healing was achieved with rest and temperature increases [Zhang 2000].

Rest periods

When subjected to rest periods, asphalt concrete has a potential to heal the damage, restore its mechanical properties and improve its durability by closing the cracks inside. The beneficial effects of rest periods on healing have been shown by many researchers [Bazin and Saunier 1967 ; van Dijk et al 1972, Francken 1979, Lytton 2000, Little et al 2001, Kim et al 2002, Kim et al 2003]. Rest periods help to restore the stiffness and strength, and extend the fatigue life of asphalt concrete. However, healing even occurs without rest periods [Pronk 2005].

Water

Water also plays a role in healing. According to Hefer and Little, water has a negative effect on healing of adhesive bond, because water has a greater affinity for the aggregates than bitumen and therefore promotes fracture and prevents healing [Hefer and Little 2005]. However, Zollinger concluded in his thesis that water increases the bitumen's ability of long term healing (an increase in the acid-base component) and reduces its resistance to fracture (a decrease in the total fracture bond energy) [Zollinger 2005]. As explained by

Cheng et al, the hydrogen atoms in the water have good interaction or affinity with those of the Lewis acid and base components of surface energy density of the bitumen; hence, water makes the hydrogen bonds stronger and enhances the healing capability [Cheng et al 2002]. As the bonding of those hydrogen atoms take time, it is associated with long term healing of asphalt [Good and Van Oss 1991].

Based on the previous literature review, the factors influencing the healing rate of asphalt mixtures are summarized in Table 2.3.

Table 2.3 Factors influencing healing of asphalt mixtures

Factors influencing healing	Bitumen properties	Bitumen type
		Chemical compositions
		Viscoelastic properties
		Surface free energy
		Ageing
		Diffusion
		Modifiers
	Asphalt mixture compositions	Bitumen content
		Aggregate structure
		Gradation
		Thickness
	Environments	Temperature
		Loading history
		Rest period
Water / moisture		

As discussed previously, asphalt concrete has a potential to heal itself. However, its healing rate is not sufficient at ambient temperatures, especially at low temperatures. Besides, it is not wise to stop the traffic circulation on the road to allow full healing. Thus, it is a challenge task to increase the self healing rate of asphalt concrete in road engineering.

From the literature, it becomes clear that the temperature dependent nature of healing offers a potential to heal the damage in asphalt pavement through bitumen diffusion and flow at high temperatures. To do this, an induction heating approach will be used in this thesis to heat the pavement to activate the self healing ability of porous asphalt concrete. The cracks will be closed by induction heating and the durability of the pavement be extended.

2.5 Induction healing of porous asphalt concrete

2.5.1 Induction heating technology

An alternating magnetic field will induce currents in an electrical conductor. The process of generating electrical currents in a conductor by placing it in an alternating magnetic field is called Faraday electromagnetic induction. The induced currents flow against the electrical resistivity of the

conductor, generating heat in the conductor because of the "Joule effect". This heating method is often called induction heating.

Induction heating, which uses high frequency electricity to heat electrically conductive materials, has advantages over convection, radiation, open flame or other heating methods. First, induction heating can convert 90% of the consumed energy to useful heat. So, it is very efficient. Second, induction heating is a non-contact heating, the heating process does not contaminate the work piece heated. Third, as the heat is induced within the part itself by Joule heating, product warpage, distortion and reject rates are minimized. Fourth, as heat is developed directly and instantly inside the heating material, induction heating works very quickly. The startup of induction heating is almost instantaneous and there is no warm up or cool down cycle. Fifth, induction heating also eliminates the inconsistencies and quality issues associated with open flame, torch heating and other methods. Once the system is properly calibrated and set up, there is no guess work or variation; the heating pattern is repeatable and consistent. Finally, Induction heating improves working conditions by eliminating smoke, waste heat, noxious emissions, open flame and loud noise [GH IA 2010].

One special benefit of induction heating of porous asphalt concrete is that the material is locally heated in the mastic, without damaging the aggregate skeleton.

Induction heating has already found wide applications in modern manufacturing processes like bond hardening or soften metals or other conductive materials. The existing induction heating techniques offer a possibility to apply induction heating on asphalt pavement to increase the temperature and close the cracks by high temperature self healing of bitumen.

The first step of applying induction heating in porous asphalt concrete is to make it electrically conductive, because only conductive materials can be heated with induction energy. Conductive asphalt concrete has been prepared successfully by many researchers. In the next paragraph, a brief review will be conducted on conductive asphalt concrete.

2.5.2 Conductive asphalt concrete

Electrically conductive asphalt concrete is a functional material developed to achieve good electrical conductivity. To reach this property, conductive components like graphite or fibers should be added to the mixture. The first attempt of making electrically conductive asphalt test plots for control of snow and ice accumulation dates back to the 1960s [Minsk 1968]. This conductive asphalt concrete was made by the addition of graphite.

Only very recently, Wu et al conducted a research on electrically conductive asphalt concrete at Wuhan University of Technology. They made electrically conductive asphalt mixtures for deicing or self monitoring purposes by adding conductive carbon fibers, carbon black or graphite to asphalt mixtures [Wu et al 2002, 2005, 2006].

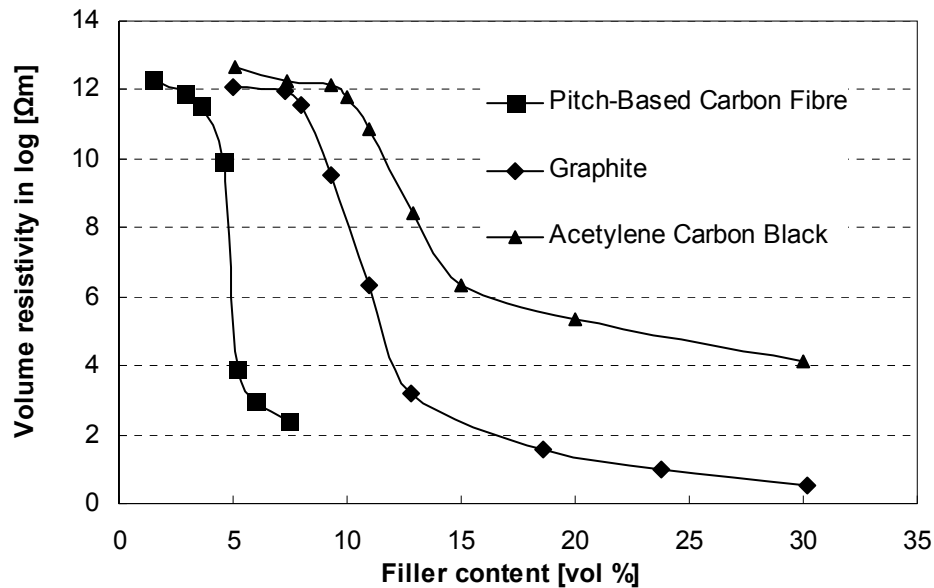


Figure 2.16: Effect of the conductive filler content on the electrical resistivity of asphalt concrete [Wu S et al 2005]

As shown in Figure 2.16, Wu et al demonstrated that the conductivity of asphalt concrete is proportional to the volume of conductive graphite or fibers added. However, adding excess conductive additives above a certain level does not reduce the resistivity anymore, but strongly influences the mechanical strength or the workability of the mixture. It was shown that adding conductive carbon fibers to the mixture is much more effective to increase the conductivity than adding conductive fillers like graphite or carbon black. Wu et al also explained how the conductivity of asphalt concrete can be highly improved by adding small volumes of carbon fibers to the aggregates-bitumen-conductive powder system: conductive fillers exhibit short range contacts in the form of clusters, whereas fibers have a bridging effect between these clusters. Finally, they indicated that it was very difficult to prepare well dispersed fiber modified asphalt mixture, because fibers tend to aggregate into clusters in the mixture.

In addition, García et al made conductive asphalt mastic by addition of steel fiber and used induction heating to heat the mastic to enhance its self healing properties [García et al 2011]. García et al showed how the conductivity is proportional to the volume of electrically conductive particles in the mixture and how there is an optimum volume content of electrically conductive particles for each mixture [García et al 2009].

These authors explain the conductive mechanism by means of the percolation theory. With a low volume of conductive particles in the mixture, the resistivity of asphalt concrete is similar to that of a nonconductive material, but when the volume of conductive particles is above the percolation threshold, the resistivity drops and the mixture becomes conductive.

As discussed previously, the existing induction heating technology and the knowledge on conductive asphalt concrete make it possible to use induction heating to close cracks in conductive porous asphalt layers by high temperature

self healing of bitumen. This approach, using induction heating to activate the self healing process of bitumen, is named induction healing.

2.6 Summary of the literature review

Based on the previous literature review, the following observations can be outlined.

- 1) Porous asphalt concrete is the most commonly used surface material on Dutch highways. The open nature of porous asphalt concrete brings significant benefits. However, porous asphalt surface wearing course does not last long because of ravelling, which is the dominant defect of porous asphalt and the main cause for maintenance or resurfacing.
- 2) Asphalt concrete has a potential to restore its stiffness and strength by closing micro-cracks inside when subjected to rest periods. The self healing rate of asphalt concrete is influenced by bitumen properties, asphalt mixture composition and environments. The healing behavior of asphalt concrete is very temperature dependent. An increase of temperature improves the self healing rate of asphalt concrete and shifts the healing response to a shorter time. The temperature dependent nature of healing offers a potential for us to heal the damage on highways at high temperatures. To do this, induction heating approach will be used in the project.
- 3) The induction heating technology has developed considerably, making it possible to use this technique in the asphalt industry. Besides, conductive asphalt concrete has been designed successfully by adding conductive additives to the mixture. This is a requirement to be able to use induction heating.
- 4) The existing induction heating technique and the knowledge on the conductive asphalt concrete make it possible to use induction heating to heat a porous asphalt layer and to heal the cracks by high temperature self healing of the bitumen (named induction healing). Induction heating was first used to improve the self healing properties of asphalt mastic by García et al. In this thesis it will be further developed and applied to heal porous asphalt concrete.

Chapter 3 Materials and Sample Preparation

The materials and the sample preparation method used in this research are introduced in this chapter. The materials consist of stone, sand, filler, steel fiber, and bitumen. The samples include asphalt mastic beams, porous asphalt concrete cylinders and beams.

3.1 Raw materials

The raw materials used in this research to make mastic beams (sand-bitumen system, no filler is involved) are five different fractions (<0.12, 0.12-0.25, 0.25-0.50, 0.50-1.0, 1.0-2.0 mm, 20% by weight of each fraction for simplicity) of crushed sand and penetration grade bitumen 70/100. The crushed sand has an average density of 2.67 g/cm³. The bitumen was obtained from Kuwait Petroleum and the properties of bitumen are shown in Figure 3.1.

Table 3.1 Properties of bitumen

Binder grade	Penetration	Softening point	Penetration Index	Specific gravity
70/100	89 dmm	45.8 °C	-0.91	1.03 g/cm ³

The raw materials used to prepare porous asphalt concrete cylinders include stone, sand, filler, steel fiber and bitumen. The stone is Bestone (Bremanger Quarry, Norway). It is a sand stone supplied by Graniet Import BV. The stone fraction has an average density of 2.77 g/cm³ and a size between 2.0 mm and 22.4 mm. The sand used is crushed sand with size between 0.063 mm and 2.0 mm and density of 2.69 g/cm³. The filler used is limestone filler Wigro 60K with size smaller than 0.063 mm and density 2.64 g/cm³. This filler consists of 25% hydrated lime by weight. The bitumen used is also 70/100 Pen, shown in Table 3.1.

To make the mastic and asphalt concrete electrically conductive and suitable for induction heating, three types of steel fibers were used as additives in the mixture. The properties of these three types of steel fibers are summarized in Table 3.2.

Table 3.2 Properties of steel fibers

Fiber type	Diameter μm	Length mm	Resistivity $\Omega\text{ cm}$	Density g/cm^3
Steel fiber 1	29.6 – 191.1	< 1	$7 \cdot 10^{-7}$	7.6
Steel wool 00	8.89 – 12.7	3.2; 6.4; 9.5	$7 \cdot 10^{-7}$	7.6
Steel wool 000	6.38 - 8.89	7	$7 \cdot 10^{-7}$	7.6

Steel fiber type 1 and steel wool type 000 were bought from the market and steel wool type 00 was supplied freely by Global Material Technologies Company (America). No treatment was needed for steel fiber type 1 and type 00. Steel wool type 000 had to be chopped by hand. To find the size distribution of the conductive fillers, more than 100 pieces of fibers of each type were checked by taking photographs under the optical microscope and measuring their length with an image processing program, obtaining the length distribution shown in Figure 3.1 and Figure 3.2 respectively. Steel wool type 00 has three different lengths: 3.2 mm, 6.4 mm or 9.5 mm respectively. The length of steel wool type 00 is very homogeneous, so the length distribution of this steel wool is not shown in this research.

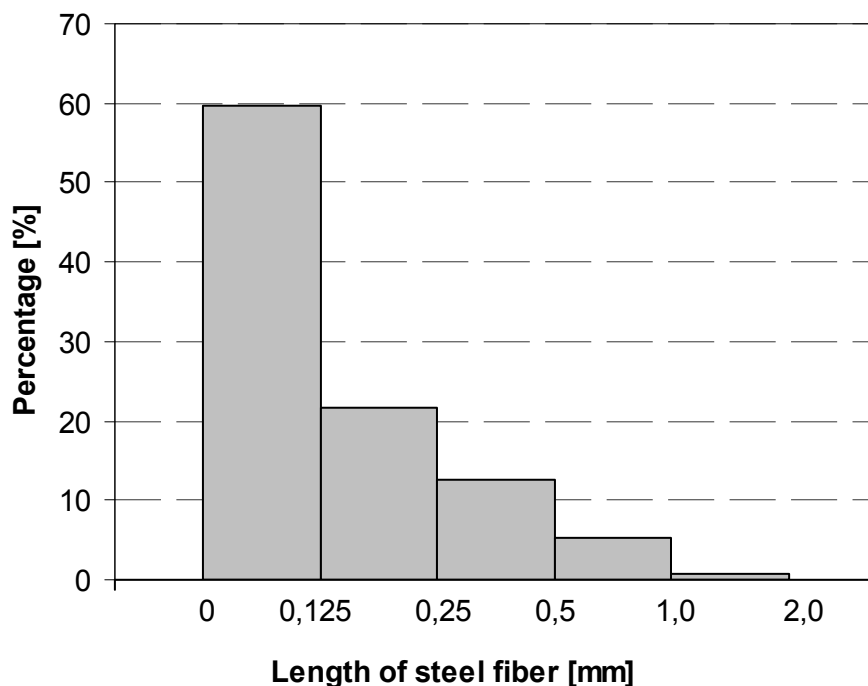


Figure 3.1 Length distribution of steel fiber type 1

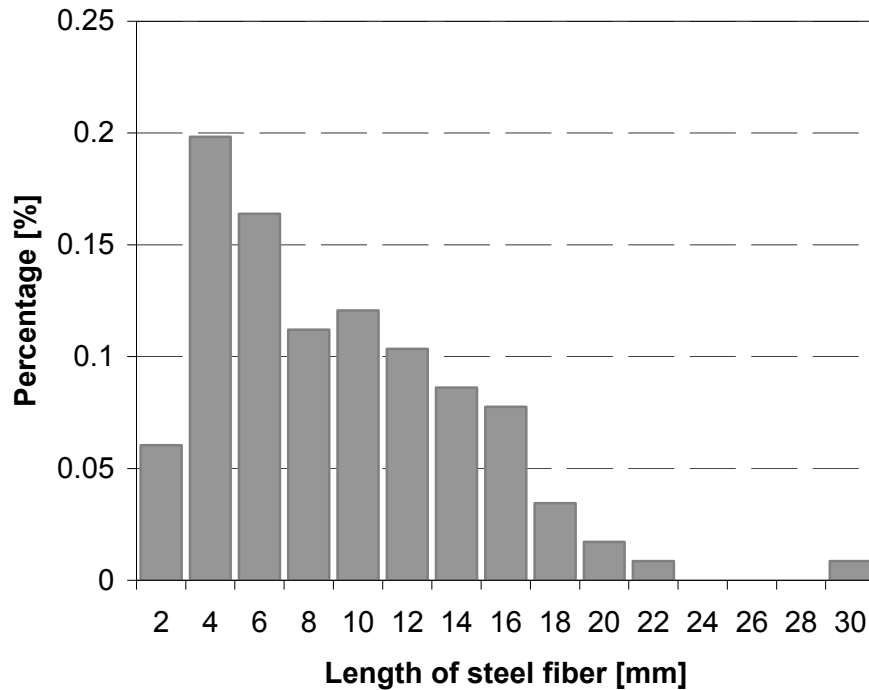


Figure 3.2: Length distribution of steel wool fiber type 000

3.2 Mastic beams

Two types of mastic beams are used in this research. The beams have the size shown in Figure 3.3 and Figure 3.4. The first beam type is used in electrical resistance testing and induction heating testing. The second beam type used in healing detection testing has a triangular notch in the centre to create a concentration here and let the samples break always at the same position.

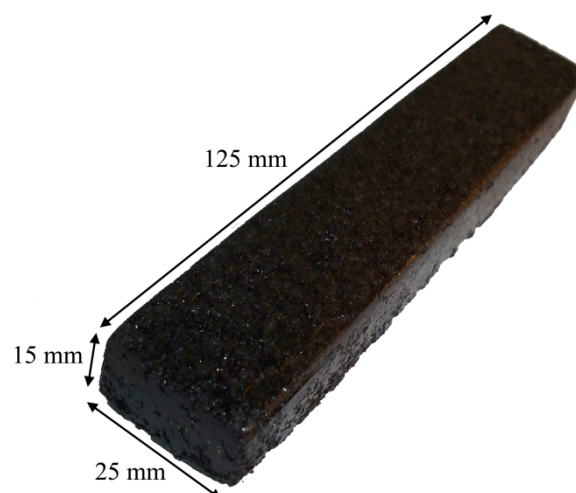


Figure 3.3: Asphalt mastic beams used in resistance and induction heating tests [García et al 2009]

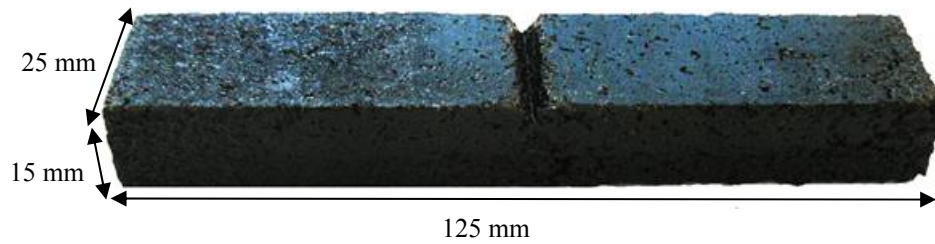


Figure 3.4 Asphalt mastic beam with a notch used in healing detection test

To prepare the beams, the materials are mixed with a Hobart Mixer (shown in Figure 3.5) for 15 minutes at 160 °C (this is not indicating the asphalt production in asphalt plant). After mixing, the mixtures are compacted into the moulds, which are shown in Figure 3.6 and Figure 3.7 respectively. The weight of the mixture compacted in the mould was accurately controlled. After cooling for 2 hours at -20 °C in the fridge, the mastic beams can be attained by detaching the mould.



Figure 3.5 Mixer used in the research



Figure 3.6 Mould used for preparing mastic beam samples for electrical resistance and heating tests



Figure 3.7 Mould used for preparing notched mastic beam samples for healing test

A Nanotom Computed Tomography (CT) scanner from Phoenix/X-ray Systems and Services Inc. was used to check the fiber distribution in the beams. In Figure 3.8 nano CT-Scan reconstructions of a sample with 6.54% steel wool (by volume of bitumen) and a sand-bitumen volume ratio of 2.90 are shown. In Figure 3.8 (a) all the fibers inside the sample are shown, and in Figure 3.8 (b) only the fibers connected. In Figure 3.8 (a) it cannot be clearly appreciated that due to the high density of fibers, clusters of fibers appeared during the mixing process. In Figure 3.8 (b) it can be seen that the volume of fibers connected is lower than the total volume of fibers in the sample and how clusters of fibers can be observed visually once the non-connected fibers have been removed. In both images, it can be seen how fibers are distributed all around the sample independently if they are connected or not, which is especially positive when trying to reach uniform heating.

To analyze the images, a burning algorithm, initially developed at NIST [Garboczi et al 1991], was adapted to the CT-scan data. The burning algorithm is a kind of algorithm similar to point diffusion: to check the continuity, the fiber pixels are thought as combustible. Fiber pixels are set on fire along one face of the test sample, and fire diffuses to adjacent connected points until no more pixels can be burned. If all the pixels are connected, the fire will extend completely across the sample. For the sample with sand-bitumen volume ratio 2.90, it was found that the total volume of fibers in the mixture was 2.14%, and if burning from one side, 74.16% of fibers were connected in a through path to the other side. Otherwise, for the sample with sand-bitumen volume ratio 2.26, the total volume of fibers in the mixture was 3.38% and 86.4% of them were connected in a through path to the other side. In both cases, fibers were connecting both sides of the sample. From these values it is confirmed how in a mixture with the volume of fibers fixed, if the sand-bitumen ratio is increased above the optimum, the total volume of fibers and the percentage of fibers connected are reduced, and how if the sand-bitumen ratio is increased, the total length of the shortest conductive path is also increased. Finally, this also means that it is possible to use CT-scan reconstructions to check if the volume of fibers is enough to be fully connected.

Besides, from the visual inspection of the pictures it is evident that the fibers are connected in closed-loop circuits. This is very important for induction heating, because a condition imposed on the material is that closed-

loop circuits must be present for eddy currents to be induced: when a magnetically susceptible and electrically conductive material is placed in the vicinity of the coil, eddy currents are also induced in the material, with the same frequency of the magnetic field [Ahmed et al 2006]. Heat is generated through the energy lost when eddy currents flow against the resistance of the material.

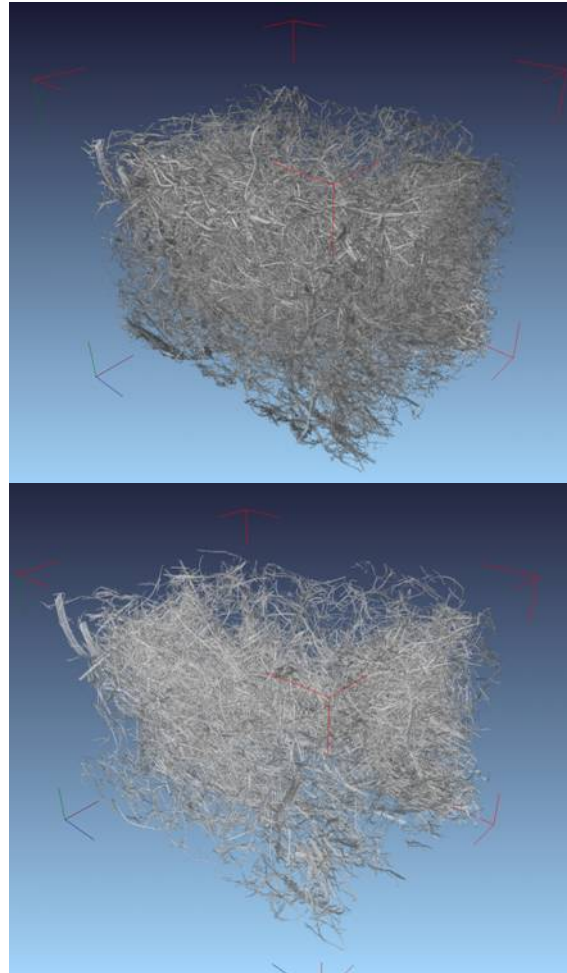


Figure 3.8 Nano CT-scan images of a test sample with 6.54% steel wool and sand-bitumen volume ratio 2.90 showing (top) all the fibers and (bottom) only the connected fibers

3.3 Porous asphalt concrete cylinders

Porous asphalt PA 0/16, the most commonly used surface material on the highways in the Netherlands, was chosen as the mixture in this research. As shown in Table 3.3, the mixture composition was fixed based on the Dutch Standard, RAW 2005.

The mixing process of steel fiber into porous asphalt mixture is of great importance, but there is no specification for this mixing procedure. There are two potential methods for the introduction of the fibers: the wet process and the dry process. In the wet process, the fibers are blended with bitumen prior to incorporating the binder into the mixture. The dry process mixes the fibers with

the aggregates before adding bitumen. Generally, the dry method is used more due to several advantages. Experimentally, the dry process is the easiest to perform and allows for the best fiber distribution in the mixture. Meanwhile since the fibers used do not melt in the binder there are no apparent special benefits to the wet process. In addition, in the field work done on fiber-reinforced asphalt mixtures generally the dry process is used [Echols 1989, Munn 1989, Hejazi 2007], possibly due to the production problems of introducing the fibers directly into the asphalt. Another reason for using the dry process is that it minimizes the major problem of clumping or balling of fibers in the mixture [Labib and Maher 1999]. However, both the dry mixing process and the wet mixing process do not work alone in this research, a combination of them is used in the laboratory experiments.

Table 3.3: Composition of the PA 0/16 mixture for gyratory samples based on the Dutch standard (RAW 2005)

Sieve size (mm)	Density (g/cm ³)	RAW Spec. % retained	Cumm % ret.	% ret. by weight
22.4 - 16.0	2.778	0-7	4	4
16.0 - 11.2	2.774	15-30	25	21
11.2 - 8.0	2.762	50-65	57	32
8.0 - 5.6	2.765	70-85	80	23
5.6 - 2.0	2.781	85	85	5
2.0 - 0.063	2.688	95.5	95.5	10.5
< 0.063	2.638	100	100	4.5
Bitumen70/100	1.032	4.5% by wt.		

The mixtures were mixed with a Hobart Mixer at 160 °C. The procedure of blending steel fibers into the mixture is summarized as follows:

1. Heat stone, sand, filler, bitumen, mixing bowl and rotor to the required mixing temperature of 160 °C;
2. Pour the required bitumen into the mixing bowl;
3. Add the required steel fiber;
4. Set up the mixing bowl and rotor;
5. Add the heated stone, sand and filler;
6. Blend the mixture at low speed for 1 min;
7. Blend the mixture at high speed until the steel fibers are dispersed quite well (about 15 minutes).

After mixing, a Servopac Gyratory Compactor was used to prepare the samples (Ø100 mm × 70 mm shown in Figure 3.9) according to the European specification NEN-EN 12697-31. The compaction mould was heated at the compaction temperature of 145 °C for 2 hours before compaction. The settings of the gyratory compactor are:

- Compaction pressure: 600 KPa;
- Gyratory angle: 0.820;
- Gyratory speed: 30 gyrations / min.



Figure 3.9 Servopac Gyrotory Compactor used in this research and the sample compacted

To obtain the target density of the compacted sample, it is necessary to know the maximum theoretical density of the mixture, which was calculated as the total weight divided by the total volume of all the materials before compaction. This calculated value was 2.569 g/cm^3 for the plain mixture. After mixing, the maximum theoretical density of the loose mixture was also measured using an ultracycrometer 1000 (America, Quantachrome Instruments), which is an instrument for measuring the true volume and density of powders, foams and bulk solids. The maximum theoretical density measured with this apparatus was 2.571 g/cm^3 , very close to the previously calculated value. So, it is not necessary to determine the maximum theoretical density of the mixture with steel fiber using an ultracycrometer. The maximum theoretical density of the mixture changes with the variation in volume of steel wool in the mixture and can be computed according to the total weight and volume of all materials in the mixture.

The Dutch standard calls for a minimum air voids content of 20%. In this case, the air voids content was assumed to be 21%. Based on the maximum theoretical density, the calculated target density of the specimen after compaction and the weight of the mixture, the gyrotory compactor can control the height of the specimen to obtain the ultimate target density. The air voids content can be computed after moulding the specimens by determining their dimensions (to compute their volumes) and weights. The maximum and assumed densities of the mixtures with different volume contents of the fibers (the fiber-bitumen volume ratio) were calculated to obtain the same air void content in all samples studied. All samples were compacted until an air voids content of 21% was obtained.

To determine the mixing time needed for a sufficient mixing, the materials with 14% steel wool type 00 was mixed for 10 minutes, 12 minutes, 15 minutes or 20 minutes, respectively and compacted to have an air void content of 21%.

To check the fiber distribution, small cores ($\text{Ø}40$ mm) drilled from the samples with 14% steel wool (volume fraction of bitumen) were scanned with Nano-CT scanner and the CT-Scan images of the samples are shown in Figure 3.10. The resolution of the images is not high enough to show a clear distribution of single steel wool. However, these images are sufficient to distinguish bad mixing (for 10 minutes and 12 minutes mixing) and good mixing (for 15 minutes and 20 minutes mixing without clusters) of steel wool in the samples. The bright dots in Figure 3.10 (a) and (b) are clusters of steel wool, which indicate a bad distribution of steel wool in the concrete. The clusters disappear in Figure 3.10 (c) and (d) where the mastic is much more homogeneous. It seems that steel wool forms clusters before being mixed evenly and further mixing tends to disperse the clusters. 15 min mixing is sufficient to produce a good distribution of steel wool in the samples.

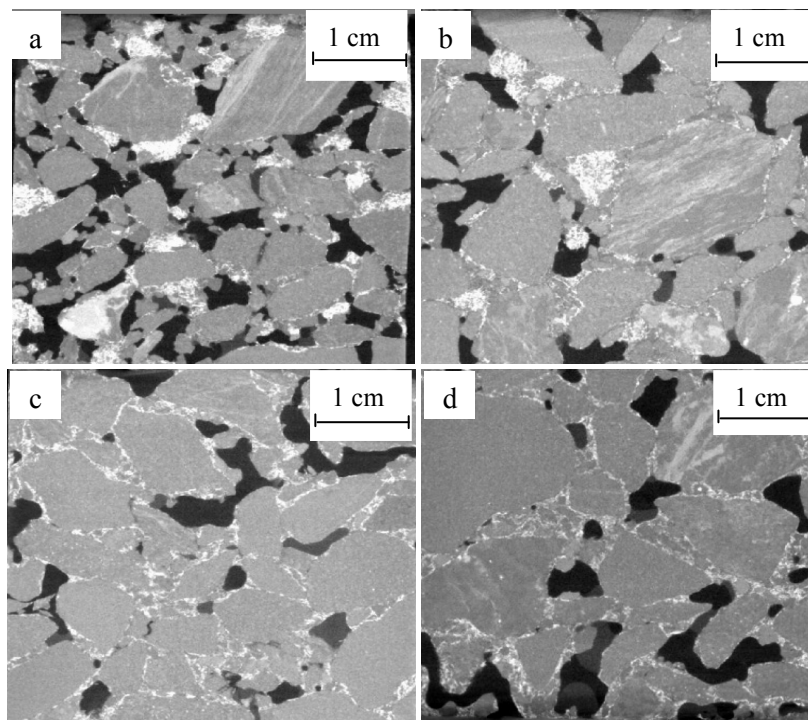


Figure 3.10: CT-Scan images of porous asphalt concrete samples with 14% steel wool (volume fraction of bitumen) at different mixing times: (a) 10 minutes; (b) 12 minutes; (c) 15 minutes; (d) 20 minutes

It was expected that the mixing time (corresponding to the distribution of steel wool) would greatly influence the properties of porous asphalt concrete. The effect of the steel wool distribution on the electrical resistance of the samples was first studied, because only conductive material could be heated with induction energy. The electrical resistance of the samples with 14% steel wool was measured with a resistance tester at room temperature 20 °C. The

samples, with a diameter of 100 mm and a thickness of 50 mm were sawn from the gyratory compacted specimens. The details of resistance measurement will be discussed in Chapter 4.

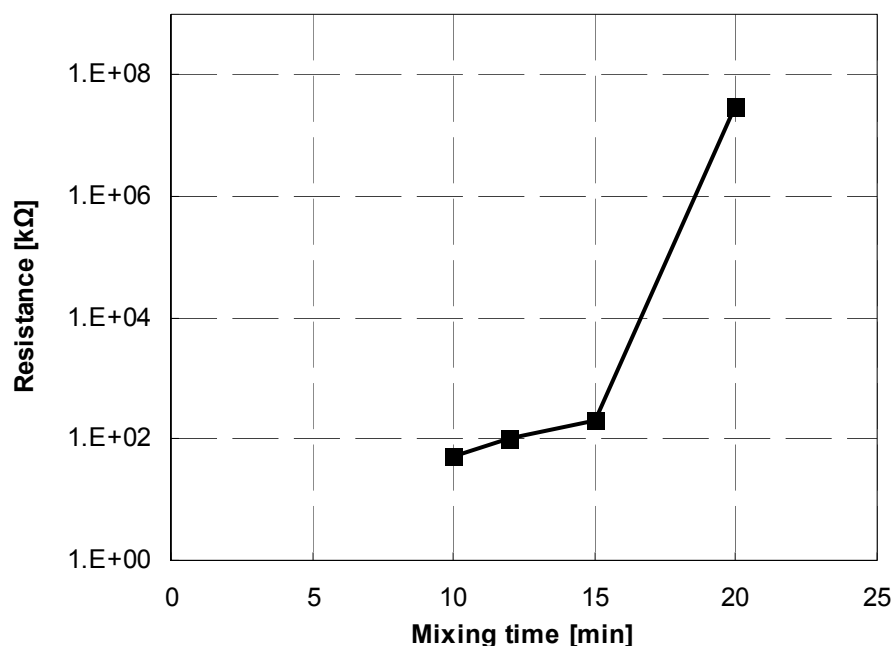


Figure 3.11 Electrical resistance of porous asphalt concrete samples with 14% steel wool after different mixing time

The effect of the mixing time (corresponding to the distribution of steel wool) on the electrical resistance of the samples is shown in Figure 3.11. It is interesting to note that the electrical resistance is lower for the samples with shorter mixing times. This phenomenon can be explained according to the distribution of steel wool. The conductive paths in the bad mixing samples are formed by clusters of steel wool, which are conductive. When the mixtures are mixed for 10 minutes, many clusters of steel wool formed and existed as conductive elements, so the sample is electrically conductive and the resistance is quite low. With the increase of the mixing time, the clusters of steel wool become less and the conductive paths become longer, thus the resistance of the sample increases gradually. When the steel wool is homogenously dispersed after 20 minutes mixing, the fibers are coated with bitumen and no longer conductive, thus the resistance of the sample increases sharply.

Secondly, the effect of the mixing time (corresponding to the distribution of steel wool) on the indirect tensile strength of the samples with 14% steel wool 00 was studied, because the indirect tensile strength (ITS) is often used as an indicator of mixture cohesion. In this study, indirect tensile tests were performed at 5 °C on cylindrical samples $\text{Ø } 100 \text{ mm} \times 50 \text{ mm}$ sawn from gyratory specimens. The equipment used in this part is a uniaxial compression setup. The indirect tensile strength of the specimen is determined by applying a vertical displacement at a rate of 50 mm per minute until failure according to the European Norm EN 12697-23.

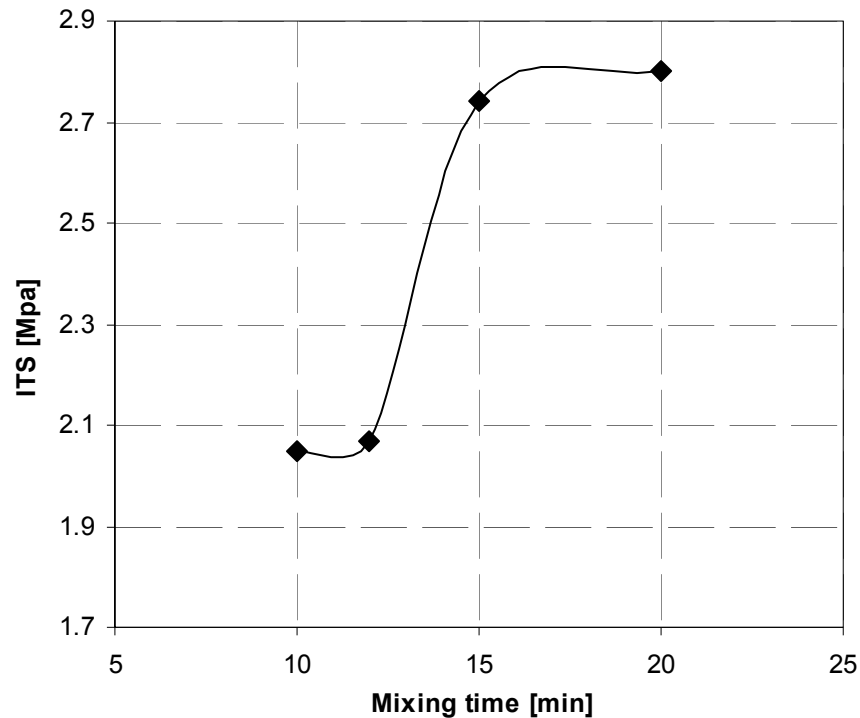


Figure 3.12 ITS of porous asphalt concrete samples with 14% steel wool at different mixing time

The effect of the mixing time (corresponding to the distribution of steel wool) on the indirect tensile strength (ITS) of the sample is plotted in Figure 3.12. It is clear that the ITS of samples with a non-uniform distribution of steel wool is quite lower than that of samples with a uniform distribution of steel wool. The ITS of samples after 10 minutes, 12 minutes, 15 minutes or 20 minutes mixing is 2.05 MPa, 2.07 MPa, 2.74 MPa or 2.80 MPa respectively. To explain this, clusters of steel wool can be seen as weak points in the samples. When steel wool are not mixed well with 10 min mixing, the clusters of steel wool decrease the thickness of bitumen film and result in a bad adhesion between aggregated particles by absorbing a large amount of bitumen, so the clusters of steel wool create weak spots in the sample and tend to induce damaged. As a result of this, the ITS of the sample with non-uniform distribution of steel wool is relative low. With the increase of the mixing time, the weak points of clusters became less, resulting in an increase of ITS. Once the steel wool are dispersed uniformly, the ITS of porous asphalt concrete does not increase anymore.

Finally, the effect of the mixing time on the induction heating speed of the samples with 14% steel wool was investigated. The induction heating experiment was performed by using an induction generator with a capacity of 50 kW and at a frequency of 70 kHz. The heating samples were the same as the ones used to measure the electrical resistance. The distance between the coil of the induction machine and the top surface of the heating sample was 30 mm. Each sample studied was heated for 3 minutes and its temperature variation at the top surface was measured with a 320 x 240 pixel, full colour infrared camera (FLIR, Type A320).

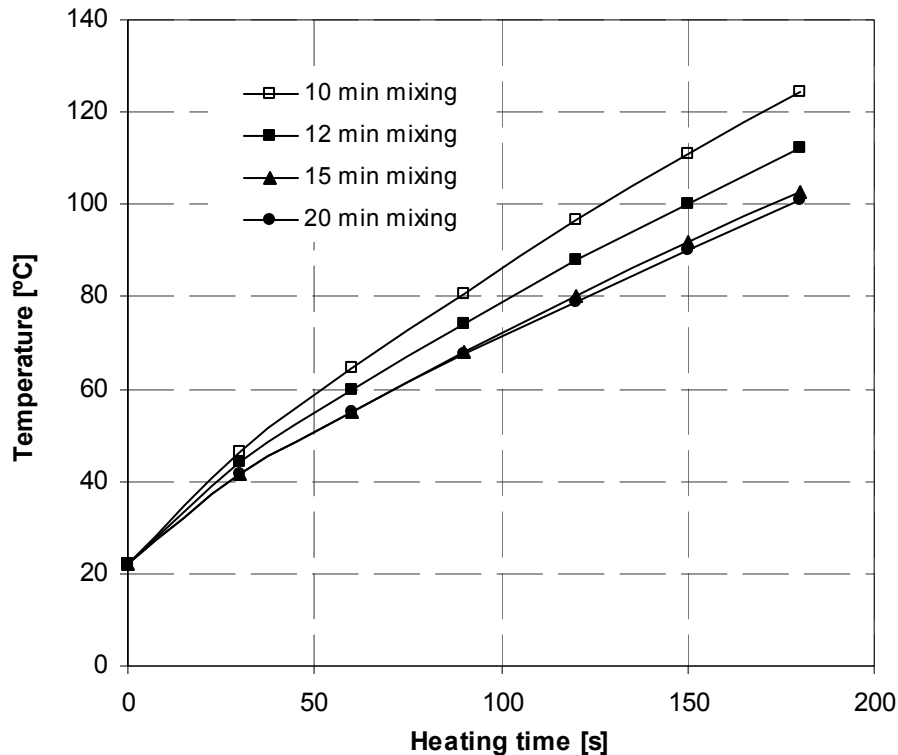


Figure 3.13 Induction heating speed of the samples with 14% steel wool at different mixing time

The effect of the mixing time (corresponding to the distribution of steel wool) on the induction heating speed of the sample is presented in Figure 3.13, where the mean temperature at the top surface of the sample is used. The induction heating speed of the samples (the slopes of the temperature-heating time curves) decreased with increase of the mixing time. The induction heating speed of the samples with 15 minutes and 20 minutes mixing were almost the same. This can be explained in relation to the distribution of steel wool. As only conductive material can be induction-heated, it can be assumed that the conductive paths within the sample formed by clusters are heating units. These heating units of clusters are heated more quickly, which is proven in the test by the fact that the temperatures of the clusters are higher than the temperature at other places. With 10 minutes mixing, there are many heating units (clusters of steel wool) within the sample, so the induction heating speed of the sample is quite high. With the increase of the mixing time, the heating units become less, resulting in a lower induction heating speed. After 15 minutes mixing, there are no clusters anymore, so the induction heating speed stops to decrease. Besides, the temperature in the samples after 15 minutes and 20 minutes mixing is more homogenous than in the samples with 10 minutes and 12 minutes mixing, which can be seen from the infrared images of the heated samples.

According to the results of the former experiments, 15 minutes mixing is sufficient to disperse the steel wool to a uniform distribution in porous asphalt concrete, resulting in high indirect tensile strength and homogenous heating of the sample. So, all the samples prepared in the laboratory of Delft

University of Technology for subsequent research were mixed for 15 minutes. However, this mixing time is not realistic when mixing the mixture in asphalt plant. This long time mixing will result in extra ageing of bitumen, making aggregate stripped easily from the pavement surface. So, it is necessary to modify the mixing method when applying porous asphalt with steel fiber.

In the asphalt plant of Heijmans-Breijn, it is found that the mixing procedure can be optimized a lot with a high speed mixer. By first mixing the bitumen with steel wool and filler, and then adding the aggregates and sand, the mixing time can be reduced to 3 minutes. However, this mixing procedure is not yet used in the laboratory of Delft University of Technology, because a standard laboratory Mixer (Hobart Mixer) is used for its simplicity.

3.4 Porous asphalt concrete beams

Porous asphalt concrete beams used in this research were prepared by Heijmans-Breijn with standard porous asphalt PA 0/16 plus 4% steel wool (volume content of bitumen). The same materials were also used in an induction healing trial section on Dutch motorway A58. The composition of the mixture is shown in Table 3.4.

Table 3.4: Composition of the mixture used for porous asphalt beams based on the new specification

Sieve size (mm)	Passing (%)	Specification	
		Min (%)	Max (%)
C 16.0	97.7	93.0	100
C 11.2	69.8	64.0	76.0
C 8.0	34.7		
C 5.6	20.5		
2.0	16.0	11.0	19.0
0.063	4.5	3.0	6.0
Bitumen 70/100	5.2%	4.7%	5.7%
Steel wool 00	4% by volume of bitumen		

The beams, shown in Figure 3.14, were sawn from porous asphalt slabs. The dimension of these beams is 50 mm × 50 mm × 400 mm. The beams will be used to study the fatigue resistance and induction healing effect of porous asphalt concrete with steel wool.



Figure 3.14 Porous asphalt concrete beam used in this research

Chapter 4 Electrical Conductivity and Induction Heating Speed of Asphalt Mastic and Porous Asphalt Concrete with Steel Fiber

4.1 Introduction

In Chapter 2 it was shown that asphalt concrete in itself is a self-healing material. However, the self healing potential of asphalt concrete is not sufficient at ambient or even higher temperatures to close all the cracks inside, especially when the binder is aged. Furthermore, self-healing of asphalt concrete is a quite slow process at ambient temperatures. It is impossible to stop the traffic flow on a road to allow enough self healing recovery at ambient or even at somewhat higher temperatures. There is a common consensus among researchers that the self-healing capacity and speed of asphalt concrete will be enhanced when the material is subjected to a higher temperature during the rest period [Bonnaure et al 1982, Jo and Richard 2001, García 2011]. So, increasing the temperature with induction heating will enhance the self healing capacity of asphalt concrete. In such a way, cracks can be closed by high-temperature bitumen flow and diffusion (healing) and in the end ravelling be delayed.

Only an electrically conductive material can be induction-heated, so the electrical conductivity of the material which is going to be heated is important for the heating efficiency. Moreover, the conductivity also influences the heating uniformity inside the samples. In this chapter, the electrical conductivity and induction heating speed of asphalt mastic and porous asphalt concrete with steel fiber are discussed.

This chapter is partly based on:

García A, Schlangen E, van de Ven M, Liu Q. Electrical conductivity of asphalt mortar with conductive fibers and fillers. *Construction and Building Materials* 23(2009):3175-3181;

Liu Q, Schlangen E, van de Ven M, García A. Induction heating of electrically conductive porous asphalt concrete. *Construction and Building Materials* 24 (2010):1207-13.

4.2 Electrical resistivity of asphalt mastic and porous asphalt concrete with steel fiber

4.2.1 Experiments

To study the electrical conductivity of asphalt mastic (sand-bitumen mixture, no filler involved) and porous asphalt concrete, their electrical resistance was measured in experiments at a room temperature of 20 °C. The asphalt mastic samples are beams, with dimensions as shown in Figure 4.1. The composition of these mastic beams is given in chapter 2.

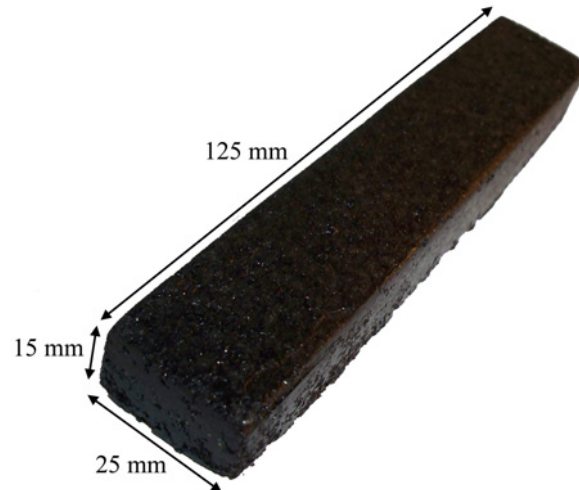


Figure 4.1: Asphalt mastic beam used in resistance testing [García et al 2009]



Figure 4.2: Porous asphalt concrete cylinder used in resistance testing

Porous asphalt concrete samples are cylinders with diameter 100 mm and thickness 50 mm (as shown in figure 4.2). They were cut from the gyratory compacted specimens to obtain flat surfaces, which allow good contact between the sample and the electrodes for resistance measurement. After cutting, the samples were placed in an oven at 40 °C for 8 hours to remove the

moisture and prevent the steel fibers from corroding on the surface of the samples. Inside the sample, the steel fibers do not corrode, because they are completely coated with bitumen.

A Fluke digital multimeter (as shown in Figure 4.3) was used to measure the resistance below $36 \times 10^6 \Omega$. A gage installation tester was used to measure the resistance higher than this value. As shown in Figure 4.4 and Figure 4.5, two 30 mm \times 25 mm copper plates electrodes connected with the multimeter were placed at both ends of the mastic beam sample to measure its electrical resistance. A small pressure was applied to the copper electrodes to obtain a good contact with the surface of the sample.



Figure 4.3: Fluke digital multimeter (left) and gage installation tester (right)



Figure 4.4: Self-made electrodes used in measuring the resistance of asphalt mastic beams



Figure 4.5: The testing method of resistance measurement on a asphalt mastic beam

Similarly, two 160 mm × 100 mm copper plate electrodes (shown in Figure 4.6) connected with the multimeter were placed at both ends of the porous asphalt concrete cylinder to measure its electrical resistance (shown in Figure 4.7).

The contact resistance between the two electrodes when directly connected is lower than 1 Ω , which is negligible with respect to the great resistances studied (higher than 100 k Ω in the samples). The electric field of the resistance tester is assumed constant and the end-effects are considered negligible.

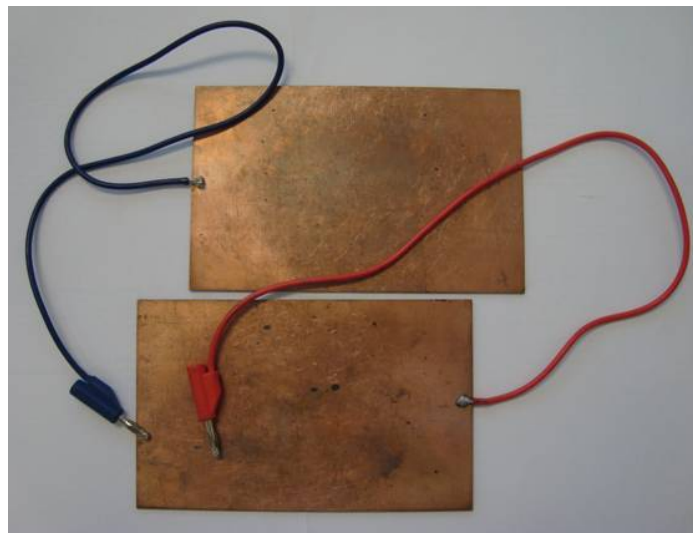


Figure 4.6: Self-made electrodes used in measuring the resistance of porous asphalt concrete cylinders



Figure 4.7: The testing method of resistance measurement on a porous asphalt concrete cylinder

After measuring the resistance, the electrical resistivity of sample was obtained from the second Ohm-law in Equation 4.1:

$$\rho = \frac{RS}{L} \quad (4.1)$$

Where:

ρ = the electrical resistivity, [Ω m];

L = the length of the beam or the thickness of the cylinder, [m];

R = the measured resistance, [Ω];

S = the electrode conductive area, [m^2].

The effects of the sand-bitumen volume ratio and steel fiber content (steel fiber-bitumen volume ratio) on the electrical conductivity of asphalt mastic and porous asphalt concrete were studied.

4.2.2 Results and discussion

4.2.2.1 Effect of the sand-bitumen volume ratio on the electrical conductivity of asphalt mastic

The electrical resistivity variation against different sand-bitumen volume ratios for the samples with constant volume content of steel wool type 000 (steel wool-bitumen volume ratio) is displayed in Figure 4.8. The objective of this graph is to show that the electrical resistivity cannot be considered separately from the sand-bitumen volume ratio (s-b) and to quantify the influence of the sand-bitumen ratio on the conductivity of asphalt mastic.

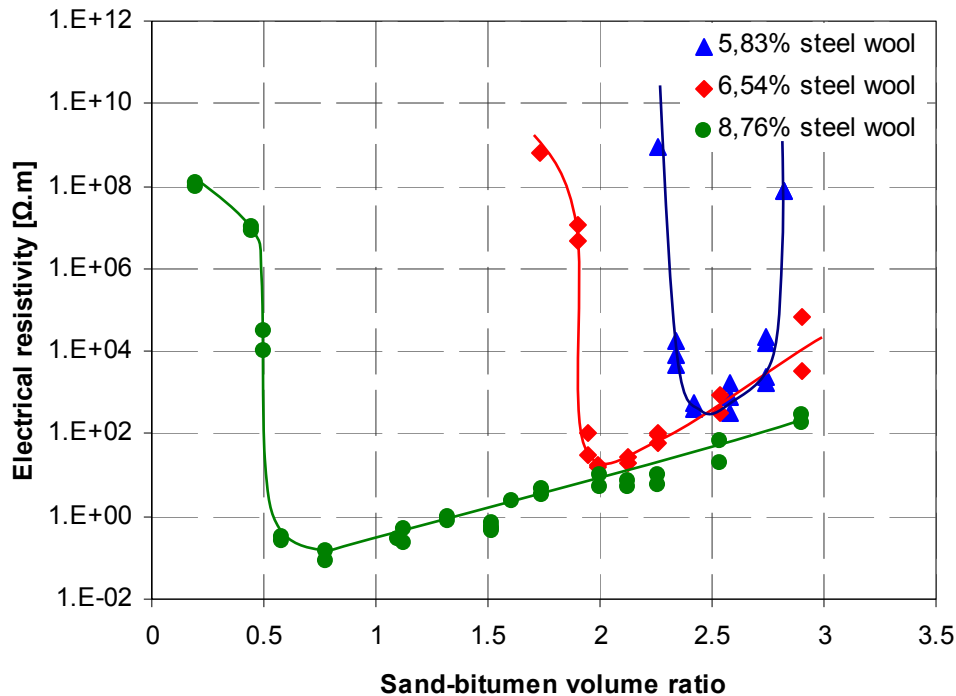


Figure 4.8: Effect of the sand-bitumen ratio on the electrical resistivity of the mastic beams with steel wool type 000 [García et al 2009]

In Figure 4.8, an optimum sand-bitumen volume ratio for each steel wool volume content can be detected, where the electrical resistivity decreases to a minimum: s-b 2.50 for 5.83%, s-b 2.00 for 6.54% and s-b 0.77 for 8.76% (percentages related to the total volume of bitumen in the mastic). Besides, a sudden increase in the electrical resistivity takes place when reducing the sand-bitumen ratio below the optimum. This area is called percolation threshold region in the resistivity. It can also be observed how the electrical resistivity in the optimum decreases almost exponentially with less volume of sand in the mixture: $82.50 \times 10^{-2} \Omega \text{ m}$, $17.54 \Omega \text{ m}$ and $420.00 \Omega \text{ m}$ for sand-bitumen ratios 0.77, 2.00 and 2.50, respectively.

Above the optimums, for each volume content of steel wool, the electrical resistivity is increased quickly with the increase of the sand-bitumen ratio in the mixture. During the mixing process, it was observed that the samples with sand-bitumen ratio above the optimal point were difficult to mix, with clusters of steel wool that grew when increasing the volume of sand in the mixture. Besides, as can be appreciated in the curve of 5.83% steel wool, if the volume of sand is increased above a certain limit, the electrical conductivity depercolates and the resistivity increases suddenly. Samples with sand-bitumen ratio higher than 2.74 and 5.83% steel wool simply lost all the conductive properties. Besides, they looked porous and weak. Definitely there was not enough bitumen to make a resistant asphalt mastic or enough fibers to attach the sands, because the total volume of fibers inside the mixture is reduced when the sand-bitumen ratio is increased.

It has been reported that the conductivity of carbon fiber reinforced cement-based composites decreases with increasing sand-cement ratio for a

given carbon fiber volume fraction [Chen et al 2004]. In Figure 4.8, it can be appreciated that this is true only when a very high volume of fibers is added to the mixture. Then, the maximum conductivity takes place when the sand-bitumen ratio is zero or almost zero. This is just because the volume of fibers inside the mixture is inversely proportional to the sand-bitumen ratio. When decreasing the volume of fibers, the optimum sand-bitumen ratio grows, and the resistivity below it increases to that of a nonconductive material. This happens because the fibers can only be in the free spaces around big sands. If these spaces are too big and the volume of fibers is not enough, they simply do not percolate; the same happens when varying the volume of fibers by fixing the sand-bitumen ratio. When these fibers start to get in contact, the resistivity starts to decrease, and when the resistivity reaches its minimum an optimum sand-bitumen ratio was obtained. When increasing the sand-bitumen ratio above the optimum, the mixture becomes difficult to work with, and fibers are not easily mixed: there is not enough bitumen for a uniform dispersion of the fibers, clusters of fibers appear and the resistivity grows exponentially. As can be seen in the curve of 5.83% steel wool, the fibers simply depercolate if the sand bitumen is increased too much and the volume of fibers is too low, and the sample becomes nonconductive; besides, in this phase, addition of fibers does not improve the conductivity but also negatively affects the mechanical properties of asphalt mastic.

4.2.2.2 Effect of the volume content of steel fiber on the electrical conductivity of asphalt mastic

The relationships between the electrical resistivity and the conductive additives (fibers and graphite) volume content (conductive additives-bitumen volume ratio) of the asphalt mastic with a fixed sand-bitumen ratio 2.25 are presented in Figure 4.9.

For small volumes of fibers or graphite powder (with a particle size of less than 20 μm and an electrical resistivity of $10^{-4} \Omega \text{ cm}$) the resistivity is similar to that of a plain asphalt mastic sample, exhibiting insulating behavior. Both with fibers and graphite, a sudden change in the resistivity takes place after a certain volume of conductive additives have been added, for example 6.02% in the case of steel wool type 000. Differently from with the sand-bitumen ratio variations, when the volume of fibers added is higher than the content, the resistivity remains constant or decreases very slowly. 6.02% can be considered as the optimal content for conductivity purpose, because adding more steel wool above this content to the mixture does not improve its electrical conductivity, but makes it difficult to disperse the steel wool and clusters of steel wool start to appear during the mixing process.

In Figure 4.9 it can be seen that steel wool has much greater influence on the electrical resistivity than the graphite powder in term of volume content. For example, the resistivity of the asphalt mastic with steel wool drops from 750 $\text{M}\Omega \text{ m}$ to 89.12 $\Omega \text{ m}$ with steel wool volume increasing from 5.83% to 6.02%. The influence of graphite on the resistivity of the samples with sand-

bitumen ratio 2.25 is quite low. The resistivity seems to drop slowly, but with high volumes of graphite, asphalt mastic is difficult to prepare, and its mechanical properties are highly reduced. It can be concluded that steel fiber is more effective than graphite to increase the electrical conductivity of asphalt mastic without damaging its mechanical properties.

Finally, the combination of fiber and graphite was analyzed. For that, the steel wool volume was fixed at 6.54% steel fiber type 000 and different volumes of graphite were added. It was found that the resistivity will continue reducing slowly with increasing volume of graphite. This phenomenon can be attributed to the bridging effect of graphite, which fills the gap between steel fibers and shorten the conductive path resulting in a slight decrease of electrical resistivity. With the increase of the graphite volume content, the electrical resistivity of the mastic system tends to a certain value, constant and independent of the volume of graphite added. A higher graphite concentration does not produce any effect on the asphalt mastic electrical conductivity, because the shortest conductive path has been attained.

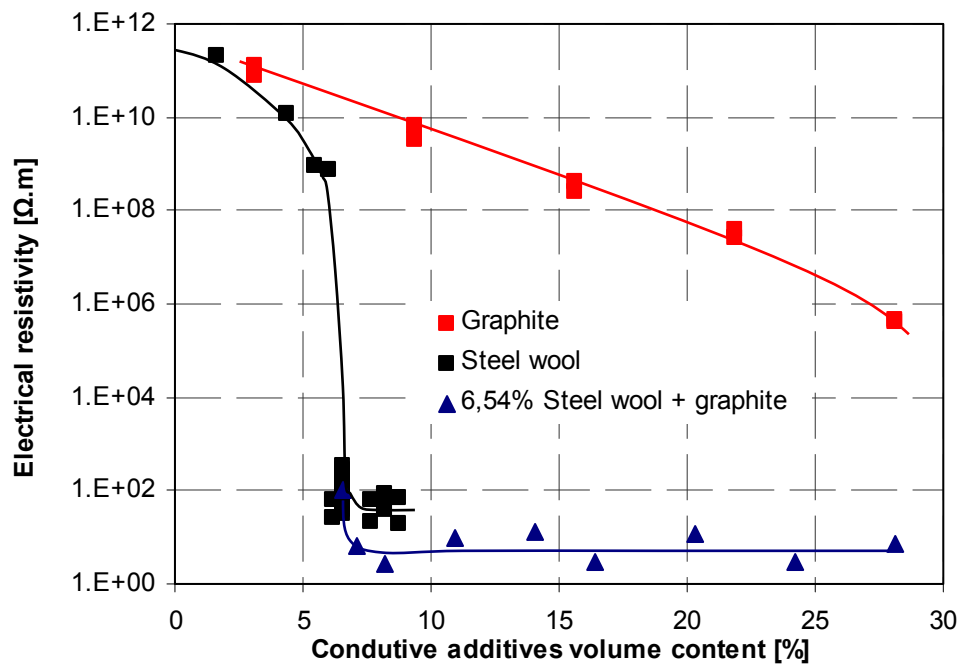


Figure 4.9: Effect of the volume content of conductive additives on the electrical resistivity of the asphalt mastic system with sand-bitumen ratio 2.25 [García et al 2009]

4.2.2.3 Effect of the volume content of steel fiber on the electrical conductivity of porous asphalt concrete

The absolute fiber size determines the number of fibers per unit of batched weight and the number per cubic meter of matrix. Since the total weight rather than the absolute size reflects the material cost of the fibers, the question arises whether a large number of small fibers offer better conductive effectiveness than the same weight of a small number of large fibers. So, three different types of steel fiber with different diameters and lengths were used in

this research to see which one is best to make porous asphalt concrete electrically conductive.

The effects of the volume contents of steel fibers on the electrical resistivity of porous asphalt concrete are shown in Figure 4.10. It can be seen in Figure 4.10 that the addition of all three types of steel fibers decreases the electrical resistivity of porous asphalt concrete, resulting in an increase in the electrical conductivity. All three electrical resistivity curves show three stages: 1) a high resistivity stage, exhibiting insulating behavior with resistances higher than $10^9 \Omega \cdot \text{m}$; 2) a transit stage, when the electrical resistivity of samples suffers a sharp decrease from $10^9 \Omega \cdot \text{m}$ to $10^4 \Omega \cdot \text{m}$; and 3) a low resistivity stage, exhibiting conductive behavior with resistivity of $10^4 \Omega \cdot \text{m}$.

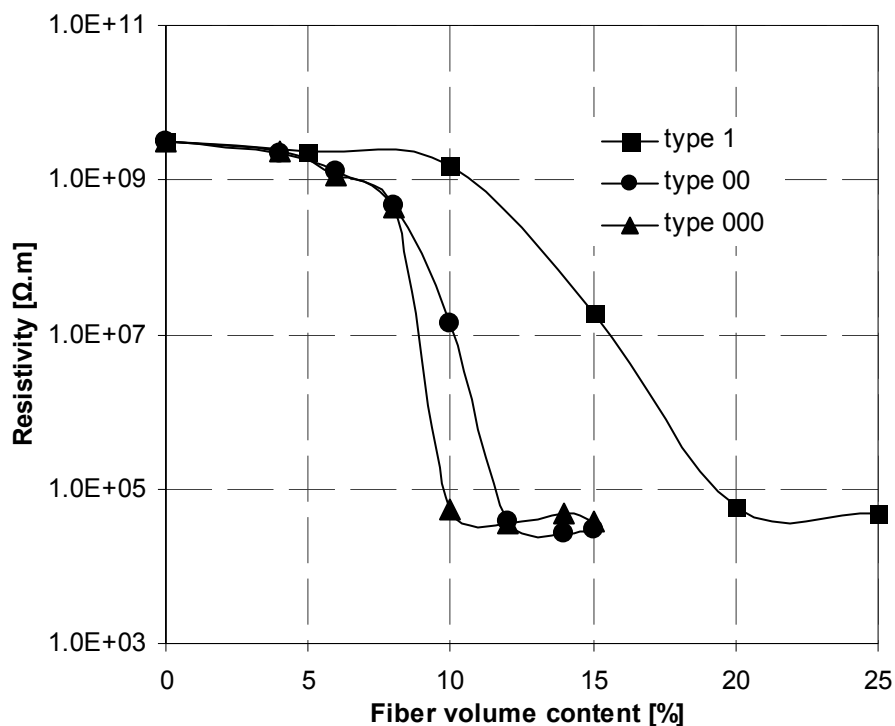


Figure 4.10: Effect of the volume content of steel fiber on the resistivity of porous asphalt concrete

When a small amount of steel fibers is added to the mixture, the fibers are uniformly distributed in the porous asphalt concrete samples and do not contact each other, having a similar resistivity to that of a plain sample without steel fibers. When more steel fibers are added to the mixture, they start contacting each other, which causes a gradual increase in the electrical conductivity showing a gradual decrease in the electrical resistivity. If the volume content of steel fiber reaches more than a certain value (so called percolation threshold) [Miyasaka 1982 and Reboul 1982], the first conductive paths are formed in the sample. This corresponds to a sharp decrease of the electrical resistivity. Beyond the percolation threshold, the conductive network develops and spreads gradually in three dimensions with the increase of the volume content of steel fiber. When the volume content of steel fibers reaches a certain value (the optimal content), steel fibers contact each other in all

directions and many conductive networks and passages are formed, corresponding to a very low value of resistivity at which adding more steel fibers doesn't reduce the resistivity anymore.

However, there are some differences between the three electrical resistivity curves. From the three different types of steel fiber, the diameter of steel fiber type 1 is largest and the diameter of steel wool type 000 is smallest. The percolation threshold comes earlier and the transit stage of the resistivity curve is sharper for the steel fiber with smaller diameter. The optimal volume contents of steel fiber to make porous asphalt concrete conductive are 20%, 12% and 10% by volume of bitumen for steel fiber type 1, steel wool type 00 and steel wool type 000 respectively, which means that the smaller the diameter, the less fibers are needed to make porous asphalt concrete electrically conductive. So, steel wool type 000 is most effective from the three fiber types to make porous asphalt concrete electrically conductive.

Adding steel fiber to asphalt concrete can reduce the drainage problem, offering a possibility of using higher bitumen content in the mixture. In this section, higher bitumen contents were used to check how the electrical conductivity of porous asphalt concrete was affected. The volume content of steel fiber type 1 was fixed at 20% by volume of bitumen in porous asphalt 0/16 mixture (for optimal electrical conductivity purpose) and the bitumen content was gradually increased from 4.5% to 5.4%. The effect of bitumen content on the electrical resistivity of porous asphalt concrete samples is shown in Figure 4.11. It can be seen that an increase in the bitumen content causes a reduction in the electrical resistivity of porous asphalt concrete. It means that higher bitumen content can be used to ensure the durability of this porous asphalt with steel fiber without decreasing the electrical conductivity.

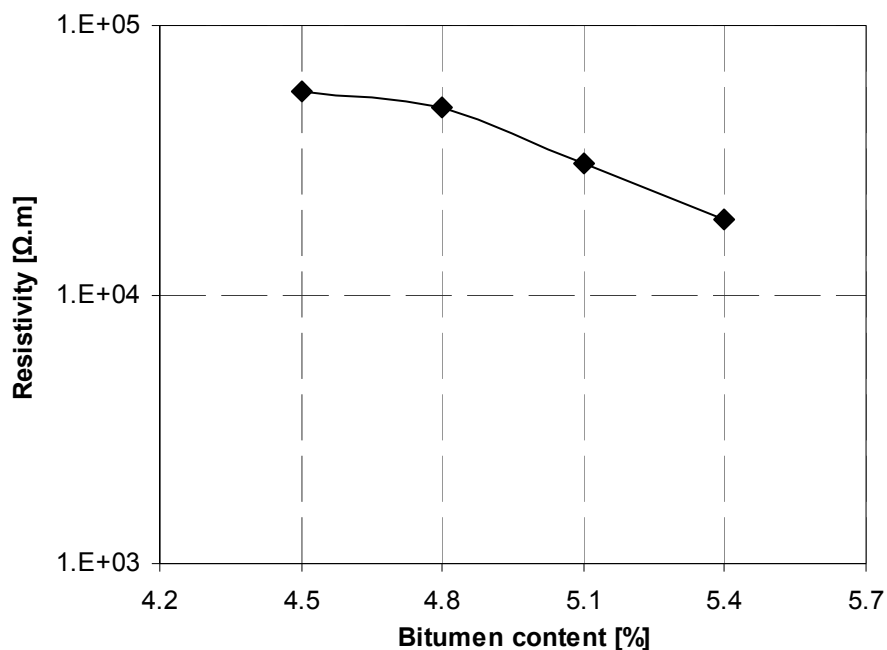


Figure 4.11: Effect of the bitumen content on the electrical resistivity of porous asphalt concrete

4.2.2.4 Effect of the length of steel fiber on the electrical resistivity of porous asphalt concrete

The differences between the electrical resistivity of porous asphalt concrete with different types of steel fiber can be mainly attributed to the differences in the diameters of them. To study the effect of the length of steel fiber on the electrical resistivity and induction heating speed of porous asphalt concrete, steel wool type 00 with three lengths 3.2 mm, 6.4 mm and 9.5 mm is used in this experiment. Figure 4.27 shows the effect of the length of steel fiber type 00 on the electrical resistivity of porous asphalt concrete.

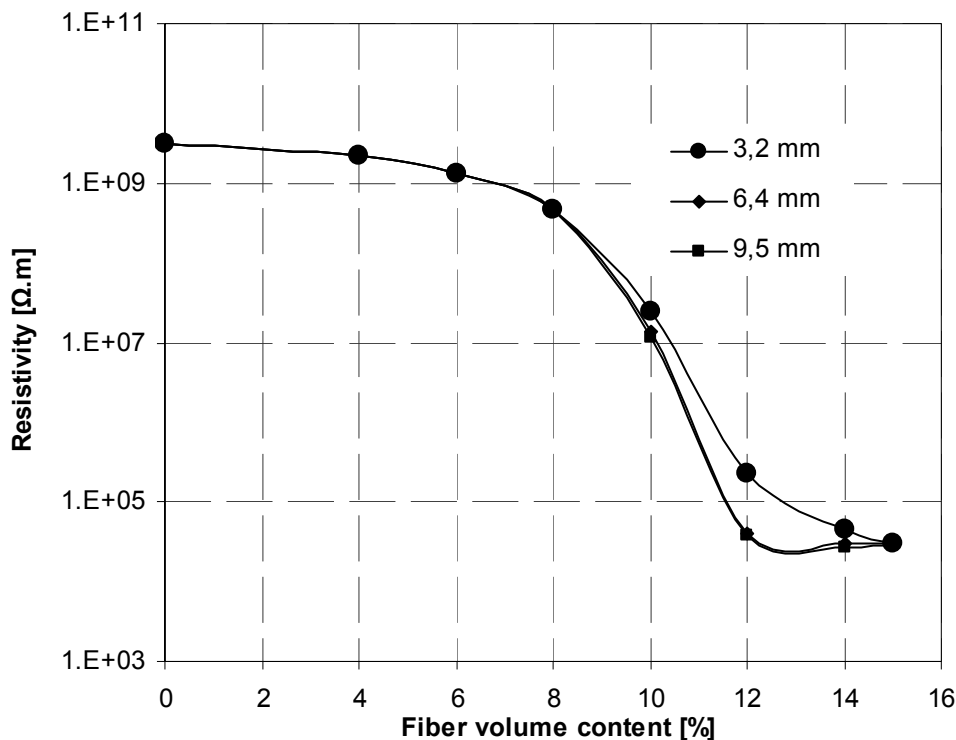


Figure 4.12: Effect of the length of steel wool type 00 on the electrical resistivity of porous asphalt concrete

No apparent differences exist among the three resistivity curves when a small amount of steel fiber is added to the porous asphalt concrete. The differences between the three resistivity curves can be seen when the steel fiber volume content reaches 8% (percolation threshold point), above which the resistivity curves of porous asphalt concrete decrease sharply. The differences become bigger with the increase of steel wool volume content. The two resistivity curves for steel wool with length of 6.4 mm and 9.5 mm decrease more sharply than that for steel wool with length of 3.2 mm. For steel wool with a length of 6.4 mm and 9.5 mm, porous asphalt concrete becomes electrically conductive when the steel wool volume content reaches 12%. For steel wool with a length of 3.2 mm, 15% of steel wool is needed to make porous asphalt concrete highly electrically conductive. It seems that longer steel wool is more effective to make porous asphalt concrete electrically conductive and 9.5 mm is long enough for electrically conductive purpose.

4.2.2.5 Analysis and discussion

To understand how steel fibers make porous asphalt concrete electrically conductive, let us imagine conductive steel fibers as small paths for electrons [García et al 2009]. In the beginning, when few steel fibers are added to the mixtures, if they are well distributed, they will remain completely isolated from each other. If then the electrical resistivity of the sample is measured, it is found that it is a little lower or very close to that of a plain asphalt mastic or porous asphalt. Electrons find high electrical resistances through the bitumen, but suddenly they find an electrically conductive fiber that makes their way easier. If more steel fibers are added to the mixture, electrons will have more conductive paths and the resistivity will continue decreasing. Eventually, there will be so many fibers that they will connect both ends of the sample, and electrons will not need to go through the bitumen anymore but through the conductive path of steel wool. This first conductive path will be a very tortuous one (as shown in Figure 4.13). Adding more steel fibers to the mixture make electrons pass along this conductive path, straightening and shortening it. This increases the conductivity a lot. It is logic that, once the conductive path has reached its shortest length, adding more conductive steel fibers to the mixture will not reduce its electrical resistivity anymore. Following these ideas, it is logic that steel fibers are much more effective than other fillers when reducing the composite resistivity: they form long conductive paths, while the same volumetric amount of filler will be dispersed all around the mixture. This is one of the reasons why steel fiber instead of other conductive fillers is used in this research.

In Figure 4.13, a schematic representation of the electrical resistivity variation versus the volume content of steel fiber is showed. As stated in the percolation theory [Stauffer 1985, Weber and Kamal 1997], it is possible to observe that the electrical resistivity strongly decreases with the increase of fiber content once there is enough volume of fibers. Based on the results shown above, changes in the resistivity as a function of volume content of steel fiber can be divided into three phases: Insulated Phase (1), where the fibers are so separated that there is no conductive paths between both ends of the test sample; here the resistivity of the system is presumably similar to that of plain asphalt concrete. Transition Phase (2), where the percolation paths are forming and the resistivity drops very fast. In this phase, samples are becoming conductive, and fibers start being in contact; this phase ends with a minimum in the electrical resistivity in Figure 4.10, where the shortest conductive paths of steel fiber have formed in the mixture; this minimum in the electrical resistivity corresponds to the optimal content of steel fiber for this mixture. Finally, in the conductive phase (3), there are so many fibers that the length of conductive paths does not decrease anymore and the electrical resistivity of the mixture stops decreasing with the increase in fiber content: once the shortest conductive path has been reached, an increase in the volume of conductive particles does not produce any increment in the conductivity. So, the volume content of steel fiber is excess in the conductive phase. In fact, excess of steel fiber can be

easily distinguished during mixing, because the fibers volume is so high that they are impossible to mix and clusters of fibers start appearing.

Following the same idea, results shown in Figure 4.9 for asphalt mastic (sand-bitumen system) mixed with conductive graphite and fibers seem to be completely logic. Graphite decreases a little the optimum resistivity because, if there is enough concentration, its particles tend to be bridges between the fibers, minimizing the conductive path length [Wu et al 2005]. Anyway, this conductivity increment has a limit imposed by the minimum conductive path length, equaling to the length of the samples studied. Once in the optimum, statistical deviations in the values obtained will come through different aggregate configurations inside the sample.

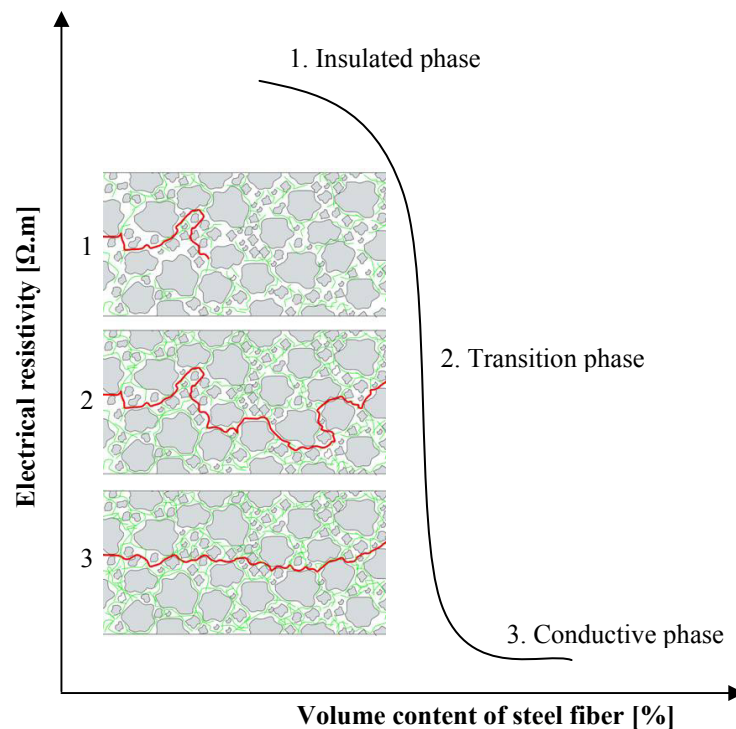


Figure 4.13: Electrical resistivity versus volume content of steel fiber schematic [García et al 2009]

In Figure 4.14, the electrical conductivity surface of asphalt mastic depending on the sand-bitumen ratio and on the total volume of conductive additives is shown. This Figure was made to show the dependence between both parameters studied and that both cannot be studied separately: there is an optimum volume of fibers for each sand-bitumen ratio. In the optimum, fibers are easy to mix, and the resistivity is at a minimum. Above the optimum, the resistivity increases exponentially and the fibers are difficult to mix. Each mixture is different and the optimum volume of fibers should be found for each sand-bitumen ratio or for each aggregates type. In Figure 4.9 it is shown how this optimum can be increased by adding graphite to the mixture. The problem of graphite is that it reduces the mechanical properties of the material, so it should be limited to a minimum, just to stabilize the mixture and avoid the conductivity dropping when the volume of fibers is relatively low. In this

Figure it can be seen how to obtain the lowest electrical resistivities, volume of fibers should be in the optimum or above it. If the volume of fibers is lower, then the volume of graphite needed is very high; whereas if the volume is higher, with a very low quantity of graphite, the conductivity will be improved, but clusters of fibers will appear in the mixture.

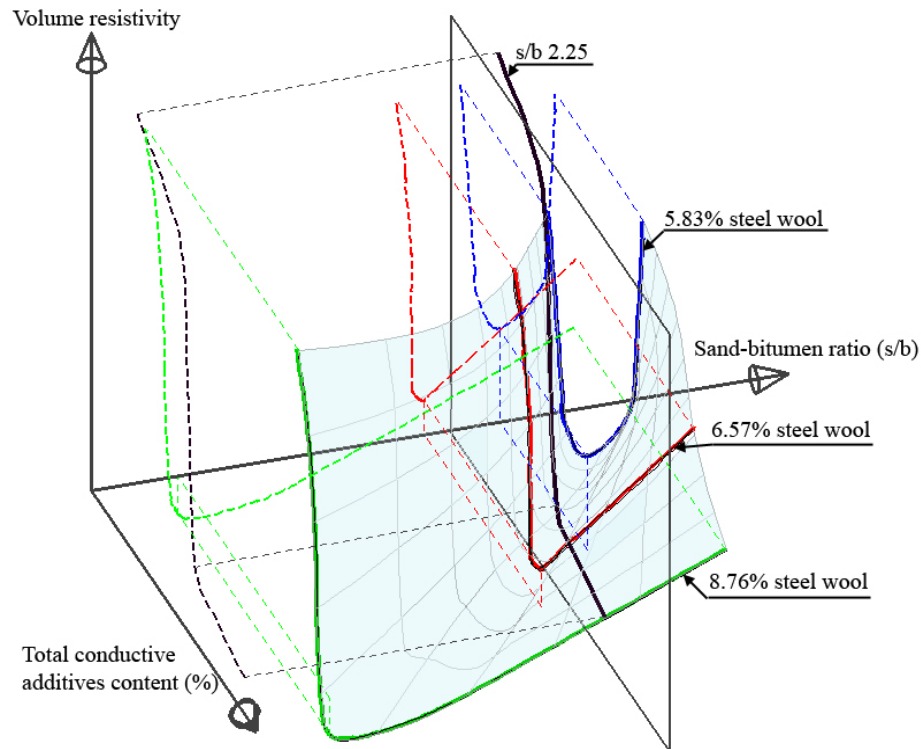


Figure 4.14: Electrical conductivity surface of asphalt mastic against the sand-bitumen ratio and the volume content of steel wool by bitumen [García et al 2009]

4.3 Induction heating of asphalt mastic and porous asphalt concrete with steel fiber

4.3.1 Induction heating principles

In this research, steel fibers are added to asphalt mixture to make it suitable for induction heating. The schematic representation of induction heating on conductive pavement is illustrated in Figure 4.15. The principles of induction heating are electromagnetic induction and Joule heating. According to Faraday's law of electromagnetic induction, when an electrically conductive, non-magnetic material is exposed to an alternating magnetic field, an induced electromotive force is generated in the material. The electromotive force generated in the material is proportional to the power induced on it.

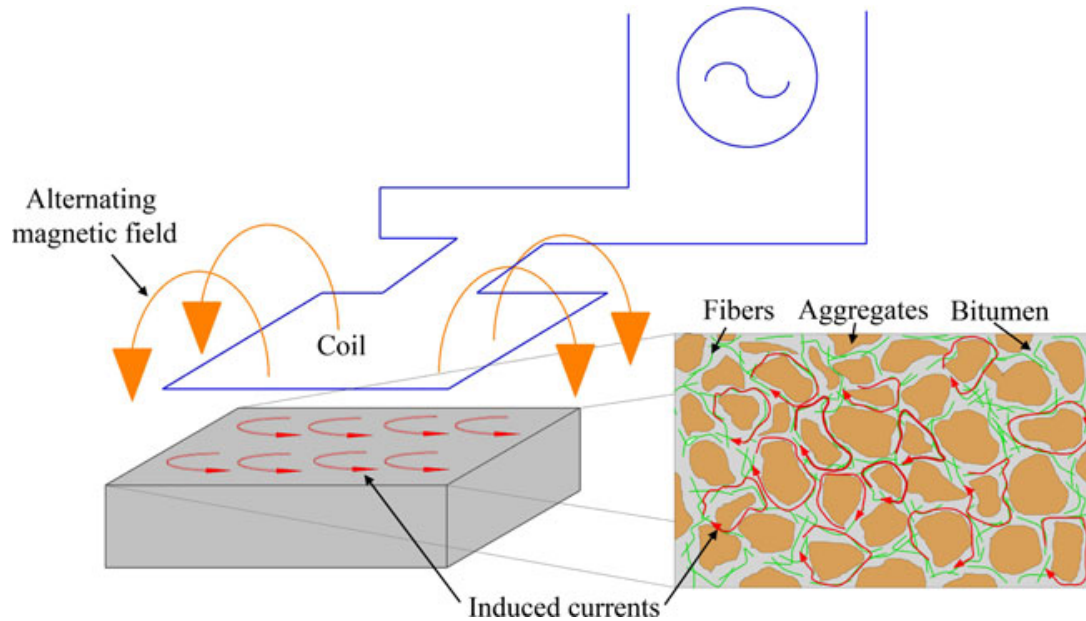


Figure 4.15: Schematic representation of induction heating on conductive pavement [García et al 2011]

The relationship between the source and the induced electromotive force can be expressed in Equation 4.2 [Frohne 1994, Rudolf et al 2000].

$$\varepsilon = \omega \cdot B \cdot A = 2\pi \cdot f \cdot \mu \cdot H \cdot A \quad (4.2)$$

Where:

ε = the electromotive force, [V];

ω = the angular frequency of the magnetic field, [rad/s];

B = the magnetic flux, [Wb];

f = the frequency of the magnetic field, [Hz];

μ = the magnetic permeability of the workpiece material, [H·m⁻¹];

H = magnetic field intensity, [T];

A = the area enclosed by the conductive fiber loop, [m²].

The induced electromotive force depends on the magnetic field intensity and the rate of change of the magnetic field flux. For this heating system, a constant frequency and constant current intensity in the induction equipment will generate a constant magnetic field and a constant electromotive force.

In practice, this means that an electrical current is induced through the fibers when the magnetic flux touches them. The electrical current generates heat when it flows through the conductive fibers. This is Joule heating. The heating rate induced by Joule heating is inversely related to the electrical resistance of the sample. The lower the resistance, the higher the heating rate is.

The Joule's first law is shown in Equation 4.3:

$$P = I^2 R \quad (4.3)$$

Where:

P = the heat generated per unit time, [W];

I = the constant current, [A];

R = the electrical resistance of a conductor, [Ω].

This law applies to any circuit that can be characterized by a resistance. Ohm's law states that for a voltage ε across a circuit of resistance R the current will be:

$$I = \frac{\varepsilon}{R} \quad (4.4)$$

By substituting this formula for current into one or both factors of current in Joule's law, the power dissipated by induction heating can be written in the equivalent form:

$$P = \left(\frac{\varepsilon}{R} \right)^2 R = \frac{4\pi^2 \cdot f^2 \cdot \mu^2 \cdot H^2 \cdot A^2}{R} \quad (4.5)$$

4.3.2 Induction heating equipment and setup

The induction heating experiment was performed by using an induction heating generator with a capacity of 50 kW and at a frequency of 70 kHz (from HÜTTINGER Electronic Germany, shown in Figure 4.16). The configuration of the induction machine and the setup of the induction heating experiment are shown in Figure 4.17 and Figure 4.18, where 6 capacitors are used. The system was not fully optimized and the magnetic field emitted by the coil could not be measured due to the difficulty of measuring fields at high frequencies, but it had no influence on the research objective: to show that asphalt mastic and porous asphalt concrete with steel wool can be heated with induction energy.

The mastic beams and porous asphalt concrete cylinders used for heating were the same as the ones used to measure the electrical resistance. The cylindrical samples cut from gyratory specimens were used to avoid the problem of binder concentration on the surfaces of samples and to get a more homogenous heating for that thinner samples mean less temperature difference between the top and the bottom of the samples. The distance between the coil of the induction machine and the top surface of the heating sample was 20 mm. The heating speed is lower with a bigger distance and the coil will block the sight of the infrared camera with a smaller distance. A 320×240 pixel full color infrared camera (FLIR, Type A320) was used to record and analyze the temperature variations of the samples during induction heating.

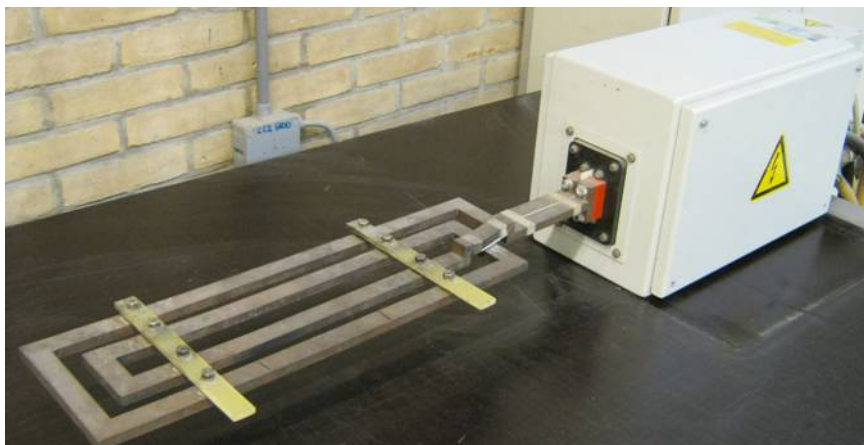


Figure 4.16: Induction heating generator



Figure 4.17: Configuration of the induction heating generator with 6 capacitors: the number of the capacitors can be varied to change the frequency of the magnetic field



Figure 4.18: Induction heating setup

4.3.3 Results and discussion

4.3.3.1 Temperature distribution in the sample

A porous asphalt concrete sample and the infrared camera image of this sample are presented in Figure 4.19 to show how the sample is heated. It can be seen clearly that the temperature of mortar is higher than that of aggregates (aggregates are darker than mortar). Besides, it is proven that plain sample without steel fiber cannot be heated with induction heating. These two facts mean that induction heating primarily heats up the mortar with steel fiber other than aggregates. However, the heat transfers from the mortar to the aggregates very quickly. Given sufficient heating speed, induction heating can heat up the mortar to close the cracks inside without damaging the skeleton structure of aggregates. Otherwise, too much energy is lost to the stones. For this reason, a higher heating speed is preferred.

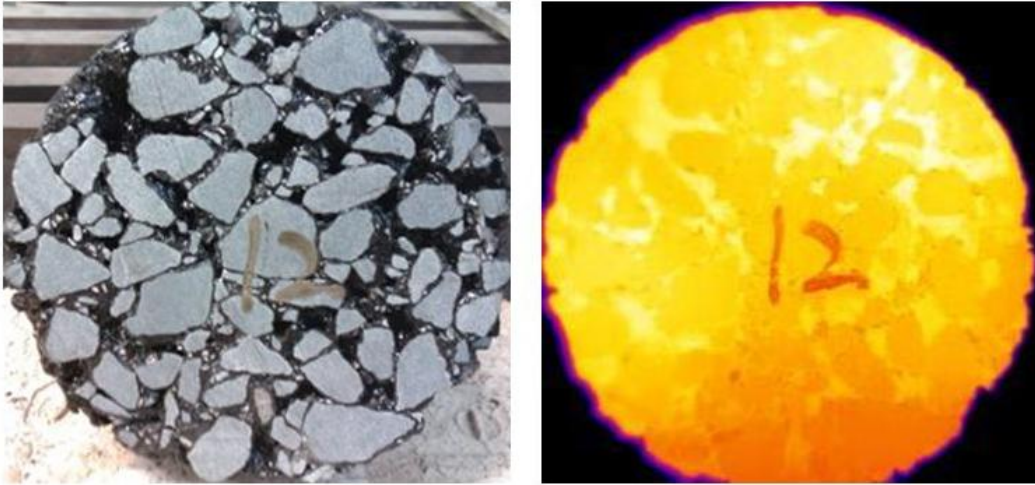


Figure 4.19: Infrared camera image of the sample

During induction heating, the samples were not heated homogeneously and a temperature gradient existed over the sample's thickness. As shown in Figure 4.20, the temperature decreased from the top of the sample (14% steel wool 00) to the bottom. The temperature at the top and bottom is 110 °C and 60 °C respectively. The temperature gradient over the 50 mm (sample's thickness) is 50 °C, which means that the temperature decreases 1 °C / mm over the samples thickness for this set up (the distance between the coil of the induction generator and the top surface of this heated sample is 20 mm).

The temperature gradient over the sample's thickness could be caused by two phenomena. First, a temperature gradient can be caused by skin effect when the skin depth is smaller than the thickness of the sample. Second, the decrease of the magnetic field intensity over the thickness of the sample also causes a temperature gradient [García et al 2012].

The eddy currents induced in the conductor have a tendency to distribute themselves so that the current density is the biggest on the outside and diminish towards the center. So, most of the heat is generated on the outside of the conductor (between the skin depth and the surface). The decline in current density versus depth is known as the skin effect and the skin depth is a measure of the distance over which the current density falls to about 37% of its original value [Ahmed et al 2006]. The skin depth is defined in Equation 4.6:

$$\delta = \sqrt{\frac{\rho}{\pi \cdot f \cdot \mu}} \quad (4.6)$$

Where:

δ = the skin depth, [m];

ρ = the electrical resistivity of the heated material, [$\Omega \cdot \text{m}$];

f = the electromagnetic frequency, [Hz];

μ = the magnetic permeability, [$\text{H} \cdot \text{m}^{-1}$].

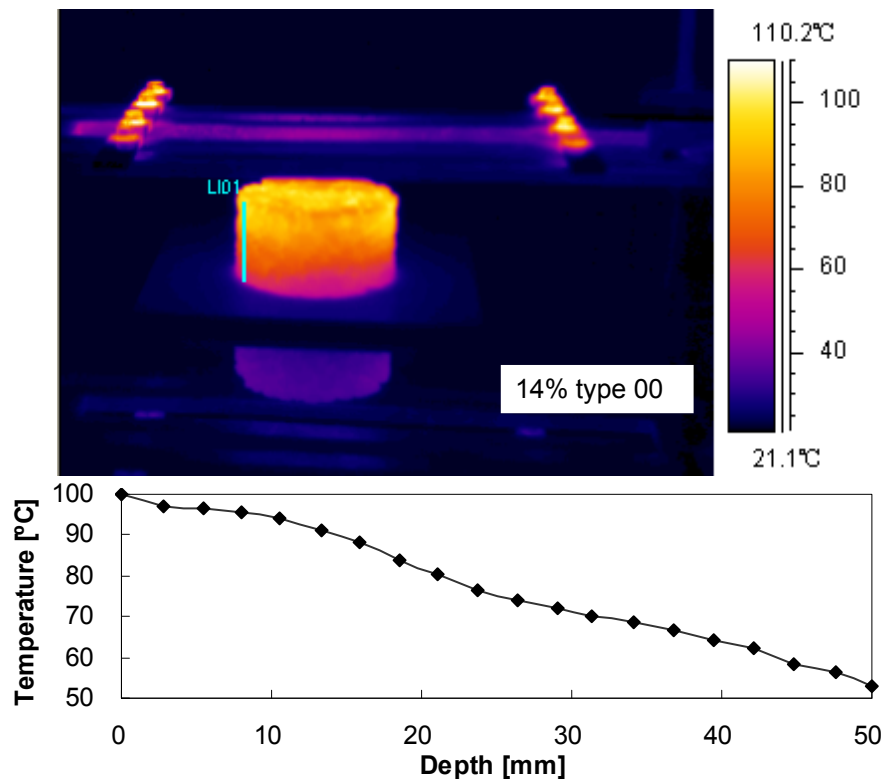


Figure 4.20: Vertical temperature distribution within the sample

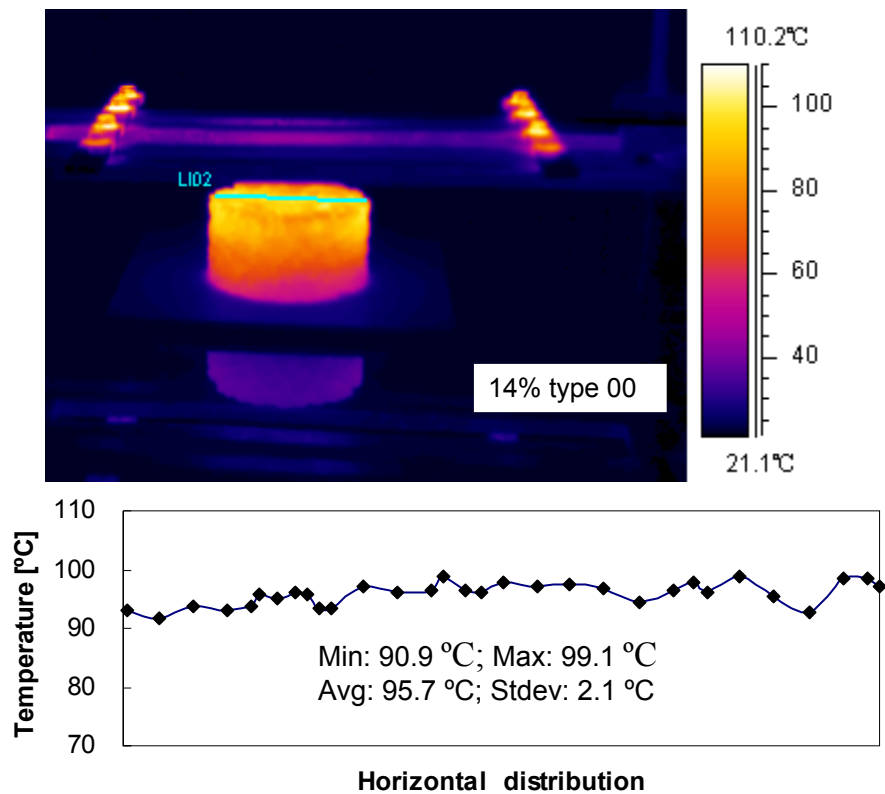


Figure 4.21: Horizontal temperature distribution within the sample

The electromagnetic frequency of the induction generator used in this research is 7×10^4 Hz. The minimal electrical resistivity of the heated samples is $10^4 \Omega \cdot \text{m}$. For non-ferromagnetic materials like porous asphalt concrete, the

magnetic permeability is equal to that of air: 1.256×10^{-6} H/m. So, the minimal skin depth of this induction heating system is about 19.25 m, far bigger than the thickness of the heated cylinder samples. So, it can be concluded that there is no skin effect when heating porous asphalt cylinders with this induction generator. The temperature gradient over the sample's thickness is caused by the decrease of the magnetic field intensity from top to bottom.

The horizontal temperature distribution at the top surface of the sample is shown in Figure 4.21, showing that the temperature distributes almost homogeneously in horizontal direction. This distribution can be attributed to two reasons: firstly, steel wool was dispersed very well in the sample. Secondly, the magnetic field intensity is equal along the line.

However, the magnetic field intensity is not homogenous under the coil of the induction heating generator, which results in inhomogeneous heating in the sample. Figure 4.22 shows the temperature distribution at the top surface of the sample. Most parts (85%) of the top surface of the sample have a temperature between 83.4 °C and 101.2 °C and the a temperature is 91.8 °C.

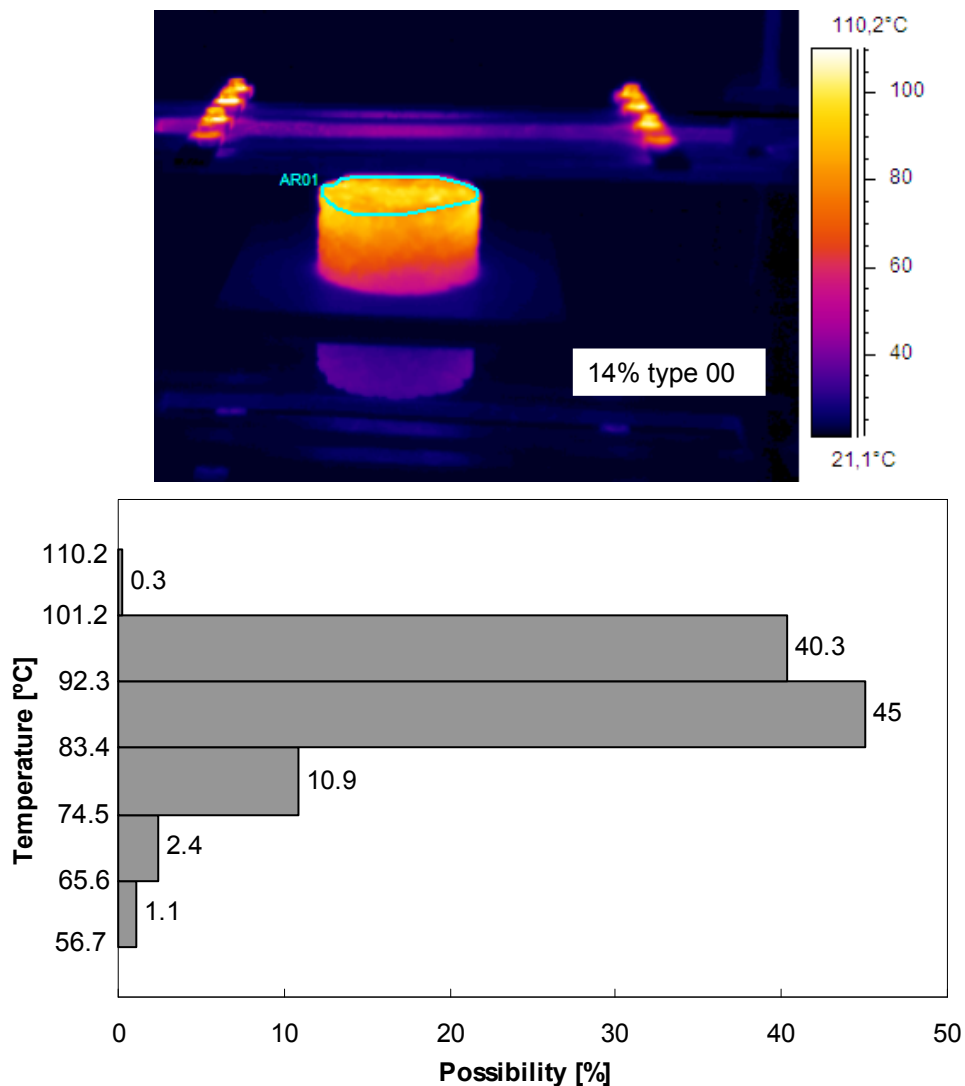


Figure 4.22: Temperature distribution at the top surface of the sample

4.3.3.2 Ageing potential of bitumen during induction heating

The Fourier Transform Infrared Spectroscopy (FTIR) test was used to examine the ageing potential of bitumen during induction heating. For that, a porous asphalt concrete cylinder was induction-heated to 100 °C. Then, bitumen was extracted from the heated sample and unheated sample in the asphalt plant of Heijmans-Breijn. Finally, FTIR test was conducted on the extracted bitumen. The FTIR absorbance spectra of unheated and heated bitumen are shown in Figure 4.23.

It can be seen in Figure 4.23 that the absorbance spectrum of the bitumen does not change after heating, meaning that there is no extra ageing problem during induction heating. Specifically, the peak height and peak area of the two groups C=O at 1705 cm⁻¹ and S=O at 1030 cm⁻¹ would increase if oxidation ageing happens [Lu et al 2002].

Besides, García did Gel Permeation Chromatography (GPC) test on unheated and heated bitumen (heated to 110 °C) to measure the molecular weight of the bitumen. He did not find any change in the molecular weight of bitumen before and after induction heating [García et al 2011]. It means that there is no ageing problem when heating the sample to 110 °C.

Based on the results of FTIR and GPC tests, it can be concluded that there is no ageing problem during induction heating. One possible reason is that probably there are no cracks in the fresh mastic sample for oxygen to penetrate into the heated bitumen. But, the main reason could be that the heating time is very short. It is believed that induction heating will cause no extra ageing to the bitumen in the field.

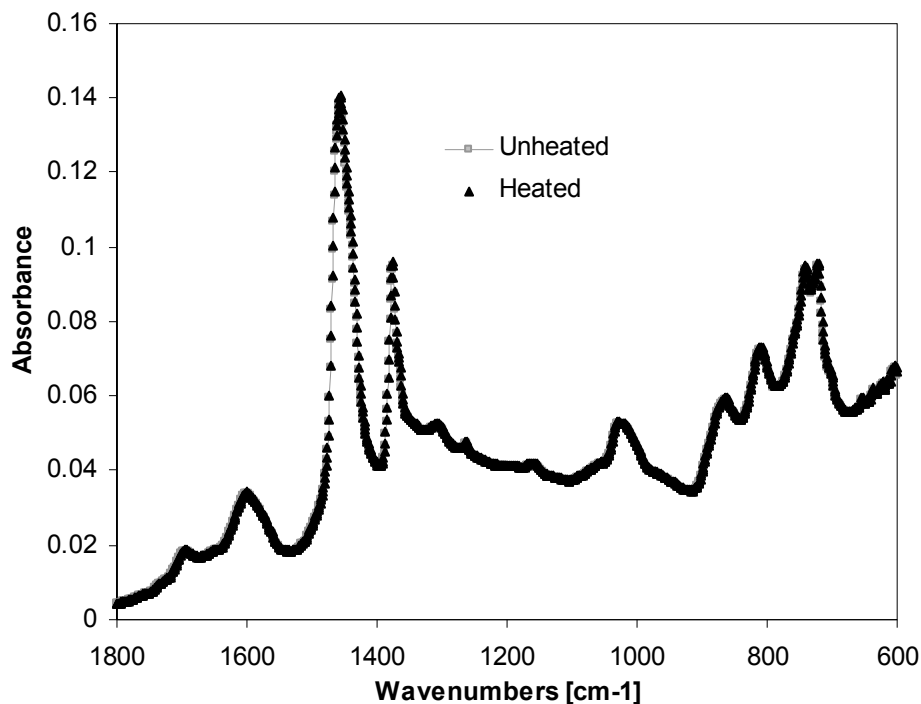


Figure 4.23: FTIR absorbance spectra of bitumen from unheated and heated sample

4.3.3.3 Effect of the volume content of steel fiber on the induction heating speed of asphalt mastic

The mastic beam samples used for induction heating have a sand-bitumen ratio of 2.25. Each sample studied was heated for 60 s, 120 s and 180 s respectively. During heating, the temperature variations in a certain time were recorded and used to denote the induction heating speed.

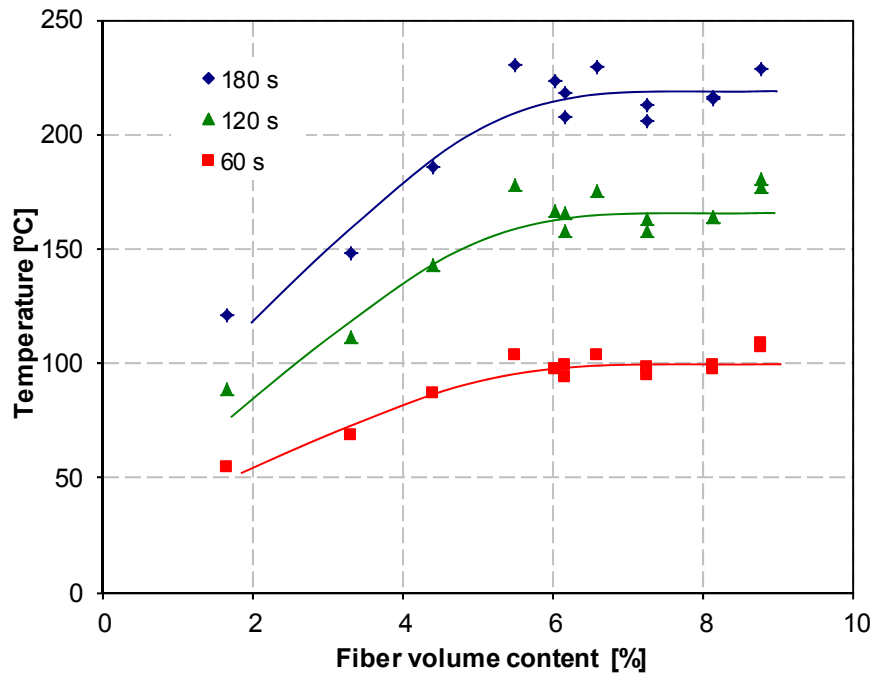


Figure 4.24: Steel fiber volume content versus surface temperature reached for mastic beam samples with sand-bitumen ratio 2.25 [García et al 2011]

Figure 4.24 presents the relationship between the volume content of steel fiber and the surface temperature reached at three different heating times [García et al 2011]. The maximum temperature here refers to the mean temperature at the surface of the heated mastic beams. These curves show two stages. When a small volume content of steel wool is added to the mastic, the reachable temperature (temperature reached in a certain time) increases with the increase of steel wool volume content. However, when steel fiber volume content exceeds 6%, the reachable temperature does not increase anymore. Despite the fact that more steel wool is added to the mastic, the temperature levels off. 6% can be seen as the optimal content for highest induction heating speed for this mastic composition. This percentage coincides with the optimal content for lowest electrical resistivity in Figure 4.9, which means that the lowest electrical resistivity corresponds to the highest induction heating speed (as can be explained with Equation 4.5).

As shown in Figure 4.9 and Figure 4.24, induction heating speed and electrical resistivity behave differently with the increase of the volume content of steel wool. This difference can be explained as follows. When a small content of steel wool is added to the mastic, they are separated with each other

inside the mastic. So, the electrical resistivity of the mastic does not change much. However, every steel wool fiber can serve as a heating unit when subjected to an alternating magnetic field, resulting in an increase of the temperature. When more steel wool is added to the mastic, the electrical resistivity of the mastic decreases slightly because some steel wool begins to contact each other. Also, more heating units are created when more steel wool is added to the mastic. So, the mastic can be heated much faster. With the increase of the steel wool volume content, more and more steel wool contact with each other until the shortest conductive path is created, where the electrical resistivity decreases sharply and then levels off when more steel wool is added to the mastic. The induction heating speed of mastic keeps increasing with the increase of the heating units formed by steel wool until the maximum heating speed is obtained, where adding more steel wool to the mastic does not increase its heating speed anymore, because excess steel wool form clusters which are exposed to air instead of coated with bitumen and lose heat very fast to the environment. Besides, when clusters of steel wool are present, the temperature increase will not be uniform in the sample.

4.3.3.4 Effect of the volume content of steel fiber on the induction heating speed of porous asphalt concrete

The induction heating speeds of porous asphalt concrete with steel fibers are discussed in this section. Three types of steel fiber, i.e. steel fiber type 1, steel wool type 00 and steel wool type 000 are used for optimizing purpose. Porous asphalt concrete samples without steel fibers cannot be heated with induction energy, so the temperature of the plain samples does not change during induction heating. Porous asphalt concrete with all three types of steel fiber can be heated with induction generator. The relationships between mean temperature at the top surface of the sample and the volume content of steel fiber for three types of steel fiber are presented in Figure 4.25, Figure 4.26 and Figure 4.27 respectively. In these figures, it can be appreciated how the mean temperature at the top surfaces of the samples differs with the volume content of steel fibers in the mixture.

For all three steel fibers, the mean temperatures reached at the top surfaces of the samples increase with the volume content of steel fibers in the mixture, but the heating speed (increase of the temperature in a certain time during induction heating) can't be increased any faster when the steel fiber volume content reaches a certain value (optimal content). This finding is the same as the results of mastic heating tests.

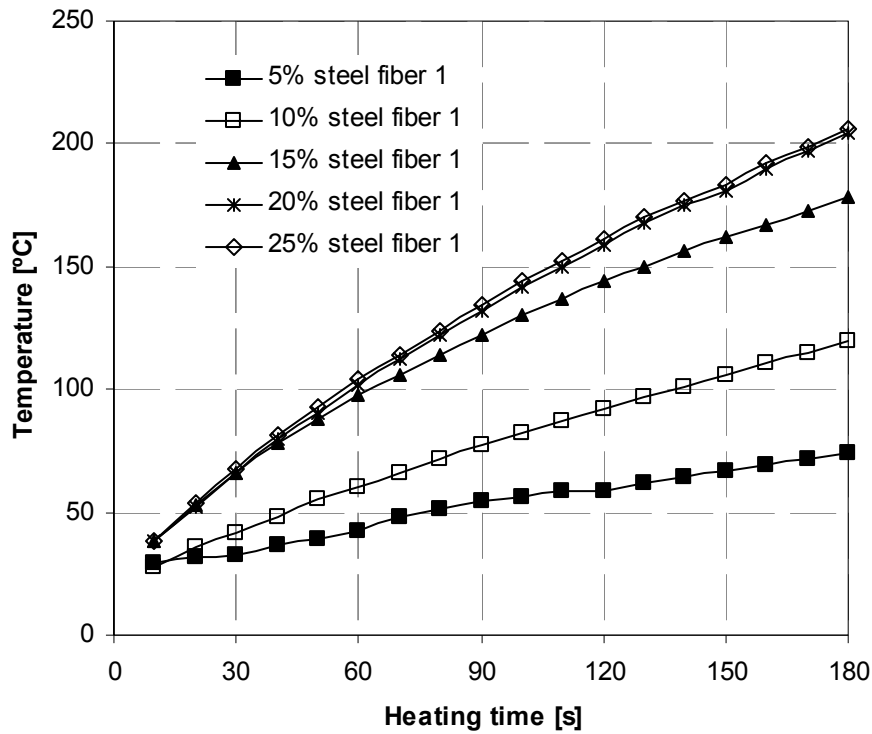


Figure 4.25: Effect the volume content (as fraction of bitumen) of steel fiber type 1 on the induction heating speed of porous asphalt concrete

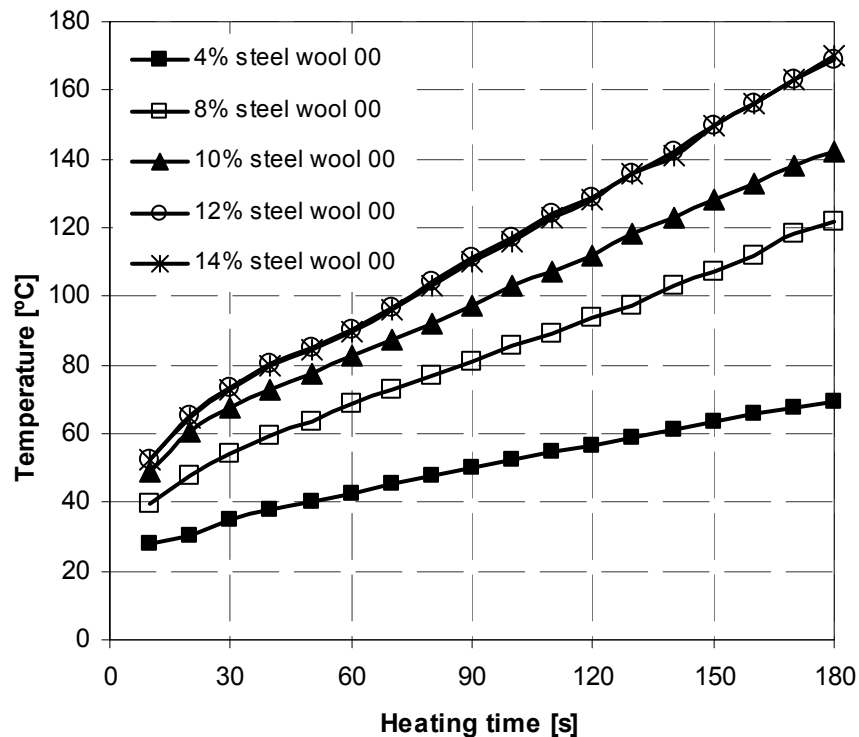


Figure 4.26: Effect of the volume content (as fraction of bitumen) of steel wool type 00 on the induction heating speed of porous asphalt concrete

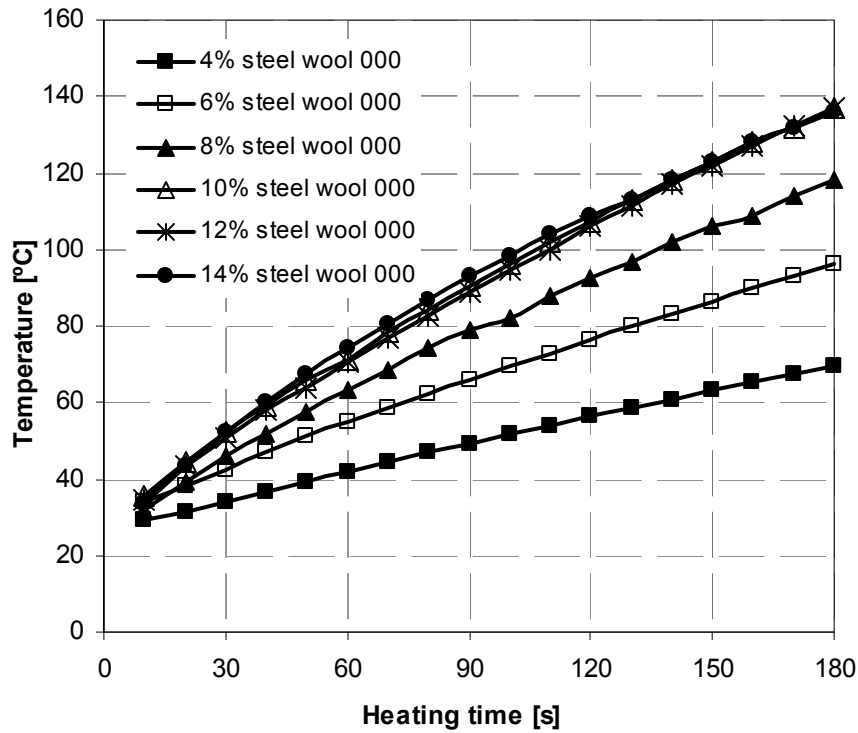


Figure 4.27: Effect the volume content (as fraction of bitumen) of steel wool type 000 on the induction heating speed of porous asphalt concrete

Table 4.1: Mean heating speeds at the surfaces of the samples with different types and contents of steel fibers

Steel fiber type	volume content of steel fiber (by volume of bitumen)	Mean heating speed (°C /s)
Type 1	5%	0.2928
	10%	0.5461
	15%	0.8683
	20%	1.0127
	25%	1.0239
Type 00	4%	0.2611
	8%	0.5572
	10%	0.6683
	12%	0.8183
	14%	0.8239
Type 000	4%	0.2661
	6%	0.3618
	8%	0.5183
	10%	0.6406
	12%	0.6461
	14%	0.6461

To compare the heating speed of the samples with different types and contents of steel fibers, the mean heating speed during this heating process is defined as the temperature increase divided by the heating time. The mean heating speeds of the samples are summarized in Table 4.1.

It is clear from Table 4.1 that, for all 3 types of steel fiber, the mean induction heating speed of the sample increases with the volume content of steel fiber until a certain volume content. When this volume content of steel fiber is reached, adding more steel fiber to the sample does not increase its induction heating speed anymore. This volume content can be seen as the optimal content of steel fiber to obtain the maximum induction heating speed. The optimum volume contents for the three types of steel fibers studied to obtain the maximum induction heating speeds are summarized in Table 4.2. The optimum volume contents are 20%, 12% and 10% for steel fiber type 1, steel wool type 00 and steel wool type 000, respectively. These values coincide with the optimal contents of fiber to obtain the minimum resistivity in Figure 4.10. The maximum heating speeds at the surfaces of the samples with optimum content of fibers are 1.0127 °C/s, 0.8183 °C/s and 0.6406 °C/s, respectively. Adding excess steel fibers doesn't increase the induction heating speeds and will result in a decrease of the indirect tensile strength and particle loss resistance of porous asphalt concrete (as shown in Chapter 5).

Table 4.2: Optimal volume content and maximum heating speed for different types of steel fibers

Steel fiber type	Optimal volume content (by volume of bitumen)	Maximum heating speed, °C /s
Type 1	20%	1.0127
Type 00	12%	0.8183
Type 000	10%	0.6406

In summary, it seems that steel wool type 00 is most effective to make porous asphalt obtain higher induction heating speed.



Figure 4.28: Swelling appearance of the over-heated sample

However, overheating can totally damage the sample. When the top surfaces of the samples are heated to above 160 °C, swelling of the mastic and deformation can occur in the samples shown in Figure 4.28 (the appearance of unheated sample can be seen in Figure 4.2). In this case, the air voids inside the sample cannot absorb the excess expansion of the mortar caused by temperature increase. When heating the sample moderately, the expansion of the mortar retains very small, resulting in no damage to the sample.

Besides, bitumen will drip down when the sample is over-heated. In practice, the dripping of binder in the asphalt layer should be avoided to prevent ravelling.

Thus, the temperature should be controlled when heating the pavement surface using this technology. The optimal heating temperature will be determined later in the study.

4.3.3.5 Effect of the initial length of steel fibers on the induction heating speed of porous asphalt concrete

The difference concerning the induction heating speed of porous asphalt concrete with different types of steel fiber can be mainly attributed to the differences in the diameters. To study the effect of the initial length of steel fiber on the induction heating speed of porous asphalt concrete, steel wool type 00 with three lengths 3.2 mm, 6.4 mm and 9.5 mm is used in this part experiment. The differences among the induction heating speeds of porous asphalt concrete with 12% steel wool type 00 (optimal content of this type fiber for maximum heating speed) with different lengths are presented in Figure 4.29.

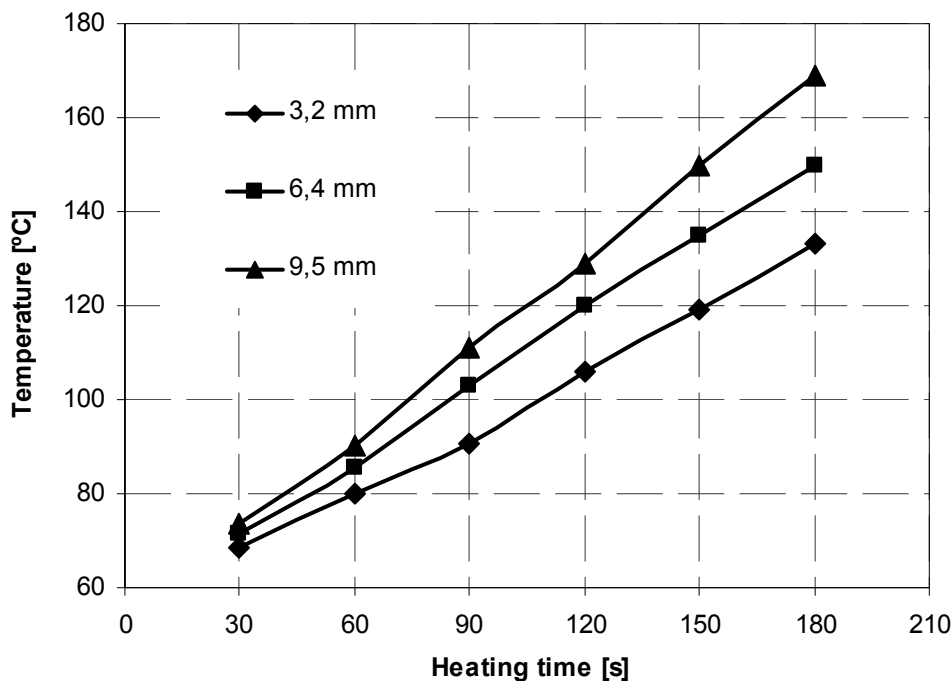


Figure 4.29: Effect of the initial length of steel wool type 00 (12%) on the induction heating speed at the top surface of porous asphalt concrete

It is shown that the induction heating speed at the top surface of porous asphalt concrete with longer steel wool is higher than that of porous asphalt concrete with shorter steel wool. Steel wool type 00 with initial length of 9.5 mm is the best one of the three to make porous asphalt concrete electrically conductive and able to heat with induction energy.

However, too long steel wool should be avoided, because it is very difficult to blend too long fibers with asphalt and the so called “balling” problem could appear, i.e. some of the fibers may lump together to form clusters. In this case, the mechanical properties of the mixture would not be good, because the degree of homogeneity of dispersion of the fibers determines the strength of the resulting mixtures [Mills and Keller 1982]. Furthermore, as the clusters of steel wool will be heated faster than other places, the induction heating speed of the mixture will be less homogenous.

As a conclusion, 9.5 mm is considered as a reasonable length of steel fiber type 00 for the laboratory research with a Hobart mixer and is therefore used in the subsequent healing research.

4.3.3.6 Effect of the distance between the coil of the induction generator and the top surface of heated sample on the induction heating speed of porous asphalt concrete

In the mechanical study (shown in Chapter 5), 8% steel wool 00 is considered as the optimal content for porous asphalt concrete. To study the induction heating capacity of the samples with 8% steel wool 00 and to study how the distance between the coil and the sample affects the induction heating speed, samples were heated with the distance from the coil varied from 30 mm to 20 mm and 10 mm. When the distance was 30 mm or 20 mm, the samples were heated for 180 seconds and an infrared camera was used to monitor the temperature changes of the samples during heating. However, when the distance was 10 mm, the infrared camera cannot monitor the temperature anymore, because the coil blocked the sight of the camera. In this case, the samples were heated for 30 seconds, 60 seconds, 90 seconds, 120 seconds, 150 seconds, and 180 seconds respectively. The samples were moved into the sight of the camera immediately after heating. According to the cooling rate of the samples in the first several seconds (a linear cooling rate was assumed), the temperature reached after heating can be known.

The effect of the distance between the coil of the induction generator and the sample on the induction heating speed of the samples is shown in Figure 4.30. Subjected to the same time of induction heating, the surface of the sample reached a higher temperature when the distance was smaller. It means that the samples were heated faster with a smaller distance from the coil of the induction machine. For each constant distance, the temperatures of the samples increased almost linearly. The slope of the line could be seen as the mean induction heating speed of the samples. The mean heating speeds at difference distances are summarized in Table 4.3. A small distance is preferred to obtain high heating speed, because the magnetic field is stronger.

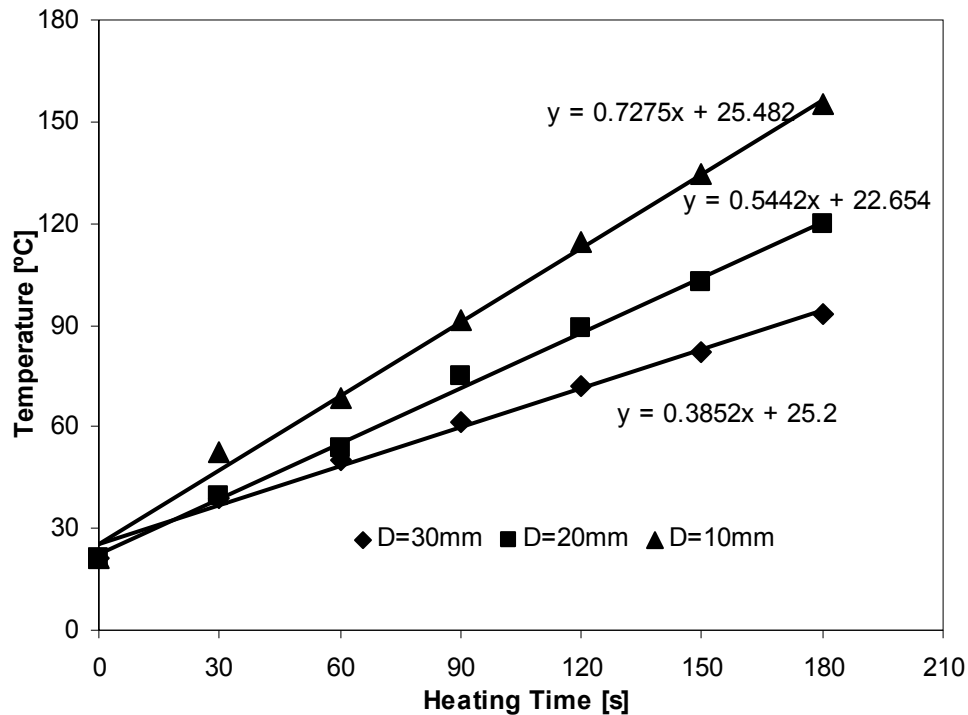


Figure 4.30: Effect of the distance between the coil of the induction generator and the sample on the temperature changes of porous asphalt concrete with 8% steel wool type 00

Table 4.3 Mean induction heating speed of the sample (8% steel wool 00) with different distance between coil and the sample.

Distance (mm)	Mean heating speed (°C/s)
10	0.7275
20	0.5442
30	0.3852

As shown in Figure 4.31, the relationship between the distance (in the range between 10 mm and 30 mm) and the mean heating speed of the samples was linear: the mean induction heating speed of the samples decreased linearly with the increase of the distance between the coil of the heating machine and the sample.

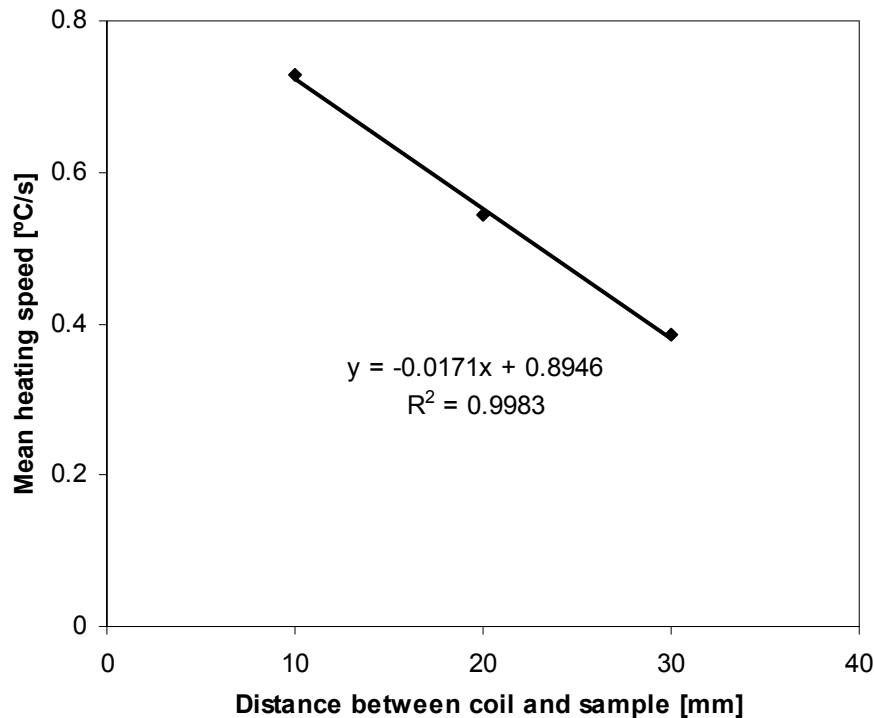


Figure 4.31: Effect of the distance between coil of the induction generator and sample on mean heating speed of the samples with 8% steel wool 00

4.3.3.7 Temperature profile in porous asphalt concrete after induction heating

To get an impression of the temperature decrease of porous asphalt concrete after induction heating, the sample with 8% steel wool was heated for 90 seconds with a distance of 10 mm between heating coil and the sample, after which the mean temperature at the surface of the sample was measured with an infrared camera for 3 hours. The temperature profile of porous asphalt concrete during and after induction heating was presented in Figure 4.32.

After heating, the temperature increased to 91.3 °C. Then, the heat will transfer from the surface of the sample to both the ambient air (21.5 °C) and the lower part of the sample. The surface temperature of the sample decreased very rapidly immediately after heating because of the high temperature difference between the surface and the lower parts. The temperature reduced to 42.3 °C after 30 min. With the heat transfer, the temperature difference between different parts within the sample became smaller, so the temperature decreasing rate became slower and slower. The temperature was 32.2 °C after 60 min. As the healing mainly happens at high temperatures, the short period of time after induction heating is very important for the healing rate of porous asphalt concrete, because later on the temperature becomes too low for healing. After 1 hour, the temperature gradually cooled down and after 3 hours the temperature of the sample was only 1.9 °C higher than the original temperature of the sample. It can be concluded that the sample was already cooled down after 3 hours.

Besides, it is found in Chapter 6 that the significant healing has been obtained 3 hours after induction heating.

According to the cooling rate and the healing rate of the sample, it is recommended that the pavement can be open for traffic after 3 hours cooling to allow the temperature to drop to the ambient temperature. In this way, the permanent deformation potential caused by induction heating can be avoided. If the heating speed is increased with a better induction heating machine (probably only bitumen is heated), the cooling time needed can be less.

Finally, wind was not taken into account in this experiment. The effect of wind speed on the cooling rate of the heated asphalt layer will be simulated in Chapter 7.

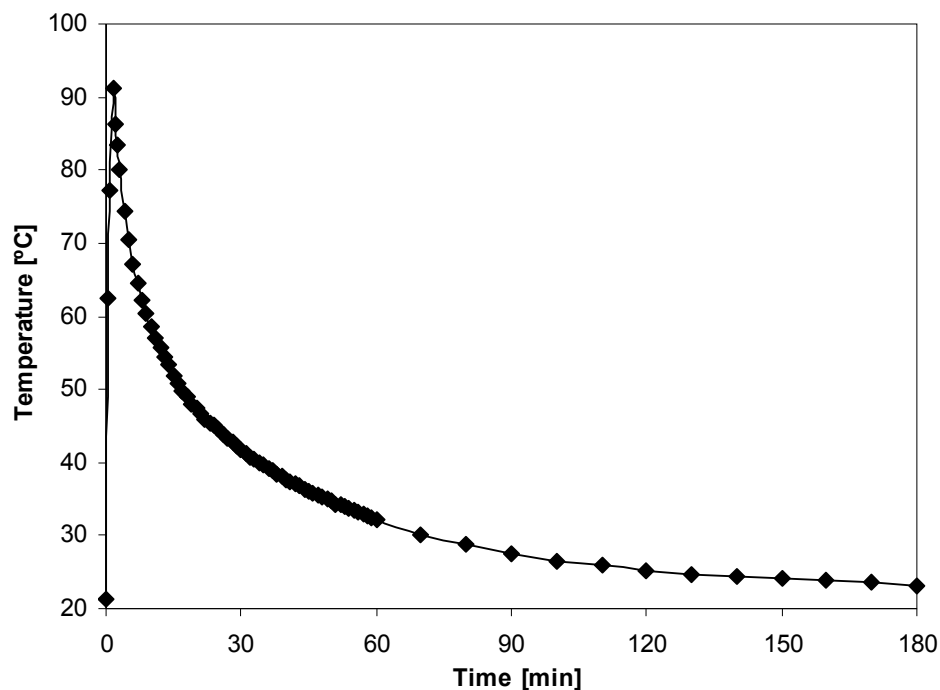


Figure 4.32: Temperature profile of the sample during and after heating

4.4 Summary and Conclusions

The electrical conductivity and induction heating speed of asphalt mastic and porous asphalt concrete were studied in this chapter.

Asphalt mastic and porous asphalt concrete are electrically conductive if they contain sufficient amount of steel fibers. There is an optimal content of steel fiber in asphalt mastic or porous asphalt concrete to obtain the best electrical conductivity. Excess steel fibers do not improve the conductivity anymore, and make the mixture difficult to mix and cause clusters of steel fiber. Excess steel fibers also have a negative effect on the mechanical properties of asphalt concrete, because the film thickness of binder around the aggregates is reduced.

Asphalt mastic and porous asphalt concrete with steel fibers can be heated with induction energy. There is also an optimal volume content of steel fiber in asphalt mastic or porous asphalt concrete to obtain the highest

induction heating speed. Adding more steel fiber above this optimal volume content does not increase the induction heating speed anymore. Compared with the electrical resistivity, the highest induction heating speed corresponds to the minimum electrical resistivity. However, porous asphalt concrete does not need to be fully conductive for induction heating. Every single steel wool fiber is a heating unit. Nonconductive samples with steel fiber can still be heated with induction heating, but at a lower heating speed. When the samples are conductive, they can be heated more evenly, because the steel fibers are distributed homogeneously everywhere in the mortar of the samples.

The type (diameter) and content of steel wool fiber are important to the electrical conductivity and induction heating speed of porous asphalt concrete. The optimal contents of steel fiber are 20%, 12% and 10% for steel fiber type 1, steel wool type 00 and steel wool type 000, respectively, to make porous asphalt concrete conductivity and to obtain highest induction heating speed. This difference is mainly attributed to the differences in the diameters of the three steel fibers.

The initial length of steel wool fiber is also important to the induction heating speed of porous asphalt concrete. Samples with 9.5 mm steel fiber type 00 can be heated much faster than samples with the same content of steel fiber with a length of 6.4 mm or 3.2 mm. However, too long steel wool fibers should be avoided, because it is very difficult to blend too long fibers with asphalt and the so called “balling” problem would appear. Clusters of steel fiber can decrease the mechanical properties of porous asphalt concrete and make heating less homogeneously.

Induction heating speed is highly dependent on the distance between the sample and the coil of the induction generator. The lower the distance, the higher the induction heating speed is. Considering the flatness of the pavement in practice, it is recommended that 10 mm is a reasonable distance for induction heating.

Induction heating can only heat mortar with conductive steel fibers. The aggregates cannot be induction-heated. However, the heat transfers from the mortar to the aggregate very quickly. The temperature of the induction-heated sample is almost homogeneous in horizontal direction and decreases vertically from surface to the bottom.

Heating the sample to 110 °C causes no ageing to the sample. After heating asphalt mastic to 110 °C, no change was found in the molecular weight of bitumen. Induction heating causes no change to the FTIR absorbance spectrum of bitumen extracted from heated sample.

However, overheating can cause swelling problem, where the mortar in porous asphalt concrete cannot bear the excess expansion caused by induction heating. Swelling of the mortar has a negative influence on the property of porous asphalt concrete. In chapter 6, it is found that overheating decrease the healing rate of porous asphalt beams.

It takes 3 hours to cool down when increasing the temperature of the pavement by 70 °C. The heat transfer within the pavement after induction heating will be simulated in chapter 7.

Chapter 5 Mechanical Properties of Porous Asphalt Concrete with Steel Fiber

5.1 Introduction

Fiber reinforced asphalt concrete has long been studied by many researchers. Addition of fiber to asphalt concrete mixtures is very popular to improve properties of the material. The addition of a large variety of fiber to asphalt concrete was reported by many researchers.

Fiber reinforcement is usually used as a crack barrier whose function is to carry the tensile loads as well as to prevent the formation and propagation of cracks [Maurer and Gerald 1989]. Some fibers have high tensile strength relative to asphalt mixtures, so these fibers have the potential to improve the cohesive and tensile strength of bituminous mixes. This may increase the amount of strain energy that can be absorbed during the fatigue and fracture process of the mix [Mahrez et al 2003]. Fibers are believed to impart physical changes to asphalt mixtures [Brown et al 1990]. It is thought that adding fibers to asphalt enhances the material strength and fatigue characteristics while at the same time increases ductility because of the inherent compatibility of fibers with bitumen and their excellent mechanical properties [Fitzgerald 2000]. Fiber changes the viscoelasticity of the modified asphalt [Huang and White 1996], increases the dynamic modulus [Wu et al 2007], moisture resistance [Putman and Amirghanian 2004], creep compliance, rutting resistance [Chen et al 2004] and freeze-thaw resistance [Echols 1989], while reducing the reflective cracking of asphalt mixtures and pavements [Echols 1989, Tapkın 2008, Maurer and Malasheskie 1989]. Research also shows that fiber-reinforced asphalt materials (FRAM) develop good resistance to ageing, fatigue cracking, moisture damage, bleeding and reflection cracking [Goel and Das 2004].

Fibers are also used to prevent drain down of asphalt mixtures [Hassan and Al-Oraimi 2004, Peltonen 1991, Hansen 2000]. Finely dispersed fibers provide a high surface area per unit weight and behave much like filler materials. Fibers also tend to increase the viscosity of the mastic, so it will not

run off the aggregates during construction. In terms of efficiency, mixtures with fibers showed a slight increase in the optimum binder content compared to the control mix. In this way, adding fibers to asphalt is very similar to the addition of very fine aggregates to it. Thus, fiber can stabilize bitumen to prevent bitumen drainage [Peltonen 1991]. That is why fibers are used in stone matrix asphalt (SMA) and open graded friction-course (OGFC).

Fibers are also used as conductive additives to improve the electrical conductivity of asphalt concrete as reported by Wu [Wu et al 2002, 2005 and 2006]. Wu et al made conductive asphalt concrete for deicing application by adding conductive fibers [Wu et al 2002 and 2005]. Thermo-electrical techniques can be used to remove snow and ice on conductive highways in winter. Wu et al also made conductive asphalt concrete for self-monitoring purposes, because the resistance change can denote the variation of its interior structure [Wu et al 2006]. A conductive asphalt pavement has also been developed as solar collector for the heating and cooling of adjacent buildings as well as to keep the pavement ice-free directly [Wu et al 2008].

In this research, the principal function of steel (wool) fiber is to make porous asphalt concrete electrically conductive and suitable for induction heating so that the pavement can be heated by induction to increase its healing capacity to close cracks and prevent ravelling. The addition of steel fiber to porous asphalt concrete for induction heating purposes will definitely influence the mechanical properties of the matrix, which are very important to the durability of this type of pavement. So the addition of steel fiber to porous asphalt shouldn't influence its mechanical properties negatively, to make sure that the mixture satisfies the durability requirements.

In this chapter the effects of steel wool on the mechanical properties of porous asphalt concrete are evaluated. The mechanical properties include particle loss resistance, indirect tensile strength, water sensitivity, indirect tensile stiffness, indirect tensile fatigue, nano indentation modulus and hardness. Table 1 shows the testing plan of the experiments.

Table 5.1: Testing plan for the mechanical experiments

Experiment	Purpose
Particle loss resistance test	Particle loss value (ravelling resistance)
Indirect tensile strength test	Strength
Retained indirect tensile test	Water damage, durability
Indirect tensile stiffness test	Stiffness
Indirect tensile fatigue test	Fatigue resistance, durability
Nano indentation test	Indentation modulus and hardness of mortar

The composition of the reference mixture is reported in Chapter 3 and steel (wool) fibers are directly added to the reference mixture. The bitumen content (4.5%) and air voids content (20%) are kept constant for all the mixtures studied in this chapter.

5.2 Cantabro test

5.2.1 Test description

As ravelling is the main damage on porous asphalt highways, the particle loss (ravelling) resistance of porous asphalt concrete with steel wool was first studied to check if the addition of steel fibers for induction heating purpose has an impact on the particle loss (ravelling) resistance of porous asphalt concrete. In spite that some researchers did not find a direct correlation between Cantabro test and field performance [Tolman et al 1996, Voskuilen et al 2004], Cantabro test is the most widely recommended test to evaluate the ravelling resistance of porous asphalt concrete during mix design and production [Ruiz et al. 1990, Phil et al 2005 and Allex et al 2010]. The samples used in this test were gyratory samples ($\varnothing 100$ mm \times 60 mm) prepared according to the European Norm EN 12697-31. Five samples were prepared for each mixture tested.

The test was done at 21.5 °C in a Los Angeles abrasion machine (shown in Figure 5.1) without steel balls according to the European Norm EN 12697-17.



Figure 5.1: Los Angeles abrasion machine used in this research

Each gyratory compacted specimen was initially weighed (W_1) and placed separately into a Los Angeles drum. The drum was rotated at a speed of 30 rpm for 300 revolutions. After the test, the specimen was removed from the machine and slightly cleaned to eliminate the loose particles. Then, each cleaned specimen was weighed again (W_2) in order to determine the weight loss during testing. This weight loss is an indicator of the cohesive properties of the mix. Lower weight loss means better cohesion and better particle loss (ravelling) resistance. To check the data reproducibility, five specimens of each

composition were tested and the average value was obtained. The test results were expressed as a percentage of weight loss in relation to the initial weight as given in Equation 5.1:

$$PL = \frac{W_1 - W_2}{W_1} \times 100 \quad (5.1)$$

Where,

PL = particle loss (%);

W_1 = the initial specimen mass (g);

W_2 = the final Specimen mass (g).

5.2.2 Particle loss resistance of porous asphalt concrete with steel (wool) fiber

The particle loss resistances of porous asphalt concretes with three different types of steel wool were studied and the optimal type and content of steel wool was determined according to the results.



Figure 5.2: Porous asphalt concrete samples after particle loss testing

Figure 5.2 shows porous asphalt concrete samples after particle loss testing. It is visible that the plain porous asphalt sample lost a lot of aggregate particles because of the abrasion in the Los Angeles abrasion machine. However, the porous asphalt concrete sample with steel fiber (such as samples with 8% steel wool 00) lost much less aggregates.

The effect of the steel fiber volume content (by volume of bitumen) on the particle loss resistance of porous asphalt concrete is shown in Figure 5.3, where each particle loss is the mean value of five samples. The separate results can be found in Appendix 1. The mean particle loss value of plain porous asphalt concrete samples is 14.84%. It can be seen that the particle loss of porous asphalt concrete decreases with the increase of the fiber volume content and reaches a minimum, after which adding more steel fibers will result in an increase of particle loss. Moderate amount of fibers reinforces the mastic, but excess fibers would reduce the bitumen film thickness, causing a bad cohesion

between the mastic components. The minimum values of particle loss are 8.77%, 8.27% and 8.01% for three different types of fibers and about 15%, 8%, 8% of steel fiber is needed to optimize the particle loss resistance of porous asphalt concrete for steel fiber type 1, steel wool type 00 (with length of 9.5 mm) and steel wool type 000 respectively. At the contents for optimal conductivity (20% for steel fiber type 1, 12% for steel wool type 00 and 10% steel wool type 000), the particle losses are 10.31%, 13.49% and 13.66% respectively. This implies that adding the optimal amount of fibers for conductivity, results in an increase of the particle loss.

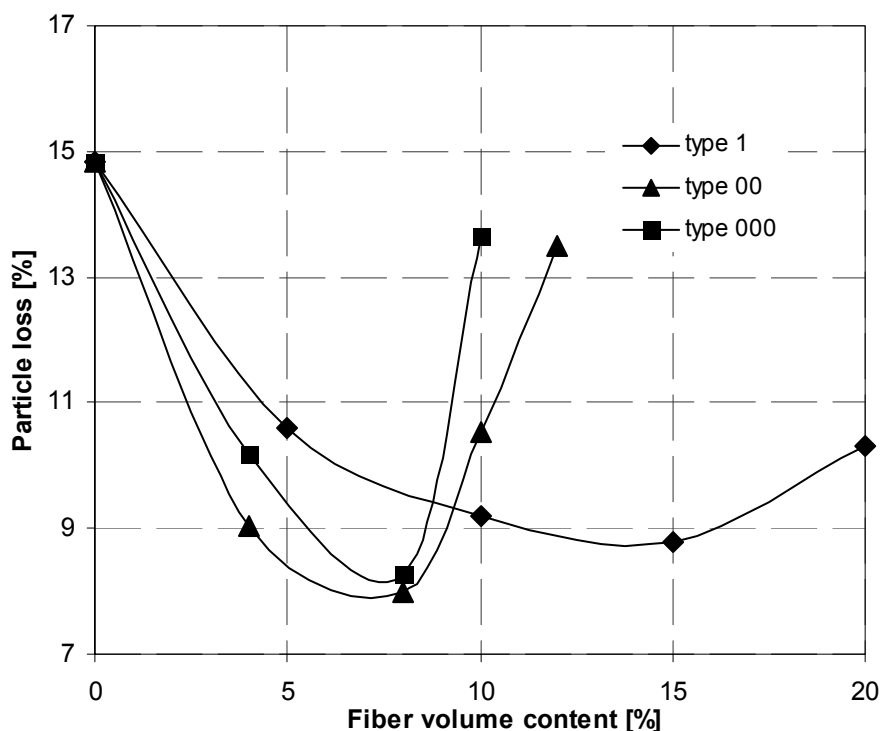


Figure 5.3: Effect of the steel fiber volume content on the particle loss of porous asphalt concrete

Among the three different steel fibers, steel wool type 00 with a length of 9.5 mm gives the best result of the particle loss resistance of porous asphalt concrete. The best particle loss resistance of this porous asphalt concrete is obtained at 8% (volume fraction of bitumen) of steel wool type 00. It is expected that porous asphalt concrete with steel fiber used for induction heating should have good particle loss resistance in itself, which can delay ravelling and in this way improve the durability. For this reason, 8% of steel wool type 00 is considered as the optimal content for this induction heating application of steel fiber.

The particle loss resistances of wet samples and aged samples were also investigated. The wet samples were soaked in a 40 °C water bath for 72 hours and dried for 24 hours before particle loss testing. The ageing process included holding the samples in a forced draft oven for 240 hours (10 days) at a temperature of 85 °C. During the ageing process, some control samples without steel fiber just fell apart, but the majority one could resist this long term high

temperature ageing. Besides, after 240 hours at 85 °C no obvious binder drain down was observed for all samples in CT scanning test [Liu et al 2012]. It is obvious that a lower temperatures and a shorter test period are more desirable for porous asphalt concrete ageing. However, this long term oven ageing is quite simply and highly related to field ageing. According to the binder properties after ageing (softening point, stiffness master curve and FTIR spectrum), this 240 hours oven treatment is estimated as being approximately equivalent to 5 years ageing in the field [Liu et al 2012]. After ageing, the samples were cooled for 24 hours before particle loss testing.

It was concluded that 8% of steel wool type 00 is the optimal option for induction heating application of porous asphalt concrete. So, only control samples and samples with 8% steel wool type 00 are used in this section. The particle loss values of wet samples and aged samples are presented in Figure 5.4 and Figure 5.5 respectively.

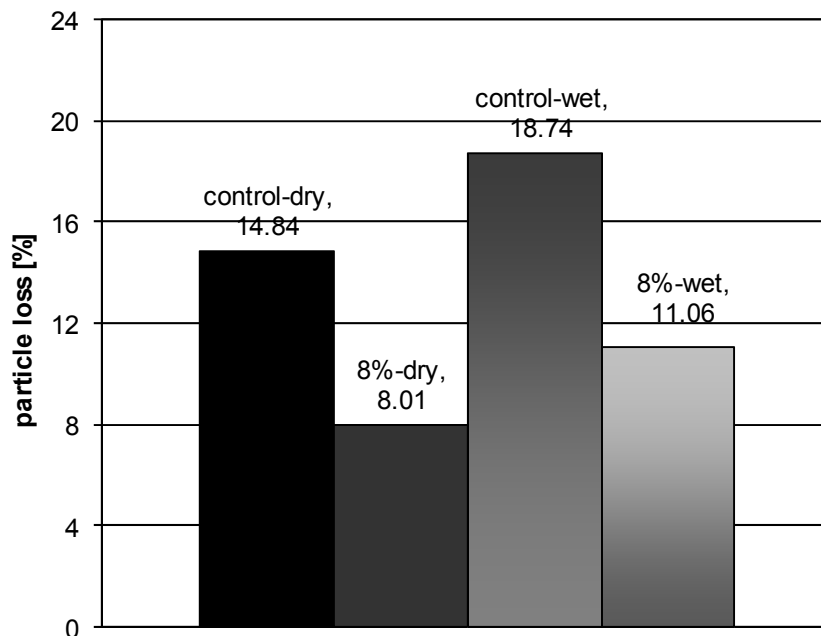


Figure 5.4: Particle loss of fresh and wet porous asphalt concrete

The particle loss of the control porous asphalt sample in dry condition and wet condition is 14.84% and 18.74% respectively. The increase of 3.9% in particle loss of porous asphalt concrete is caused by water damage. The particle loss value of the samples with 8% steel wool type 00 increases from 8.01% to 11.06% when they are subjected to water damage. However, after suffering the water damage, the particle loss resistance (value) of samples with 8% steel wool type 00 is still much better (lower) than that of control samples.

In case of ageing, the particle loss of the control porous asphalt concrete sample in fresh condition and aged condition is 14.84% and 17.43% respectively. An increase of 2.59% in particle loss of porous asphalt concrete is caused by ageing. The particle loss value of the samples with 8% steel wool type 00 increases from 8.01% to 9.77% after ageing. The particle loss increase is 1.76%, lower than that of control samples which means that porous asphalt

concrete with 8% steel wool type 00 is more resistant to ageing. The reason is probably that it is more difficult for oxygen to penetrate into the steel wool reinforced binder or the oxygen only reacts with the steel wool. After ageing, the particle loss resistance (value) of the samples with 8% steel wool type 00 is still much better (lower) than that of the control samples.

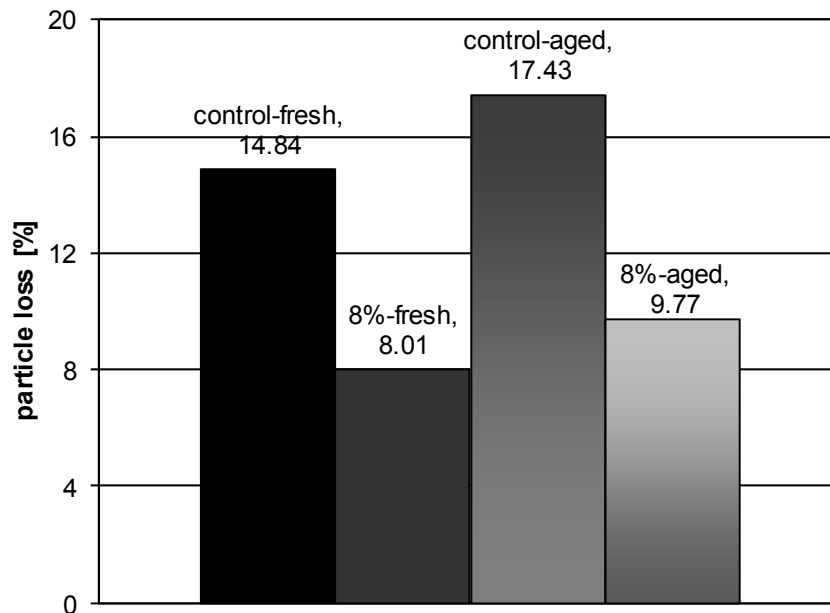


Figure 5.5: Particle loss of fresh and aged porous asphalt concrete

5.3 Indirect tensile strength test

5.3.1 Test description

Indirect tensile strength (ITS) is a parameter that indicates the bond of the binder with the aggregates and the cohesion in the mastic, so it can be used as an indicator of mixture cohesion strength [Li 2007, Behbahani et al 2009]. In this study, indirect tensile tests were conducted to characterize the effect of the volume content of steel fiber on the mechanical behavior of porous asphalt concrete. Indirect tensile strength tests were conducted on cylindrical samples cut from gyratory compacted specimens. The samples had a diameter of 100 mm and a thickness of 50 mm. The equipment used in this experiment is a uniaxial compression setup shown in Figure 5.6, in which the compressive load is applied to the specimen via two loading strips.

This experiment was performed at a standard test temperature of 5 °C, to obtain a "correct" indirect tensile break line. The indirect tensile strength of the specimen is determined by applying a displacement at a rate of 50 mm per minute until the peak load is reached according to the European Norm EN 12697-23. The indirect tensile strength is the maximum horizontal tensile stress calculated from the peak load applied at break and the dimensions of the specimen. For reproducibility reasons, three specimens of each composition were tested and the average value was obtained. After the tests, the indirect tensile strength of the samples could be calculated using the Equation 5.2:

$$ITS = \frac{2F}{\pi DH} \quad (5.2)$$

Where:

ITS = the indirect tensile strength (MPa);

F = the total applied vertical load at failure (N);

D = the diameter of specimen (m);

H = the height of specimen (m).

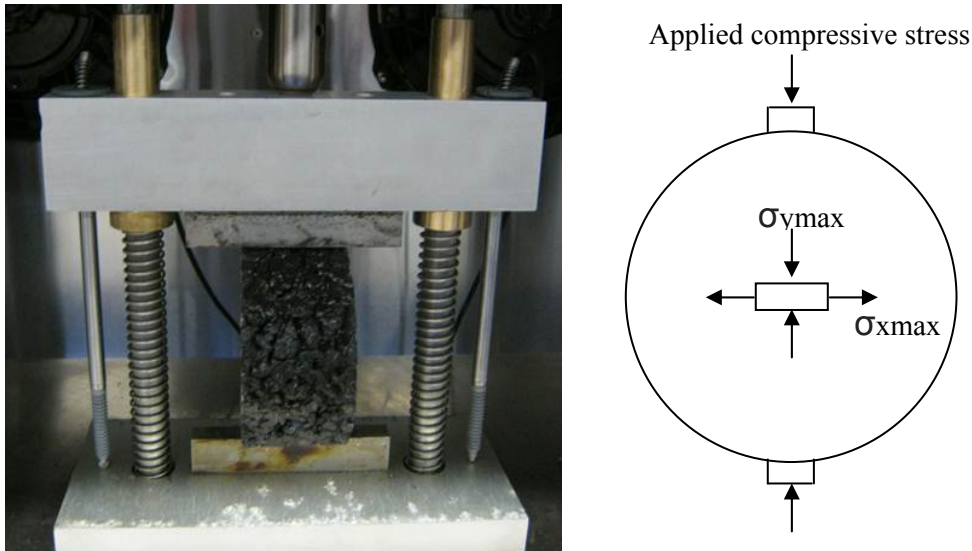


Figure 5.6: The set-up and schematic of the ITS test

5.3.2 Indirect tensile strength of porous asphalt concrete with steel (wool) fiber

After breaking the samples, the type of the failure was observed. As shown in Figure 5.7, the possible types of failure of a sample in the indirect tensile strength test are categorized as: (a) "clear tensile break" – Samples clearly broken along a diametrical line, except perhaps for small triangular sections close to the loading strips; (b) "deformation" – Samples without a clearly visible tensile break line – or (c) "combination" – Samples with a limited tensile break line and larger deformed areas close to the loading strips.

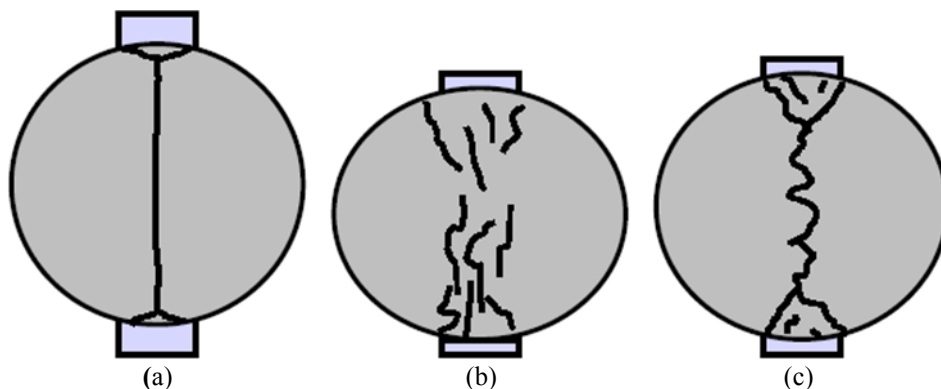


Figure 5.7: Possible types of failure in indirect tensile strength test

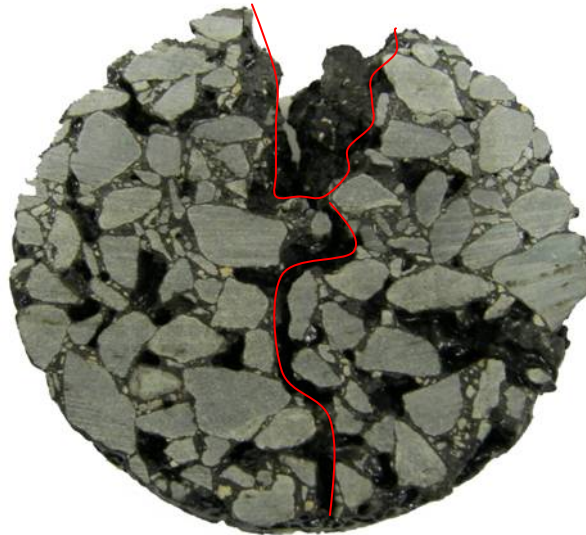


Figure 5.8: Typical failure geometry of porous asphalt concrete in indirect tensile strength test

The typical failure geometry of porous asphalt concrete specimens is shown in Figure 5.8. Both plain porous asphalt concrete specimens and specimens with steel fiber showed the same type of failure. It is interesting to note that the type of failure is a combination of a limited tensile break line and larger deformed areas close to the upper loading strip. The break line does not occur exactly along the diametrical line. The reason for this failure line may be the non-uniform air void distribution and consequently non-uniform strength inside the sample.

Figure 5.9 shows the appearance of the fracture surface of the sample after indirect tensile strength (ITS) test. The fracture predominately took place through the mastic (cohesion failure). Most stones are intact, but some broken aggregates at the fracture surface can be seen for both plain samples and samples with steel fiber. As it was found in CT scanning test that there was no broken stone after compaction, the stones had to be broken in indirect tensile strength testing. This failure may give an indication that the aggregates and binder in this porous asphalt concrete are bonded quite firmly at 5 °C, thus some cracks go through the weak aggregates.



Figure 5.9: Appearance of the fracture surface of the sample after ITS test

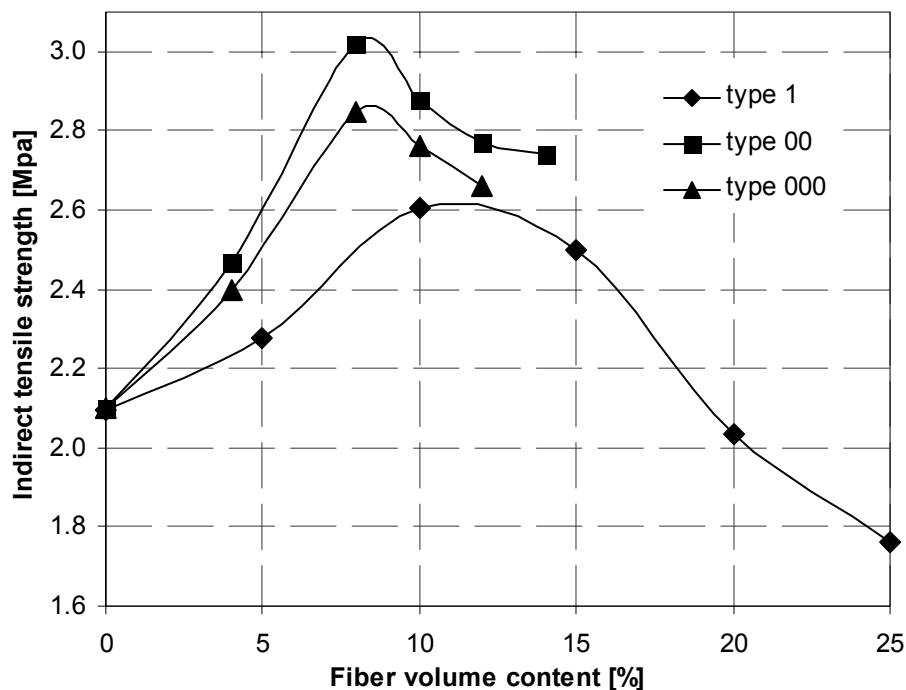


Figure 5.10: Effect of steel fiber volume content on the indirect tensile strength of porous asphalt concrete at 5 °C

The indirect tensile strength values (each value is a mean value of three samples) of porous asphalt samples with different volume contents of steel fiber are presented in Figure 5.10. The separate results of indirect tensile strength test are shown in Appendix 2. It can be seen in Figure 5.10 that adding all three types of steel fiber to porous asphalt concrete can increase its indirect tensile strength, but adding excess steel fiber may result in a decrease of the indirect tensile strength. This finding coincides with the conclusion of particle loss testing: a moderate amount of fibers reinforces the mastic, but excess fibers would cause a bad cohesion between the mastic components, resulting in a decrease of strength. The mean indirect tensile strength of plain porous asphalt concrete samples is 2.06 MPa. The maximum values for the indirect tensile strength of the samples are 2.60 MPa, 3.02 MPa, and 2.87 MPa for three different types of fibers and about 11%, 8%, 8% of steel fiber is needed for porous asphalt concrete to obtain the highest indirect tensile strength for steel fiber type 1, steel wool type 00 and steel wool type 000 respectively. At the contents for optimal conductivity and induction heating speed (20% for steel fiber type 1, 12% for steel wool type 00 and 10% steel wool type 000), the indirect tensile strengths are 2.03 MPa, 2.77 MPa, and 2.76 MPa respectively. It can be concluded that adding steel fiber to porous asphalt concrete in an amount that is optimal for induction heating speed purpose will increase its indirect tensile strength.

Among the three different types of steel fiber, steel wool type 00 with a length of 9.5 mm is most effective to increase the indirect tensile strength of porous asphalt concrete. The highest indirect tensile strength of this porous asphalt concrete can be obtained at 8% (volume fraction of bitumen) of steel wool type 00. This percentage is equal to the amount that required for best

particle loss resistance of porous asphalt concrete, because both low temperature indirect tensile strength and particle loss resistance indicate the cohesive strength of asphalt mortar.

A typical plot of the load versus vertical deformation curve is given in Figure 5.11. All mixtures studied show a similar behavior. However, the deformation at failure, the indirect tensile strength, the fracture work (the area under the load-deformation curve shown in Figure 5.11) and the fracture energy of porous asphalt concrete are increased by the addition of steel fiber. As shown in Table 5.2, the deformation at failure, the ITS, the fracture work and the fracture energy of porous asphalt concrete with steel wool type 00 all increase with the increase of the steel wool volume content until the maximums of 2.21 mm, 3.02 MPa, 33.79 J and 4302 Pa are reached with a steel wool content of 8%. This content can be seen as an optimal content to resist fracture. Above this optimal content, addition of more steel wool to the mixture would result in a decrease in the fracture resistance of the porous asphalt concrete, because excess steel wool will reduce the mastic film thickness, which causes a bad adhesion between the asphalt components.

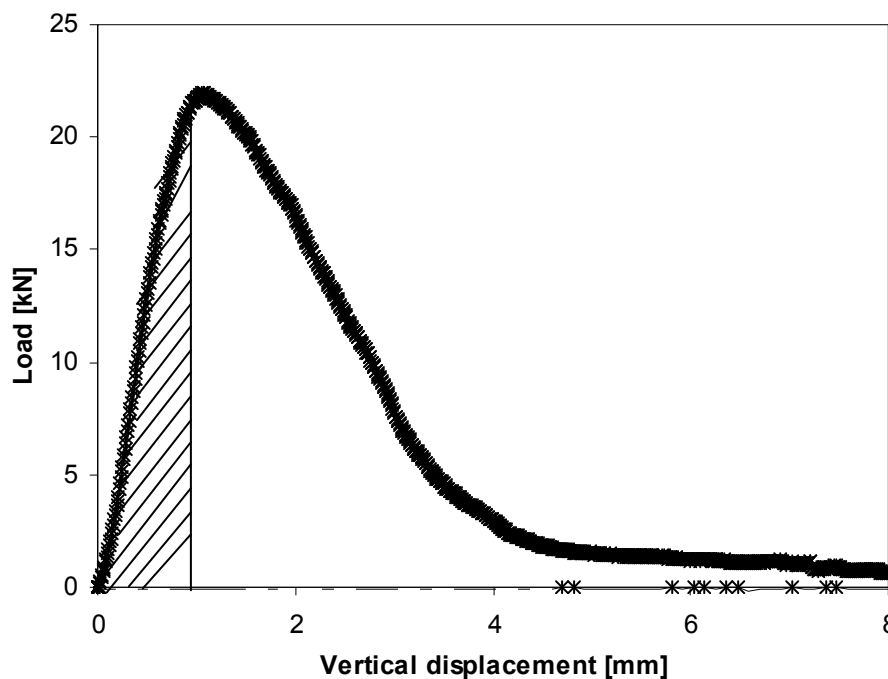


Figure 5.11: Typical plot of load versus vertical displacement in indirect tensile test at 5 °C, 50 mm/ min

Table 5.2: Results of indirect tensile strength (ITS) test for steel wool type 00

Samples	Plain	4% wool	8% wool	10% wool	12% wool
Deformation, mm	1.00	1.35	2.21	1.45	1.28
ITS, MPa	2.06	2.52	3.02	2.88	2.77
Fracture work, J	11.00	18.26	33.79	18.10	14.45
Fracture work, Pa	1400	2324	4302	2304	1801

5.4 Retained indirect tensile strength test

5.4.1 Test description

Moisture (water) can result in loss of adhesion between the asphalt binder and the aggregate surface, and can accelerate the development of other distresses such as potholes, cracking and ravelling. So, water sensitivity is an indication of the adhesion between bitumen film and aggregate. The retained indirect tensile strength test was done here to study the effect of steel wool on the adhesion of the porous asphalt specimens. The specimens were divided into a dry and a wet group. The dry group was directly used to test the indirect tensile strength at 15 °C according to the European Norm EN 12697-12. The wet group was soaked in a 40 °C water bath (as shown in Figure 5.12) for 72 hours and then used to test the indirect tensile strength.



Figure 5.12: The water bath used in this research

The indirect tensile strength ratio (ITSR) was used to denote the water sensitivity of specimens. ITSR was calculated with Equation 5.3:

$$ITSR = \frac{ITS_w}{ITS_d} \times 100 \quad (5.3)$$

Where

$ITSR$ = the indirect tensile strength ratio (%);

ITS_w = the average indirect tensile strength of three wet samples (MPa);

ITS_d = the average indirect tensile strength of three dry samples (MPa).

5.4.2 Water sensitivity of porous asphalt concrete with steel fiber 00

It has been shown that steel wool type 00 (with a length of 9.5 mm) is the best among the three different steel fibers for porous asphalt concrete to obtain best particle loss resistance, highest indirect tensile strength and high induction heating speed. The water sensitivity of porous asphalt concrete with this fiber is investigated in the section. The indirect tensile strength values (m at 15 °C) of the dry and wet samples are given in Appendix 3.

As shown in Figure 5.13, the indirect tensile strength ratio (ITSR) of plain samples is 92.7%, higher than the requirement in the Dutch specification RAW 2010 (80%). For the samples with 4% and 8% steel wool type 00, the ITSR is 95.9% and 101.4%, respectively, higher than that of plain samples. So, the addition of steel wool to porous asphalt concrete increases its ITSR. The increase of ITSR means that the addition of steel wool type 00 to porous asphalt concrete for induction heating purpose can also increase its resistance to water damage (adhesion between aggregate and mortar). With an ITSR of 101.4% (higher than 100% because of experimental error), the samples with 8% steel wool type 00 will show a very strong resistance to water damage.

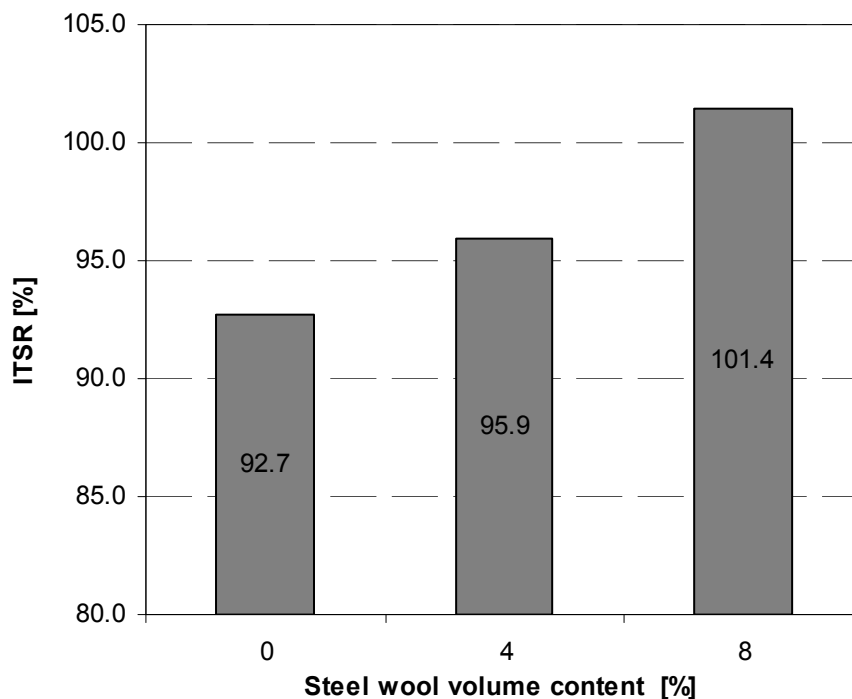


Figure 5.13: ITSR of porous asphalt concrete with steel wool type 00

5.5 Stiffness modulus test

5.5.1 Test description

The stiffness modulus tests were performed on cylindrical specimens with 100 mm diameter and 50 mm thickness according to the European Norm EN 12697- 26. As shown in Figure 5.14, the equipment used was UTM 5.

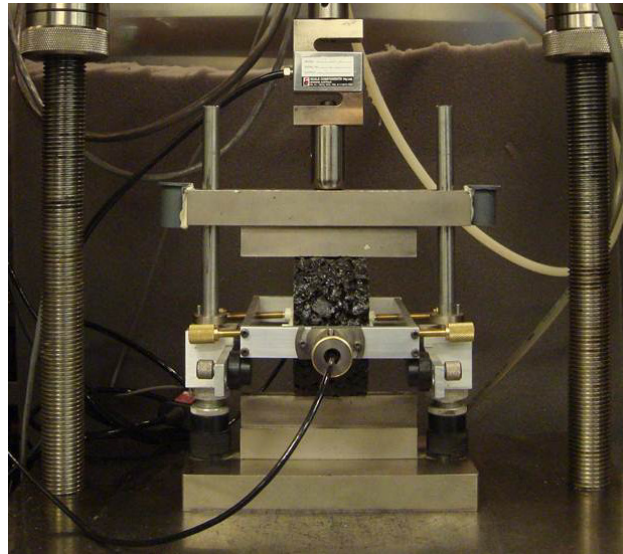


Figure 5.14: The set-up of indirect tensile stiffness test

The tests were done at four different temperatures (5 °C, 10 °C, 20 °C and 30 °C) and for each temperature at five different frequencies (8 Hz, 4 Hz, 2 Hz, 1 Hz and 0.5 Hz). For each selected test temperature and loading frequency, five loading pulses were applied. From the five load pulses, the measured stiffness modulus value for each loading pulse was determined with Equation 5.4 and the average stiffness modulus can be attained from the five measured stiffness modulus:

$$S_m = \frac{F \times (\nu + 0.27)}{Z \times h} \quad (5.4)$$

Where

S_m = the measured stiffness modulus (MPa);

F = the peak value of the vertical load (N);

Z = the amplitude of the horizontal deformation during the load cycle (mm);

h = the mean thickness of the specimen (mm);

ν = the Poisson's ratio. For porous asphalt concrete, the Poisson's ratio was assumed as 0.22 at 5 °C [Merine 2009].

5.5.2 Stiffness of porous asphalt concrete with steel fiber type 00

The master curve of a bituminous mixture at a reference temperature describes the relationship between its stiffness modulus and the so-called reduced frequencies at the reference temperature and can be constructed with the time temperature superposition principle.

Figure 5.15 shows the resilient stiffness modulus of a sample with 8% steel wool at different temperatures. The experimental resilient stiffness of the plain samples is reported in Appendix 4. In constructing the master curves (as shown in Figure 5.15), the data points obtained at test temperatures above the

reference temperature are horizontally shifted to the left (lower frequencies) and the data points obtained at test temperatures below the reference temperature are shifted to the right (higher frequencies), while the data at the reference temperature (20 °C) remain unchanged. The resulting master curve of the stiffness, as function of the reduced frequency, describes the time dependency of the material. The shift factor (at each temperature) required to form the master curve describes the temperature dependency of the material.

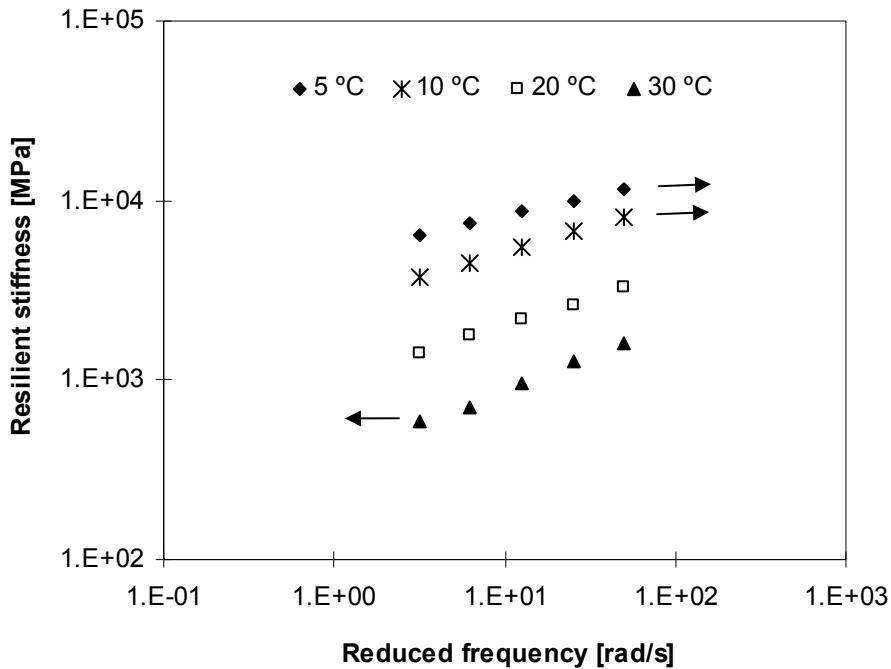


Figure 5.15: Stiffness modulus of a sample with 8% steel wool at different temperatures

The master curves were mathematically modeled with a sigmoidal-shape function described in Equation 5.5 [Bahia et al 2001 and Mo 2010]:

$$G^* = G_e^* + \frac{G_g^* - G_e^*}{[1 + (f_c / f_{red})^k]^{m_e/k}} \quad (5.5)$$

Where:

$G_e^* = G^*(f \rightarrow 0)$, equilibrium stiffness, $G_e^* = 0$;

$G_g^* = G^*(f \rightarrow \infty)$, glass stiffness;

f_c = local parameter with dimensions of frequency;

f_{red} = reduced frequency;

k, m_e = model constants.

The reduced frequency was determined by multiplying the test frequency f with a temperature shift factor a_T :

$$a_T = f_{red} / f \quad (5.6)$$

The shift factor was determined using the Williams-Landel-Ferry (WLF) formulation:

$$\log(a_T) = -\frac{C_1(T - T_{ref})}{C_2 + T - T_{ref}} \quad (5.7)$$

Where:

T = test temperature, [°C];

T_{ref} = reference temperature, [°C];

C_1, C_2 = model constants.

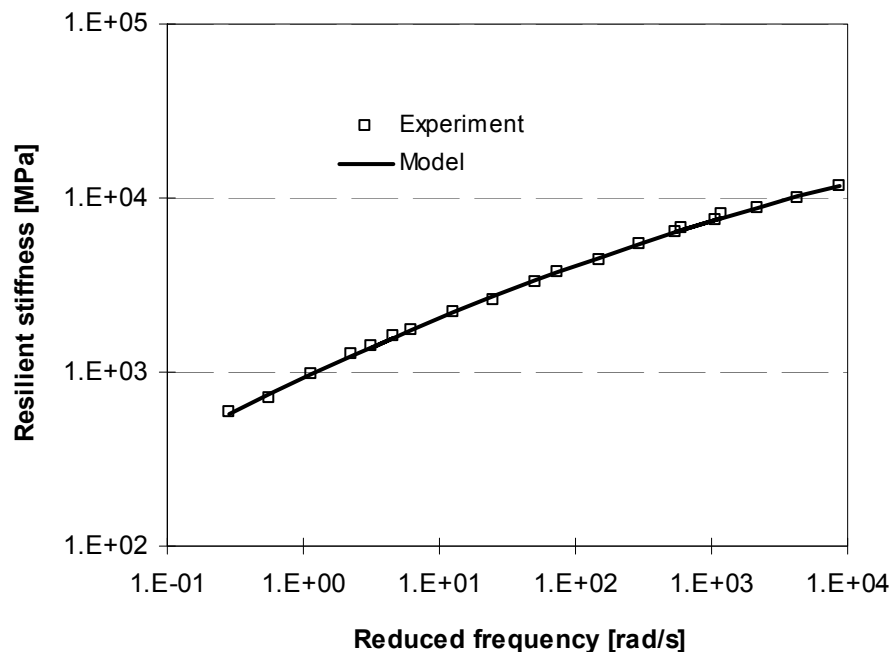


Figure 5.16: Resilient stiffness master curve of porous asphalt concrete with 8% steel wool at a reference temperature of 20 °C

To construct the master curves, the experimental data were fitted to the sigmoidal-shape function given by Equation 5.5 in combination with a shift factor as described in Equation 5.7. The model parameters were automatically obtained by minimizing the mean relative error using the Solver function in the Excel spreadsheet. Figure 5.16 shows the stiffness master curve of porous asphalt concrete with 8% steel wool at a reference temperature of 20 °C. It can be seen that the experiment data fits the model quite well.

Figure 5.17 compares the resilient stiffness master curves of plain porous asphalt concrete and porous asphalt concrete with 8% steel wool type 00 at a reference temperature of 20 °C. The model parameters and the amount of shift of the stiffness master curves are listed in Table 5.3 and Table 5.4 respectively.

It can be seen in Figure 5.17 that porous asphalt concrete with 8% steel wool type 00 shows a higher resilient stiffness than plain porous asphalt concrete over the whole frequency range. Besides, the constructed master

curve of plain mixture is composed of a wider range of frequency. The amount of shift in constructing the master curve, $\text{Log}(a_T)$, represents the gap between two temperatures: the higher the shift factor, the more temperature-dependent the material is [Chailleux et al 2006]. It is shown in Table 5.4 that the amount of shift for plain mixture is higher than for the mixture with steel wool. It means that the addition of steel wool to the mixture decreases the temperature-dependency of the mixture, which narrows frequency range in the master curve.

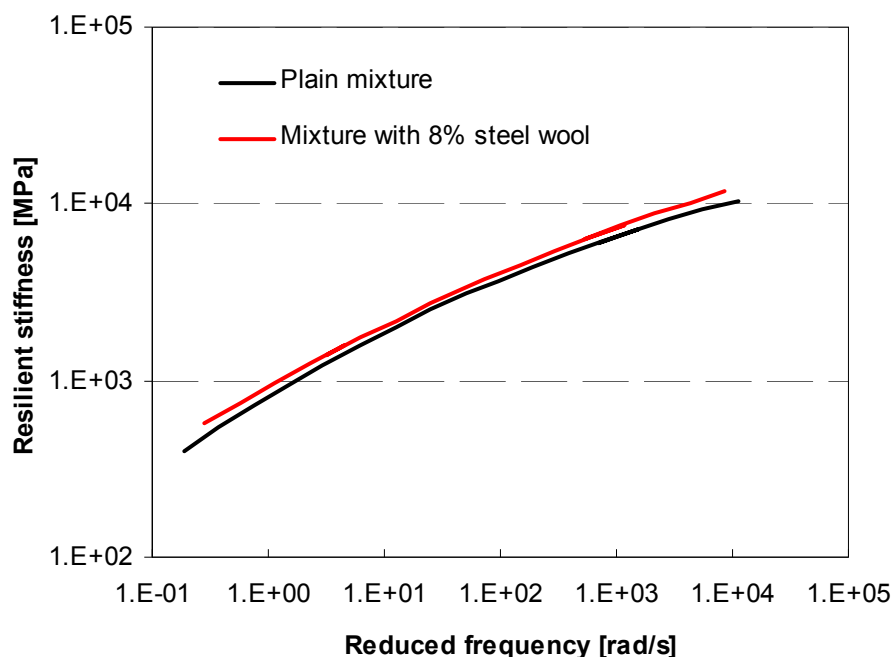


Figure 5.17: Resilient stiffness master curves of plain porous asphalt concrete and porous asphalt concrete with 8% steel wool type 00 at reference temperature of 20 °C

Table 5.3: Model parameters for the stiffness master curves

Model parameters	Plain mixture	Mixture with 8% steel wool
C_1	14.26453	8.763313
C_2	106.225	73.86532
G_e [Mpa]	40649.71	90107.35
G_g [Mpa]	0	0
f_c [Hz]	1.284141	4.541412
m_e [-]	0.775032	0.67572
k [-]	0.140691	0.11569

Table 5.4: The amount of shift in constructing master curves: $\text{Log}(a_T)$

Temperature	$\text{Log}(a_T)$	
	Plain mixture	Mixture with 8% steel wool
5 °C	2.3455	2.2331
10 °C	1.4824	1.3722
20 °C	0	0
30 °C	-1.2273	-1.0449

Voskuilen [Voskuilen et al 2004] states that a higher initial stiffness of the binder reduces the initial loss of stones, which is usually the cause of premature ravelling. He considered the higher initial stiffness of the binder as the primary effect of modified bitumen. So, the modification of steel wool, which increases the resilient stiffness and decrease of the temperature (frequency) dependency of porous asphalt concrete, can probably reduce the premature ravelling tendency of porous asphalt concrete.

5.6 Indirect tensile fatigue test

5.6.1 Test description

Fatigue resistance of both plain samples and samples with steel fiber were studied with the indirect tensile fatigue (ITF) test. It has been concluded that 8% of steel wool type 00 is the optimal content for the induction heating application of steel fiber, so the fatigue resistance of samples with 8% of steel wool type 00 is evaluated compared with plain samples. The samples used in the fatigue test were the same as those used in indirect tensile strength test. The loading mode of the fatigue test was stress controlled shown in Figure 5.18 and these fatigue tests were done at four continuous haversine loading levels at 5 °C with a frequency of 8 Hz (the maximum reliable frequency of the machine) according to the European Norm EN 12697- 24. The test was done at 5 °C to avoid permanent deformation as much as possible during fatigue. The fatigue test ran until the failure of the sample.

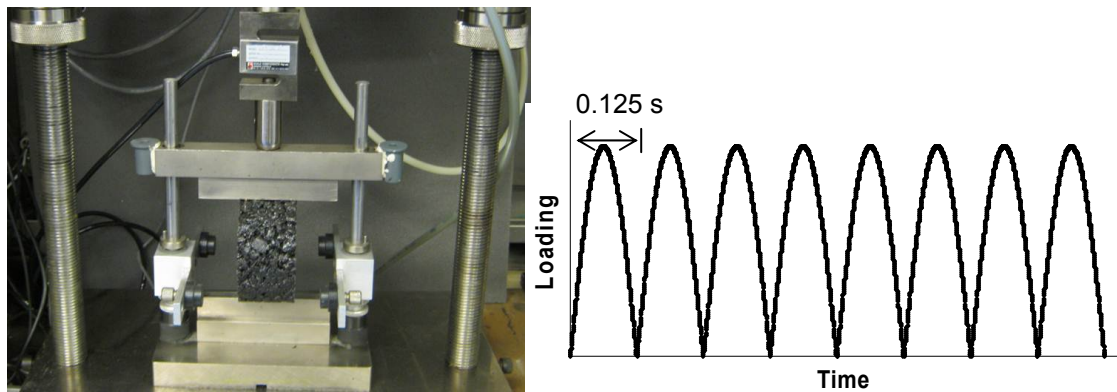


Figure 5.18: The set-up of ITF and loading configuration

To predict the fatigue life of these two mixtures at a reasonable stress range, the fatigue lives of both mixtures were measured at four different loading levels. After testing the fatigue life of the sample at each loading level, the regression fatigue lines of these two mixtures were determined according to the Equation 5.8:

$$N_f = k\sigma^{-n} \quad (5.8)$$

$$\sigma = \frac{2F}{\pi DH} \quad (5.9)$$

Where

N_f = the number of loading cycles to failure;

σ = the horizontal tensile stress at the specimen center (MPa);

k and n = fatigue regression constants;

F = the total applied vertical load at failure (N);

D = the diameter of specimen (m);

H = the height of specimen (m).

5.6.2 Fatigue life of porous asphalt concrete with 8% steel fiber 00

As 8% (by volume of bitumen) of steel wool type 00 was considered to be the optimal option for this induction heating application of steel fiber, the fatigue resistance of porous asphalt concrete with this percentage of steel wool type 00 was studied in this section. For comparison, the fatigue resistance of plain porous asphalt concrete was also investigated.

In the fatigue test, the vertical deformation of the sample during loading was monitored to indicate the development of damage during the fatigue process, because monitoring the variation of vertical deformation was much easier than measuring the change of stiffness.

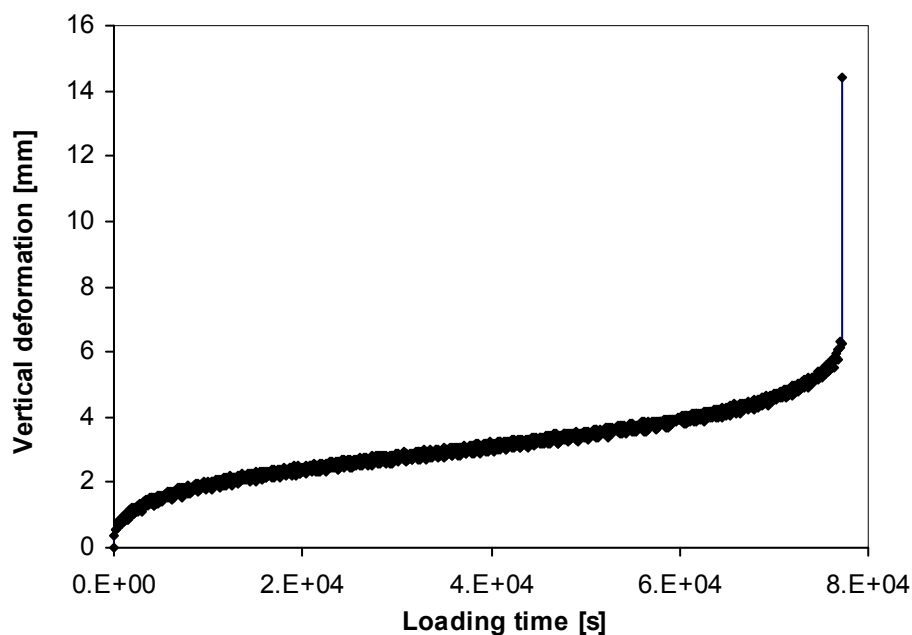


Figure 5.19: Typical fatigue curve of porous asphalt concrete

As an example, the vertical deformation versus loading time at 0.6 MPa for porous asphalt concrete with 8% steel wool type 00 is shown in Figure 5.19, where the development of vertical deformation can be seen as an indicator for damage development. The vertical deformation of the tested sample varies with the loading time and can be divided into three stages. The vertical deformation developed relatively fast at the beginning of the loading, this phenomenon could be attributed to the settlement of the load strips in the first few minutes of the test. After that, the vertical deformation increased slowly with the

assumption that damage accumulates due to the repetitive application of loads. At the final stage of fatigue, the vertical deformation grows very rapidly due to the fact that micro cracks merge into macro cracks.

Figure 5.20 compares the fatigue lines of both types of mixtures studied, with and without 8% steel wool type 00. It can be seen that porous asphalt concrete with 8% steel wool type 00 has a better fatigue resistance than plain porous asphalt concrete. At the same load levels, samples with 8% steel wool type 00 have a longer fatigue life, which means that the fatigue damage develops slower than in plain samples. At high load levels, it takes a very short time to break plain porous asphalt concrete, because damage develops very rapidly in it. The fatigue life of porous asphalt concrete with 8% steel wool type 00 is much longer, which indicates that these samples can resist higher fatigue loading without developing huge damage prone to failure.

However, it should be noted that some creep taking place during the test could have influenced the results.

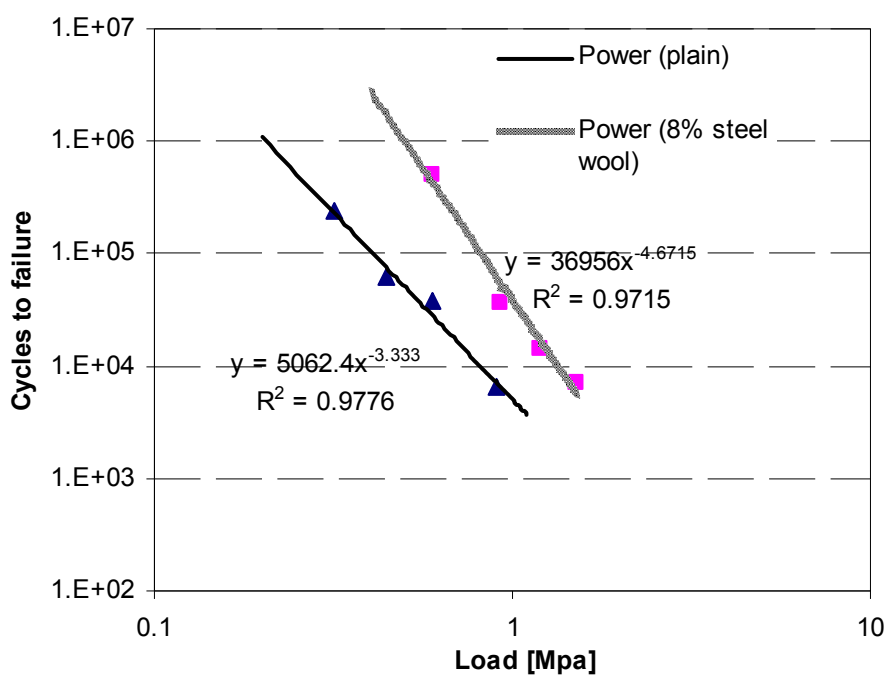


Figure 5.20: Fatigue lines of two mixtures, with and without 8% steel wool type 00 at 5 °C, 8 Hz

Table 5.5: Fatigue regression constants for plain mixture and mixture with 8% steel wool

Mixtures type	Fatigue regression constants	
	k	n
Plain mixture	5062.4	3.3330
Mixture with 8% steel wool	43094	4.7795

5.7 Nano indentation test

5.7.1 Test description

The Nano-indentation test was conducted to compare the mechanical properties of the mortar of porous asphalt concrete with or without steel wool at nanometer scale. The indentation modulus and hardness of the mortar can be measured with a nano indenter and higher indentation modulus and hardness can be seen as an indication of steel wool reinforcement.

To prepare the samples for nano indentation measurement, porous asphalt cores (40 mm) drilled from gyratory compacted samples were firstly impregnated with a two component epoxy resin under vacuum condition. With this impregnation process the voids were filled with epoxy and in this way the sample can be kept intact during the subsequent cutting and polishing process. Without impregnation, crumbling problems would happen during cutting and polishing (Scott, 1993). To impregnate the sample, it was placed in a paper cup and then placed into the vacuum barrel for 1 hour to allow the air come out so that the epoxy resin can impregnate the voids. After impregnation, the impregnated samples were kept in the vacuum condition for another 20 min to allow the epoxy resin to fill the very small voids and cracks. The impregnated sample is also shown in Figure 5.21.



Figure 5.21: The set-up of impregnation and the sample before and after impregnation

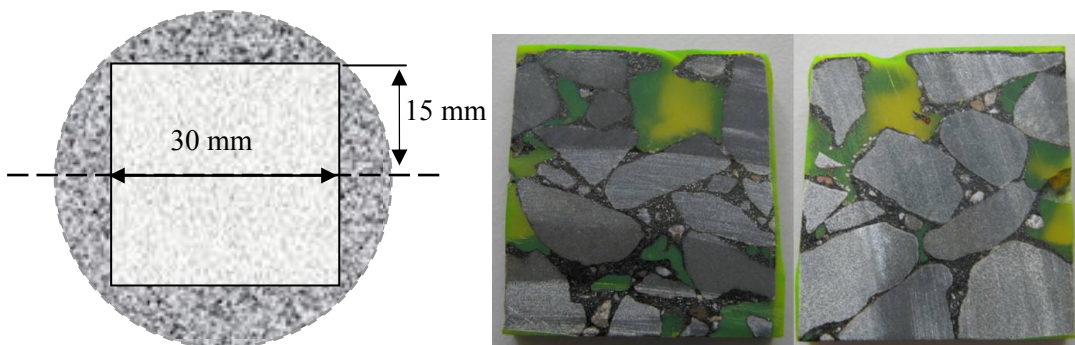


Figure 5.22: Typical blocks cut from each sample

As shown in Figure 5.22, two $30 \times 4 \text{ mm}^2$ blocks were cut from the middle of each impregnated sample. This dimension was determined according to the size of the cooling plate of the nano indenter.

After Cutting, the samples were ground and polished as follows:

Grinding phase:

- Grind the sample with 320 # silicon carbide paper for 3 minutes, ice water was used to lubricate the sample during grinding (Figure 5.23).
- Grind the sample with 800 # silicon carbide paper for 3 minutes.
- Grind the sample with 1200 # silicon carbide paper for 3 minutes.
- Grind the sample with 4000 # silicon carbide paper for 3 minutes.

Polishing phase:

- Polish the sample with $6\mu\text{m}$ diamond powder for 2 minutes.
- Polish the sample with $3\mu\text{m}$ diamond powder for 2 minutes.
- Polish the sample with $2\mu\text{m}$ diamond powder for 2 minutes.
- Polish the sample with $0.25\mu\text{m}$ diamond powder for 2 minutes (Figure 5.8).

After polishing, the sample is ready for Nano indentation testing. A Nano indentation sample is shown in Figure 5.24.

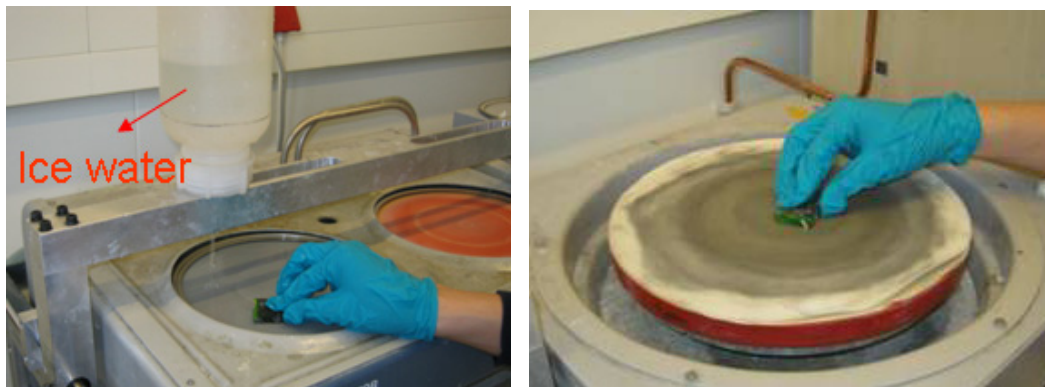


Figure 5.23: Grinding the sample with silicon carbide paper (left) and Polishing the sample with diamond powder (right)



Figure 5.24: Sample ready for nano-indentation testing

The equipment used for indentation testing in this research was an Agilent Nano Indenter G200 (as shown in Figure 5.25). This nano indenter G200 system consists of a microscope and an indenter. The microscope can be used to determine the testing points on the sample. The indenter was used to apply a load on the sample to determine the hardness and modulus of the sample. As shown in Figure 5.26, all the testing points were set in the mortar region to determine the indentation modulus and hardness, because steel wool will most probably influence the properties of the mortar.

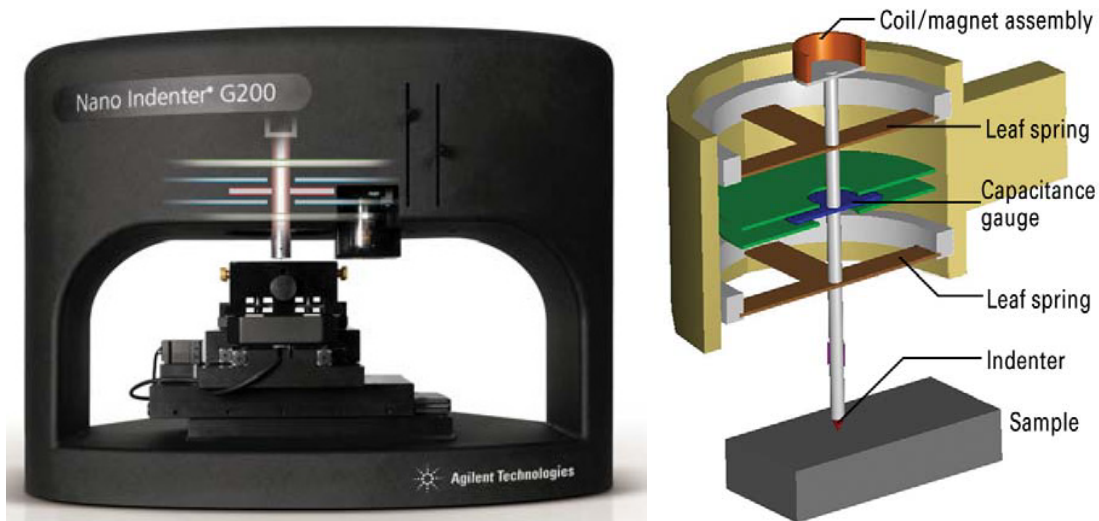


Figure 5.25: Nano Indenter G200 and its actuating and sensing mechanisms

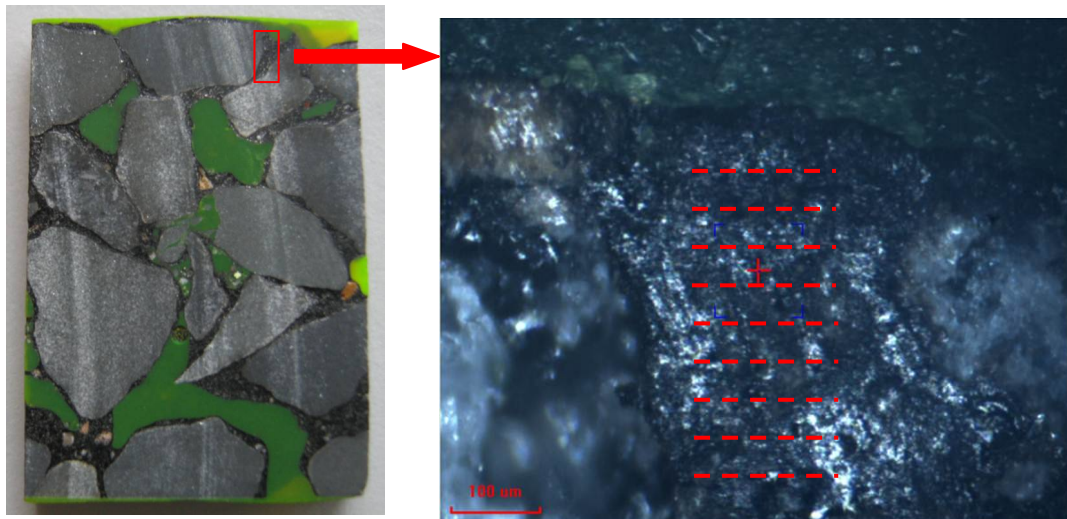


Figure 5.26: Nano indentation region on the sample (left) and indentation measurements on the sample (right)

The local indentation modulus and hardness of the sample were measured at a depth of 1000 nm at $-20\text{ }^{\circ}\text{C}$. Figure 5.27 shows a typical curve for an indentation test. Each measurement consists of three phases: loading phase, peak holding phase and unloading phase. The indenter was first positioned into the sample for 1000 nm, and then held at the peak load for 1 s and finally was unloaded. The recorded indentation data can be automatically

converted into two parameters, the hardness and the indentation modulus. The hardness is calculated by the maximum force divided by contact area. The modulus is calculated using the initial slope of the unloading branch in the force-penetration curve [Oliver and Pharr 2004, Testworks 2002].

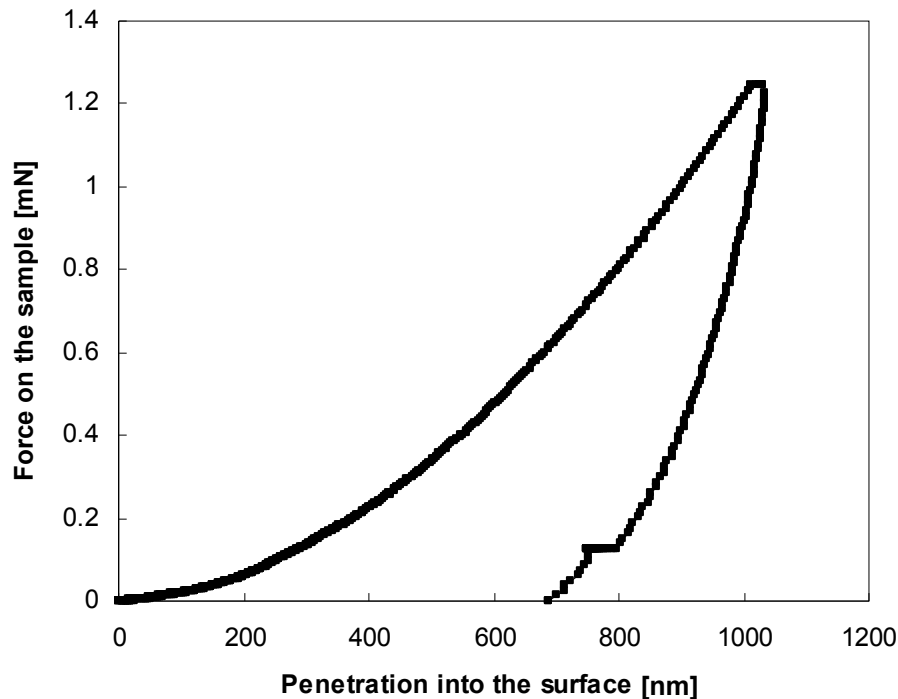


Figure 5.27: A typical indentation force-penetration curve for an indentation test

5.7.2 Indentation modulus and hardness of the mortar in porous asphalt concrete with steel fiber 00

To determine the indentation modulus and hardness of the mortar in the samples, 200 measurements were done in the mortar (at different locations) for each sample. The average values of the measurements are determined with exclusion of the modulus higher than 5 GPa (sand involved). The testing result is presented in Table 5.6.

Table 5.6: The average indentation modulus and hardness of the mortar in the samples

Source of the sample	Indentation modulus (Standard deviation)	Hardness (Standard deviation)
Plain porous asphalt	2.0 (0.87) GPa	24.2 (12.2) MPa
With 4% steel wool	2.2 (0.80) GPa	37.2 (13.4) MPa
With 8% steel wool	2.62 (0.67) GPa	38.2 (15.7) MPa

The nano indentation modulus and hardness of plain porous asphalt concrete is 2.0 GPa and 24.2 MPa, respectively. The addition of steel wool increases the nano indentation modulus and hardness of the mortar in porous

asphalt concrete. With 8% steel wool, the mortar shows much higher indentation modulus and hardness: 2.62 GPa and 38.2 MPa, respectively. The higher indentation modulus and hardness indicate that the addition of steel wool reinforces the mortar. The steel wool containing mortar also shows higher ductility in the previous indirect tensile strength test. So, it can be concluded that the mortar in porous asphalt concrete with steel wool is stronger and more ductile than the plain mortar, both improving the ravelling resistance of porous asphalt concrete.

5.8 Summary and Conclusions

The effects of steel fiber on the mechanical properties of porous asphalt concrete (Particle loss resistance, indirect tensile strength, water sensitivity, indirect tensile stiffness and fatigue, nano indentation modulus and hardness of the mortar) were studied in this chapter.

Porous asphalt concrete samples with steel fiber showed less particle loss in the Cantabro test, indicating that a moderate amount of steel fiber could increase the ravelling resistance of porous asphalt concrete. However, adding excess steel fiber will reduce the bitumen film thickness, causing a bad cohesion between the mastic components. Among the three different types of steel fiber (steel fiber type 1, steel wool type 00 and steel wool type 000), steel wool type 00 is most efficient to improve the particle loss (ravelling) resistance of porous asphalt concrete and the optimal content of steel wool is 8% (volume fraction of bitumen) to obtain the lowest particle loss value or highest particle loss resistance. Both ageing and water damage can decrease the ravelling resistance of porous asphalt by increasing its stone loss. Aged or water damaged samples with steel wool showed less particle loss than aged or water damaged plain samples.

Porous asphalt concrete samples with a moderate amount of steel fiber showed much higher indirect tensile strength than plain porous asphalt concrete, which is another indication that addition of steel wool for induction heating purposes can reinforce porous asphalt concrete rather than worsening its mechanical properties. Among the three different types of steel fiber, steel wool type 00 is most effective to increase the indirect tensile strength of porous asphalt concrete and 8% is the optimal content to obtain the highest indirect tensile strength and fracture work in porous asphalt concrete. Addition of steel wool above this optimal content results in a decrease of the indirect tensile strength and fracture energy.

For durability purposes, porous asphalt concrete should have a good ravelling resistance and high strength in itself. So, 8% of steel wool type 00 is considered as the optimal content for this application of steel wool.

Porous asphalt concrete with 8% steel wool type 00 shows higher indirect tensile strength ratio than plain porous asphalt concrete, meaning that adding steel wool to porous asphalt concrete also increases its resistance to water damage.

Addition of 8% steel wool type 00 to porous asphalt concrete increases its resilient stiffness and decreases its temperature dependency, which can probably improve the premature ravelling resistance of porous asphalt pavement.

Addition of 8% steel wool type 00 to porous asphalt concrete also increases its fatigue resistance in the indirect tensile fatigue test: porous asphalt concrete with 8% steel wool type 00 shows much longer fatigue life and can resist higher fatigue loading.

The addition of steel wool to porous asphalt concrete reinforces the mortar by increasing its nano indentation modulus and hardness. This is also a sign for less drainage in porous asphalt concrete with steel wool.

Chapter 6 Induction-Healing of Asphalt Mastic and Porous Asphalt Concrete with Steel Fiber

6.1 Induction healing of asphalt concrete

Asphalt concrete is a self healing material in itself [Little and Bhasin 2007, Jo and Richard 2001]. When subjected to rest periods, asphalt concrete has a potential to heal damage and restore its mechanical properties by closing the cracks inside [Qiu 2008]. The self healing capability of asphalt concrete has been shown both in laboratory tests and in the field since the 1960s [Bazin and Saunier 1967, van Dijk et al 1972, Castro and Sánchez 2006, Little and Bhasin 2007]. Bazin and Saunier found that asphalt concrete beams, tested until failure under uniaxial tensile loads could recover 90% of their original strength when they were rested under pressure at 25 °C [Bazin and Saunier 1967]. Meanwhile, they found that fatigue damaged beam samples could regain over a half of the original fatigue life after introducing a one day rest period to the failed samples and pressing the crack faces together with a small pressure during this rest period. The recovery of both strength and fatigue life were proof of healing caused by rest periods. After that, more laboratory experiments were done to study the strength recovery and the fatigue life extension of an asphalt mixture when rest periods were introduced to the loading. Laboratory experiments done by van Dijk, Castro and Little demonstrated that the fatigue life of an asphalt mixture could be extended when rest periods were introduced in the normally continuous loading test [van Dijk et al 1972, Castro and Sánchez 2006, Little and Bhasin 2007].

This chapter is partly based on:

Liu Q, Schlangen E, van de Ven M, García A. Induction healing of asphalt mastic and porous asphalt concrete. *Construction and Building Materials* 25(2011):3746-3752;

Liu Q, Schlangen E, van de Ven M. Evaluation of the induction healing effect of porous asphalt concrete through four-point bending fatigue test. *Construction and Building Materials* 29 (2012) 403-409;

Liu Q, Schlangen E, van de Ven M. Induction healing of porous asphalt concrete beams on an elastic foundation. Accepted for publication in *Journal of Materials in Civil Engineering*.

Healing of asphalt concrete was also shown in field experiments: Williams et al used surface wave measurement to assess the stiffness of a pavement before, immediately after, and 24 hours after loading passes. It was found that the stiffness recovered completely after 24 hours of rest [Williams et al 2001]. It was also reported by many researchers that cracks observed in winter time disappeared in summer time. As a consequence, in the shift factor required to translate the laboratory fatigue life into the in-situ fatigue life healing plays an important role [Lytton et al 1993].

However, the self healing capacity of asphalt concrete is not enough at service temperatures and the ageing of the binder further decreases the self healing capacity of asphalt concrete [Edward 2006]. It is well known that self healing of asphalt concrete is a temperature dependent phenomenon: an increase in the test temperature increases the healing rate of asphalt concrete and shifts the recovery response to a shorter time [Grant 2001, Uchida et al 2002, Kim and Roque 2006]. Grant concluded that healing occurs almost immediate at high temperature [Grant 2001]. Also Kim's work showed that asphalt concrete heals better at higher temperatures [Kim and Roque 2006]. Castro and Sánchez explained the self healing mechanisms of asphalt mixture by sol-gel theory: At high temperature, healing happens due to the transition of bitumen from sol to gel and, if the rest period is enough, damage recovery will be complete. At low temperature, rest periods do not allow the healing of structural damage created by the loading cycles and recovery would only be partial [Castro and Sánchez 2006].

Based on these mechanisms, induction heating of steel wool reinforced porous asphalt concrete will increase its self healing capacity by means of high temperature healing of bitumen (diffusion and flow). This healing mechanism is called induction healing in this research. It has been already proven previously that asphalt mastic and porous asphalt concrete with steel wool can be heated quickly with induction heating to temperatures above the maximum service temperature. For this reason, the objective of this chapter is to detect the induction healing effect of asphalt mastic and porous asphalt concrete induced by induction heating.

In this research, the basic approach to heal asphalt mastic and porous asphalt concrete consists of damaging the samples with cyclic loading, and then heating them via induction energy. Healing is defined as the difference between the mechanical resistance before and after heating. Strength recovery, stiffness recovery and fatigue life extension are used to quantify the healing capacity of asphalt mastic and porous asphalt concrete. Firstly, strength recovery of asphalt mastic was measured by successively breaking and healing asphalt mastic beams in three point bending test. After that, the stiffness and strength recovery and fatigue life extension of porous asphalt concrete cylinders and beams were studied with the indirect tensile test, bending test on elastic foundation and four point bending test, respectively, to show their induction healing effect. The overall test plan for the healing experiments is shown in Table 6.1.

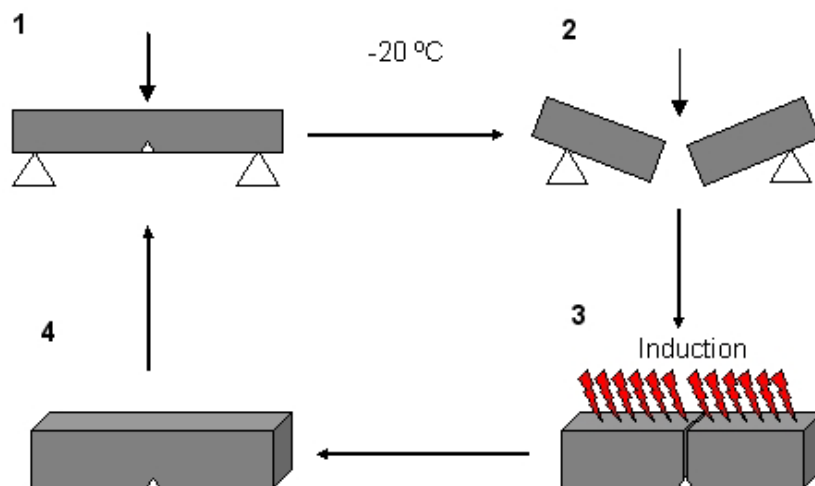
Table 6.1: Test plan for the healing experiments

Samples	Healing experiments
Asphalt mastic beams	Healing in three point bending test
Porous asphalt cylinders	Healing in indirect tensile test
Porous asphalt beams	Healing in bending test on elastic foundation
Porous asphalt beams	Healing in four point bending test

6.2 Healing of asphalt mastic beams in three point bending test

6.2.1 Test description

Healing of asphalt mastic beams (with 5.66% steel wool and sand-bitumen volume ratio 1.60) was characterized by testing the fracture resistance recovery of beam samples after fracture. The test procedure is shown in Figure 6.1, and also described in [Liu et al 2011]. First, five mastic beams were frozen at $-20\text{ }^{\circ}\text{C}$ and broken in three point bending test (as shown in Figure 6.2). This temperature was chosen to avoid permanent deformation and to create a brittle fracture in the sample. Then, both pieces were put together in the same mould where they were originally made and induction-heated for 2 minutes, until the temperature was close to $120\text{ }^{\circ}\text{C}$ at the surface of the samples. Finally, the samples were frozen to $-20\text{ }^{\circ}\text{C}$ and broken again by means of three point bending test. This process was repeated until the beams did not resist anymore loads. In these heating experiments, the distance between the coil of the induction heating machine and the top surface of the sample was about 30 mm, as shown in Figure 6.3.

**Figure 6.1:** Test procedures for strength recovery of mastic beam

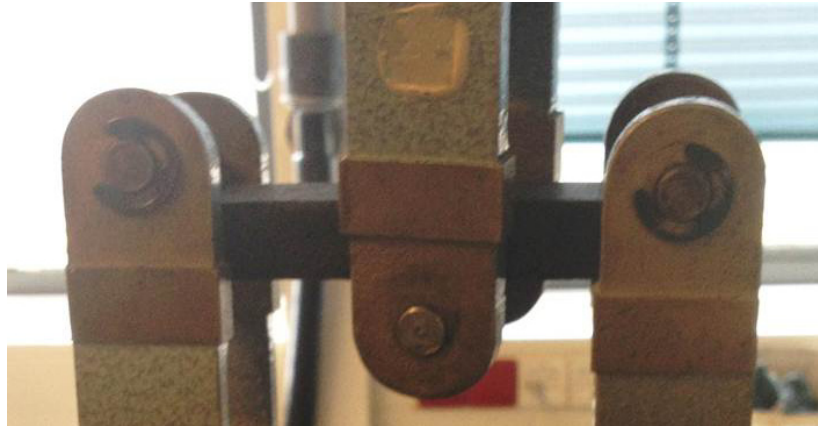


Figure 6.2: Three point bending set-up

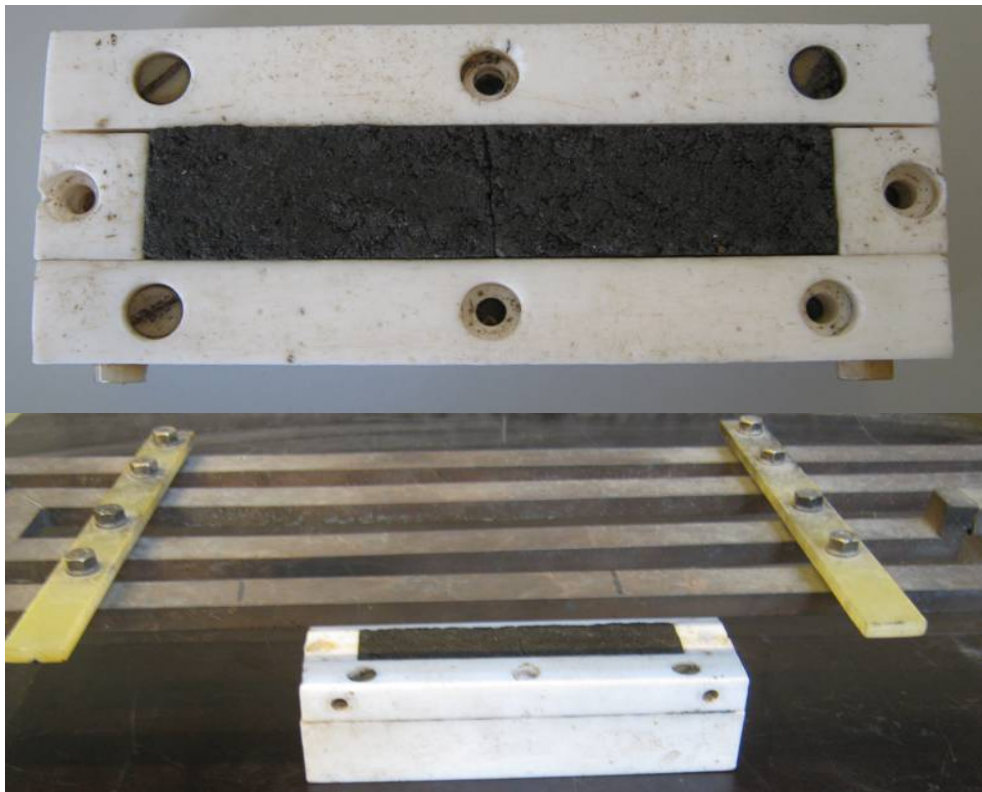


Figure 6.3: Fractured asphalt mastic beam in the mould (top) and induction heating of the fractured beam (bottom)

6.2.2 Test result

The evolution of the bending strength of asphalt mastic samples through successive damage-healing cycles is shown in Figure 6.4. This process was repeated until the accumulated damage in the material was too high to continue the healing process. In Figure 6.4, the strength recovery of the samples after the first healing is about 85% of the original value. In the successive cycles, it becomes stable at about 70% of the original value. Finally, it decreases sharply after the sixth healing step. The strength recovery is not complete for two reasons. The crack represents a weak point and the sample suffers some kind of structural damage due to the induction heating. It should be noted that the

specimens were completely fractured in two pieces, which might not fit perfectly together anymore. In the situation of porous asphalt concrete cylinders the intention is to apply healing at an early stage when there are only just micro-cracks (before major cracks develop).

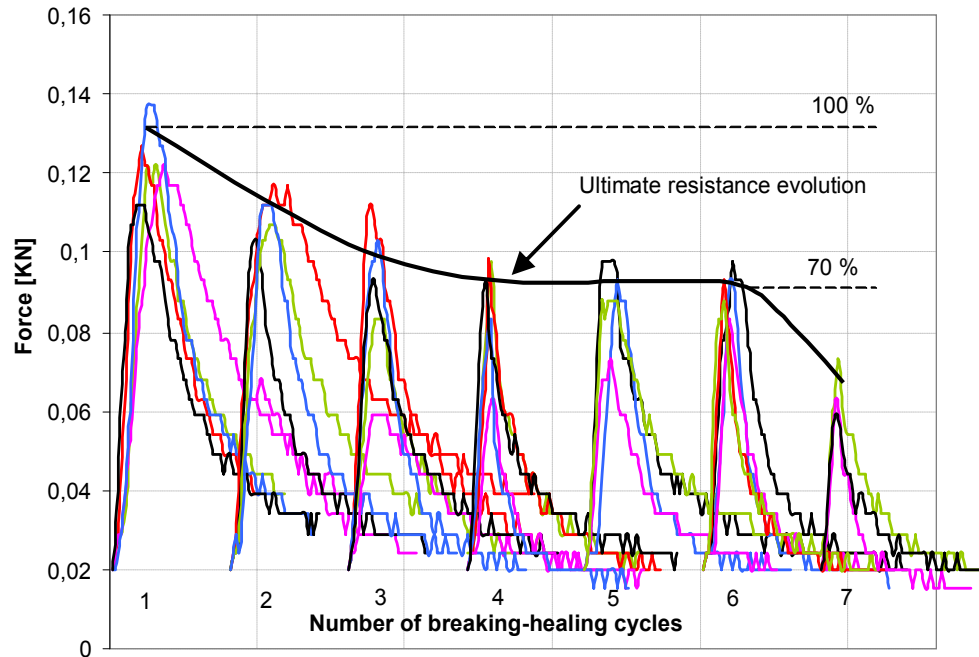


Figure 6.4: Load-displacement curves for samples with 5.66% steel wool 000 and sand-bitumen volume ratio 1.60 [García et al 2011, Liu et al 2011]

It could be seen that cracks disappeared because of the flow of bitumen during the induction heating process. It could also be observed that the volume of the mastic increased through the cycles, maybe because the heating was excessive and the air voids in the mixture suffered an expansion.

Based on the visual observations of crack closure and the strength recoveries shown in Figure 6.4, it can be concluded that asphalt mastic with steel wool can be healed very fast with 2 minutes induction heating.

6.3 Healing of porous asphalt concrete cylinders in indirect tensile fatigue test

6.3.1 Test description

To prove that damage in porous asphalt concrete can be healed via induction heating, indirect tensile fatigue tests at 5 °C were done, with rest periods to heat them with induction energy. The idea was to introduce some damage to the material, then the samples were induction-heated and they were rested for some time to see if the damage can be healed by induction heating.

For a first impression about the healing capacity of porous asphalt concrete in the beginning of the research, indirect tensile fatigue tests were conducted on the samples with 10% steel wool type 000 (volume fraction of

bitumen). For these tests, a 0.2 seconds haversine load followed by a rest period of 0.3 seconds at a frequency of 2 Hz was applied on the sample and a Poisson's ratio of 0.22 was assumed for this porous asphalt concrete to determine its resilient stiffness modulus. The maximum stress applied was 0.82 MPa (which is about 32% of the ITS of this material). Fatigue tests were stopped when the resilient modulus of the samples reduced to 70% or 80% of their original values. Then, the samples were induction-heated for 2 minutes and they were rested for 24 hours. Finally, fatigue tests were continued until the resilient modulus reduced to 70% and 80% of its initial value for the second time. After the tests, two values of loading cycles C_1 and C_2 , were obtained (Figure 6.5). The healing was characterized according to Equation 6.1.

$$HI = \frac{C_2}{C_1} \quad (6.1)$$

Where

HI = the healing index (%), where 100% means the entire healing of damage and 0% means no healing at all;

C_1 = number of the loading cycles for the first time loading;

C_2 = number of the loading cycles for the second time loading.

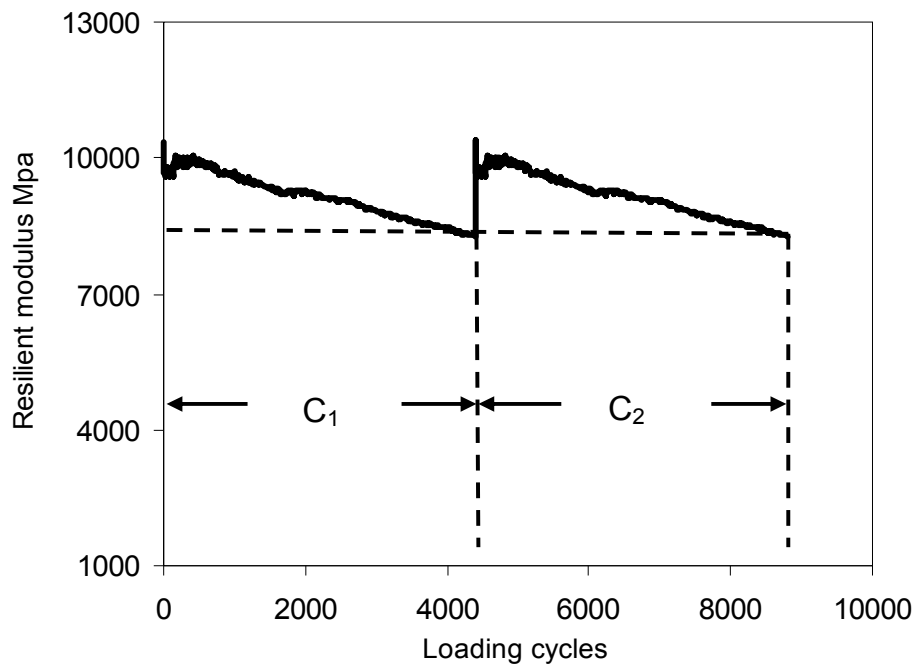


Figure 6.5: Fatigue recovery of porous asphalt concrete cylinder for resilient modulus reduction to 80%

During the test, the increasing horizontal deformation of the sample was out of the range of the linear variable differential transformer (LVDT). At such a moment, it is necessary to adjust the LVDT for the stiffness measurement, which means opening the temperature cabinet and affecting the temperature. So, the stiffness was not measured anymore in further healing test.

Second, to quantify the healing recovery for different rest periods, the stiffness recovery of fatigue damaged samples was measured. The comparison with the original stiffness was used as the healing indicator. The stiffness recovery testing procedure is as follows:

1) The original stiffness of the samples with 8% steel wool type 00 was measured at 5 °C.

2) A cyclic stress of 0.60 MPa (which is a medium load used to measure the fatigue line of the material in Chapter 5), at a frequency of 8 Hz, was applied to the samples for 3 or 8 hours, respectively.

3) The samples were rested for different times from 0 to 20 hours and the stiffness of each sample was monitored.

4) A third set of samples was induction-heated immediately after the 8 hours cycle loading and before the rest period. These samples were heated for 1.5 minutes; until their average surface temperature was 70 °C (the bottom temperature is around 30 °C). This heating process was repeated on both faces of the samples.

As shown in Figure 6.6, the fatigue loading time of the samples at 0.60 MPa was 77,191 s. For 3 or 8 hours loading, the fatigue damage level was 0.14 or 0.37 times the value of the fatigue time, respectively (in Table 6.2).

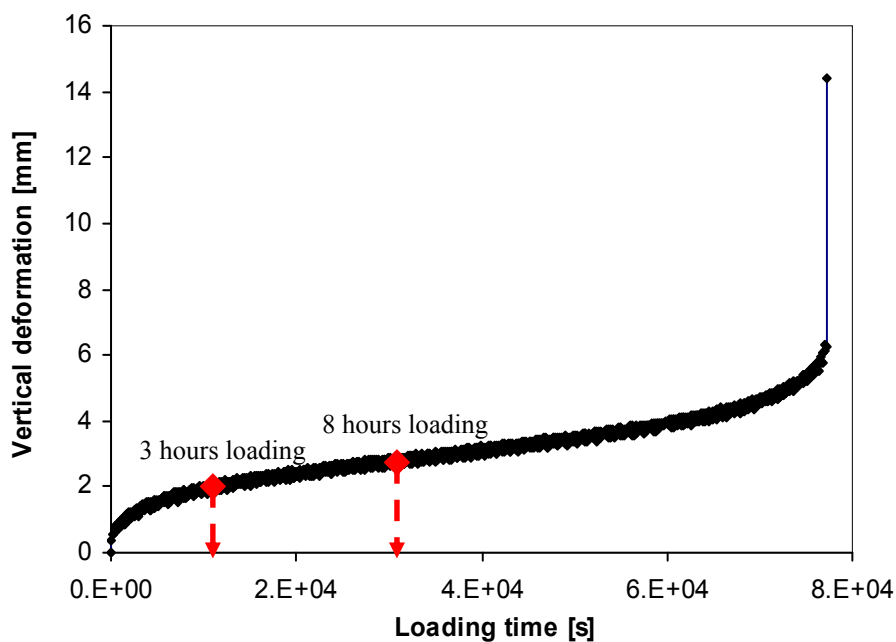


Figure 6.6: Damage loading time in stiffness recovery testing

Table 6.2: Fatigue damage level in stiffness recovery testing

Fatigue time	77,191 s	1
3 hours loading	10,800 s	0.14
8 hours loading	28,800 s	0.37

Third, fatigue life extension of porous asphalt concrete cylinders with 8% steel wool type 00 was also used to characterize the healing effect and to compare natural healing, with induction healing and with no healing at all.

These fatigue tests were done at 5 °C, and a maximum stress of 0.60 MPa. For comparison purposes, three sets of tests were prepared. This test procedure is as follows:

- 1) In the first set, fatigue experiments were run until failure.
- 2) In the second set, 8 hours of cyclic loading were applied to the samples; then they were let to rest for 20 hours and finally, fatigue tests were run until failure.
- 3) The third set of experiments was the same as the second one, with the difference that before the resting period, the samples were induction-heated for 1.5 minutes, until their mean surface temperature was 70 °C. This heating process was repeated in both surfaces of the samples.

6.3.2 Test results

6.3.2.1 Fatigue recovery of porous asphalt concrete cylinders

The healing indices of plain samples (without fibers) and samples with 10% steel wool 000 after 24-hour rest are shown in Table 6.3. Each one of these values has been obtained from three samples. In this table, $HI_{70\%}$ and $HI_{80\%}$ mean that fatigue tests are stopped for healing when the resilient modulus of the sample decreases to 70% and 80% of its original value, respectively. In both cases, samples with fibers show better healing than plain samples. Additionally, the healing effect of conductive samples increases after the induction heating is applied. In the case where fatigue tests are stopped for healing when the resilient modulus decreases to 70% of its original value, 11.4% and 18.0% of the damage in plain samples and in samples with steel wool is healed after 24 hours rest. But when a 1.5 minutes induction heating is applied on the samples with steel wool, 23.1% of the damage is healed. In this case, the healing is relatively low because structural damage, such as permanent deformation or broken aggregates, has developed. Induction healing can repair micro-damage, not structural damage, so in this case, it is too late to heal the damage in the asphalt concrete. But if fatigue tests are stopped when the resilient modulus reduces to 80% of its original value (to avoid structural damage in the sample), 52.1% and 83.8% of the damage in plain samples and in samples with fibers, respectively, are healed after 24 hours rest. Finally, with 2 minutes induction heating, the damage in samples with steel wool can be completely healed.

Table 6.3: Healing indexes of the samples studied

Samples	Plain samples	Samples with steel wool	
		Without heating	With heating
$HI_{70\%}$	11.4%	8.0%	23.1%
$HI_{80\%}$	52.1%	83.8%	100%

6.3.2.2 Stiffness recovery of porous asphalt concrete cylinders

Results quantifying the stiffness recovery (healing) after different rest periods are shown in Figure 6.7. The original stiffness of the samples with 8% steel wool type 00 is 14,654 MPa. In the case where the cyclic load is applied for 3 hours, the stiffness decreases to 11,809 MPa. The stiffness of the sample can recover to its original value after a rest time of 4 hours. This happens because the damage induced is low enough to allow natural healing. In the case where the cyclic load is applied for 8 hours, the stiffness decreases to 8,702 MPa. In Figure 6.7, it can be seen that the maximum possible stiffness, even after 20 hours healing is 11,544 MPa (78.8% of the original value). This happens because the induced damage is too high to be naturally repaired. Finally, in the case where the cyclic load is applied for 8 hours and induction heating is used, after 4 hours rest (which is needed to cool down the samples from 70 °C to 5 °C), the stiffness is almost fully recovered, with a value of 14,524 MPa (99.1% of the original stiffness). The stiffness does not change anymore over time, which means that full healing has been achieved due to induction heating.

Based on the stiffness recovery, it can be concluded that induction heating increases the healing capacity of damaged porous asphalt concrete samples with steel wool and that the rest time needed for full healing is reduced.

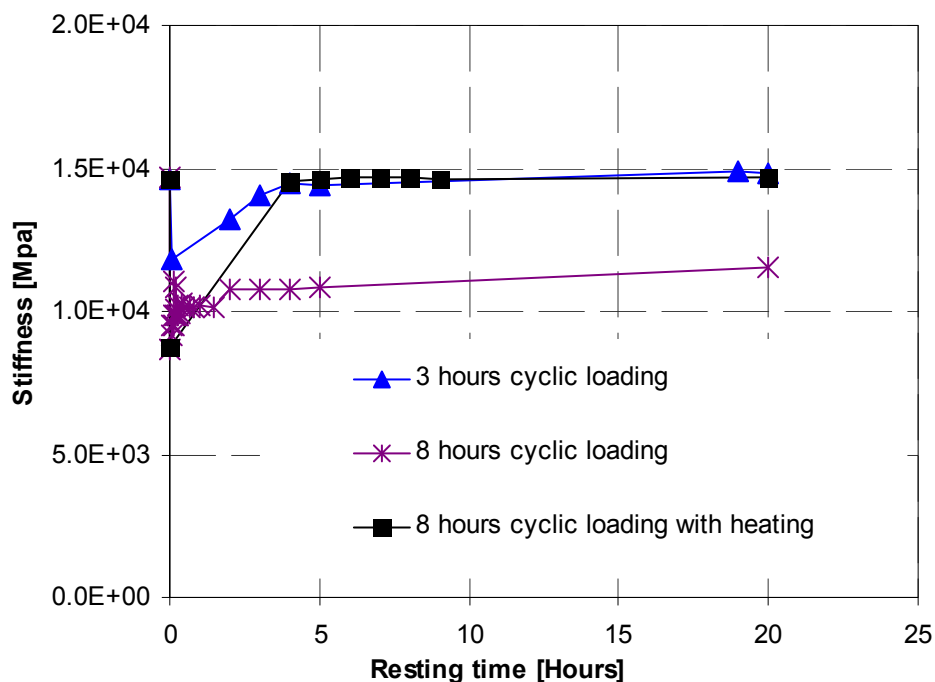


Figure 6.7: Stiffness recovery of porous asphalt concrete samples with 8% steel wool type 00 (ITT, 5 °C, 8 Hz)

6.3.2.3 Fatigue life extension of porous asphalt concrete cylinders

The comparison between natural healing, induction healing and samples with no healing at all is shown in Figure 6.8, where it can be seen that the total fatigue life of porous asphalt concrete, without rest periods is 617,528 cycles.

In the case where the samples are rested after 230,400 cycles fatigue loading, the fatigue life after the rest period is 486,864 cycles, which represents a final decrease of 21.16% in the total fatigue life of the material. This means that, although some recovery took place in the sample (no recovery would mean that the final decrease would be 37.31%, the equivalent time to 8 hours testing), it has not been complete. The overall fatigue life is 717,264 cycles, which is 99,736 cycles longer than the original fatigue lifetime without rest period. This extension H_1 , as shown in Figure 6.8, is caused by the rest period. However, 20 hours is a very unrealistic time to let the pavement heal in a real life situation. In the case when induction heating is applied after 8 hours fatigue loading, the total fatigue life of the specimens after the rest period is 622,296 cycles, which almost coincides with the total life when compared to the fatigue experiments without rest periods. In this case, the specimens are completely recovered. The whole fatigue life in this case is 852,672 cycles, which is 235,144 cycles longer than the original fatigue life. This fatigue life extension H_2 is caused both by induction heating and by rest periods. The difference between H_2 and H_1 is 135,408 cycles, which is the fatigue life extension H_3 caused by induction heating. So, it can be concluded that the fatigue life of porous asphalt cylinder is extended by induction healing. It is expected that the induction healing effect will be more significant if the samples suffer a shorter rest period than 20 hours.

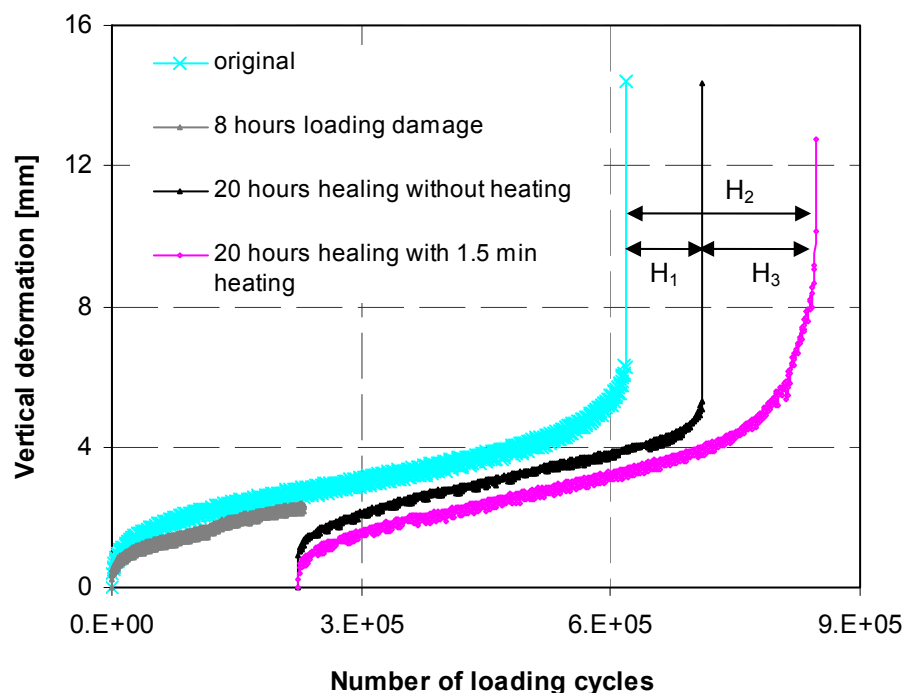


Figure 6.8: Fatigue life extensions of porous asphalt concrete samples with 8% steel wool type 00 (ITT, 5 °C, 8 Hz)

6.4 Healing of porous asphalt concrete beams on elastic foundation setup

6.4.1 Background of beam on elastic foundation test

The beam test on elastic foundation has been reported by many researchers. Majidzadeh conducted fatigue test of beams on an elastic foundation (soft art gum rubber) to characterize the fatigue resistance of asphalt mixes. Majidzadeh found that the creep effect during fatigue test can be neglected due to the elastic foundation [Majidzadeh et al 1971 and 1976]. With respect to the fatigue crack growth, the parameter n of Paris's law obtained from beam on elastic foundation fatigue test was around 3.7, which was in agreement with what was expected from theory [Molenaar 1983].

Molenaar also investigated the fatigue behavior of asphalt beams on an elastic rubber foundation [Molenaar 1983]. He concluded that the asphalt beam should be glued on the rubber foundation in order to simulate full contact and full friction. When no glue was used, partial slip could occur between the beam and the rubber. Due to the full contact, the crack propagation speed under a symmetric load decreased strongly when the crack length reached about 60% of the height of the beam; then the crack entered the compression zone and no further propagation was observed.

In addition, Molenaar conducted the beam on elastic foundation tests to investigate the effect of a stress absorbing membrane interlayer [Molenaar et al 1986]. Both vertical deflection and horizontal tensile displacements were monitored during the test and a special clamp with a strain gauge was developed to monitor the vertical crack propagation displacement. It was observed that the crack was retarded by using the stress absorbing membrane interlayer. A similar setup was adopted successfully by Brown [Brown et al 2001] and Rowe [Rowe et al 2009] for characterizing reinforcing interlayer materials.

Furthermore, Roesler and Gaedicke conducted the three point bending test on notched concrete slabs and beams placed on a low-plasticity clay foundation to study crack initiation, crack growth, and the flexural load capacity of concrete slabs [Gaedicke 2009, Roesler and Gaedicke 2010]. Compared with results of simply supported beams, the maximum load of the beam on elastic foundation was observed to be higher because of the presence of the elastic foundation.

Qiu conducted the beam on elastic foundation test to investigate the healing potential of asphalt mixtures [Qiu et al 2011]. He states that the notched beam on an elastic foundation setup is useful for cracking and healing investigation for two reasons: (a). The elastic foundation absorbs most of the deformation, which eliminates the influence of permanent deformation and helps for healing investigations; (b). After a loading-unloading cycle, the elastic foundation will help to close the crack during unloading thus support the healing process of asphalt mixtures.

A notched beam on elastic foundation setup is used to qualify the healing properties of porous asphalt concrete with steel wool in this study.

6.4.2 Beam on Elastic Foundation Setup

The beams used in this beam on elastic foundation test have a size of 50 mm × 50 mm × 450 mm. The beams used in this research were prepared by the construction contractor Heijmans-Breijn with the same materials used for the induction healing trial section on Dutch motorway A58. The mixtures of the beams consisted of standard porous asphalt concrete PA 0/16 and 4% steel wool type 00 instead of the optimal content of 8% (volume fraction of the bitumen). It was found in the Heijmans-Breijn's asphalt plant that it was difficult to disperse 8% steel wool to the mixture evenly. Considering the fact porous asphalt concrete with 4% steel wool was also heatable with induction heating previously shown in Table 4.1, the percentage of steel wool was reduced to 4% (1.3% by mass of the total mixture) to solve the mixing problem and reduce the cost of the material.

A small notch was created by cutting in the middle of the beam with 4.5 mm in width and 20 mm in depth. White paint was used to make the cracks visible in the subsequent tests. The notched beam on elastic foundation setup is shown in Figure 6.9.

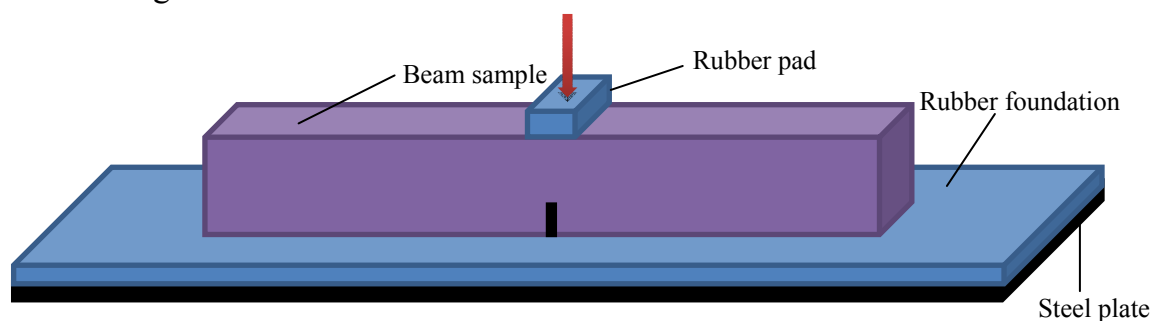


Figure 6.9: Beam on elastic foundation setup

A Neopreen rubber, with a hardness of 40° shore and a thickness of 20 mm, was selected as the elastic foundation. The Young's modulus of this rubber foundation is 6.5 MPa and its Poisson's ratio is 0.5.

Another type of rubber with a size of 20 mm × 10 mm × 50 mm, a Young's modulus of 15 MPa and Poisson's ratio of 0.5 was used as a loading pad on top of the beam (See Figure 6.9) to prevent local damage to the beams around the loading area.

A steel plate with a thickness of 10 mm was used as a support to the rubber. The rubber-steel interface was fully glued with a Rengel SW 404 glue for its excellent workability.

The porous asphalt beam was not glued to the rubber foundation, because significant permanent deformation at the loading region of the beam was observed in the fracture test when the beam was fully or half glued to the rubber foundation (porous asphalt beam is more susceptible to permanent deformation and big displacement is needed to fracture the beam). Without glue in the beam-rubber interface, no permanent deformation occurred in this bending test on elastic foundation.

The loading setup of the beam on elastic foundation test is shown in

Figure 6.10, where an LVDT placed near the loading area is used to record the displacement of the beam during the test, which is different from the displacement of the loading cell because of the rubber loading pad.

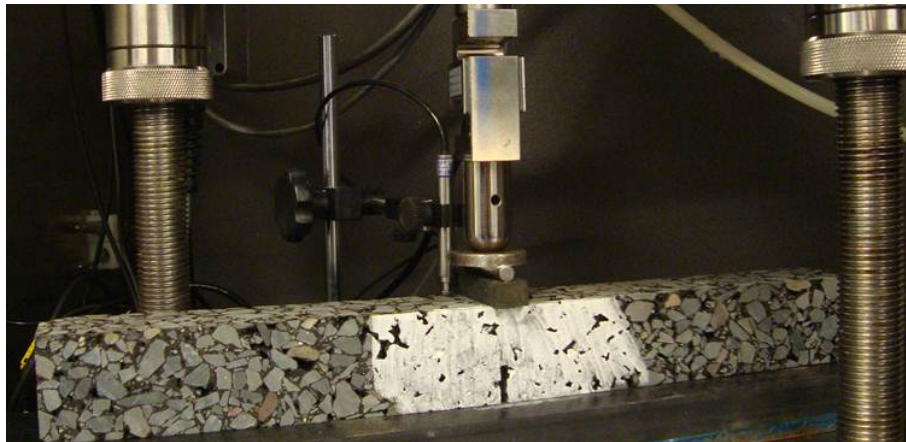


Figure 6.10: Loading setup of beam on elastic foundation test

6.4.3 Test procedure for beam on elastic foundation test

The test procedure for the beam on elastic foundation test consists of three steps: 1) The notched porous asphalt beam is fractured on the elastic foundation at 5 °C with a displacement speed of 50 mm/min (the fracture surfaces of the sample are shown in Figure 6.11); 2) The fractured beam is heated and rested for 6 hours at 5 °C or rested for 6 hours directly at 5 °C; and 3) The healed beam is fractured again with the same loading speed.

The loading was applied on the elastic rubber pad at a speed of 50 mm/min, causing a smaller displacement rate of the beam. The displacement rate of the beam at the loading area was 5.37 mm/min, recorded by LVDT.



Figure 6.11: Fractured beam (with broken stone)

To heal the fractured beam (shown in Figure 6.11) with induction heating, the two fractured pieces were put together and heated with the induction machine. Figure 6.12 shows the placement of heating of the fractured beam, where the beam is placed perpendicular to the coil of the induction generator. The notch is under the center of the coil and the distance between the

beam and the coil of the induction generator is 10 mm, resulting in a heating speed of $0.34\text{ }^{\circ}\text{C/s}$ at the surface of the beam.



Figure 6.12: Induction heating of a fractured beam

6.4.4 Test results

To study how induction heating influences the healing rate of the fractured beams, the fractured beams were induction-heated to different temperatures ($30\text{-}50\text{-}70\text{-}85\text{-}100\text{ }^{\circ}\text{C}$), respectively, and then the corresponding fracture resistance of the heated beams was tested after cooling.

The original and the healed loading force-loading time curves are compared in Figure 6.13, where the recovered flexural resistance of the fractured beam can be used as an indicator of healing. The healing index (recovered flexural resistance ratio) was defined as the recovered bending resistance f_2 divided by the original bending resistance f_1 .

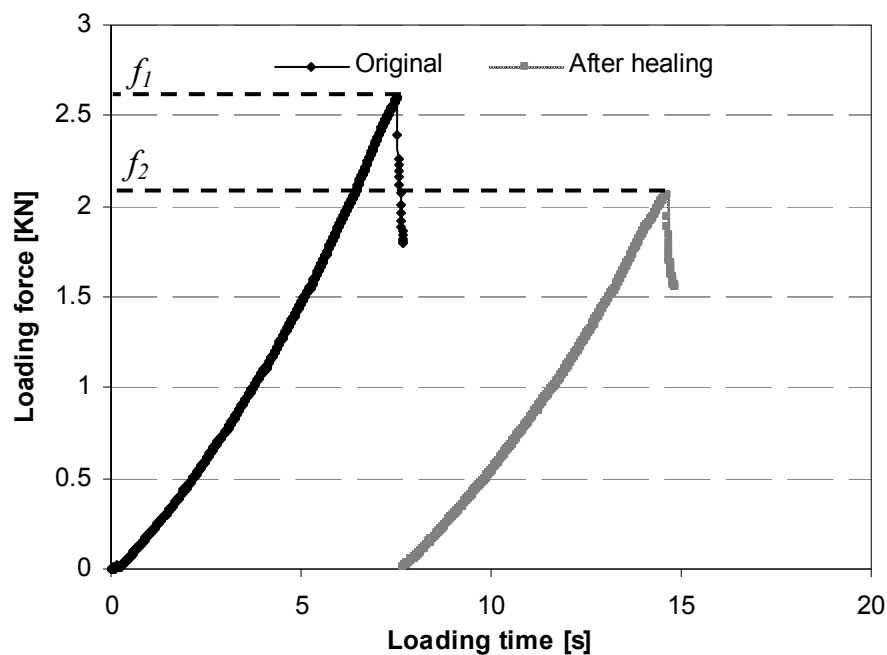


Figure 6.13: Definition of healing in fractured beam: healing ratio = f_2/f_1

Figure 6.14 and Figure 6.15 present the fractured beam before and immediately after induction heating (85 °C). It can be seen in Figure 6.15 that the crack in Figure 6.14 disappears after heating, meaning that induction heating heals the crack.

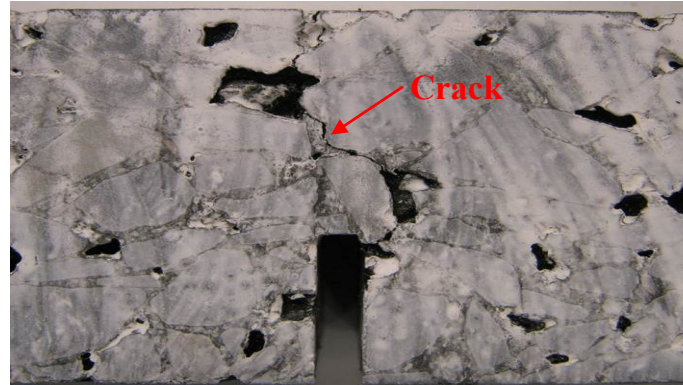


Figure 6.14: Fractured beam before induction heating



Figure 6.15: Fractured beam immediately after induction heating

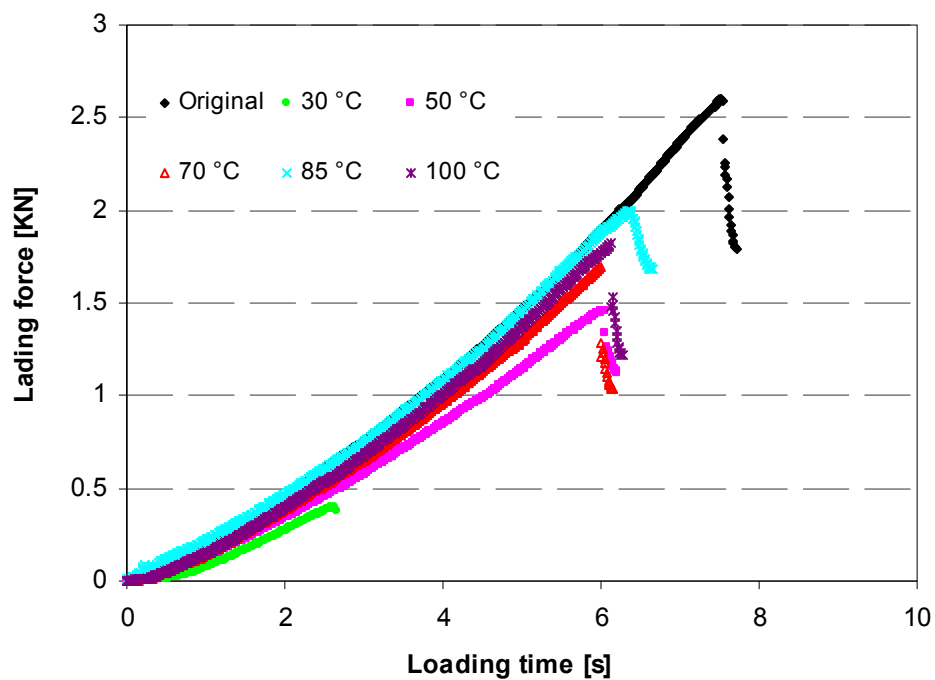


Figure 6.16: Typical loading curves of original beam and induction healed beams

Figure 6.16 shows the typical fracture curves of the original beam and healed beam after different induction heating temperatures. The corresponding healing rates (recovered fracture resistance ratios) are compared in Figure 6.17. Without induction heating, the fractured beams cannot heal themselves at 5 °C. Heating the fracture beams to 20 °C doesn't cause any healing either. As a thermally activated capillary flow of bitumen, healing of asphalt concrete is higher at higher temperatures. So, the recovered fracture resistance of the beam increases from 14.9% to 78.8% when the heating temperature is increased from 30 °C to 85 °C. The optimal heating temperature for the highest recovered fracture resistance is 85 °C. The maximum healing ratio is 78.8%, not complete. The reason for this probably lies in the fact that some aggregates were broken during the test, which cannot be healed. The temperature gradient also contributed to this limited healing rate. Overheating will cause structural damage to the sample. Swelling of the mortar can be observed in the samples that are heated to 100 °C, which explains why the healing rate at 100 °C is lower than that at 85 °C. Binder drainage problem may also occur in these overheated samples. This also decreases the beneficial effect of heating.

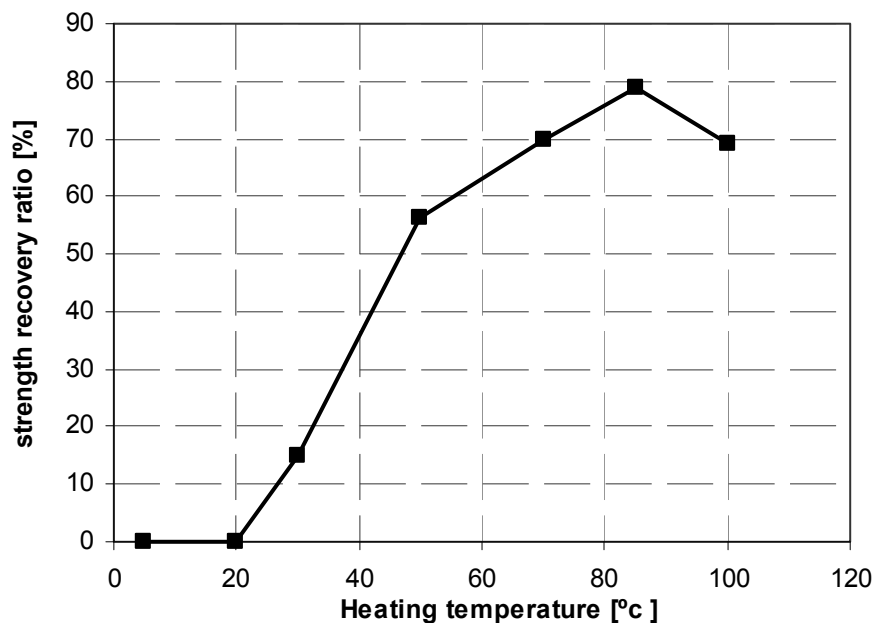


Figure 6.17: Strength recovery ratios with different induction heating temperatures

To prove that induction heating can be repeated when cracks appear again, the cyclic fracturing-healing process was repeated on the sample for five times. The heating temperature was fixed at 85 °C to obtain the best healing effect. Figure 6.18 shows the results of the cyclic fracturing-healing test. In Figure 6.18, the healed fractured beams show equal fracture resistance, which means that repeated induction heating doesn't decrease the healing ratio of the fractured beam. It also proves that there is no accumulated damage in the sample during the cyclic fracturing-healing test on elastic foundation. Otherwise, the first time healing ratio would be higher than the latter ones.

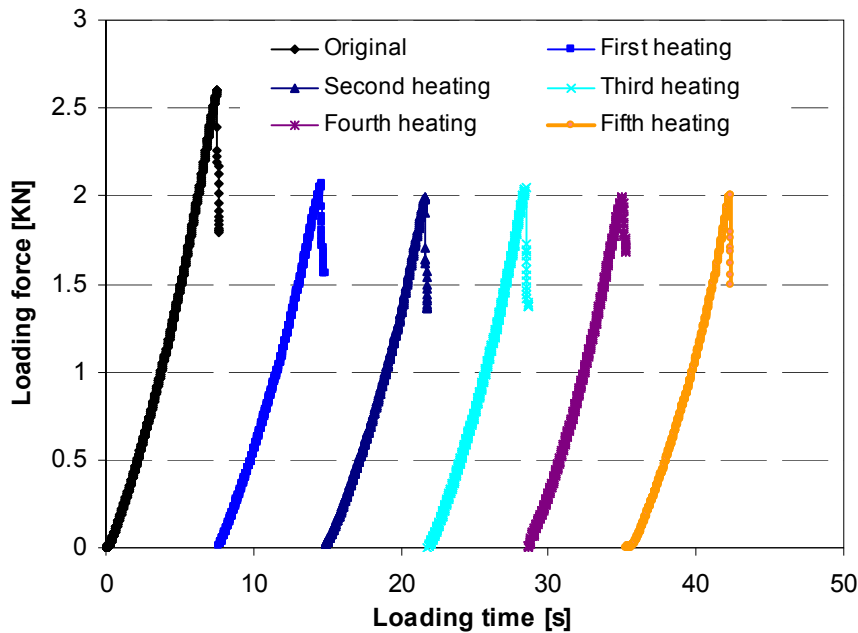


Figure 6.18: loading force-loading time curves of cyclic fracturing-healing test with 6 hours rest after induction heating

6.5 Healing of porous asphalt concrete beams in four point bending fatigue test

6.5.1 Fatigue resistance of porous asphalt concrete beams with steel wool

The four point bending fatigue test was done on porous asphalt concrete beams with steel wool to evaluate their fatigue resistance and effect of induction healing [Liu et al 2012]. The dimension of the porous asphalt concrete beams used in this research was 50 mm × 50 mm × 400 mm.

Before healing measurements, the fatigue resistance of the beams was firstly determined in four point bending fatigue test according to European Norm EN 12697-24. The purpose of this test was to obtain the fatigue life of the beams in microstrain controlled test so that the damage content in the subsequent healing test could be calculated. The schematic diagram and set up of this test was presented in Figure 6.19 and Figure 6.20 respectively.

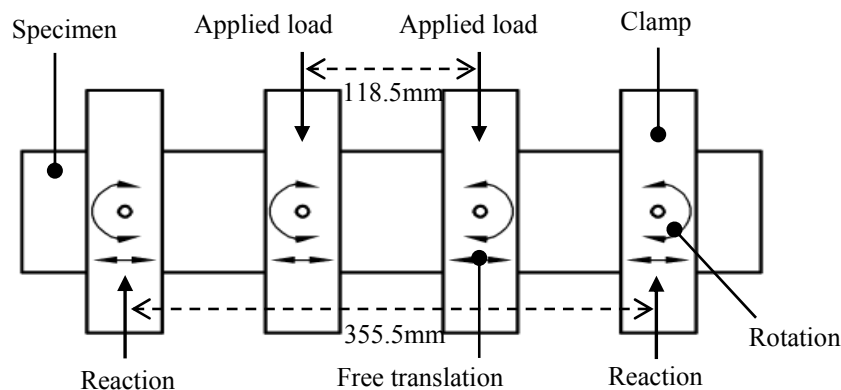


Figure 6.19: The schematic diagram of four point bending fatigue test



Figure 6.20: The set-up of four point bending fatigue test

The test was done at 20 °C with a frequency of 8 Hz (the maximum frequency of the machine). The initial value of the flexural stiffness modulus was calculated from the measured values for force, displacement and phase lag after hundred cycles ($n = 100$) with the following equations:

$$\varepsilon = \frac{12\delta h \times 10^6}{(3G_o^2 - 4G_I^2)} \quad (6.2)$$

$$\sigma = \frac{G_o P}{Wh^2} \quad (6.3)$$

$$S = \frac{1000 \times \sigma}{\varepsilon} \quad (6.4)$$

Where,

ε is the maximum microstrain applied on the beam, σ is the peak deflection at the center of the beam, h is the average beam length (mm), G_o is the outer support length (355.5 mm), G_I is the inner support length (118.5 mm), σ is the maximum tensile stress (kPa), P is the peak force (kN), W is the average beam width (mm), and S is the flexural stiffness of the beam (MPa).

The fatigue test was continued until the calculated stiffness modulus dropped to half its initial value. After testing the fatigue life of the beams at 6 strain amplitudes (150, 200, 250, 300, 350 and 400 microstrain) under sinusoidal displacement controlled testing, the fatigue line of the beam was determined according to the Equation 6.5:

$$N_f = a\varepsilon^{-b} \quad (6.5)$$

Where,

N_f = the number of loading cycles to fatigue;

ε = the microstrain amplitude used in fatigue testing;

a and b = fatigue constants.

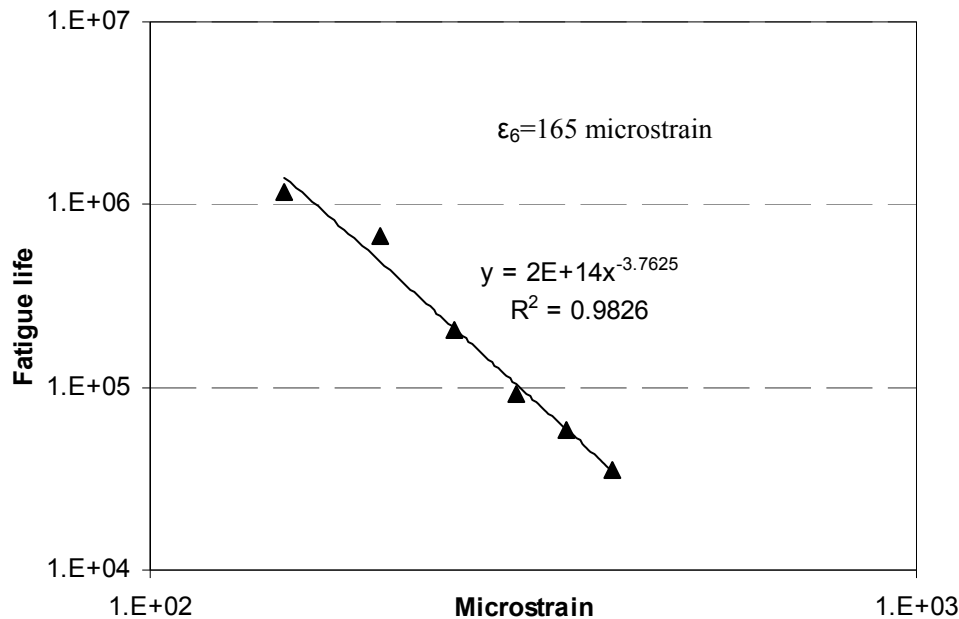


Figure 6.21: Four point bending fatigue line of the porous asphalt concrete beams with 4% steel wool 00 (volume fraction of bitumen)

The fatigue line of the porous asphalt concrete beams is shown in Figure 6.21 and the initial strain corresponding with a fatigue life of 10^6 cycles ϵ_6 was determined according to the fatigue line. The ϵ_6 of this mixture with 4% steel wool type 00 equals to 165 microstrain. To evaluate the fatigue resistance of this mixture, dense graded asphalt mixtures are used as references, because there are no plain porous asphalt beams to be tested and no references on porous asphalt concrete. Pang et al conducted four point bending fatigue test on 3 mixtures at 20 °C / 10 Hz and obtained ϵ_6 ranging from 158, 168 to 184 microstrain [Pang et al 2010]. Compared with the results from Pang's work, the fatigue resistance of this porous asphalt is quite good, comparable to that of dense graded asphalt concrete.

6.5.2 Natural healing and induction healing of porous asphalt concrete beams

Firstly, to compare natural healing and induction healing and to analyze the influence of the strain amplitude on the healing rate, the fatigue life extension of the beams after natural rest periods and induction heating were studied at four different strain amplitudes (200-250-300-400 microstrain), at a frequency of 8 Hz. The test procedure is to fatigue the beam in four-point bending fatigue test until its flexural stiffness reduces to 50% of the initial value, then rest the beam for 18 hours directly or heat the beam to 70 °C with an induction heating machine and then rest it for 18 hours, and finally damage the beam again with fatigue loading. The second time fatigue life can be seen as a healing indicator caused by resting and induction heating. As shown in Figure 6.22, the healing index (fatigue life extension ratio) is defined as the extra fatigue life Δf after healing divided by the original fatigue life f .

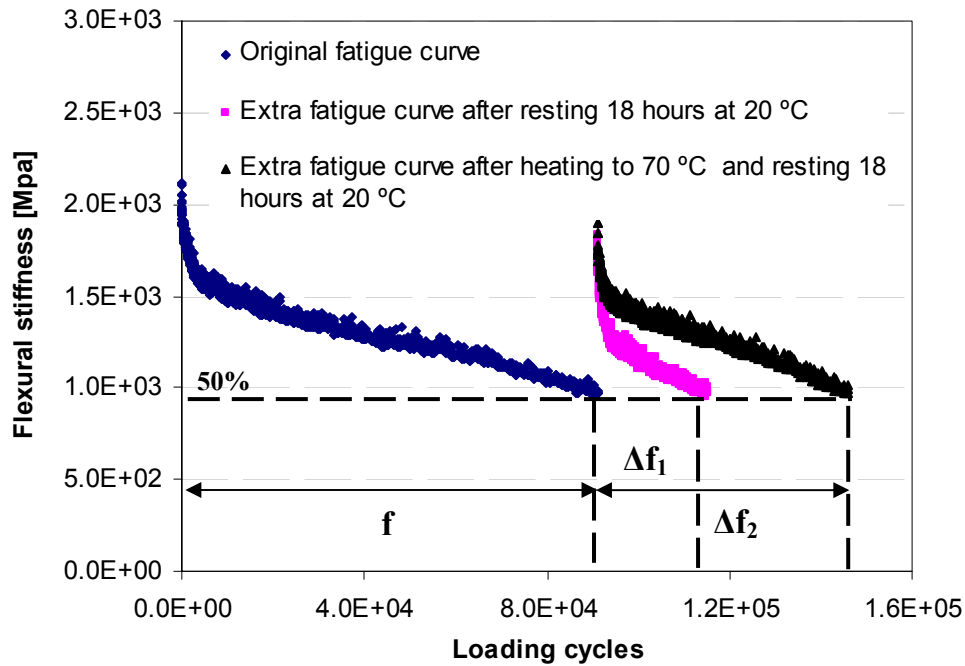


Figure 6.22: Definition of fatigue life extension ratio ($\Delta f/f$) in four point bending fatigue test

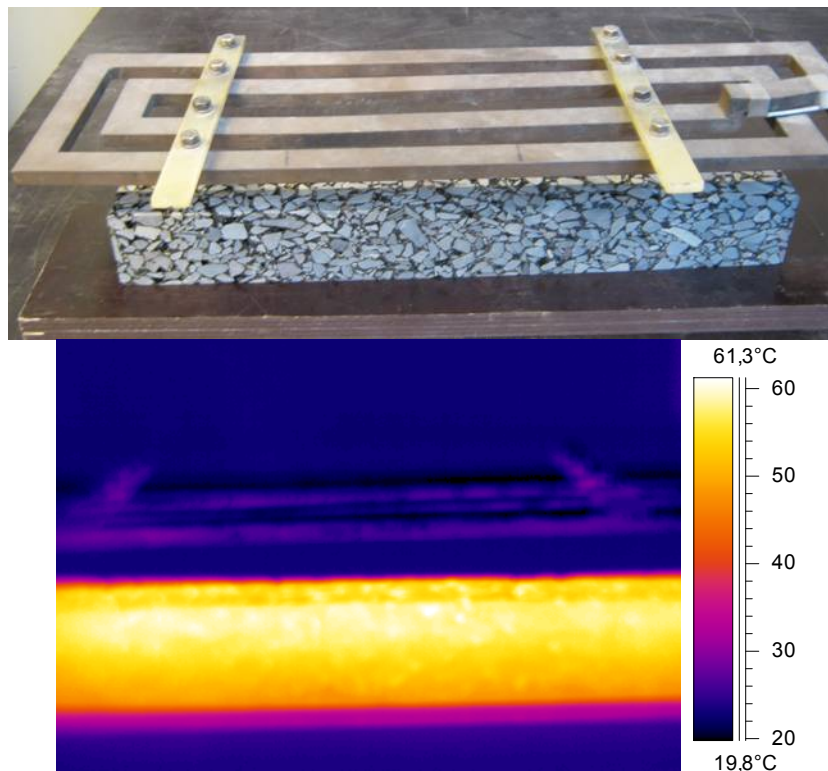


Figure 6.23: The setup and image of induction heating

To better understand the induction heating system, an induction heating image of a porous asphalt concrete beam is shown in Figure 6.23. As the main goal of this induction heating approach is to prevent ravelling at the pavement surface, the surface temperature of the pavement after heating is most important. So, in this experiment the focus is on the heating speed at the top

surface of the beams during induction heating. It is already found that the samples can be heated much faster when they are closer to the coil of the induction heating machine. To get a high induction speed, the distance will be fixed at 10 mm when heating the samples in subsequent healing tests, where an induction heating speed of 0.34 °C/s can be obtained. Given this heating speed, the heating time needed to get a certain temperature can be calculated. For instance, to increase the surface temperature from 20 °C to 85 °C, the beams should be heated for 191 seconds. The heating speed can be enhanced a lot with an optimized induction heating machine.

The fatigue life extension ratios of porous asphalt concrete beams with natural healing (no heating/only rest) and induction healing (with induction heating) are plotted in Figure 6.24. It can be seen that under all 4 microstrain amplitudes induction heating increases the fatigue life extension ratios of the beams. However, these healing increments are not very high. The first reason for this is that the temperature increment after induction heating is very limited, because the temperature decreases to rest temperature 20 °C very quickly in 3 hours. The temperature difference is only in the first 3 hours, so the healing difference in these two cases is not very big. It is expected that the healing increment will be pronounced when the rest period takes place at lower temperatures. Another reason for the low increment of healing can be the temperature gradient in the sample. The sample is damaged over its full height, but induction heating tends to only heal the damage in the top part of the beam, where the temperature is much higher than in the lower part after induction heating. However, the healing of the surface is just what we need to prevent ravelling at the pavement surface, without damaging the structure in the lower part.

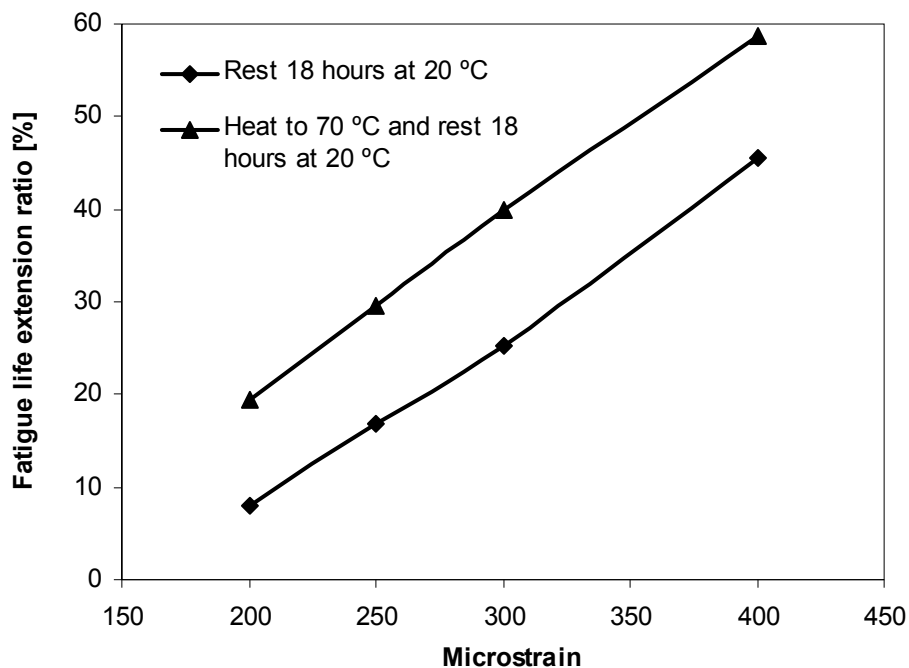


Figure 6.24: Natural healing and induction healing of the samples under different micro strain amplitudes

It is also clear from Figure 6.24 that the fatigue life extension ratio is highly strain dependent. The fatigue life extension ratio is higher at higher microstrain amplitudes for both natural healing and induction healing. This can be explained with the amount of the accumulated dissipated energy during the fatigue damage process, which is the cause of the damage in the sample and can be obtained automatically. There is less energy dissipated at higher microstrain amplitude, resulting in less damage in the sample. Besides, the thixotropic effect is more apparent at higher strain amplitudes, also causing less real fatigue damage in the sample [Shan et al 2011]. So it is easier to heal the fatigue damage in the fatigued beams under higher strain amplitude condition.

6.5.3 Healing of porous asphalt concrete beams at different temperatures

To quantify the effect of temperature on the healing rate and to determine the optimal heating temperature, the extra fatigue life of the damaged beams with different heating and rest temperatures was investigated. For that, the beams were fatigued with constant fatigue loading strain amplitude of 300 microstrain (8Hz). Then, the beams were induction-heated to 70 °C/85 °C/100 °C and rested at 20 °C for 18 hours or directly rested at 20 °C/5 °C for 18 hours. Finally the fatigue life of beams was measured again with the same strain amplitude.

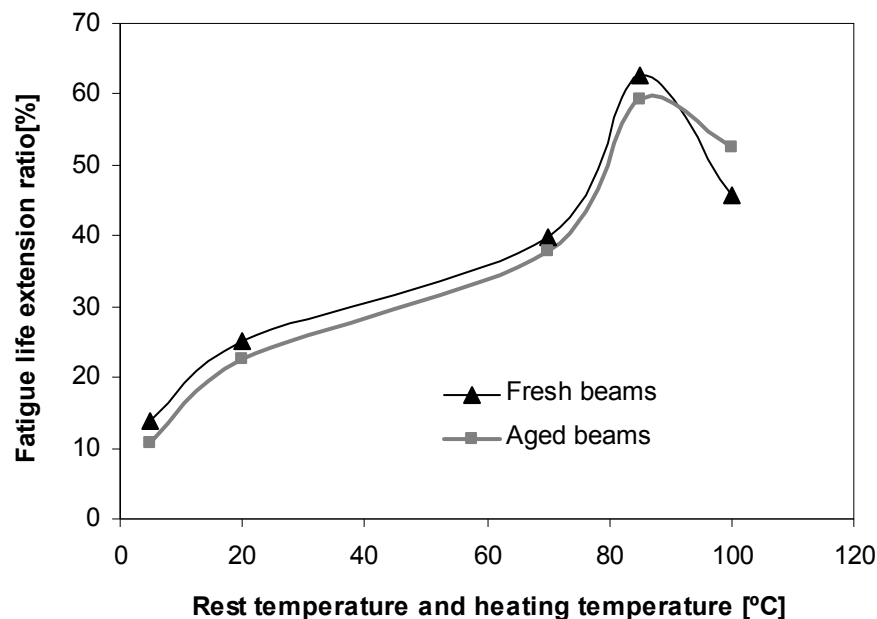


Figure 6.25: Fatigue life extension ratio of the samples versus heating and rest temperature

Figure 6.25 presents the effect of temperature on the fatigue life extension ratio of porous asphalt beams. As shown in Figure 6.25, the fatigue life extension ratio of the beams (healing) is very temperature dependent. The fatigue life extension ratio is quite low at a low rest temperature of 5 °C and increases with the increase of the rest temperature. There is a dramatic increase when the heating temperature is increased from 70 °C to 85 °C. After that,

further increase in the heating temperature results in a decrease of the fatigue life extension ratio. The reason for this decrease can be attributed to the geometry damage and binder drainage problem caused by overheating. In this case, the swelling problem showed up in the mortar, because the mortar cannot bear the excess expansion caused by temperature increase. The binder in the sample tends to drain down at such a high temperature, also probably reducing the healing rate. Based on these results, it is concluded that 85 °C is the optimal heating temperature for the samples to obtain the best healing effect.

It also can be seen in Figure 6.25 how ageing influences the fatigue life extension ratio of the beams. On average, ageing slightly decreases the fatigue life extension ratio by 3%. It means that ageing does not decrease the healing rate of porous asphalt concrete a lot. For severe ravelling of aged porous asphalt wearing course, the accumulated damage during the service life (ageing) caused by traffic and environmental loading plays an important role. At a heating temperature of 100 °C, the healing rate of the ageing beam is higher than that of the fresh beam. The reason for this can be attributed to ageing hardening behavior of the binder. With ageing, the binder becomes harder and its softening point increases, reducing binder drainage at 100 °C. As a result of less binder drainage, the healing of the aged beams increases a bit.

6.5.4 Healing of porous asphalt beams with different damage degree

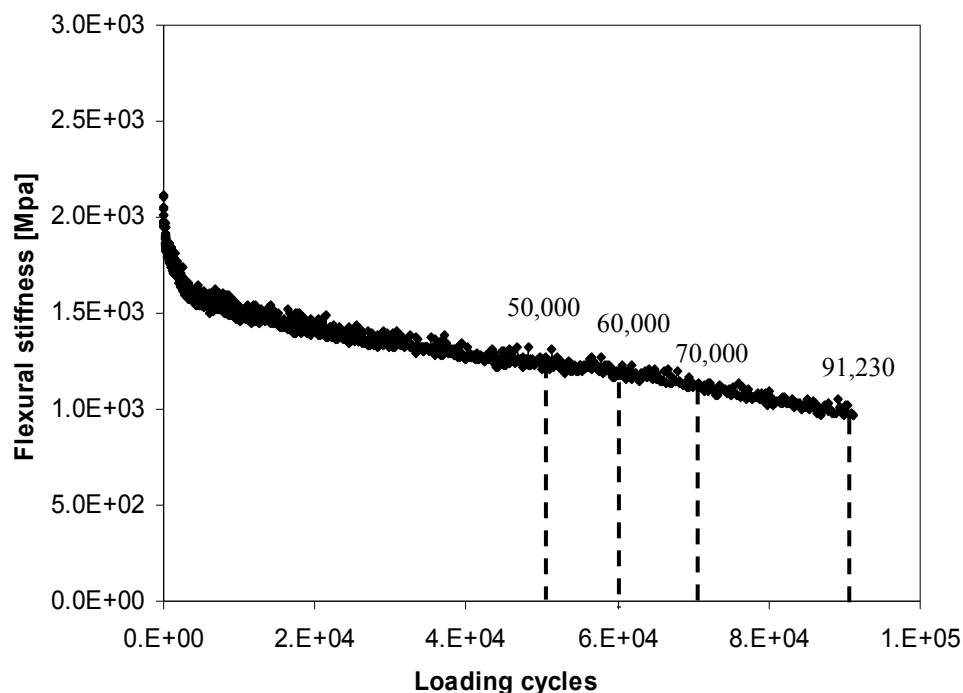


Figure 6.26: Different damage loading cycles in fatigue life extension test

The relationship between the damage degree and the healing rate was studied to get an idea of the optimal timing to start induction heating. As shown in Figure 6.26, the beams were loaded 50,000/60,000/70,000 cycles or loaded until fatigue, respectively, at 300 microstrain and at a frequency of 8 Hz. The

damage degree can be described as the loading cycles divided by the original fatigue life (95,700 determined from the fatigue line). So 50,000/60,000/70,000 cycles' loading corresponds to a damage degree of 52.2%/62.7%/73.1%. Then the damaged beams were heated to 85 °C and rested for 18 hours. Finally, the fatigue life of healed beams was measured at the same strain amplitude of 300 microstrain.

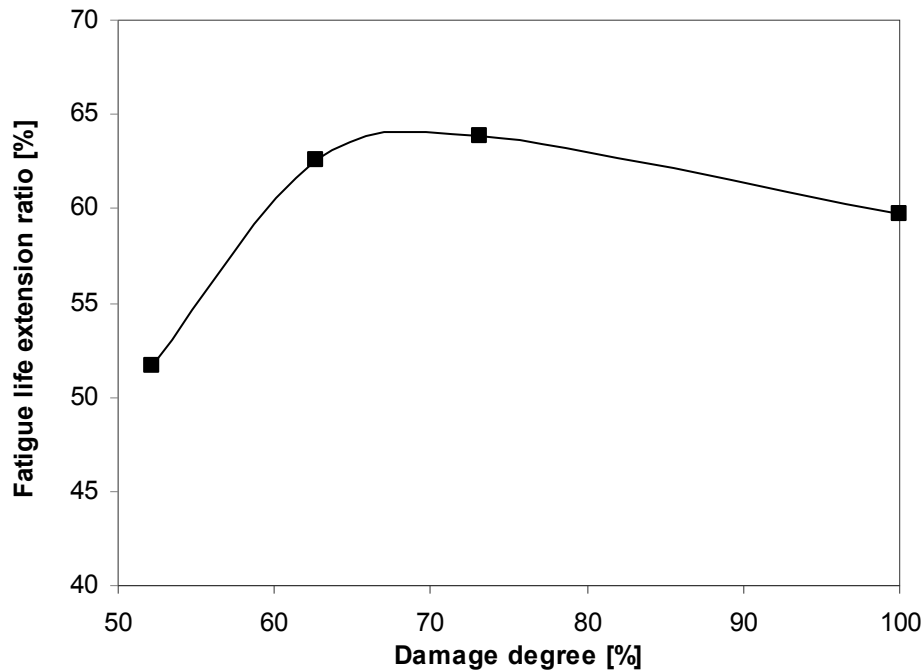


Figure 6.27: Fatigue life extension of the samples versus damage degree at a heating temperature of 85 °C

Figure 6.27 presents the relationship between the damage degree and the fatigue life extension ratio. It can be seen from the curve that a highest fatigue life extension ratio of 63.9% is obtained when the damage degree is 73.1% with 70,000 cycles' damage loading. The damage degree is the maximum fatigue life extension ratio that the sample can possibly obtain when induction heating heals all the damage. 50,000 cycles' damage loading applied on the beam results in a damage degree of 52.2% and induction heating causes a relatively lower fatigue life extension ratio of 51.7%. In this case, as the fatigue life extension can only be as high as 52.2% when full healing happens, a fatigue life extension ratio of 51.7% means that almost all the damage is healed by induction heating. However, the low fatigue life extension ratio means that sufficient damage is necessary to obtain a high fatigue life extension ratio with induction heating. To get long fatigue life extension, induction heating should not be applied too early. When the beam sample is fully fatigue damaged, the fatigue life extension ratio is also relatively low. In this case, the damage might be too huge to heal. According to the experimental results, it is the best moment to heat the sample when it is damaged to around 70%. However, it is difficult to link the experiment result to field pavement performance. Field inspection is necessary to determine the situation of the pavement and the

moment to start induction heating on pavement. It is recommended that induction heating is applied on the pavement just before the first stones are coming out.

6.5.5 Flexural stiffness recovery of damaged porous asphalt concrete beam

The flexural stiffness recovery of a damaged beam was measured in this research to characterize how the healing recovery developed with rest time and to compare the differences between natural healing and induction healing. Firstly, the flexural stiffness of the porous asphalt concrete beam was measured in four point bending stiffness test at a strain amplitude of 50 microstrain at 20 °C. Secondly, 70,000 cycles fatigue loading of 300 microstrain were applied to the beam at 20 °C with a frequency of 8 Hz to damage the beam. Then, the flexural stiffness recovery of the beam with rest time was monitored in four point bending stiffness test. When the stiffness did not recover anymore, the beam was heated to 85 °C with induction heating and was rested for 3 hours at 20 °C to cool down. Finally the stiffness of the healed beam was measured.

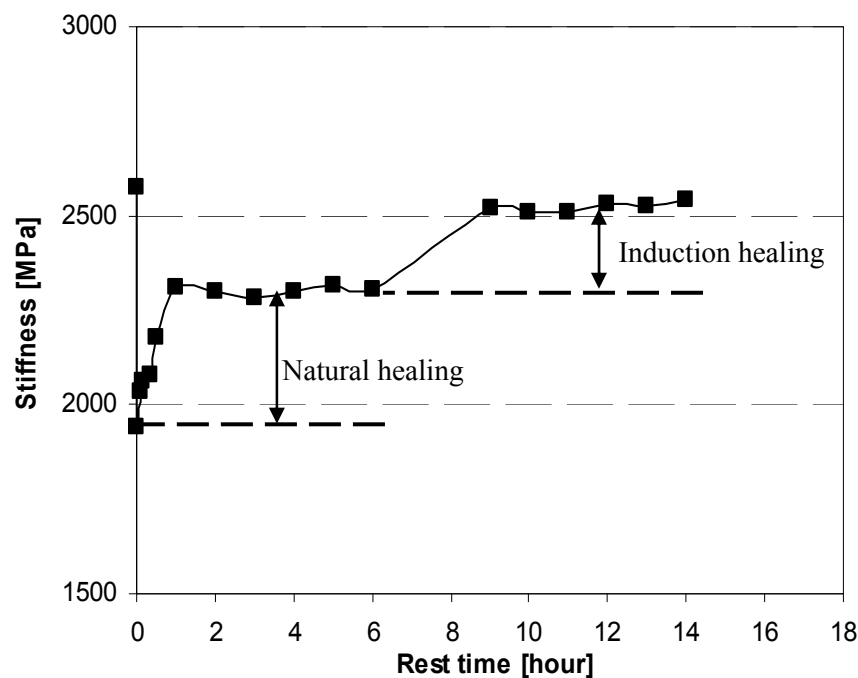


Figure 6.28: Stiffness recovery of damaged sample with natural and induction healing

Figure 6.28 shows how the flexural stiffness of the damaged sample develops with natural and induction healing. The initial flexural stiffness of the sample is 2,578 MPa at 20 °C and the stiffness reduces to 1,940 Mpa after 70,000 cycles damage loading. The stiffness restores itself very quickly by self healing immediately after loading and increases to 2,308 MPa after 1 hour rest. After that, the stiffness is monitored for another 5 hours, but there is no recovery anymore. It means that the self healing of the damaged sample at 20 °C is not enough to heal all the damage. However, when the sample is heated to

85 °C with the induction heating machine and rested for 3 hours, the stiffness is found to recover to 2,522 MPa, very close to the original stiffness value. This extra stiffness recovery is a proof of healing which is caused by induction heating. So, it can be concluded that induction heating helps to restore the stiffness of this porous asphalt concrete. Compared with the fatigue life extension ratio of 63.9% with the same damage degree in Figure 6.27, the stiffness is more recovered. It means that stiffness is easier to recover than fatigue life. This can be explained using Phillips' three steps diffusion model [Phillips 1998]: the first two steps of healing (surface approach and wetting) cause the recovery of the stiffness and the third step of healing (diffusion and randomization of asphaltene structures) causes the recovery of the strength.

6.5.6 Application of multiple times induction heating on porous asphalt concrete beams

The possibility of multiple times induction heating was examined to show that induction heating could be repeated when cracks appear again after healing. A strain amplitude of 300 microstrain, at a frequency of 8 Hz, was applied on the porous asphalt concrete beam for 50,000 cycles. Then, the sample was induction-heated to 85°C and rested for 18 hours for the first time. After that, another 50,000 cycles fatigue loading was applied on the beams, followed by the second time heating and rest process. The damaging, heating/rest and re-damaging process was repeated four times. Finally, the fatigue life of the beam was measured.

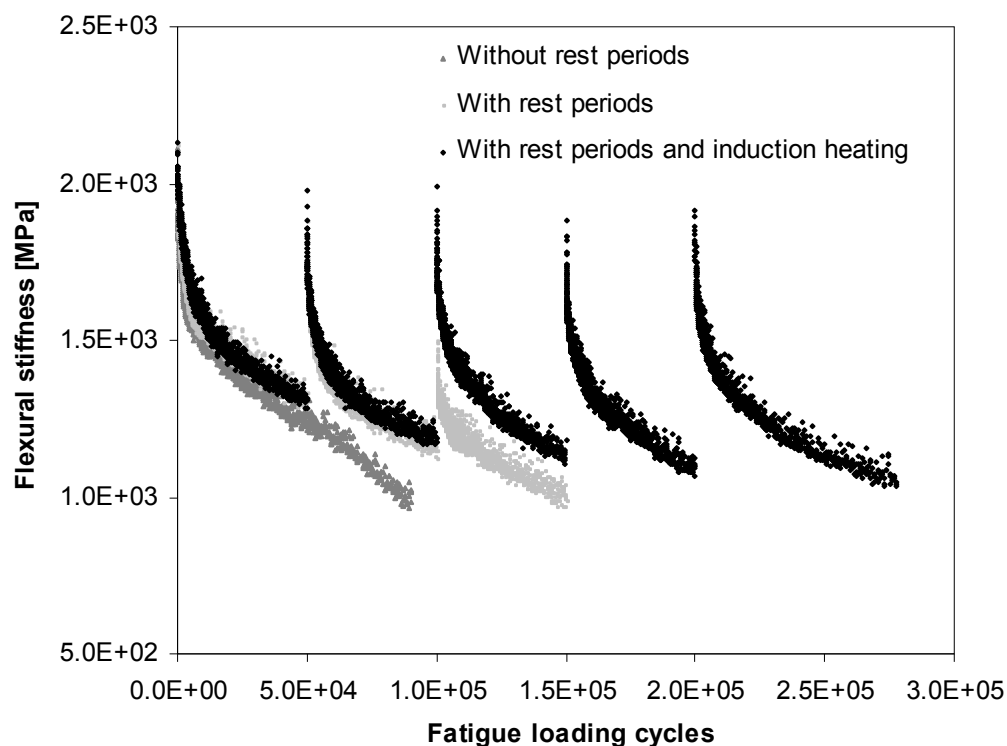


Figure 6.29: Fatigue life extension of the sample caused by multiple induction heating

The original fatigue curve and the multiple times induction heating modified fatigue curve of the samples are shown in Figure 6.29. The original fatigue life of the sample is 95,700 cycles. With 4 times damage loading of 50,000 cycles followed by 4 times induction heating and resting, the modified fatigue life is 277,720, which is 2.9 times the original fatigue life. The fatigue life extension ratio is 190%. However, if only rest periods are introduced to the sample, the sample will be fatigued after two cycles of fatigue/resting. In this case, the fatigue life of the sample is 150,000 cycles and the fatigue life extension ratio is only 56.7%, much lower than with induction heating. Although the moment of heating the pavement and the frequency of heating are not fully optimized yet in this research, it is definite that multiple times heating can greatly increase the fatigue life of porous asphalt concrete.

6.5.7 Induction healing of aged porous asphalt concrete beams

Finally, the healing potential of aged beams (10 days ageing at 85 °C in the oven) was also investigated. This ageing method was equivalent to 5 years field ageing [Liu et al 2012]. The aged beams were divided into two sets, used for natural healing and induction healing measurements respectively. The first set of samples was first fatigued at 20 °C with a loading of 300 microstrain and 8 Hz, then rested for 3 hours or 18 hours, and finally fatigued again with the same loading. The fatigue criterion was reduction of stiffness to half of its initial value. The second set of samples was first damaged like the first set of samples, then induction-heated to 85 °C and rested for 3-24 hours and finally fatigued again. The fatigue life extension ratio (the second time fatigue life divided by the original fatigue life) was used as a healing indicator.

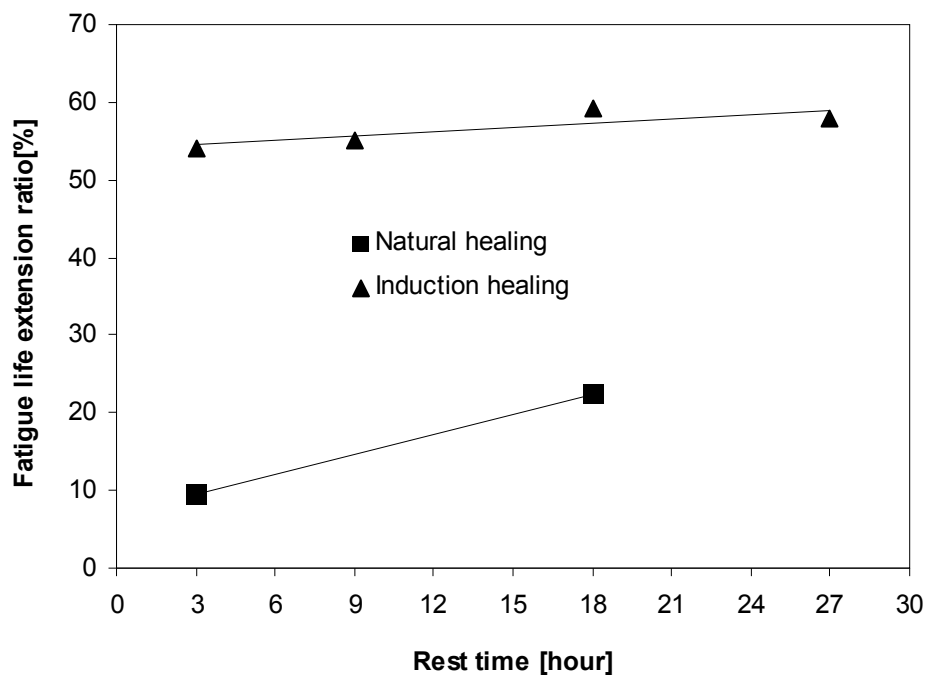


Figure 6.30: Fatigue life extension ratio of the aged beams with natural and induction healing

Figure 6.30 presents how the fatigue life extension ratio of the aged beams with natural and induction healing develops with rest time. With induction heating (to 85 °C) and 3 hours' rest, the fatigue life of the aged beam recovers 54.1%, while the fatigue life of the aged beam only recovers 9.6% with 3 hours' rest alone. For a rest time of 18 hours, the fatigue life extension of the aged beam with natural healing is 22.5%, still much lower than that with induction healing. It means that induction healing is much higher and faster compared with natural healing. For induction healing, the difference among the fatigue life extension ratios with different rest durations is very small. It means that the significant healing is already obtained after 3 hour's rest, which is the time needed for the heated beams to cool down. For this reason, it is proposed that the pavement cool 3 hours after heating, which is further supported by numerical modeling as explained in Chapter 7.

6.6 Summary and Conclusions

The healing potential of asphalt mastic and porous asphalt concrete with steel wool was investigated in this chapter. The strength/stiffness recovery and fatigue life extension caused by induction heating were used as healing indicators.

First, the strength (flexural resistance) recovery of fractured asphalt mastic was measured to characterize its induction healing effect. It is found that completely fractured asphalt mastic beams with steel wool can be healed many times with induction heating. During the induction heating, it can be seen that cracks in asphalt mastic beams disappear because of the flow of bitumen.

Second, the stiffness recovery and fatigue life extension were measured to quantify the healing rate of porous asphalt concrete cylinders. It is found that porous asphalt cylinders with steel wool show a better healing effect than plain samples. In this case, the stiffness of porous asphalt concrete with steel wool recovers much more when induction heating is applied. The rest time needed for full healing is also shortened due to induction heating. In addition, fatigue damage in the sample can be totally healed via induction heating. It is also noted that the fatigue life of porous asphalt concrete samples with steel wool is significantly increased by induction heating. In addition to its higher healing rates, porous asphalt concrete with steel wool has better fatigue resistance than the plain material: it can resist higher loads with less damage due to the reinforcement of steel wool.

Third, the induction healing capacity of porous asphalt concrete beams was evaluated in bending test on elastic foundation. The fractured beams cannot heal themselves at low temperatures. With induction heating, the beams can be healed up to 78.8%. The optimal heating temperature is 85 °C. Further heating causes swelling and drainage problems of the binder, which offset the benefits of induction heating. Reheating doesn't decrease the healing ratio of the sample, which means that heating can be repeated when cracks appear again.

Fourth, the healing potential of porous asphalt concrete beams with steel wool was also evaluated in four point bending fatigue test. The healing ratio (fatigue life extension ratio) of porous asphalt concrete is strain dependent with higher healing ratio at higher microstrain amplitude. Healing is also very temperature dependent. Healing is higher when induction heating is applied on the samples. The optimal heating temperature is 85 °C and overheating decreases the healing ratio, which is consistent with the result of the beam on elastic foundation test. Damage degree affects the healing ratio. Heating should not be applied too early or too late. If it is applied too early, porous asphalt concrete can heal the damage by itself and heating is not necessary. But, if porous asphalt concrete is heated too late, the healing efficiency will be very poor, because structural damage such as permanent deformation or broken stones can occur, which is beyond the healing capability of asphalt concrete. The stiffness of the fatigue damaged beams can recover much more with induction heating. With multiple times induction heating, the fatigue life of porous asphalt beam can be greatly increased. Ageing doesn't influence the healing of porous asphalt beams very much. Induction heating significantly increases the healing rate and speed of aged porous asphalt.

Based on the strength recovery, stiffness recovery and fatigue life extension of asphalt mastic and porous asphalt concrete, it is concluded that the healing capacity of porous asphalt concrete is increased and the crack/damage is healed by induction heating.

Chapter 7 Application of Induction Healing on the Trial section

In the previous chapters, it has been demonstrated in the laboratory that the addition of steel wool fiber to porous asphalt concrete will improve the durability of a porous asphalt layer due to the following two aspects: (1) Steel wool reinforces porous asphalt concrete by increasing its strength, fatigue life and particle loss resistance. So, porous asphalt pavement with steel wool will suffer less cracking and ravelling problems. (2) In case of cracking, porous asphalt concrete with steel wool fiber can be heated with induction energy and subsequently cracks will be healed by capillary flow of bitumen at high temperature. So, induction heating and healing will be useful to improve the durability of porous asphalt pavement by closing cracks.

To apply the induction healing technology in real porous asphalt (PA) pavement, a trial section was constructed on a Dutch motorway. The research plan regarding this induction healing porous asphalt trial section is shown in Table 7.1.

Table 7.1: Research plan regarding the induction healing porous asphalt trial section

Research	Purpose
Experiments in the laboratory of Heijmans	To assess the porous asphalt with steel wool developed at TU Delft
Trial production of the porous asphalt mixture with steel wool	To develop a suitable mixing procedure in the asphalt plant
Construction of the porous asphalt trial section	To conduct a real application of the induction healing approach
Experiments on the filed cores	To characterize the material from the trial section
Modeling of the thermal transfer in the field trial section	To predict the cooling rate of the trial section after induction heating

7.1 Assessment of the porous asphalt mixture with steel wool in the laboratory of Heijmans-Breijn in Rosmalen

One of the challenges in translating the laboratory research of induction healing porous asphalt to practice is how to homogeneously disperse steel wool into porous asphalt mixture. In the laboratory of Delft University of Technology, a standard mixer (Hobart mixer) was used for the small scale research described in the previous chapters. However, the mixer in an asphalt plant usually mixes much more intensively than a Hobart mixer, especially the pug mill in a batch plant. So, the steel wool fiber might be shortened by mixing in the asphalt plant, which will certainly influence the properties of the mixture. To assess the mixture produced by intensive mixing, a preliminary study was conducted in the road engineering laboratory of Heijmans-Breijn, which was the construction contractor of the trial section on the motorway.

In the laboratory of Heijmans-Breijn, steel wool was blended into asphalt mixture with an intensive mixer. The intensive mixer used is shown in Figure 7.1. The mixture used here is the same as the mixture used for the trial section: porous asphalt concrete PA 0/16 with 4% steel wool type 00 (volume percentage of bitumen). Table 7.2 shows the composition of the PA mixture.



Figure 7.1: Mixer used in the laboratory of Heijmans-Breijn

Table 7.2: Composition of mixture used on the trial section based on the new specification RAW 2010

Material	Size mm	Passing percentage %	Specification
Stones	16	97.7	93-100
	11.2	69.8	64.0-76.0
	8	34.7	-
	5.6	20.5	-
Sand	2	16.0	11.0-19.0
Filler	< 0.036	4.5	3.0-6.0
Bitumen	5.2% of the total weight of stone, sand and filler		B _{min4.5}
Steel wool	4% of the volume of bitumen		

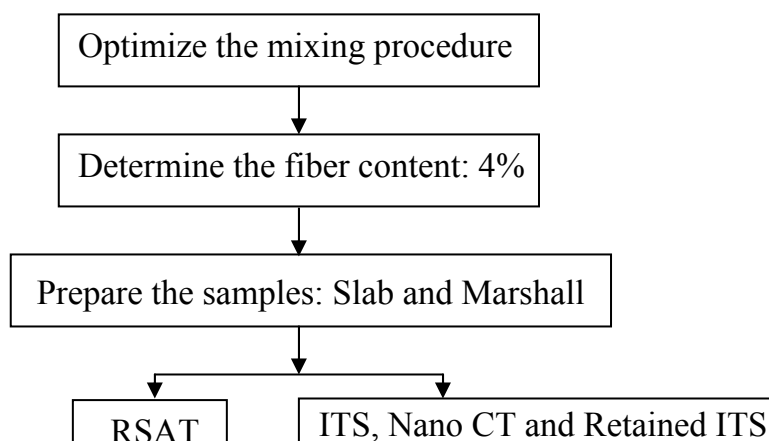


Figure 7.2 Test plan in the laboratory of Heijmans-Breijn

Figure 7.2 shows the test plan in the laboratory of Heijmans-Breijn.

It was still difficult to disperse steel wool into porous asphalt concrete even with an intensive mixer in the laboratory of Heijmans-Breijn in Rosmalen. Adding more than 4% steel wool caused balling problem (steel wool forms ball clusters in the mixture), causing segregation which will decrease the strength of porous asphalt concrete. So, 4% of steel wool type 00 was selected for the trial section. Also, the mixing procedure was optimized to homogeneously disperse steel wool in an acceptable mixing time. The optimal mixing order is to mix bitumen and steel wool first, where steel wool is saturated with bitumen and becomes sticky and tough. Then by adding stone, sand and filler, the steel wool clusters are pulled apart by the rest of the mixture. With this mixing procedure, a good asphalt mixture can be produced. However, the required mixing time is 2 minutes, 2 times the normal mixing time in an asphalt plant.

After mixing, steel wool was extracted from the mixture and no clusters of steel wool were found. It meant that the steel wool dispersed well in the mixture. However, the steel wool was strongly shortened by mixing, which probably influences the induction heating speed and strength of the subsequent concrete. Since the desired content of steel wool is higher (8%) and the steel wool was significantly shortened by the intensive mixer, it is necessary to evaluate the mixture with 4% shortened steel wool. For that, Marshall Samples and RSAT (rotating surface abrasion test) samples were prepared and induction heating, indirect tensile strength (ITS), Nano CT scanning and RSAT tests were done on these samples.

Three Marshall Samples were heated with the induction heating machine at a frequency of 70 KHz and a distance between the sample and the coil of 10 mm. Chapter 4 explains the details of the heating test. The average heating speed at the top surface of the samples is 0.3412 °C /s. This heating speed is not very high, but it can be improved a lot by optimizing the induction generator.

The indirect tensile strength ratios (ITSR) of the Marshall Samples were tested at 15 °C according to the European Norms EN 12697-12:2003 and EN 12697-23:2003. Table 7.3 shows the results of the samples, where each value is

an average of four samples. It can be seen that the samples with 4% steel wool have a higher indirect tensile strength and indirect tensile strength ratio than plain samples. It means that the addition of steel wool reinforces the concrete and decreases its water sensitivity.

Table 7.3: Indirect tensile strength (ratio) of the samples

Samples	ITS _{dry}	ITS _{wet}	ITSR
Plain	0.927	0.768	85%
With 4% steel wool	0.987	0.932	94%

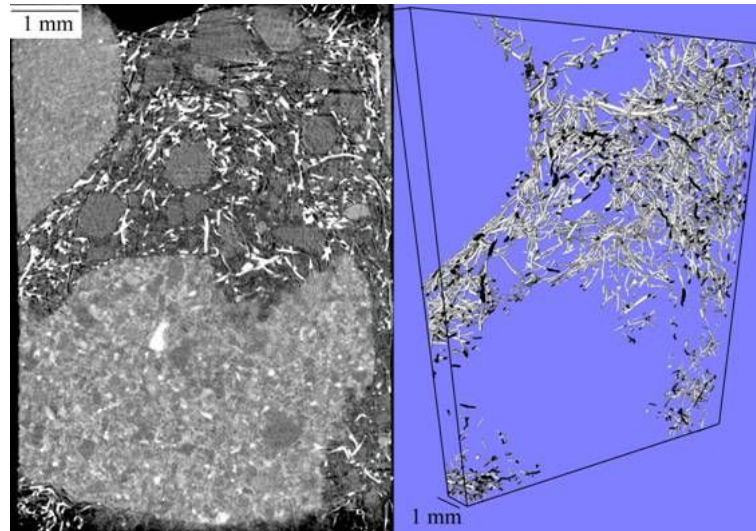


Figure 7.3: steel wool distribution in the sample [García et al 2012]

After determination of the strength of samples, a small piece was sawn from one waste sample and scanned with a Phoenix X-ray Nano CT scanner. After scanning, a reconstruction was made to analyze the steel wool distribution in the sample. Figure 7.3 shows the distribution of steel wool in the sample. It shows that the steel wool fiber is distributed homogeneously and no clusters of steel wool can be seen.



Figure 7.4: RSAT slabs with 4% steel wool 00 prepared by Breijn-Heijmans

The Rotating Surface Abrasion Test (RSAT) was specially developed at Breijm-Heijmans to study the ravelling resistance of porous asphalt mixtures. Figure 7.4 shows the RSAT samples used in this research, which are 8-right prism slabs with a side length of 180 mm and a height of 50 mm. These slabs were prepared by Breijm-Heijmans from the sample mixture as used in the field trial section: 3 slabs of plain porous asphalt PA 0/16 and 3 slabs of porous asphalt with 4% steel wool (volume fraction of bitumen).

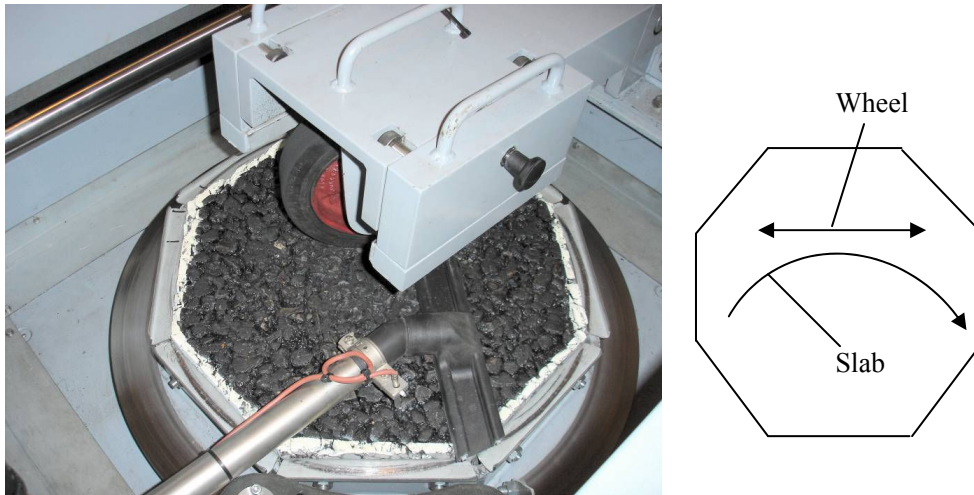


Figure 7.5: Setup and schematic of Rotating Surface Abrasion Test (RSAT)

The rotating surface abrasion test is usually done at 20 °C. Figure 7.5 shows the setup of the rotating surface abrasion test, where the contact pressure between the tire and the sample is 0.6 Nmm². To simulate ravelling on the pavement, the tire rotates 24 hours on the whole sample at a speed of 3607 r/h, resulting in 690 times at the same location. 24 hours' tire rotating on the sample is assumed to simulate 7 years' traffic on the pavement. During the test, a vacuum cleaner is used to suck the lost stones from the surface of the sample.

The stone loss is determined after the test. Figure 7.6 shows the sample with stone loss after the test.



Figure 7.6: Sample with stone loss after rotating surface abrasion test

Figure 7.7 shows a typical stone loss curve of a porous asphalt concrete. The stone loss in the rotating surface abrasion test is an indicator of the ravelling resistance of the mixture. The tendency of the stone loss is consistent with the ravelling process on a porous asphalt pavement: it starts slowly but develops quickly.

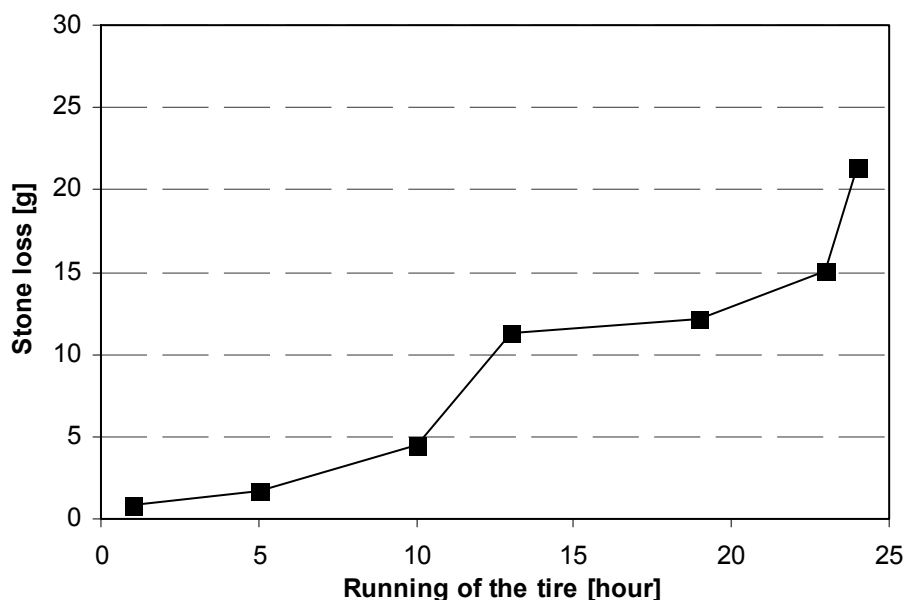


Figure 7.7: Stone loss in rotating surface abrasion test

Table 7.4 compares the stone loss of the RSAT samples with and without steel wool. It can be seen in Table 7.4 that the stone loss value of plain RSAT samples is more than two times that of the samples with 4% steel wool. It means that porous asphalt concrete with steel wool has better particle loss resistance. If the stone loss of plain slab 3 is considered as an outlier and this result is ignored, the plain RSAT slabs and slabs with 4% steel wool will have similar stone loss value. In this case, the conclusion is that the addition of steel wool doesn't adversely influence the stone loss resistance of porous asphalt concrete.

Table 7.4: Stone loss of RSAT sample with and without steel wool

Sample	Slab 1	Slab 2	Slab 3	Average
plain	5.32 g	3.82 g	24.18 g	11.11 g
With 4% steel wool	4.27 g	2.57 g	8.64 g	5.16 g

It is expected that induction heating will stop the process of stone loss by closing the cracks in the stone-stone contact region. If induction heating is applied in the pavement in time, ravelling will be definitely delayed.

Based on the studies above, the provisionally selected content of steel wool of 4% (volume fraction of bitumen) in the asphalt provides acceptable induction heating capacity and does not adversely influence the properties of porous asphalt concrete. So, it is decided to incorporate 4% steel wool into the porous asphalt mixture for the field trial section.

7.2 Trial production of porous asphalt mixture with steel wool in the asphalt plant of Heijmans-Breijn in Zwijndrecht

Before paving the field trial section, research was needed to develop a suitable mixing procedure in a full scale hot mix asphalt plant. In the asphalt plant of Heijmans-Breijn in Zwijndrecht, six mixing procedures were selected for the production of a good asphalt mixture [van Bochove et al 2011]. The details of the six mixing procedures are summarized in Table 7.5.

Table 7.5: Different mixing procedures used to produce asphalt mixture

Procedure	Mixing sequence	Mixing time	Total mixing time
1	Steel wool + bitumen	0 s	290 s
	Sand + stone	90 s	
	Filler	100 s	
	Final mixing	100 s	
2	Steel wool + bitumen	0 s	250 s
	Filler	50 s	
	Sand + stone	100 s	
	Final mixing	100 s	
3	Sand + stone	0 s	200 s
	Filler	0 s	
	Steel wool + bitumen	100 s	
	Final mixing	100 s	
4	Sand + stone	0 s	230 s
	Steel wool + bitumen	30 s	
	Filler	100 s	
	Final mixing	100 s	
5	Sand + stone + steel wool	0 s	300 s
	Filler	100 s	
	Bitumen	100 s	
	Final mixing	100 s	
6	Steel wool + bitumen	0 s	300 s
	Filler	100 s	
	Sand + stone	100 s	
	Final mixing	100 s	

The mixtures produced by different mixing procedures are shown in Figure 7.8, where steel wool was pre-dispersed with a wood chipper (shown in Figure 7.9) before mixing and then blown into the mixer in mixing procedure 5 and 6. Steel wool clusters are indications of bad mixing. If the mixture was mixed well, very few or no clusters of steel wool were observed. It can be seen in Figure 7.8 that the mixing procedure 6 is efficient to produce a well mixed

asphalt mixture without steel clusters. So, this mixing procedure will be used to produce the mixture for the trial section described in the following paragraphs.

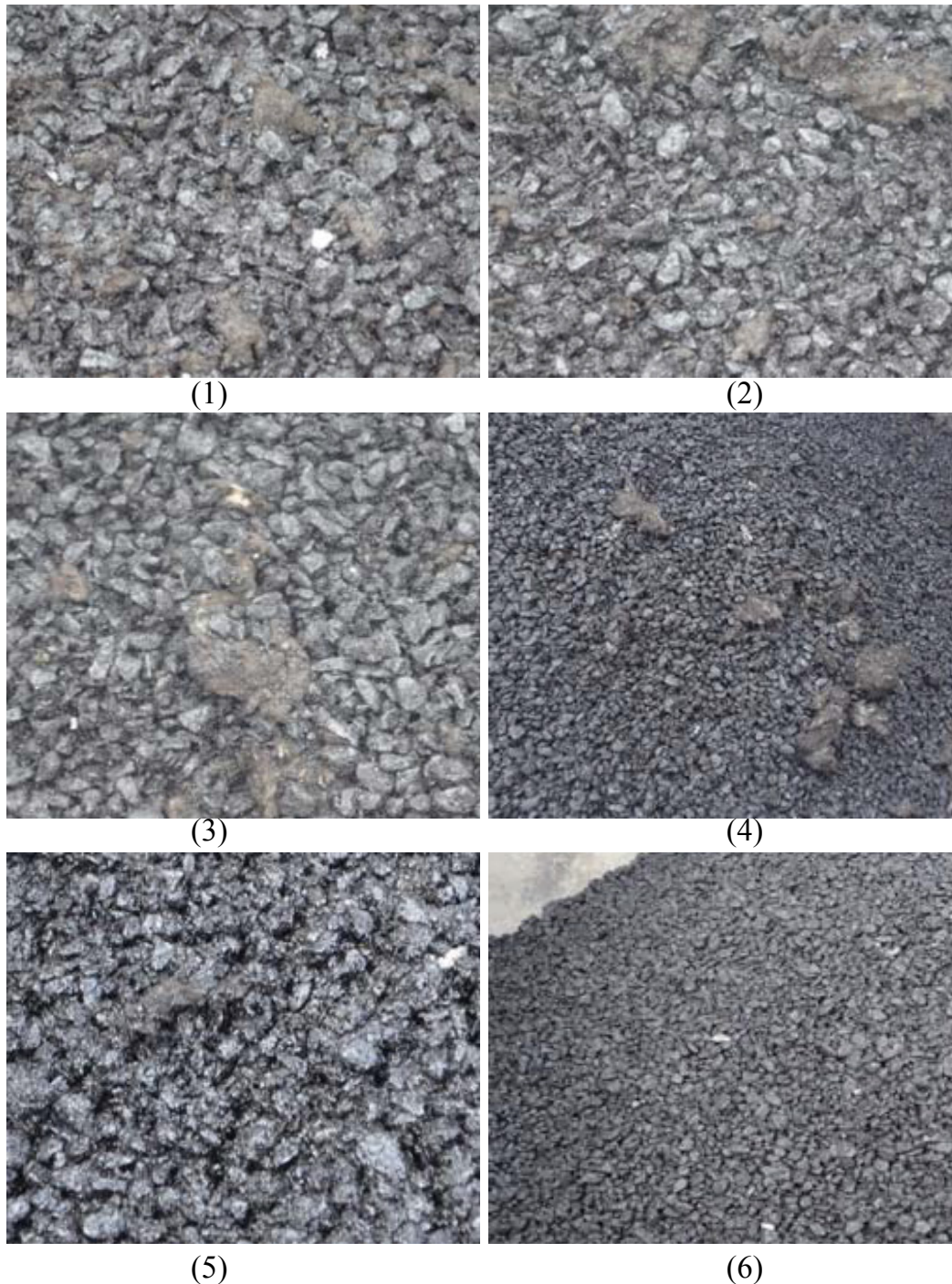


Figure 7.8: Asphalt mixtures produced by different mixing procedures: (1), (2) and (3) bad mixing, dry mixture with many steel wool clusters which absorbed a lot of bitumen; (4) very bad mixing, mixture with many steel wool clusters, (5) good mixing, well mixed mixture with a few steel wool clusters; (6) good mixing, well mixed mixture with very few steel wool clusters [van Bochove et al 2011]

However, it should be noted that the mixing time is about 6 times the normal mixing time for porous asphalt. Besides, the provisionally selected

content of steel wool is 4% and it is not feasible to blend 8% steel wool (desired content) into the mixture. So, the mixing procedure still needs to be optimized to decrease the mixing time and to make it feasible to incorporate more steel wool into the mixture. However, the sixth mixing procedure was used to produce the mixture for the trial section.



Figure 7.9: Wood chipper used to disperse steel wool

7.3 Construction of the induction heating trial section

A 400 meter long filed trial section with the induction heating porous asphalt concrete was constructed by Heijmans-Breijn on Dutch motorway A58 near Vlissingen on December 11, 2010. The ambient temperature was about 8 °C during construction. Figure 7.10 shows the location of the trial section. The construction and research of the induction heating trial section was financed by Rijkswaterstaat, Ministry of Transport, Public Works and Water Management, the Netherlands.



Figure 7.10: Location of the induction heating field trial section

The filed trial section was constructed by the construction company Heijmans-Breijn. Figure 7.11 shows some construction activities on the field trial section.



Figure 7.11: Construction of the induction heating trial section on Dutch motorway A58

The trial section survived the past two cold winters of 2010-2011 and 2011-2012 perfectly and no damage or even small cracks could be observed by the inspection of experts. A large number of cores ($\varnothing 100$ mm) were drilled from this trial section (shown in Figure 7.12). Plain cores without steel wool were also drilled for comparison purpose. To predict the performance of this trial section, the cores were used to do experiments to study the heating, mechanical and healing properties of the placed material.



Figure 7.12: Drilling cores from the induction heating trial section

7.4 Characterization of the material from the field trial section with laboratory experiments

The experiments described in this chapter include induction heating speed test, Cantabro (particle loss) test, indirect tensile strength test, indirect tensile stiffness and fatigue test, Nano indentation test, CT scan test and healing test.

7.4.1 Heating test

In the heating test, 9 cores ($\text{Ø}100\text{mm}\times 50\text{mm}$) from the field trial section were heated with the induction heating machine for 3 minutes. This induction heating machine has a power of 50 KW and 70 KHz. The distance between coil of the induction machine and the sample varied from 10 mm to 20 mm and 30

mm. During the heating process, an infrared camera was used to monitor the temperature changes at the surface of the core. Figure 7.13 shows an infrared image of an induction-heated sample. The heating speed of the cores (temperature increase in time) can be calculated after the test with the software of the infrared camera. Before and after heating, the cores were scanned with a Siemens CT scanner (Resolution in per slice: 0.294 mm times 0.294 mm). According to the result of the CT scanning, the void content over the sample's thickness does not change after induction heating. It means that there is no binder drainage problem during heating.

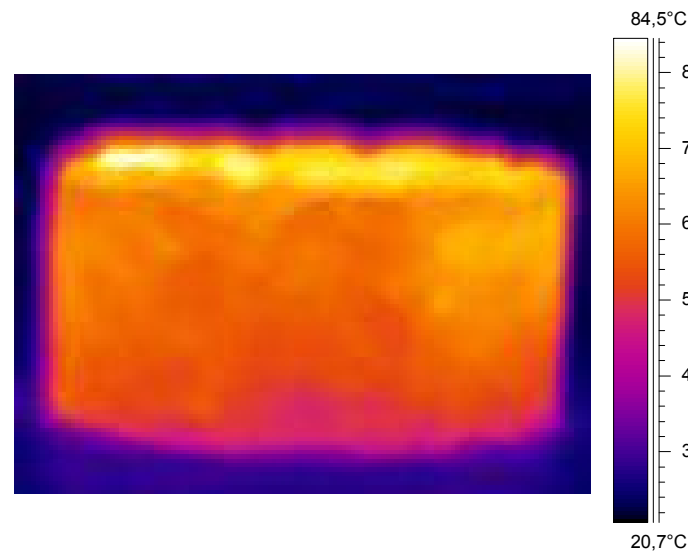


Figure 7.13: Infrared image of a heating sample

As the main goal of the induction heating approach is to prevent ravelling at the pavement surface, the surface temperature of the pavement after heating is very important. For this reason, this experiment focused on the temperature increase of the top surface of the cores during heating. With the software of the infrared camera, the mean heating speeds at the top surface of the samples were calculated (the temperature increase divided by the heating time). The heating speeds of three steel wool reinforced cores were measured for each case and the results are summarized in Table 7.6.

Table 7.6: Induction heating speed of the steel wool reinforced field cores

Distance mm	Heating speed °C/s			
	1	2	3	Average
30	0.1924	0.1811	0.2177	0.1971
20	0.2363	0.2611	0.2442	0.2472
10	0.3144	0.3383	0.38	0.3442

The cores can be heated much faster when they are closer to the coil of the induction machine. When the distance between the top surface of the sample and the coil is 10 mm, the average heating speed of the three measurements is 0.3442 °C /s. With the induction heating speed, it takes 190 s

to heat the sample surface from 20 °C to 85 °C. However, this heating time is not very practical for field heating. Therefore the induction heating machine needs to be optimized to increase the heating speed. In a recent study it has been shown that the field cores could be heated at a speed of 2.5 °C /s using a more optimized heating device in the induction generator manufacture company Huttinger in Germany.

7.4.2. Cantabro test

The Cantabro test was conducted on both plain cores (Ø100mm×50mm) and cores with steel wool to compare their particle loss resistance. The tests were done at room temperature in a Los Angeles abrasion machine without steel balls according to the European Norm EN 12697-17. Each specimen was initially weighed (W_1) and placed separately into a Los Angeles drum. Thereafter, each specimen was weighed again after 300 revolutions of the drum (W_2) in order to determine the weight loss during testing. This weight loss ($W_1 - W_2$ divided by W_1) is an indicator of the cohesive properties of the mix. Lower weight loss means better cohesion and better particle loss resistance.

The particle loss values of the plain cores and cores with steel wool, both fresh and oven aged (240 hours at 85 °C), are presented in Figure 7.14. This ageing equals to 5 years field ageing [Liu et al 2012].

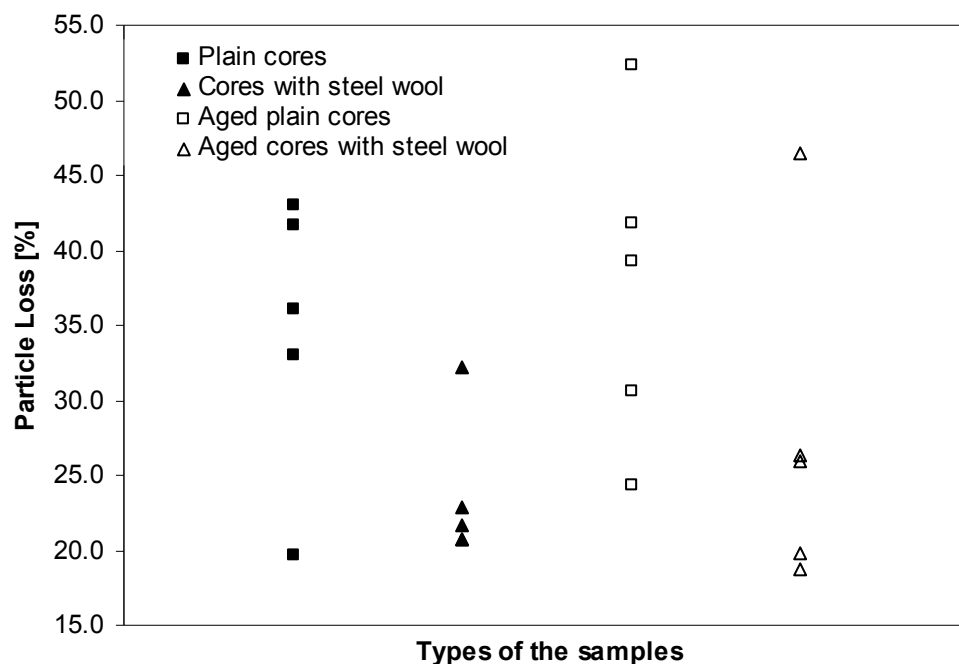


Figure 7.14: Particle loss values of the reference and steel wool reinforced cores

The particle loss values of the samples show a large scatter, which could be related to the inhomogeneous construction activity. The average particle loss value of five measurements is used as an indicator for the ravelling resistance (the lower the particle loss value, the higher the ravelling resistance). The

average particle loss of steel wool reinforced cores is 23.6%, much lower than that of reference cores 34.7%. For both cores with steel wool and reference cores, the particle loss values increase slightly due to aging. The average particle loss of aged steel wool reinforced cores is 27.5%, still much lower than that of aged reference cores 37.7%. Steel wool improves the particle loss resistance of porous asphalt concrete cores. As a result, ravelling on the trial section will be delayed.

7.4.3 Indirect tensile strength test

The indirect tensile strength of the cores ($\text{Ø}100\text{mm}\times 50\text{mm}$) with or without steel wool was tested at $5\text{ }^{\circ}\text{C}$ to avoid as much as possible the influence of permanent deformation on the test result. The indirect tensile strength of the sample is determined in a vertical displacement test at a rate of 50 mm/minute according to the European Norm EN 12697-23. The set-up of this test is shown in Figure 7.15. During the test, the horizontal deformations of the samples were measured with two horizontal LVDTs. To check the data reproducibility, 3 sample of each material type were tested and the average strength was obtained. The maximum stress and the horizontal deformation at failure of the specimens were attained from the test results.

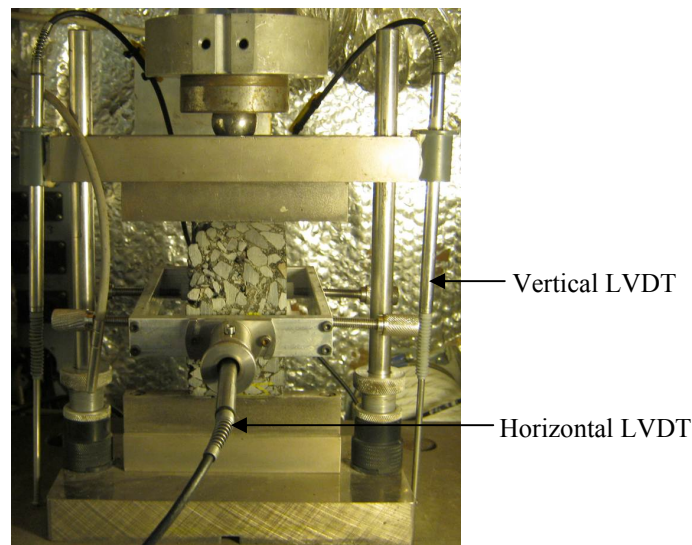


Figure 7.15: Set-up of indirect tensile strength test

The water sensitivity of the cores with steel wool was evaluated with the indirect tensile strength ratio. Six cores were divided into a dry and a wet group. The dry group (3 samples) was directly used to test the indirect tensile strength at $15\text{ }^{\circ}\text{C}$ according to the European Norm EN 12697-12. The wet group was soaked in a $40\text{ }^{\circ}\text{C}$ water bath for 72 hours and then stored in the air chamber for 2 hours before testing the indirect tensile strength. The indirect tensile strength ratio (indirect tensile strength of wet samples divided by indirect tensile strength of dry samples) was used as an indicator of the water sensitivity of the mix.

The results of the indirect tensile strength test are presented in Table 7.7. The average indirect tensile strength of the cores with steel wool is 2.13 MPa, slightly higher than that of the plain core. The steel wool reinforcement is not significant in terms of strength. The reason for this is probably the limited content of steel wool. However, the addition of steel wool strongly increases the tensile deformation at failure of the cores. As shown in Figure 7.16, the tensile deformation at failure of the cores with steel wool is increased by 42.1%. It is expected that the improvement of the ductility caused by addition of steel wool will increase the ravelling resistance of the trial section.

Table 7.7: Indirect tensile strength of the field cores (5 °C)

Sample	Average strength
Plain cores	2.06 MPa
Cores with steel wool	2.13 MPa

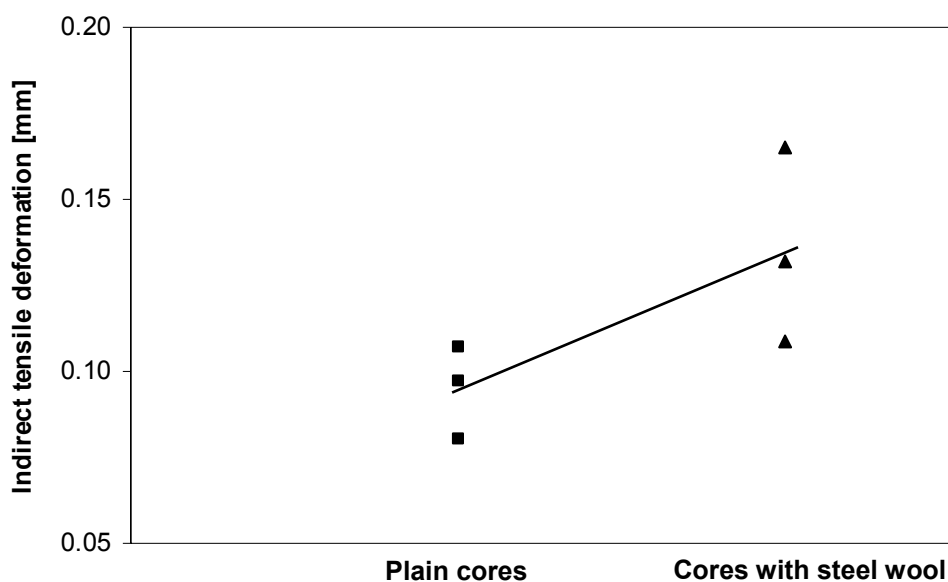


Figure 7.16: Indirect tensile deformations of the samples at failure (5 °C)

As shown in Figure 7.17, the indirect tensile strength (measured at 15 °C) of the wet cores is a bit lower than that of dry cores. The indirect tensile strength ratio is 94.1%, much higher than the requirement of 80% in the Dutch Specification. It means that the water damage resistance of this porous asphalt concrete with steel wool is good.

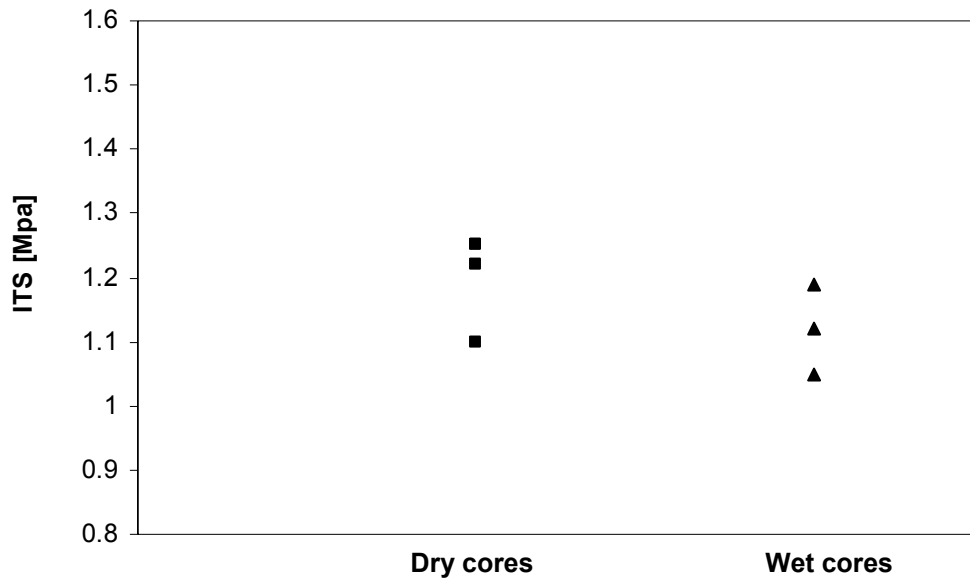


Figure 7.17: Indirect tensile strength of the cores with steel wool (measured at 15 °C)

7.4.4 Indirect tensile stiffness test

To compare the stiffness master curves of the cores ($\text{Ø}100 \text{ mm} \times 50 \text{ mm}$) with or without steel wool, the indirect tensile resilient stiffness was measured according to the European Norm EN 12697-26 at four temperatures (5°C, 10°C, 20°C, 30°C) and for each temperature at five frequencies (8 Hz, 4 Hz, 2 Hz, 1 Hz, 0.5 Hz). Figure 7.18 shows the setup of this test. The experimental indirect tensile stiffness of the samples is shown in Appendix 5.

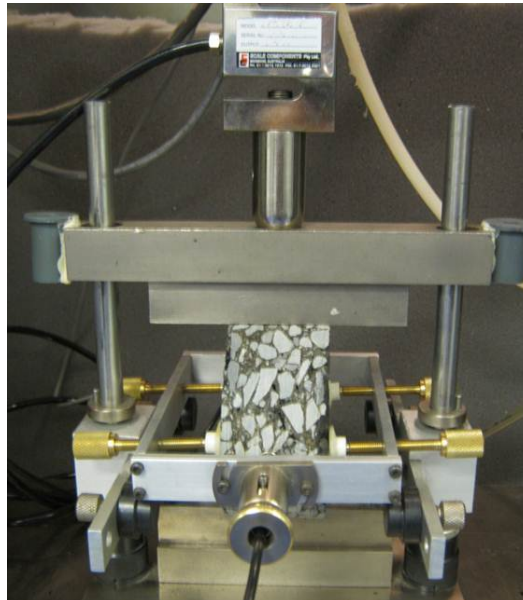


Figure 7.18: Setup of indirect tensile stiffness test

After the test, the master curves of the two porous asphalt mixtures were constructed by fitting the experimental data to a sigmoidal-shape mathematical model as described in Equation 5.5 in Chapter 5. The master curves of the two

mixtures (at a reference temperature of 20 °C) are compared in Figure 7.18. The model parameters and the amount of shift of the resilient stiffness master curves are listed in Table 7.8 and Table 7.9 respectively.

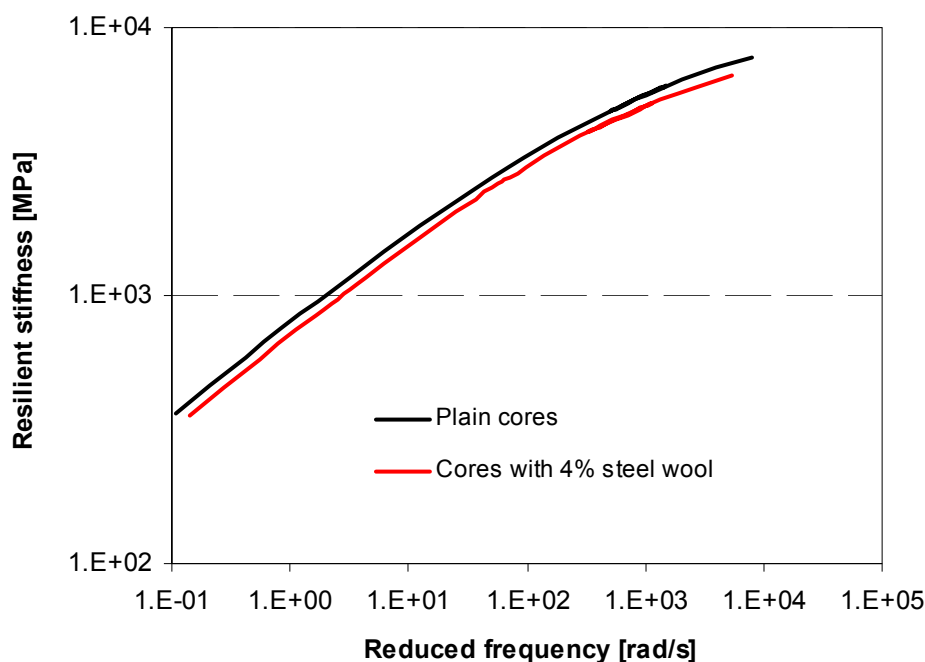


Figure 7.19: Indirect tensile resilient stiffness master curves of field cores with and without 4% steel wool at a reference temperature of 20 °C

Table 7.8: Model parameters for the stiffness master curves

Model parameters	Plain cores	Cores with 4% steel wool
C_1	547413.7	107183.5
C_2	3726107	793365.8
G_e [Mpa]	11413.51	9731.771
G_g [Mpa]	0	0
f_c [Hz]	1118.686	991.7344
m_e [-]	0.36934	0.370498
k [-]	0.371481	0.397298

Table 7.9: The amount of shift in constructing master curves: $\text{Log}(a_T)$

Temperature	$\text{Log}(a_T)$	
	Plain cores	Cores with 4% steel wool
5 °C	2.20371	2.02653
10 °C	1.46914	1.35101
20 °C	0	0
30 °C	-1.46913	-1.35098

In Figure 7.19, the master curve of the plain cores shows a wider frequency range. In Table 7.9, the amount of shift in constructing the master curve, $\text{Log}(a_T)$, is higher for plain cores than for cores with steel wool. It means that the cores with steel wool are less temperature (frequency) dependent.

It can also be seen in Figure 7.19 that the plain porous asphalt cores show higher indirect tensile resilient stiffness than the cores with 4% steel wool in the whole range of frequency. This conflicts with the steel wool reinforcement effect shown in Indirect Tensile Strength Test and Cantabro Test. The reason for the higher stiffness of plain cores is that the air void content in the plains cores is much lower than in the cores with steel wool. The cores with steel wool were drilled immediately after construction of the pavement, but the plain cores used in this test were drilled 6 months after construction (the first newly constructed plain cores were not enough for the research). The traffic load compacted the pavement gradually, resulting in lower air voids content in the pavement.

The plain core and the core with steel wool were scanned with a Siemens CT scanner to determine the air voids content. Figure 7.20 compares the air voids content of the core with and without steel wool. The average air voids content in the plain core and the core with steel wool is 8.2% and 16.1%, respectively. The plain core is much denser, which explains why it has higher resilient stiffness. Besides, the plain cores suffered ageing during the 6 months, further increasing the resilient stiffness.

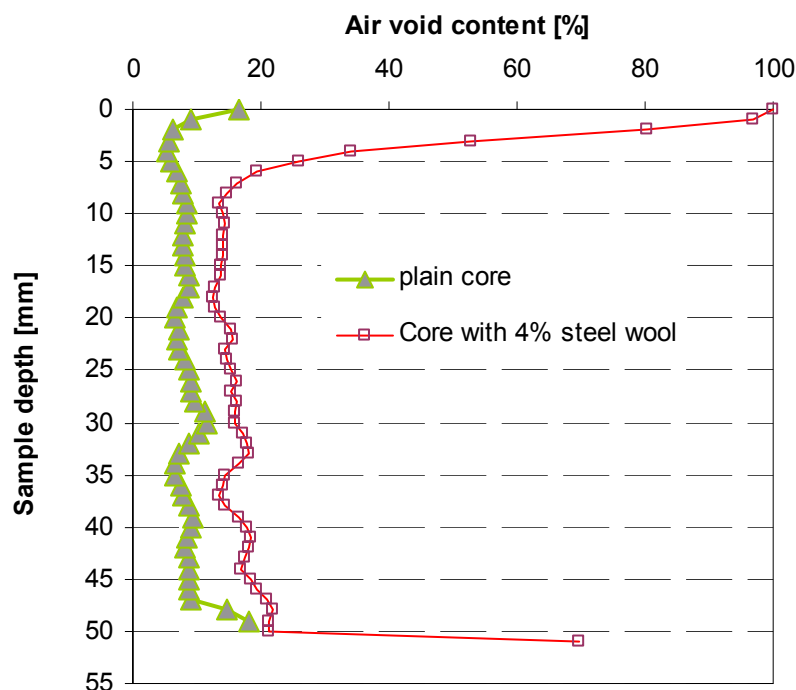


Figure 7.20: CT scan results of the air voids content in the cores

7.4.5 Indirect tensile fatigue test

The indirect tensile fatigue resistance of cores ($\text{Ø}100\text{mm}\times 50\text{mm}$) with or without steel wool is reported in this section. The fatigue test was done at 5°C to reduce the permanent deformation and the loading mode was continuous sinusoidal stress loading at 8 Hz (the maximum reliable frequency of the machine). The fatigue lives under different stress levels are tested for the two

mixtures. The results are plotted in Figure 7.21 to compare their fatigue behaviors.

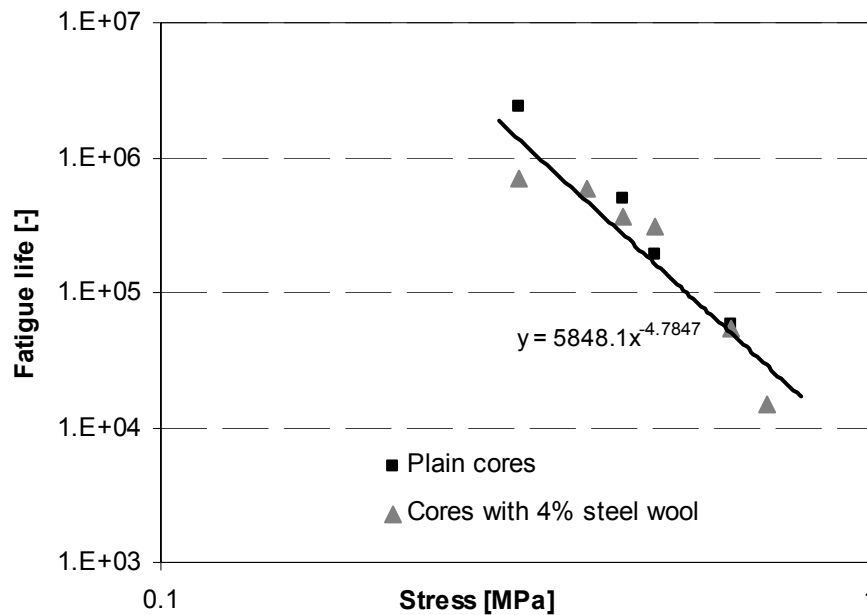


Figure 7.21: Indirect tensile fatigue life of field cores with and without 4% steel wool

In Figure 7.21 it is shown that, there is hardly any difference between the fatigue lines of the two mixtures, despite the fact that the plain cores have much lower air voids content (Figure 7.20). This could be explained by the reinforcement effect of steel wool. Without the reinforcement effect of steel wool, a mixture with a much lower voids content (plain cores) would have better fatigue behavior than a more porous mixture (cores with steel wool).

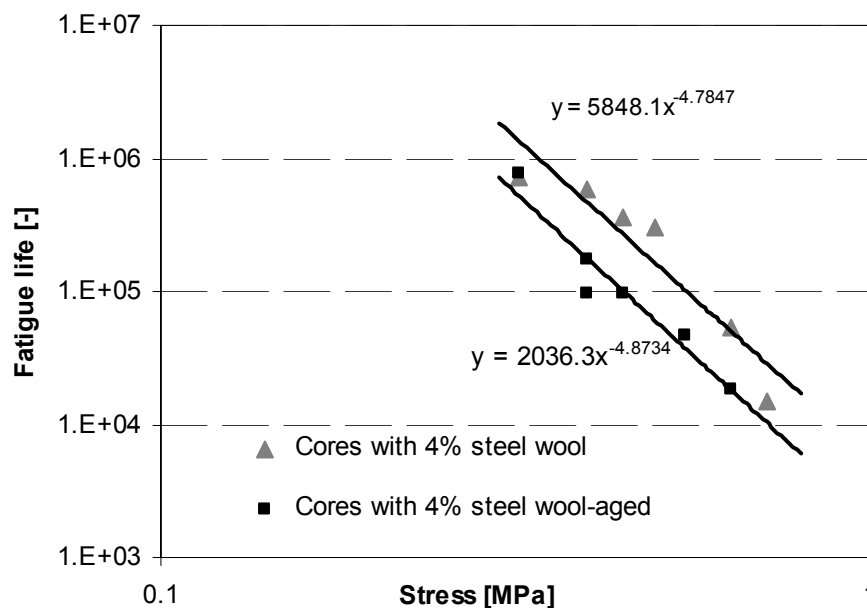


Figure 7.22: Indirect tensile fatigue lines of field cores with 4% steel wool (fresh and aged)

Figure 7.22 compares the fatigue lines of fresh and oven aged (240 hours at 85 °C) field cores with 4% steel wool. This ageing can be considered equal to approximately 5 years field ageing [Liu et al 2012]. It can be seen in Figure 7.21 that ageing decreased the fatigue life of porous asphalt cores. The aged cores show higher stiffness and are more brittle, losing the ability of resisting the stress loading without developing huge damage. This explains why aged porous asphalt layers are more susceptible to ravelling.

7.4.6 Nano indentation test

The Nano indentation test was used in this chapter to study the effect of steel wool on mechanical properties at the micro-level of the mortar bridge between stones in porous asphalt concrete cores. This chapter describes the test results. The sample preparation and the testing method for the nano indentation measurement are described in Chapter 5. The local indentation modulus and hardness of the mortar in the samples with and without steel wool were measured at an indentation depth of 1000 nm at -20 °C. To give an impression of the test, an indentation region of the mortar between stones is shown in Figure 7.23. After the test, the indentation modulus and hardness of the mortar can be obtained. To determine the average indentation modulus and hardness of the mortar in the samples, 200 measurements were done in each sample.

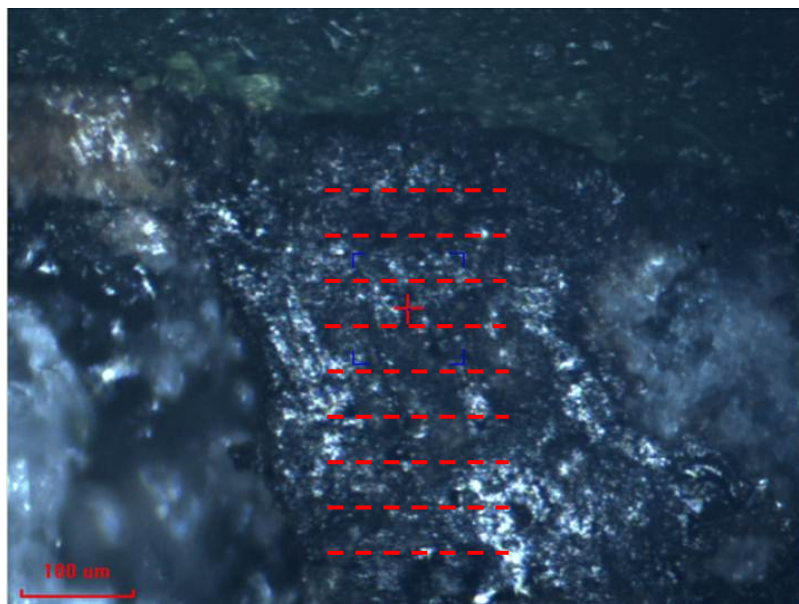


Figure 7.23: Indentation region of the bridge between stones

The average indentation modulus of the mortar was calculated with exclusion of the modulus higher than 5 GP (sand involved). The results are shown in Table 7.10. It can be seen that the mortar with steel wool shows a higher indentation modulus and a higher hardness, which indicates that steel wool reinforces porous asphalt cores. The mortar with steel wool also shows a higher ductility in the indirect tensile strength test. Based on these two findings, it can be expected that the steel wool trial section has better ravelling resistance than the reference section. Ageing increases the indentation modulus and

hardness of the mortar in both reference cores and cores with steel wool. The aged mortar in sample with steel wool is still stronger (with higher hardness) than that in aged reference sample.

Table 7.10: The average indentation modulus and hardness of the mortar in the samples with and without steel wool (both fresh and aged)

Source of the sample	Indentation modulus (standard deviation)	Hardness (standard deviation)
Plain core	2.0 (0.93) GPa	24.2 (10.2) MPa
Core with steel wool	2.28 (0.81) GPa	33.8 (11.3) MPa
Aged plain core	2.85 (0.44) GPa	34.5 (10.7) MPa
Aged core with steel wool	2.78 (0.70) GPa	43.4 (12.1) MPa

7.4.7 Nano CT scanning test

In order to get an indication of the distribution of steel wool in porous asphalt concrete, a small cube with a clear bridge of mortar was sawn from the Nano indentation sample and was scanned with a Phoenix Nanotom X-ray Computed Tomography (CT) scanner. After scanning, reconstructions were made to analyze the distribution of steel wool.

Figure 7.24 shows the distribution of steel wool in the sample. It can be seen that the steel wool is dispersed quite well in the sample and no clusters can be observed. This explains why the sample is heated homogeneously at the sample height. It is also observed that the average length of steel wool in the sample is around 1 mm, which is only 10% of its initial length. It means that serious degradation of the steel wool length occurs during mixing, which could be negative for heating and mechanical purpose. So, the mixing procedure still needs to be improved to prevent steel wool from degrading in further research.



Figure 7.24: Steel wool distributions in the sample

7.4.8 Stiffness recovery test

To detect the healing effect on cores after induction heating, the stiffness recovery is used as a healing indicator in this test. The idea of the test is to introduce some damage to the cores by fatigue loading and heat the cores with induction energy to see if the stiffness can recover. The testing procedure for the stiffness recovery test was as follows:

- 1) Conduct indirect tensile fatigue test on the sample with a cyclic load of 0.5 MPa at 5 °C and 8 Hz until its resilient stiffness reduces to 85%, 54% or 24% of its initial stiffness (The permanent deformation of the samples are 1.05 mm, 2.31 mm and 3.50 mm respectively).
- 2) Measure the resilient stiffness recovery of the sample during 2 hours (the test setup is shown in Figure 7.18).
- 3) Heat the samples to 85 °C with the induction heating machine and rest the samples for 2 hours. An infrared camera was used to monitor the temperature of the sample during heating.
- 4) Measure the additional flexural stiffness recovery over time caused by the induction heating until 8 hours.

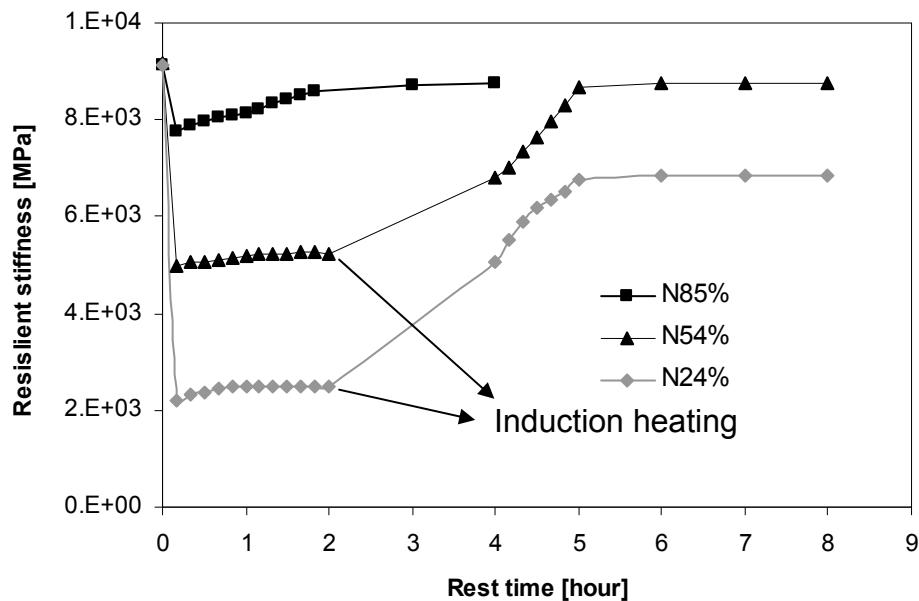


Figure 7.25: Stiffness recoveries of the field cores with 4% steel wool

The stiffness recoveries of the samples at different fatigue levels (decrease of stiffness) are presented in Figure 7.25. When the stiffness of the sample reduces to 85% of its initial value, it can recover to its initial value by itself after a rest period of 4 hours. This recovery is caused by self healing of porous asphalt concrete itself. When the stiffness of the sample reduces to 54% of its initial value, it can only recover a bit by self healing. It is believed that in this case the damage is beyond the self healing ability of the sample. However, the sample can obtain full stiffness recovery when induction heating is applied to it. The extra stiffness recovery is caused by induction healing. Based on this extra recovery of the stiffness, it can be concluded that induction heating

enhances the healing ability of porous asphalt cores. However, when the stiffness of the sample reduces to 24% of its initial value, it can not recover much by self healing and it can only partially recover with induction heating. In this case, it is too late for induction heating to heal all the damage.

7.4.9 Fatigue life extension test

The fatigue life extension thanks to the induction heating was also used as a healing index to characterize the healing effect. Two sets of fatigue test were performed at 0.5 MPa, 5 °C with a frequency of 8Hz. In the first one, the fatigue test was run on one field core with steel wool until failure to test its original fatigue life. In the second set, a number of fatigue loadings were applied on a sample until its stiffness reduced to 24% of its initial value and induction heating was used to heal the damage. After measuring the stiffness recovery of the healed sample in the stiffness recovery test (N24%), the fatigue life of the sample was tested and compared with the original fatigue life of the field core.

As shown in Figure 7.26, the original fatigue life of the core was 335,336 cycles. The applied fatigue loading was 305,520 cycles when the stiffness of the sample was reduced to 24% of its initial value. After heating the sample to 85 °C and resting it for 6 hours in the stiffness recovery test, the fatigue life of this sample was 179,880 cycles. The overall fatigue life of the sample was 485,400 cycles, which was 150,064 cycles longer than the original fatigue life. In this case, the fatigue life of the sample was extended by 44.8% due to induction heating (healing). It is already shown in the stiffness recovery test that there is almost no natural healing (no stiffness recovery) of this sample after a rest period of 2 hours. So, it can be concluded that induction heating increases the healing capacity of the field cores with steel wool.

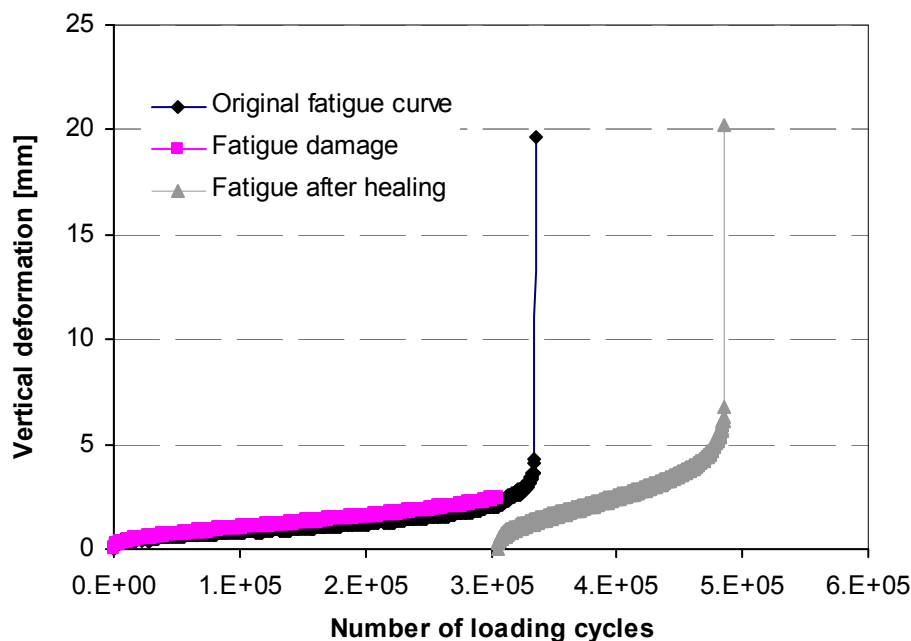


Figure 7.26: Fatigue life extension of the field cores with 4% steel wool

However, the indirect tensile fatigue life extension shown here is just an indication of induction heating. The indirect tensile test is not recommended for healing detection because of the permanent deformation in the sample during the test and the potential variations of the fatigue life of the samples. The induction heating potential of the material was already proven in Chapter 6 with beam samples in three point bending and four point bending tests, which give the same indication.

7.5 Modeling of the thermal transfer in the field trial section after induction heating

As the trial section was just placed in December 2010, it will take probably a few years before the first induction heating treatment takes place. In order to predict how long the porous asphalt layer can maintain the temperature after induction heating and to study the effects of the environment (temperature, wind speed and solar radiation) on the cooling rate of the pavement surface, a numerical simulation of the thermal transfer in the trial section is done in this chapter.

7.5.1 Thermal properties of an asphalt pavement

After induction heating, the temperature of the porous asphalt concrete layer (especially the top part) is much higher than the temperature of the environment, so the heat will transfer to the atmosphere and other layers below the porous asphalt layer. As shown in Figure 7.27, three ways of heat transfer (conduction, convection and radiation) can take place in the porous asphalt layer after induction heating. Heat will transfer to the dense asphalt layer below the porous asphalt layer and then to the base layer by conduction, and transfer to the air by surface convection and long wave radiation. At the same time, the pavement surface will absorb solar radiation.

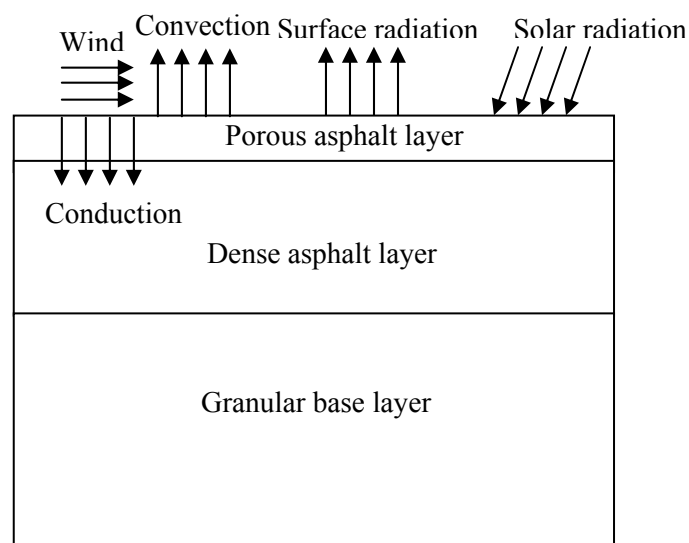


Figure 7.27: Thermal analysis of pavement after induction heating

According to Fick's second law, this one-dimensional transient heat conduction within the pavement can be described by the following differential Equation 7.1:

$$\frac{\partial}{\partial z} \left(k \frac{\partial T}{\partial z} \right) = \rho c \frac{\partial T}{\partial t} \quad (7.1)$$

Where k is the thermal conductivity in W/mK; T is the temperature in K; z is the depth below the pavement surface in m; ρ is the density in kg/m³; c is the heat capacity in J/KgK and t is the time in s.

This formula can be simplified to Equation 7.2 by assuming a constant thermal conductivity:

$$k \frac{\partial^2 T}{\partial z^2} = \rho c \frac{\partial T}{\partial t} \quad (7.2)$$

According to Ozisik [Ozisik 1985], the free convection heat transfer between the pavement surface and the air can be estimated by Equation 7.3:

$$q = h_c (T_s - T_a) \quad (7.3)$$

Where q is the heat flux in W/m²; h_c is the convection coefficient in W/m²; T_s and T_a are the temperature of the pavement surface and the air respectively, in K.

Two kinds of radiation should be considered at the pavement surface. On one hand, heat will flow to the ambient air because the temperature at the pavement surface is much higher than that of the environment. This radiation heat flux can be described by Equation 7.4:

$$q_e = \sigma (\varepsilon_s T_s^4 - \varepsilon_a T_a^4) \quad (7.4)$$

Where q_e is the heat flux in W/m²; σ is the Stefan-Boltzmann constant equal to 5.669×10^{-8} W/m²K⁴; ε_s is the pavement emittance to the air and ε_a is the emittance of air to the pavement surface.

On the other hand, the pavement will also absorb solar radiation from the sun. This radiation heat flux q_a can be represented by Equation 7.5:

$$q_a = \varepsilon_r G \quad (7.5)$$

Where ε_r is the pavement absorptance of solar radiation and to the air and G is the solar flux on the pavement surface in W/m².

So the net radiation heat flux of the pavement surface is a combination of emittance radiation and absorption radiation, shown in Figure 7.6:

$$q_r = \sigma (\varepsilon_s T_s^4 - \varepsilon_a T_a^4) - \varepsilon_r G \quad (7.6)$$

7.5.2 Introduction to the model program FEMMASSE HEAT-MLS

To predict the temperature variations within the pavement after induction heating, a finite element program FEMMASSE HEAT-MLS, which is capable to compute the heat diffusion within a multi layers system, is used in this research. The flow chart and input parameters of this program are introduced in the following paragraphs. The input parameters such as wind speed, environment temperature and solar radiation can be changed to study their effects on the temperature cooling process of the pavement surface.

The flowchart of this model is shown in Figure 7.28.

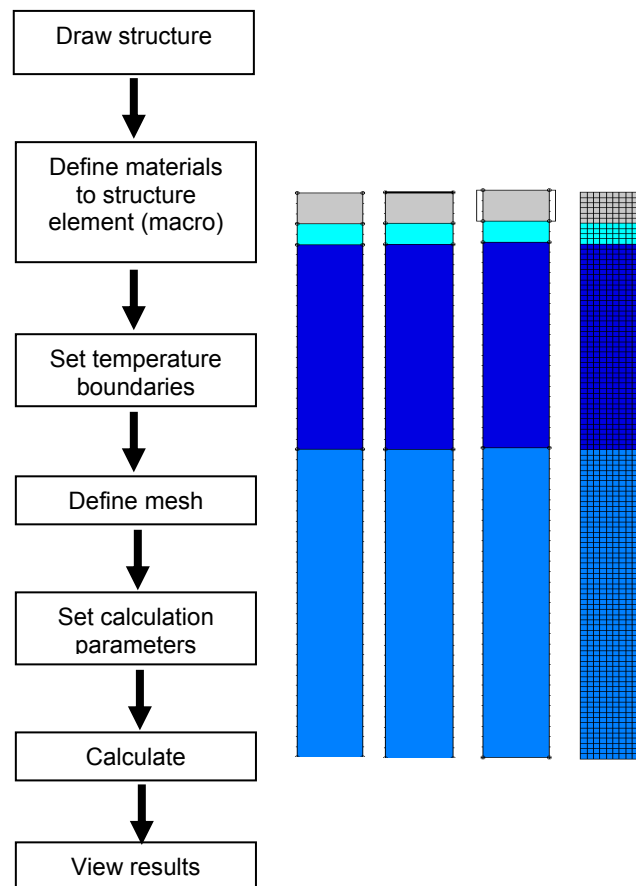


Figure 7.28: Flow chart of the modeling program FEMMASSE HEAT-MLS

Firstly, to use this model, the structure of a pavement should be defined. The pavement structure used in this model consists of 50 mm porous asphalt concrete trial section, 200 mm dense asphalt concrete and 300 mm unbound granular base. This is a normal structure of a Dutch pavement on highways.

Secondly, the properties of materials have to be defined. To simulate the heat diffusion process, the thermal properties of the materials including the heat capacity and thermal conductivity are required. For dense graded asphalt mixtures, the mostly reported intermediate values of the heat capacity and heat conductivity are used in this modeling [Wolfe et al 1980, Tegeler and Dempsey 1973, Corlew and Dickson 1968, Tuner and Malloy 1981, Luca and Mrawia 2005 and Wu et al 2008]: a thermal conductivity of 1.3 W/mK and a

heat capacity of 920 J/KgK (corresponding to 2254 KJ/m³K for dense graded asphalt concrete with a density of 2450 Kg/m³). According to the American National Asphalt Pavement Association, the thermal conductivity of an open graded friction course (OGFC) is up to 70% less than dense graded asphalt concrete. So, the thermal conductivity of porous asphalt concrete is assumed as 50% of dense graded asphalt concrete in this modeling. It is assumed that normal porous asphalt concrete and dense graded asphalt concrete have the same heat capacity of 920 J/KgK. However, this heat capacity equals to 1840 KJ/m³K for porous asphalt concrete with density of 2000 Kg/m³. For the base layer, a thermal conductivity of 1.3 W/mK and a heat capacity of 1473 J/KgK are assumed. Based on the previous literature review and analysis, the thermal properties for the three layers of the pavement are summarized in Table 7.11.

Table 7.11: Heat capacity and thermal conductivity for the three layers of the pavement

Layer	Heat capacity [KJ/m ³ K]	Thermal conductivity [W/mK]
Porous asphalt concrete	1840	0.65
Dense asphalt concrete	2254	1.3
Gravel Base	1473	1.3

Thirdly, the temperature boundaries for the pavement structure need to be defined. It is assumed that induction heating will be applied on the induction heating porous asphalt trial section in March to close possible cracks occurred in the past winter. The initial temperature of all layers and the ambient air is assumed to be 5 °C (the mean temperature in March in the Netherlands). The heat convection coefficient is required to define at the surface of the pavement. The following equation is used to determine the convection heat transfer coefficient [Alford et al 1939]:

$$h_c = 7.4 + 6.39 \times W^{0.75} \quad (7.7)$$

Where h_c is the convective heat transfer coefficient (W/m²K) and W is the wind velocity at 2 meters above the ground level (m/s).

For a medium wind speed of 7 m/s, the thermal convection coefficient is 34.90 W/m²K. This thermal convection coefficient is assumed constant at a constant ambient air temperature.

For the radiation, three coefficients ε_r (direct solar radiation on a surface), ε_s (long-wave radiation from the surface to the atmosphere) and ε_a (emissivity of the atmosphere) were defined and practical values were used for these three coefficients (shown in Table 7.12).

Table 7.12: Radiation coefficients

ε_s	ε_a	ε_r
0.95	0.94	0.81

Based on experience, the maximum global solar radiation at 12:00 hours was assumed at 284 W/m^2 and the duration of solar radiation was 10 hours. The typical global solar radiation used in this simulation is shown in Figure 7.29.

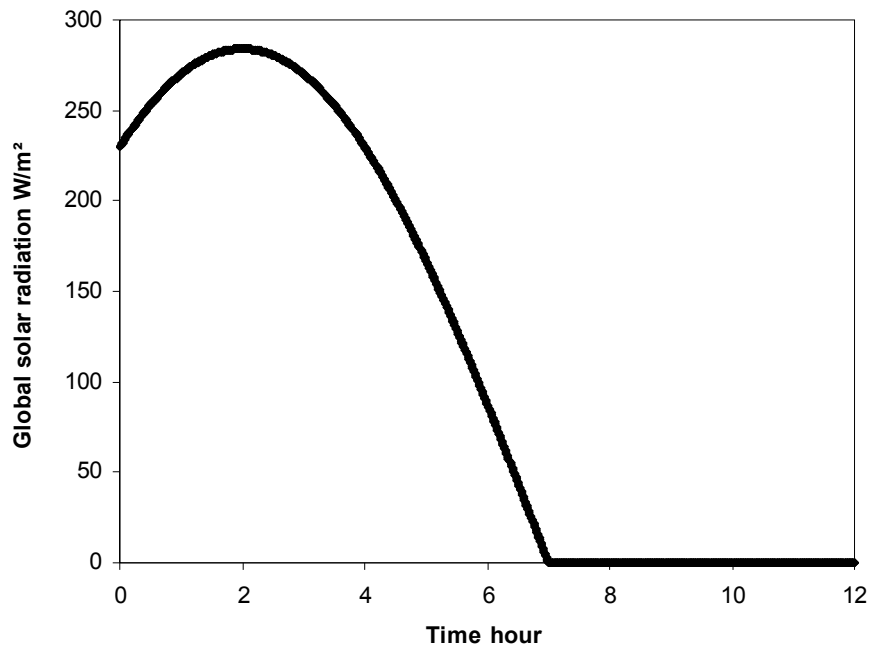


Figure 7.29: Typical global solar radiation (in March) used in the simulation

Fourthly, the temperature of the heated porous asphalt layer during induction heating should be defined. For simplicity, the porous asphalt layer is assumed to be heated only in the top 20 mm. This 20 mm layer is heated from $5 \text{ }^\circ\text{C}$ (normal temperature in March in the Netherlands) to $85 \text{ }^\circ\text{C}$ in 30 seconds. It is also assumed that the conductive porous asphalt concrete is heated homogeneously over this thickness.

After setting the temperature boundaries, we need to define a mesh on the structure element and set calculation parameters. The thermal transfer within the pavement during 12 hours was studied with this program. For the first 0.1 hour, the time increment was set as 0.0001 hour. In the following period, the time increment was changed to 0.1 hour. The number of the total calculation steps is 1119. After setting the calculation parameters, the calculation of the thermal transfer process within the pavement can be started.

7.5.3 Results and analysis

Thermal transfer within the pavement

To study the thermal transfer process in the pavement after induction heating, the temperature profiles at different layers of the pavement during 4 hours with a wind speed of 7 m/s are plotted in Figure 7.30.

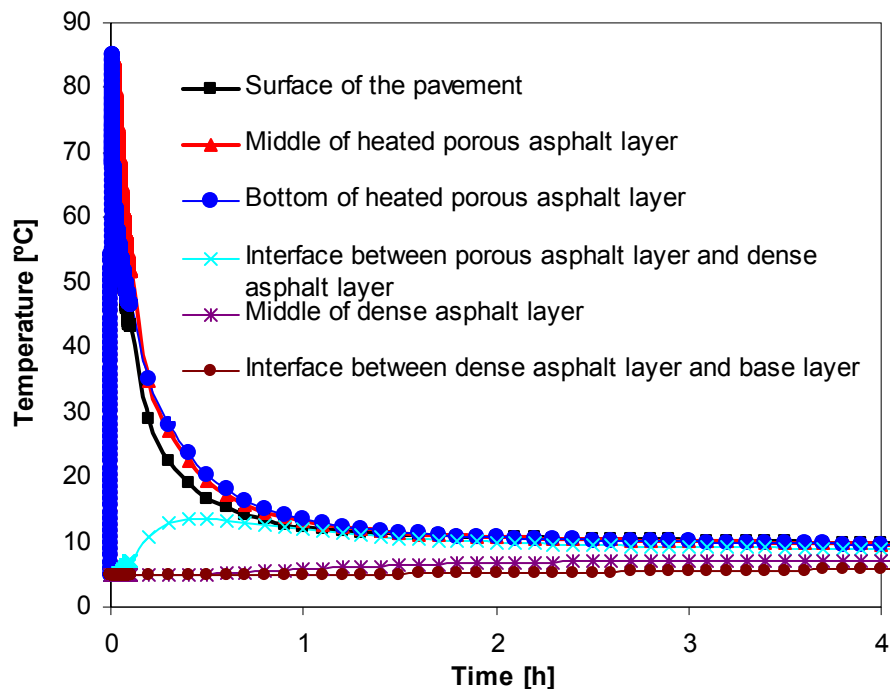


Figure 7.30: Temperature profiles at different layers

Within the heated porous asphalt concrete, the abilities of different layers to maintain the temperature are slightly different. The pavement surface is most susceptible to lose heat by means of convection and long wave radiation to the atmosphere: the temperature at the surface of the pavement decreases from 85 °C to 12.4 °C in one hour. The interface between heated and unheated porous asphalt layers will also lose heat because of thermal conduction to the layers below, which has much lower temperature: the temperature at the bottom of the heated porous asphalt layer decreases from 85 °C to 13.1 °C in one hour. The middle part of the heated porous asphalt layer is most capable to keep its temperature because of the low surrounding temperature gradient: the temperature at this part is 13.5 °C after cooling for one hour. The temperature at the interface between porous asphalt layer and dense asphalt layer reaches a maximum of 13.5 °C after 0.5 hour's thermal transfer and decreases thereafter. After 2 hours, the temperature at the heated porous asphalt layer almost levels off and the temperature differences in this layer become very small. The temperature in the middle of the dense asphalt layer only increases 2.2 °C after 4 hours. Very little heat can reach the base layer, so the temperature at the interface between the dense asphalt layer and the base layer only increases 1.3 °C.

As far as induction healing rate is concerned, the first hour after heating is most important, because thereafter the temperature is too low for healing.

Vertical temperature variations within the conductive porous asphalt layer

It is very important for the micro cracks closing rate how long the porous asphalt layer can keep warm after induction heating. For that, the

temperature within the porous asphalt layer was analyzed during 12 hours with the modeling program. The results are shown in Figure 7.31, where the temperature variations of the porous asphalt layer can be seen.

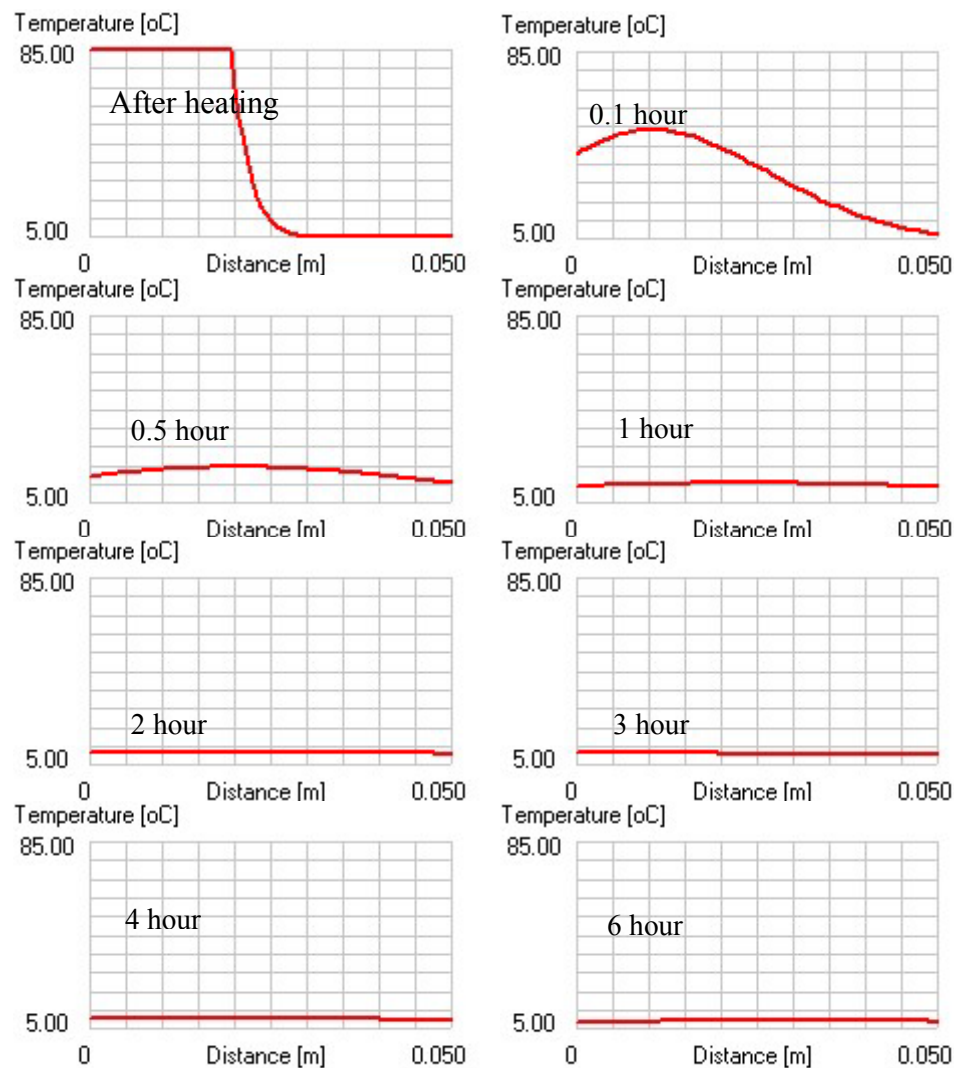


Figure 7.31: Vertical temperature variations within the porous asphalt layer

It is assumed in the modeling that the first 20 mm porous asphalt layer is heated homogeneously to 85 °C after 30 seconds' heating. On the one hand, the temperature within the heated porous asphalt layer, especially at the surface, decreases very rapidly after induction heating. On the other hand, the temperatures of the rest of the porous asphalt layer increases gradually. So, the temperature curve gradually turns into a parabolic curve in the first hour, where the temperature is highest in the middle of the porous asphalt layer. After that, the temperature over the whole thickness begins to decrease, but the temperature of the top part decreases more slowly than the bottom part because the pavement surface is absorbing solar energy. So, the temperature of the top part gradually becomes a bit higher than the bottom part. From the second hour, the temperature curve becomes linear, where the temperature decreases vertically from the top to the bottom. And then, the temperature curve keeps

linear, but the temperature difference between the top and the bottom becomes smaller. After cooling for 3 hours, the pavement surface temperature is 10.34 °C and the temperature difference within porous asphalt layer is only 1.09 °C. After that, the pavement surface cools very slowly with a temperature of 6.12 °C after cooling 12 hours. At the same time, the decrease of the solar radiation makes the pavement surface cool faster than the bottom layer.

Compared with the heating temperature of 85 °C and the atmosphere temperature of 5 °C, it is considered that the pavement surface with a temperature of 10.34 °C has already cooled down after cooling 3 hours. In chapter 6, it has been shown that the significant healing of porous asphalt concrete is already obtained after cooling 3 hours. So, it is recommended that the pavement can be open for traffic after cooling for 3 hours. If the heating speed can be increased a lot, then it is maybe possible to heat only the bitumen and not the aggregates. The cooling rate will be faster in that case. However, the healing rate will not be influenced a lot, because the healing is almost immediate at high temperatures.

Effect of the wind speed on the cooling rate of the pavement surface

To study the factors influencing the cooling rate of the conductive porous asphalt layer, the medium wind speed of 7 m/s was varied to a mild wind of 2 m/s or a strong wind of 12 m/s in the modeling program to see its effect (corresponding to the convective heat transfer coefficient of 18.15 W/m²K or 48.60 W/m²K). The effect of the wind speed on the cooling rate of the pavement surface is presented in Figure 7.32.

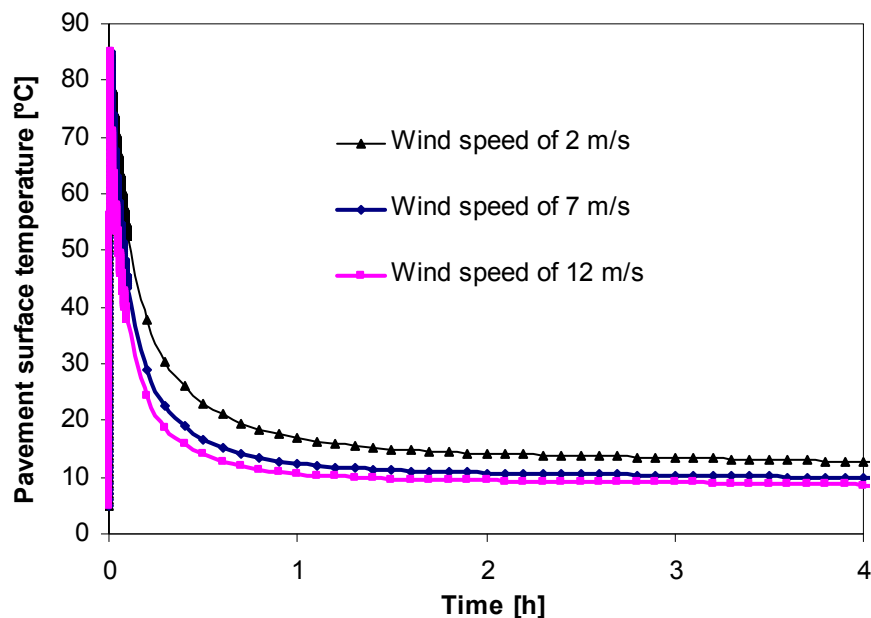


Figure 7.32: Effect of the wind speed on the cooling rate of the pavement surface

It is clear in Figure 7.32 that the wind speed significantly influences the cooling rate of the pavement surface: the decrease of the wind speed greatly increases the ability of the pavement to keep the heat and maintain its temperature and the increase of the wind speed decreases this ability. The pavement surface can maintain its temperature higher than 50 °C for 3.3 minutes, 4.5 minutes or 7.2 minutes with the wind speed of 12 m/s, 7 m/s or 2 m/s respectively. The temperature difference of the pavement surface in a mild wind or a strong wind condition can be as large as 14.8 °C. The temperature at the surface of the pavement with a mild wind is always much higher than with a strong wind during the cooling process. It is easy to understand this: an increase of the wind speed results in a higher convective thermal transfer coefficient, so the pavement loses heat more quickly in higher wind speed condition. So, to have a good healing (micro cracks closing) rate by high temperature healing, induction heating should be applied on the pavement in mild wind or no wind condition.

Effect of the environment temperature on the cooling rate of the pavement surface

The environment temperature can strongly influence the temperature reached of the conductive porous asphalt layer after induction heating. Given a constant induction heating speed, the conductive porous asphalt layer can be heated from 5 °C to 85 °C or heated from 20 °C to 100 °C after 30 seconds' heating. In the simulation, the initial temperature of the whole system was changed from 5 °C to 20 °C to study the cooling process of the pavement surface in both conditions. The results of this simulation are shown in Figure 7.33. The differences of the pavement surface temperature under two conditions are also plotted in Figure 7.33.

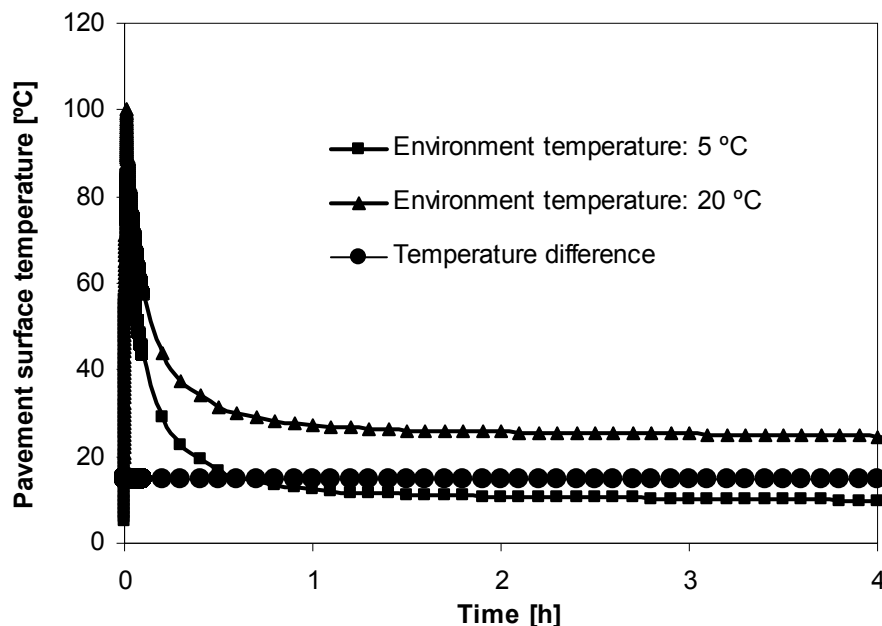


Figure 7.33: Effect of the environment temperature on the temperature variations at the surface of conductive porous asphalt layer

It is found that during the whole cooling process, the difference of the pavement surface temperature under the two conditions keeps constant at 15 °C, which is the difference of the initial environment temperatures. On the one hand, it means that the environment temperature has no effect on the cooling rate of the pavement surface temperature. It is comprehensible that the temperature gradient under these two conditions is the same when the induction heating speed is constant, and the same temperature gradient will result in the same cooling rate of the temperature. On the other hand, the environment temperature will greatly influence the high temperature healing rate of the porous asphalt layer. The pavement should be heated longer to reach the temperature required for healing in lower environment temperature condition. So, it is advised to apply induction heating on the pavement in higher temperature condition.

Effect of the solar radiation on the cooling rate of the pavement surface

The effect of the solar radiation on the cooling rate of the pavement surface temperature was also investigated by removing the direct solar radiation on the pavement surface from the input ($\epsilon_r = 0$). Figure 7.34 compares the cooling rates of the pavement surface with and without solar radiation.

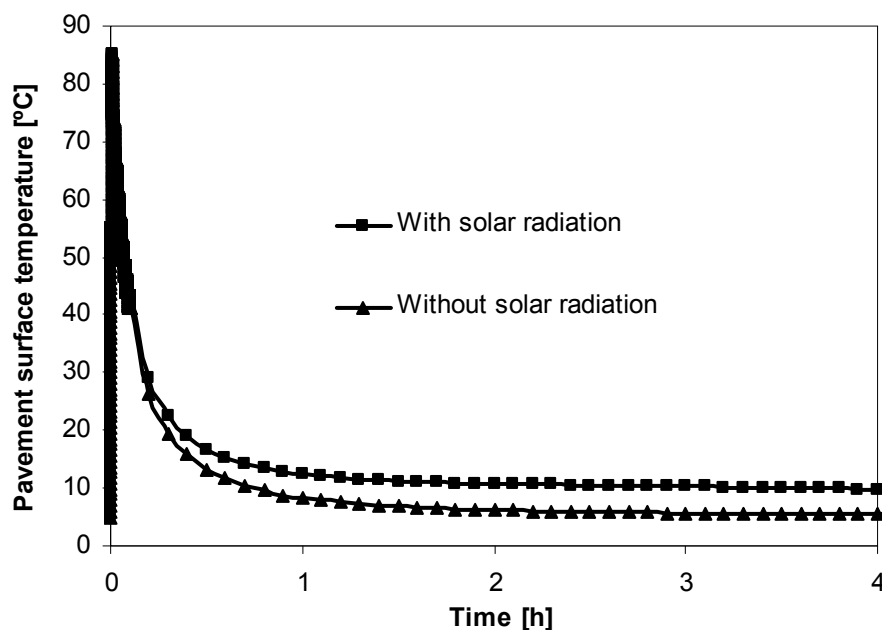


Figure 7.34: Effect of the solar radiation on the cooling rate of the pavement surface

As shown in Figure 7.34, the temperature at the pavement surface without solar radiation decreases faster than with solar radiation, because the pavement surface cannot absorb solar energy. With or without solar radiation, the difference of the pavement surface temperature can be 4.7 °C. Based on this finding, induction heating should be applied on the pavement in good solar radiation condition. However, compared to the effects of the wind speed and

environment temperature, the influence of the solar radiation on the cooling rate of the pavement surface is much lower.

7.6 Summary and Conclusions

The porous asphalt mixture with steel wool developed at Delft University of Technology was assessed in the laboratory of Heijmans-Breijn in Rosmalen. The mixing procedure was optimized. The optimal order of mixing is to first mix bitumen and steel wool. The clusters of steel wool can be pulled apart by mixing with stone, sand and filler. The volume content of steel wool (by bitumen) was reduced to 4% to solve the problems when mixing at higher quantities. Nevertheless, porous asphalt concrete Marshall Samples with 4% steel wool can be heated with induction energy and they have higher indirect tensile strength, higher indirect tensile strength ratio and higher particle loss resistance than plain porous asphalt concrete samples. So, it was decided to incorporate 4% steel wool into the porous asphalt mixture for the trial section built on a Dutch highway.

Before paving the trial section, research was done to produce a good porous asphalt mixture with 4% steel wool in the asphalt plant of Heijmans-Breijn in Zwijndrecht. A wood chipper was used to disperse steel wool before mixing and the mixing procedure was optimized. The most efficient mixing procedure is mixing steel wool, bitumen and filler for 100 seconds, then adding stone/sand and mixing for another 200 seconds. This mixing procedure produced a very good mixture and was used to produce the asphalt for the trial section. However, the mixing procedure still needs to be optimized to decrease the mixing time and to make it possible to incorporate more steel wool into the mixture.

A field trial section with the induction healing porous asphalt concrete was constructed on Dutch motorway A58 on December 11, 2010. The trial section was still fully intact after the past two winters perfectly. Cores were drilled from the trial section and experiments were done on them to study their heating, mechanical and healing properties.

Porous asphalt field cores with steel wool can be heated with induction energy, but the heating speed is not high enough with the present induction heating machine used in this research. However, tests have shown that optimizing the induction machine improves the heating speed a lot.

Both fresh and aged porous asphalt field cores with steel wool have higher particle loss resistance than fresh and aged plain porous asphalt cores in Cantabro test.

Porous asphalt field cores with steel wool have slightly higher indirect tensile strength and much higher tensile deformation at failure than plain cores. Porous asphalt field cores with steel wool also show a high indirect tensile strength ratio, indicating a good resistance to water damage.

Porous asphalt field cores with steel wool have slightly lower indirect tensile resilient stiffness and less temperature dependency than plain cores. The plain cores are gradually compacted by traffic loading and are much denser

than the cores with steel wool, which were drilled immediately after construction.

Porous asphalt field cores with steel wool and plain cores (much denser) show similar fatigue behavior. Ageing decreases the fatigue life of porous asphalt field cores with steel wool.

The mortar in porous asphalt field cores with steel wool shows a higher indentation modulus and a higher hardness than in plain cores.

Steel wool is well dispersed in the sample shown in CT scan test.

The stiffness of the damaged porous asphalt core with steel wool recovers much more with induction heating than without induction heating. The fatigue life of the porous asphalt core with steel wool is also extended by induction heating. So, induction heating enhances the healing capacity of the porous asphalt core with steel wool.

The thermal transfer process within the trial section after induction heating was simulated with the FEMMASSE HEAT-MLS program. The pavement surface cools from 85 °C to 10.34 °C after cooling for 3 hours. The effects of wind speed, environment temperature and solar radiation on the cooling rate of the pavement surface were studied. It is recommended that induction heating should be applied on the pavement on a day with low wind speed, high temperature and high solar radiation.

Based on the findings above, it is expected that the durability of the field trial section with steel wool can be enhanced by the addition of steel wool and induction heating.

Chapter 8 Conclusions and Recommendations

8.1 Introduction

In this research, the possibility of using an induction heating approach to enhance the self healing capacity of porous asphalt concrete is investigated. Induction heating activates the self healing capacity of porous asphalt concrete at high temperatures. To make induction heating/healing work, steel wool fiber is added to a porous asphalt mixture to make it electrically conductive and suitable for induction heating. When micro cracks are expected to occur in porous asphalt, induction heating can be applied to the material to increase the temperature. The micro cracks can be closed through the high temperature healing of the bitumen (diffusion and flow). The closure of the micro cracks prevents the formation of macro cracks and ravelling in the end.

The electrical conductivity, induction heating speed, mechanical properties (including particle loss resistance, indirect tensile strength, water sensitivity, indentation modulus, stiffness and fatigue resistance) and healing potential (the strength/stiffness recovery and fatigue life extension) of porous asphalt concrete with steel wool were investigated with laboratory experiments in this research. This induction healing concept was applied on a trial section on the Dutch motorway A58.

In this chapter, the conclusions and recommendations resulting from this research are presented.

8.2 Conclusions

The general conclusions with regards to the main goals of this thesis are as follows:

1. Adding steel (wool) fiber to porous asphalt concrete makes it electrically conductive. The electrical resistance of porous asphalt concrete depends on the content, diameter and length of steel fiber. There is an optimal content of

each type of steel fiber for porous asphalt concrete to obtain the highest conductivity. Above this optimal content, addition of more steel fibers does not increase the conductivity anymore. Excess steel fibers can make the mixture difficult to mix.

2. Porous asphalt concrete with steel fiber (wool) can be heated with induction energy. The diameter, length and content of the steel fiber are important for the heating speed of porous asphalt concrete. There is an optimal content of each type of steel fiber. Addition of steel fiber above the optimum does not increase the induction heating speed anymore.
3. Addition of a moderate amount of steel fiber can increase the ravelling resistance and indirect tensile strength of porous asphalt concrete. Among the three different types of steel fiber (steel fiber type 1, steel wool type 00 and steel wool type 000), steel wool type 00 proved to be the most efficient to increase the particle loss (ravelling) resistance and strength of porous asphalt concrete. The optimal content of this type steel wool is 8% (by volume of bitumen) to obtain the lowest particle loss value or highest indirect tensile strength. Aged or water damaged samples with steel wool showed higher particle loss resistance than aged or water damaged plain samples. Adding 8% steel wool type 00 to porous asphalt concrete increases its resilient stiffness and decreases its temperature dependency and water sensitivity. Adding 8% steel wool type 00 to porous asphalt concrete also increases its fatigue resistance, the indentation modulus and hardness of the mortar.
4. The healing capacity of asphalt mastic and porous asphalt concrete is increased by induction heating. The completely fractured asphalt mastic beams and porous asphalt concrete beams with steel wool cannot heal themselves at low temperatures; but they can be healed many times due to induction heating. The stiffness of fatigue damaged porous asphalt concrete cylinders and beams recovered more and faster when induction heating is applied on the samples. The fatigue life of porous asphalt concrete cylinders and beams with steel wool is significantly extended after induction heating. The optimal heating temperature is 85 °C. Induction heating can be repeated when cracks appear again. Through multiple times induction heating, the fatigue life of a porous asphalt beam can be strongly increased. Induction heating also significantly increases the healing capacity and speed of aged porous asphalt beams. Induction heating should not be applied too early or too late during the service life of pavement.
5. The durability of porous asphalt concrete roads will be improved with induction heating because of the improvements in the healing capacity and in the fatigue resistance.

6. A finely mixed porous asphalt mixture with 4% steel wool 00 (volume fraction of bitumen) can be produced in the asphalt plant by first mixing steel wool with bitumen and filler, then adding stone and sand. However, the mixing time needed is 300 seconds, 6 times the normal mixing time for porous asphalt mixtures.
7. A porous asphalt trial section with the concept of induction heating was paved on Dutch motorway A58 in December 2010. The trial section was fully intact after the two winters of 2010-2011 and 2011-2012. The trial section can be heated with induction energy and cores from the trial section show better particle loss resistance than the reference section. It is expected that the durability of the trial section will be enhanced by induction heating.
8. In terms of heating of 85 °C, the porous asphalt trial section is already cooled down and the significant healing is already obtained after cooling for 3 hours. Induction heating should be applied on the trial section on a day with a low wind speed, a high temperature and a high solar radiation.

8.3 Recommendations

Based on the experience obtained from this thesis, the following aspects of applying induction heating technology are recommended for further research:

1. Optimization of steel fiber (wool)
The diameter and length of steel fiber are very important factors affecting the electrical conductivity and induction heating speed of porous asphalt concrete incorporating steel fiber. So, it is necessary to conduct research to optimize the steel fiber used in induction heating research. At the same time, the mechanical properties (especially particle loss resistance) of porous asphalt concrete incorporating steel fiber should be taken into account when determining the optimal diameter and length of steel fiber. Furthermore, conductive powders (graphite or magnetic powder) are not recommended in this research, because they do not reduce the binder drainage (gravity segregation) problem, which is a very important issue in porous asphalt concrete layers. Addition of steel fiber should not reduce the air voids content of the mixture, which is very important for the noise reduction, spray and splash functions of a porous asphalt layer.
2. Optimization of mixing technology
To shorten mixing time and save energy consumed in dispersing steel fiber into porous asphalt mixture, the mixing technology needs to be optimized. A wood chipper can be used to pre-disperse the steel fiber before mixing. It is recommended that steel wool is first mixed with bitumen. Then by adding filler, stone and sand, the steel fiber clusters were pulled apart by the rest of the mixture. Also, the degradation of the steel fiber should be avoided during the mixing process, because the length of the steel fiber is important

to the reinforcement and binder drainage prevention effects. This will be a challenge for further research.

3. Optimization of induction generator

To enhance the induction speed, the induction generator should be optimized by changing its frequency and the shape/size of the coil. The porous asphalt trial section should be heated very quickly and locally in the mortar to close the cracks inside without heating the stones. If the heating speed is low, heat will be lost to the stones, resulting in a low heating efficiency. The workability of the induction heating generator is also important when heating the trial section in the future. Besides, the heating temperature should be carefully controlled. A surface temperature of 85 °C in the mortar is recommended. Further heating will cause binder drainage problem, offsetting the benefits of heating.

4. Modeling of induction healing in porous asphalt concrete

To fully understand the mechanisms involved in induction healing and to predict the induction heating time needed to obtain a full healing recovery of porous asphalt concrete, modeling work can be of great help. The capillary flow of the Newtonian binder in cracks under surface tension force will be simulated in further research.

References

- Abo-Qudais S, Suleiman A (2005). Monitoring fatigue damage and crack healing by ultrasound wave velocity. *Nondestructive Testing and Evaluation*, 20(2):125-145.
- Ahmed TJ, Stavrov D, Bersee HEN, Beukers A (2006). Induction welding of thermoplastic composites-an overview. *Composites: Part A* 37:1638-1651.
- Allex Eduardo Alvarez, Amy Epps-Martin, Cindy Estakhri, Richard Izzo (2010). Evaluation of durability tests for permeable friction course mixtures, *International Journal of Pavement Engineering* 11(1): 49-60.
- Alford JS, Ryan JE, and Urban FO (1939). Effect of heat storage and variation in outdoor temperature and solar intensity on heat transfer through walls. *Transactions: American Society of Heating and Ventilating Engineers* 45:369-396.
- Alvarez AE, Epps Martin A, Estakhri CK, Button JW, Glover GJ, Jung SH (2006). Synthesis of current practice on the design, construction, and maintenance of porous friction courses. FHWA TX-06/0-5262-1. Texas Transportation Institute. College Station, Texas.
- Anderson HM, Keller MW, Moore JS, Sottos NR and White SR (2007). Self healing polymers and composites. First International Conference on Self Healing Materials, Noordwijk, The Netherlands.
- Bahia HU, Hanson DI, Zeng M, Zhai H, Khatri MA, Anderson RM (2001). Characterization of modified asphalt binders in Superpave mix design, NCHRP report 459, National Academy press, Washington DC.
- Bazin P, Saunier J (1967). Deformability, fatigue, and healing properties of asphalt mixes. *Proceedings of the Second International Conference on the Structural Design of Asphalt Pavements*, Ann Arbor, Michigan, pp 553-569.
- Behbahani H, Nowbakht S, Fazaeli H, Rahmani J (2009). Effects of fiber type and content on the rutting performance of stone matrix asphalt. *Journal of Applied Sciences* 9(10):1980-1984.
- Bendtsen H, Nielsen CB, Raaberg J, Macdonald RA (2002). Clogging of porous bituminous surfacings – an investigation in Copenhagen. Danish Road Institute Report 120. Road Directorate, Danish Road Institute. Denmark.
- Bennert T, Fee F, Sheehy E, Jumikis A, Sauber R (2005). Comparison of thin-lift HMA surface course mixes in New Jersey. TRB 2005 Annual Meeting CD-ROM. Transportation Research Board. National Research Council. Washington DC.
- Bhasin A, Bommavaram R, Greenfield MI, Little DN (2011). Use of molecular dynamics to investigate self-healing mechanisms in asphalt binders. *Journal of Materials in Civil Engineering* 23(4):485-492.
- Bhasin A, Little DN, Bommavaram R, Vasconcelos KL (2008). A framework to quantify the effect of healing in bituminous materials using material properties. *International Journal of Road Materials and Pavement Design* 8:219–242.
- Blom SD, Veltman J. Self healing Asphalt. Breijn report-6710801, 2011.
- Bolzan PE, Nicholls JC, Huber GA (2001). Searching for superior performing porous asphalt wearing courses. TRB 2001 Annual Meeting CD-ROM. Transportation Research Board. National Research Council. Washington DC.
- Bonnaure FP, Huibers AH, Boonders A (1982). A laboratory investigation of the influence of rest periods on the fatigue characteristics of bituminous mixes, *Journal of the Association of Asphalt Paving Technologists* 5:104-128.
- Brown SF, Rowlett RD, Boucher JL (1990). Asphalt modification. In: *Proceedings of the conference on the United States strategic highway research program: sharing the benefits*. London: Thomas Telford (Pub.), p. 181-203.

- Brown SF, Thom NH, Sanders PJ (2001). A study of grid reinforced asphalt to combat reflective cracking. *Journal of Association of Asphalt Paving Technologists* 70:543-570.
- California Department of Transportation. Open graded friction course usage guide. Sacramento, CA, 2006.
- Carpenter SH, Shen S (2006). A dissipated energy approach to study HMA healing in fatigue. In *Transportation Research Record No:1970. Journal of the Transportation Research Board:178-185.*
- Castro M, Sánchez JA (2006). Fatigue and healing of asphalt mixtures: discriminate analysis of fatigue curves. *Journal of Transportation Engineering* 132(2):168-174.
- Chailleux E, Ramond G, Such C, de La Roche C (2008). A mathematical-based master-curve construction method applied to complex modulus of bituminous materials. *Road materials and Pavement Design, EATA 2008*, p. 75-92.
- Chen B, Wu K, Yao W (2004). Conductivity of carbon fiber reinforced cement-based composites. *Cement and Concrete Composites* 26:291-7.
- Chen H, Li N, Hu C, Zhang Z (2004). Mechanical performance of fibers-reinforced asphalt mixture. *J Chan Univ (Nat Sci Ed)* 24(2):1-5.
- Cheng D (2002). Surface free energy of asphalt-aggregate system and performance analysis of asphalt concrete based on surface free energy. Ph.D. Dissertation, Texas A&M University, College Station, Texas.
- Chowdhury A, Button J, Bhasin A (2006). Fibers from recycled tires as reinforcement in hot mix asphalt. Report No. SWUTC/05/167453-1, Texas Transportation Institute, Texas A&M University, College Station, Texas.
- Cooley L, Allen Jr, Brown ER, Watson DE (2000). Evaluation of OGFC Mixtures With Cellulose Fibers. *Transportation Research Record No: 1723. Transportation Research Board. National Research Council. Washington DC.*
- Cooper SB, Abadie C, Mohammad LN (2004). Evaluation of open-graded friction course mixture. Louisiana Transportation Research Center Technical Assistance Report Number 04-1TA.
- Corlew JS and Dickson PF (1968). Methods for calculating temperature profiles of hot-mix asphalt concrete as related to the construction of asphalt pavements. *Journal of Association of Asphalt Paving Technologists* 37:101-140.
- Craven JM (1966). Cross linked thermally reversible polymers produced from condensation poly-mers with pendant furan groups cross-linked with maleimides. US patent 3,3435,003.
- Dry C (1994). Matrix cracking repair and filling using active and passive modes for smart timed release of chemicals from fibers into cement matrices. *Smart Materials and Structures* 3(2):118-123.
- Echols J (1989). New mix method for fiber-reinforced asphalt. *Public Works* 119(8):72-3.
- Edward KOA. Fatigue resistance of hot-mix asphalt concrete mixtures using the calibrated mechanistic with surface energy measurements approach. Master thesis of Texas A&M University, 2006.
- EN 12697-12 (2004): Bituminous mixtures - Test methods for hot mix asphalt - Part 12: Determination of the water sensitivity of bituminous specimens.
- EN 12697-17 (2004): Bituminous mixtures- Test methods for hot mix asphalt- Part 17: Particle Loss of porous asphalt specimen.
- EN 12697- 23 (2004): Bituminous mixtures - Test methods for hot mix asphalt - Part 23: Determination of the indirect tensile strength of bituminous specimens.
- EN 12697- 24 (2004): Bituminous mixtures - Test methods for hot mix asphalt - Part

- 24: Resistance to fatigue.
- EN 12697- 26 (2004): Bituminous mixtures - Test methods for hot mix asphalt - Part 26: Stiffness.
- EN 12697- 31 (2004): Bituminous mixtures - Test methods for hot mix asphalt - Part 31: Specimen preparation by gyratory compactor.
- Fitzgerald RL (2000). Novel applications of carbon fiber for hot mix asphalt reinforcement and carbon-carbon pre-forms. Master thesis, Department of Chemical Engineering, Michigan Technological University.
- Francken L (1979). Fatigue performance of a bituminous road mix under realistic best conditions. *Transport Research Record* 712:30-37.
- Frick K (2005). Evaluation of new patching material for open-graded asphalt concrete (OGAC) wearing courses. Technical Memorandum TM-UCBPRC-2-5-9. California Department of Transportation.
- Frohne H (1994). *Elektrische und magnetische felder*. Stuttgart: Teubner Verlag.
- Gaedicke C (2009). Fracture-based method to determine the flexural load capacity of concrete slabs. PhD thesis, University of Illinois, Urbana-Champaign.
- Garboczi EJ, Bentz DP (1991). In: Mindess S, editor. *Advances in cementitious materials*. *Ceramics Transactions* 16:365-80.
- García A, Schlangen E, van de Ven M and Liu Q (2009). Electrical conductivity of asphalt mortar with conductive fibers and fillers. *Construction and Building Materials* 23: 3175-3181.
- García A, Schlangen E, van de Ven M, vanVliet D (2001). Induction heating of mastic containing conductive fibers and fillers. *Materials and Structures* 44:499-508.
- García A, Schlangen E, van de Ven M, vanVliet D. *Heron* Vol.56 (2011) No. 1/2.
- García A, Schlangen E, van de Ven M, Liu Q (2012). A simple model to define induction heating in asphalt mastic. *Construction and Building Materials*, *Construction and Building Materials* 31:38-46.
- García A (2012). Self-healing of open cracks in asphalt mastic. *Fuel* 93: 264-272.
- GH Induction Atmospheres (GH IA). The induction heating guide. <http://www.inductionatmospheres.com/>.
- Goel A, Das A (2004). Emerging road materials and innovative. In: National conference on materials and their application in civil engineering, Hamipur, India.
- Good RJ, Van Oss CJ (1991). The modern theory of contact angles and the hydrogen bond component of surface energies. In M.E. Schrader and G. Loeb (Eds.), *Modern Approach to Wettability: Theory and Applications*, Plenum Press, New York, p. 1-27.
- Grant TP (2001). Determination of asphalt mixture healing rate using the Superpave indirect tensile test. Master thesis, University of Florida, America.
- Hagos ET (2008). The effect of aging on binder properties of porous asphalt concrete. PhD thesis, Delft University of Technology, the Netherlands.
- Hansen R, McGennis B, Prowell B, Stonex A (2000). Current and future uses of nonbituminous components of bituminous paving mixtures. *Transportation in the new millennium*. TRB A2D02, Washington DC, USA.
- Hassan H, Al-Oraimi S, TAHA R (2005). Evaluation of open-graded fiction come mixtures with cellulose fibers and styrene butadiene rubber polymer. *Journal of Materials in Civil Engineering* 17(4):415-22.
- Hefer A, Little D (2005). Adhesion in bitumen-aggregate systems and quantification of the effects of water on the adhesive bond. ICAR/505-1.
- Hejazi SM (2007). Mechanical reinforcement of hot mix asphalt using textile

- materials. Master thesis, Isfahan University of Technology, Iran.
- Herrington P, Reilly S, Cook S (2005). Porous asphalt durability test, Transfund New Zealand Research Report No. 265.
- Huang H, White TD (1996). Dynamic properties of fiber-modified overlay mixture. *Transport Research Record* 1545:98-104.
- Huber G (2000). Performance survey on open-graded friction course mixes. *Synthesis of Highway Practice* 284. Transportation Research Board, National Research Council, Washington DC.
- Jo SD, Richard KY (2001). Laboratory evaluation of fatigue damage and healing of asphalt mixtures. *Journal of Materials in Civil Engineering* 13(6):434-440.
- Kandhal PS (2002). Design, Construction and maintenance of open-graded asphalt friction courses. *National Asphalt Pavement Association Information Series* 115.
- Khalid H, Pérez F (1996). Performance assessment of Spanish and British porous asphalts. *Performance and Durability of Bituminous Materials*, pp. 137-157. Published by E & FN Spon, London.
- Khalid H, Walsh C (1996). A rational mix design method for porous asphalt. In *Procedures, 24th European Transport Forum, PTRC, Session G22i (Road Materials & Methods—Worldwide Update)*. London.
- Kim B, Roque R (2006). Evaluation of healing property of asphalt mixture. *Proc. 2006 Annual Transportation Research Board Meeting CD-ROM*.
- Kim H, Sokolov K, Poulidakos LD, Partl MN (2009). Fatigue evaluation of porous asphalt composites with carbon fiber reinforcement polymer grids. *Transportation Research Record* 2116:108-117.
- Kim YR, Little DN (1990). One-dimensional constitutive modeling of asphalt concrete. *Journal of Engineering Mechanics ASCE* 116 (4):751-772.
- Kim YR, Little DN (1991). SEM analysis on fracture and healing of sand-asphalt mixtures. *Journal of Materials in Civil Engineering* 3 (2):140-153.
- Klomp AJG (1996). Life period of porous asphalt. *Dutch Road and Hydraulic Engineering Institute report*.
- Kneepkens A, van Hoof Th, Schaefer H, van Keulen W (2004). VIA-RAL_ for porous asphalt: a result of research and development, but most of all of implementation. *Wegbouwkundige Werkdagen*.
- Kneepkens A, Van Hoof Th, Van Keulen W, Van Gent RJ (2004) Development of via-ral ® for porous asphalt: More than just research, more pragmatism 3rd Eurasphalt & Eurobitume Congress, Vienna, [295].
- Kringos N, Schmets A, pauli T, Scarpas T (2009). A finite element base chemo-mechanical model to simulate healing in bitumen. *Chemo-mechanics of Bituminous materials, 2009 Group of the Mechanics of infrastructure materials*, ISBN 7209653.
- Labib M, Maher A (1999). Recycled plastic fibers for asphalt mixtures. Report no: FHWA 2000-04.
- Lane R (2005). Cleaning open-grade asphalt to improve safety. *International Conference on Surface Friction/ 2005 Papers*. www.surfacefriction.org.nz. Christchurch, New Zealand.
- Larsen LE, Bendtsen H (2002). Noise reduction with porous asphalt - costs and perceived effect. *Ninth International Conference on Asphalt Pavements*. International Society of Asphalt Pavements. Copenhagen, Denmark.
- Lee HJ, Daniel JS, Kim YR (2000). Laboratory performance evaluation of modified asphalt mixtures for Incheon airport pavements, *International Journal of Pavement Engineering* 1(2):151-169.

- Lefebvre G (1993). Porous asphalt. Permanent International Association of Road Congresses.
- Li VC and Yang E (2007). Self healing in concrete materials. First International Conference on Self Healing Materials, Noordwijk, The Netherlands.
- Li YZ (2007). Using compaction parameters and indirect tensile strength to evaluate asphalt concrete rutting potential. Master thesis, Changsha University of Technology, China.
- Little DN, Bhasin A (2007). Exploring mechanisms of healing in asphalt mixtures and quantifying its impact. Self Healing Materials an Alternative Approach to 20 Centuries of Materials Science, Springer Series in Materials Science 100: 205-218.
- Little DN, Lytton RL, Williams AD, Chen CW (2001). Microdamage healing in asphalt and asphalt concrete, vol I: microdamage and microdamage healing. project summary report. FHWA-RD-98-141, Texas Transportation Institution, College Station, Texas.
- Little, Dallas N., R. L. Lytton, Devon Williams, Y. R. Kim (1999). An analysis of the mechanics of microdamage healing based on the application of micromechanics first principles of fracture and healing. Journal of the Association of Asphalt Paving Technologists 68:501-542.
- Liu Q, Schlangen E, van de Ven M, García A (2011). Induction healing of asphalt mastic and porous asphalt concrete. Construction and Building Materials 25: 3746-3752.
- Liu Q, Schlangen E, van de Ven M (2012). Induction healing of porous Asphalt trial section. Report, Delft University of Technology.
- Liu Q, Schlangen E, van de Ven M (2012). Evaluation of the induction healing effect of porous asphalt concrete through four-point bending fatigue test. Construction and Building Materials 29:403-409.
- Lu XH, Isacson U (2002). Effect of ageing on bitumen chemistry and rheology. Construction and Building Materials 16: 15-22.
- Luca J, Mrawia D (2005). New measurement of thermal properties of Superpave asphalt concrete. Journal Materials in Civil Engineering 17:72-9.
- Lumley R (2007). Self healing in aluminium alloys. First International Conference on Self Healing Materials, Noordwijk, The Netherlands.
- Lytton R, Uzan J, Fernando E, Roque R, Hiltunen D, Stoffels S (1993). Development and validation of performance prediction models and specifications for asphalt binders and mixes. Strategic Highway Research Program, Report number SHRP-A-357, Washington DC.
- Lytton RL, Chen CW, Little DN (2001). Microdamage healing in asphalt and asphalt Concrete; Volume IV: A Viscoelastic Continuum Damage Fatigue Model of Asphalt Concrete with Microdamage Healing. Federal Highway Administration, Publication No. FHWA-RD-98-144.
- Mahrez A, Karim M, Katman H (2003). Prospect of using glass fiber reinforced bituminous mixes. J East Asia Soc Trans Studies 5:794-807.
- Majidzadeh K, Buranorom C, Karakouzian M (1976). Application of fracture mechanics for improved design of bituminous concrete. Report FHWA-RD-76-91, vol 1 and 2.
- Majidzadeh K, Kauffmann EM, Ramsamooj DV (1971). Application of fracture mechanics in the analysis of pavement fatigue. Journal of Association of Asphalt Paving Technologist 40:227-246.
- Maurer DA, Malasheskie GJ (1989). Field performance of fabrics and fibers to retard reflective cracking. Geotext Geomem 8:239-67.

- Maurer Dean A, Gerald M (1989). Field performance of fabrics and fibers to retard reflective cracking. *Transport Research Record* 1248:13-23.
- McDaniel RS, Kowalski KJ, Shah A, Olek J, Bernhard RJ (2009). Long term performance of a porous friction course. Joint Transportation Research Program 1284 Civil Engineering Building, Purdue University. Final report: FHWA/IN/JTRP-2009/22
- McDaniel RS, Thornton W (2005). Field evaluation of a porous friction course for noise control. TRB 2005 Annual Meeting CD-ROM, Transportation Research Board, National Research Council, Washington DC.
- Mills DR, Keller Jr T (1982). The effectiveness of synthetic fibre-reinforced asphaltic concrete overlays in Delaware. Delaware Department of Transportation. Dover.
- Minsk LD (1968). Electrically conductive asphalt for control of snow and ice accumulation. *Highway Research Record* 227:57-63.
- Miyasaka K, Watanabe K, Jojima E, Aida H, Sumita M, Ishikawa K (1982) *Journal of Materials Science* 17:1610.
- Mo LT (2010). Damage development in the adhesive zone and mastic of porous asphalt concrete. PhD thesis, Delft University of Technology, the Netherlands.
- Molenaar AAA (1983). Structural performance and design of flexible road constructions and asphalt concrete overlays. PhD thesis, Delft University of Technology, the Netherlands.
- Molenaar AAA, Heerkens JCP, Verhoeven JHM (1986). Effects of stress absorbing membrane interlayers. *Journal of Association of Asphalt Paving Technologist* 55:453-481.
- Molenaar JMM, Molenaar AAA (2000). An investigation into the contribution of the bituminous binder to the resistance to ravelling of porous asphalt 2nd Eurasphalt & Eurobitume Congress, Barcelona , [106].
- Munn D (1989). Fiber reinforced hot mix promises improved stability. *High Health Constr* 132 (10):54-56.
- Nicholls JC, and Carswell IG (2001). The design of porous asphalt mixtures to performance-related criteria. TRL Report 497. TRL, United Kingdom.
- NL Agency (2011). Self healing materials concept and application. Second edition.
- Oliver WC and Pharr GM (2004). Measurement of hardness and elastic modulus by instrumented indentation: Advances in understanding and refinements to methodology. *Journal of Materials Research* 19, 3.
- Open Graded Friction Course Usage Guide (2006). California Department of Transportation. Division of Engineering Services. Materials Engineering and Testing Services-MS #5. Sacramento, California.
- Ozisik MN (1985). *Basic Heat Transfer*, McGraw-Hill Book Company, New York.
- Padmos C (2002). Over ten years experience with porous road surfaces. ISAP 9th International conference on Asphalt Pavements, [4-3-4]. Copenhagen, Denmark.
- Pang L, Wu SP, Xie J, Hu DM (2010). Investigate of performance of asphalt concrete with gneiss. *Key Engineering Materials Vols.* 417-418:497-500.
- Peltonen P (1991). Wear and deformation of characteristics of fiber reinforced asphalt pavements. *Construction and Building Materials* 5:18-22.
- Phillips MC (1998). Multi-step models for fatigue and healing, and binder properties involved in healing. *Proceedings, Eurobitume Workshop on Performance Related Properties for Bituminous Binders*, Luxembourg, Paper No. 115.
- Poulikakos LD, Takahashi S, Partl MN (2003). A comparison of Swiss and Japanese porous asphalt through various mechanical tests. 3rd Swiss Transport Research Conference. Monte Verita/Ascona.

- Pronk AC (2005). Partial Healing, A new approach for the damage process during fatigue testing of asphalt specimen. *Asphalt Concrete* 185, 9 , ASCE.
- Punith VS, Suresha SN, Veeraragavan A, Raju S, Bose S (2004). Characterization of polymer and fiber-modified porous asphalt mixtures. TRB 2004 Annual Meeting CD-ROM. Transportation Research Board. National Research Council. Washington DC.
- Putman BJ, Amirkhanian SN (2004). Utilization of waste fibers in stone matrix asphalt mixtures, resources. *Resources Conservation and Recycling* 42:265-74.
- Qiu J (2008). Self healing asphalt: literature review. Report, Delft University of Technology, the Netherlands, 2008.
- Qiu J, Molenaar A, van de Ven M, Wu S, Yu J (2012). Investigation of self healing behaviour of asphalt mixes using beam on elastic foundation setup. *Materials and Structures* 45: 777-791.
- Qiu J (2012). Self healing of asphalt mixtures. PhD thesis. Delft University of Technology, the Netherlands.
- Reboul JP (1982). *Carbon Black-Polymer Composites*, p. 80-120, Marcel Dekker, New York.
- Roesler J, Gaedicke C (2009). Fracture-based method to determine the flexural load capacity of concrete slabs. Draft Final Report for Federal Aviation Administration. University of Illinois.
- Roesler J, Gaedicke C (2010). Flexural behavior of concrete specimens on various support conditions. Paper presented at the 7th International DUT-Workshop on Design and Performance of Sustainable and Durable Concrete Pavements, Seville, Spain.
- Rogge D (2002). Development of maintenance practices for Oregon F-mix. Publication FHWAOR-RD-02-09. Federal Highway Administration, U.S. Department of Transportation, Washington DC.
- Rowe GM, Lewandowski LH, Grzybowski KF, Rasche J (2009). Development of the beam on elastic foundation for the evaluation of Geo-synthetic materials for reinforcing of asphalt layers. Paper presented at the 2009 Annual Meeting of the Transportation Research Board.
- Rudolf R, Mitschang P, Neitzel M (2000). Induction heating of continuous carbon-fibre reinforced thermoplastics. *Composites: Part A* 31: 1191-1202.
- Ruiz AR, Alberola R, Perez F, Sanchez B (1990). Porous asphalt mixtures in Spain. *Transportation Research Record: Journal of the Transportation Research Board* 1265: 87-94.
- Scott EB (1993). Polymer/fiber modified asphalt fracture mechanisms and microstructure relationships to distresses and environmental factors. PhD Thesis, Michigan State University.
- Seo Y, Kim YR (2008). Using acoustic emission to monitor fatigue damage and healing in asphalt concrete. *KSCE Journal of Civil Engineering* 12(4):237-243.
- Shan LY, Tan YQ, Underwood BS, Kim YR (2011). Separation of thixotropy from fatigue process of asphalt binder. *Transportation Research Record: Journal of the Transportation Research Board* 1: 89-98.
- Shell Bitumen (1995). *The shell Bitumen Industrial Handbook*, Surrey, U.K.
- Shen S, Chiu HM, Huang H (2010). Characterization of fatigue and healing in asphalt binders. *Journal of Materials in Civil Engineering* 22(9): 846-852.
- Spillemaeker PE, Bauer P (2000). Development of 0/6 Porous Asphalt. 2nd Eurasphalt & Eurobitume Congress. Barcelona, Spain. pp. 553-557.
- Stauffer D (1985). *Introduction to percolation theory*. London: Taylor and Francis.

- Swart JH (1997). Experience with porous asphalt in the Netherlands. European conference on porous asphalt. Madrid. pp 1019.
- TestWorks®4 (2004) User manual for Nanoindentation Systems. MTS Systems Corporation. 2002.
- Turner, William C. and Malloy, John F (1981). Thermal insulation handbook, Robert E. Krieger Publishing Company, Malabar, Florida, p. 549.
- Tegeler, PA and Dempsey BJ (1973). A method of predicting compaction time for hot-mix bituminous concrete. Asphalt Paving Technology 1973, Proceedings: Association of Asphalt Paving Technologists Technical Sessions 42:499-523.
- Tapkın S (2008). The effect of polypropylene fibers on asphalt performance. Building and Environment 43:1065-71.
- The Highways Agency, The Scottish Office Development Department, The Welsh Office Y Swyddfa Gymreig, The Department of the Environment for Northern Ireland (1999). Design manual for roads and bridges. Volume 7: Pavement Design and Maintenance Bituminous Surfacing Materials and Techniques.
- Theyse HL, de Beer M, Rust FC (1996). Overview of the South African Mechanistic Pavement Design Analysis Method, Paper 96-1294 presented at the 75th Annual Transportation Research Board Meeting, Washington DC.
- Tolman F., Van Gorkum F. (1996). Mechanical durability of porous asphalt 1st Eurasphalt & Eurobitume Congress, Strassbourg , [076].
- Uchida K, Kurokawa T, Himeno K, Nishizawa T (2002). Healing characteristics of asphalt mixture under high temperature conditions. Proceedings of 9th International Conference on Asphalt Pavements.
- Van Benthem RATM, Ming W and de With G (2007). Self healing polymer coatings. First International Conference on Self Healing Materials, Noordwijk, The Netherlands.
- Van der Zwan J, Goeman T, Gruis H, Swart J, Oldenburger R (1990). Porous asphalt wearing courses in the Netherlands: state of the art review. Transportation Research Record 1265: 95-110.
- Van Bochove G, Blom SD, Veltman J (2011). Self healing Asphalt. Breijn report-6710801.
- Van Dijk W, Moreaud H, Quedeville A, Uge P (1972). The fatigue of bitumen and bituminous mixes. Proceedings of the 3rd International Conference on the Structure Design of pavement, London, p. 354-366.
- Van Gooswiligen G, de Hilster E, Robertus C (1994). Changing needs and requirements for bitumen and asphalts. Proc. 6th Conference on Asphalt Pavements for Southern Africa, Cape Town.
- Voskuilen JLM, Tolman F, Rutten E (2004). Do modified porous asphalt mixtures have a longer service life? 3rd Eurasphalt & Eurobitume Congress, Vienna.
- Voskuilen JLM, Huurman M (2009). Conversations, Centre for transport and Navigation of the Dutch Ministry of Transport, public Works and Water management, Delft, The Netherlands.
- Voskuilen JLM, Verhoef PNW (2003). Cause of premature ravelling failure of porous asphalt. Sixth International RILEM Symposium on Performance Testing and Evaluation of Bituminous Materials, p. 191-197.
- Watson D, Johnson A, Jared D (1998). Georgia department of transportation's progress in Open-Graded Friction Course development. Transportation Research Record 1616. Transportation Research Board. Washington DC.
- Weber M, Kamal MR (1997). Estimation of the volume resistivity of electrically conductive composites. Polymer Composites 16(6):711-25.

- White SR, Sottos NR, Geubelle PH, Moore JS, Kessler MR, Sriram SR, Brown EN, Viswanathan S (2001). Autonomic healing of polymer composites. *Nature* 409: 794-797.
- Wikipedia (2011). http://en.wikipedia.org/wiki/Self-healing_material.
- Williams D, Little DN, Lytton RL, Kim YR, Kim Y (2001). Microdamage healing in asphalt and asphalt concrete; Volume II: Laboratory and Field Testing to Assess and Evaluate Microdamage and Microdamage Healing. Federal Highway Administration, Publication No. FHWA-RD-98-142.
- Williams D, Little DN, Lytton RL, Kim YR., Kim Y (2001). Microdamage healing in asphalt and asphalt concrete. Res. Rep. 7229, A&M University, College Station, Texas.
- Wolfe RK, Heath GL, Colony DC (1980). University of Toledo time-temperature model laboratory field validation. Report No. FHWA/OH-80/006, Department of Industrial Engineering, University of Toledo, Toledo, Ohio.
- Wu S, Liu X, Ye Q, Li N (2006). self-monitoring electrically conductive asphalt-based composite with carbon fillers, *Transactions of Nonferrous Metals Society of China* 16: 512-516.
- Wu S, Ye Q, Li N, Yue H (2007). Effects of fibers on the dynamic properties of asphalt mixtures. *J Wuhan Univ Technol - Mater Sci Ed* 22:733-736.
- Wu SP, Mo LT, Shui ZH, Chen Z (2005). Investigation of the conductivity of asphalt concrete with conductive fillers. *Carbon* 43(7):1358-1363.
- Wu SP, Mo LT, and Shui ZH (2002). An Improvement on electrical properties of asphalt. *Journal of Wuhan University of Technology (Mater. Sci. Ed)*17(4):63-65.
- Wu S, Li B, Wang H and Qiu J (2008). Numerical simulation of temperature distribution in conductive asphalt solar collector due to pavement material parameters. *Materials Science Forum* Vols. 575-578:1314-1319.
- WWW.SELFHEALINGCONCRETE.BLOGSPOT.COM (2012).
- Zhang Z, Roque R, Birgisson B, and Sangpetngam B (2001). Identification and verification of a suitable crack growth law. *Journal of the Association of Asphalt Paving Technologists* 70:206-241.
- Zhang Z (2000). Identification of suitable crack growth law for asphalt mixtures using the Superpave indirect tensile test. PhD thesis, University of Florida, Gainesville.
- Zollinger CJ (2005). Application of surface energy measurements to evaluate moisture susceptibility of asphalt and aggregates. Master thesis, Texas A&M University.

Appendix

Appendix 1: Particle loss values of the samples with steel (wool) fiber

Sample	Fiber content	Particle loss value (%)					
		Sample 1	Sample 2	Sample 3	Sample 4	Sample 5	Average
Plain samples	0	16.11	16.08	12.32	14.80	14.89	14.84
Samples with steel fiber type 1	5%	15.74	8.74	10.83	11.00	11.64	11.59
	10%	7.96	11.74	8.74	9.63	8.00	9.21
	15%	8.65	8.53	7.60	10.17	8.90	8.77
	20%	10.04	8.73	9.75	12.46	10.55	10.31
Samples with steel fiber type 00	4%	6.59	9.20	11.71	8.84	8.92	9.05
	8%	8.11	5.13	9.27	9.61	7.90	8.00
	10%	9.27	8.05	13.02	11.86	10.44	10.53
	12%	13.55	13.07	13.92	13.50	13.44	13.49
Samples with steel fiber type 000	8%	8.37	10.05	12.2	10.13	10.27	10.20
	10%	8.41	7.10	9.45	8.33	8.06	8.27
	12%	13.96	12.10	10.3	16.97	14.98	13.66

Appendix 2: Indirect tensile strength of the samples with steel (wool) fiber

Sample	Fiber content	Indirect tensile strength (MPa)			
		Sample 1	Sample 2	Sample 2	Average
Plain samples	0	2.06	2.14	2.13	2.11
Samples with steel fiber type 1	5%	2.24	2.41	2.16	2.27
	10%	2.63	2.54	2.67	2.61
	15%	2.58	2.52	2.41	2.50
	20%	1.99	2.12	1.99	2.03
	25%	1.72	1.75	1.82	1.76
Samples with steel wool type 00	4%	2.44	2.47	2.51	2.47
	8%	2.91	3.12	3.04	3.02
	10%	2.97	2.9	2.76	2.88
	12%	2.75	2.77	2.80	2.77
	14%	2.69	2.80	2.72	2.74
Samples with steel wool type 000	4%	2.47	2.34	2.4	2.40
	8%	2.85	2.92	2.79	2.85
	10%	2.64	2.85	2.78	2.76
	12%	2.49	2.72	2.76	2.66

Appendix 3: Indirect tensile strength ratio of the samples with steel wool type 00

Sample		Indirect tensile strength measured at 15 °C (MPa)				
		Sample 1	Sample 2	Sample 3	Average strength	Strength ratio
Plain samples	Dry	1.10	1.18	1.03	1.10	92.7%
	Wet	0.99	1.09	0.97	1.02	
Samples with 4% steel wool	Dry	1.27	1.25	1.20	1.24	95.9%
	Wet	1.19	1.14	1.25	1.19	
Samples with 8% steel wool	Dry	1.34	1.42	1.45	1.40	101.4%
	Wet	1.47	1.35	1.43	1.42	

Appendix 4: Experimental indirect tensile resilient stiffness of the samples with and without 8% steel wool type 00

Temperature (°C)	Frequency (Hz)	Resilient stiffness (MPa)	
		Plain samples	Samples with 8% steel wool
5	8	10303	11575
5	4	9159	9953
5	2	7968	8696
5	1	6970	7442
5	0.5	6077	6409
10	8	7427	8026
10	4	6271	6789
10	2	5315	5498
10	1	4497	4426
10	0.5	3804	3741
20	8	3171	3284
20	4	2482	2579
20	2	1964	2192
20	1	1593	1761
20	0.5	1200	1421
30	8	1226	1619
30	4	933	1261
30	2	712	967
30	1	539	706
30	0.5	416	589

Appendix 5: Experimental indirect tensile resilient stiffness of the field cores with and without 4% steel wool type 00

Temperature (°C)	Frequency (Hz)	Resilient stiffness (MPa)	
		Plain cores	Cores with steel wool
5	8	7893	6804
5	4	7022	5939
5	2	6155	5122
5	1	5414	4541
5	0.5	4758	4045
10	8	6256	5469
10	4	5361	4643
10	2	4580	3942
10	1	3945	3353
10	0.5	3371	2883
20	8	2831	2550
20	4	2240	2024
20	2	1775	1617
20	1	1464	1312
20	0.5	1206	1073
30	8	974	947
30	4	741	738
30	2	578	573
30	1	449	449
30	0.5	380	362

Curriculum Vitae

Name: Quantao Liu

Date of Birth: August 15th, 1982

Place of Birth: Xihua, Henan Province, China

Email: liuquantao82@126.com

- Oct. 2008 – Oct. 2012 PhD student in Materials and Environment, Faculty of Civil Engineering and Geosciences, Delft University of Technology, Delft, the Netherlands
- Sep. 2006 – Jun. 2008 Master student in Construction Materials, Faculty of Material Science and Engineering, Wuhan University of Technology, Wuhan, China
- Sep. 2002 – Jun. 2006 Bachelor student in Material Science and Engineering, Faculty of Material Science and Engineering, Wuhan University of Technology, Wuhan, China

Publications

1. **Liu Q.** Induction healing of asphalt mastic for crack control. Submitted to Construction and Building Materials.
2. **Liu Q,** Schlangen E, van de Ven M. Induction healing of porous asphalt concrete beams on an elastic foundation. Journal of Materials in Civil Engineering (Accepted for publication).
3. **Liu Q,** Schlangen E, van de Ven M. Induction healing of porous asphalt concrete. Transportation Research Record: Journal of the Transportation Research Board (Accepted for publication).
4. **Liu Q,** Schlangen E, van de Ven M. Characterization of the material from the induction healing porous asphalt concrete trial section. Materials and Structures, DOI: 10.1617/s11527-012-9936-9.
5. **Liu Q,** Schlangen E, van de Ven M. Evaluation of the induction healing effect of porous asphalt concrete through four-point bending fatigue test. Construction and Building Materials 29(2012):403-409.
6. **Liu Q,** Schlangen E, van de Ven M. Predicting the Performance of the Self Healing Porous Asphalt Trial section. The 7th RILEM International Conference on Cracking in Pavement June 2012, Delft, The Netherlands.
7. García A, Schlangen E, van de Ven M, **Liu Q.** A simple model to define induction heating in asphalt mastic. Construction and Building Materials 31(2012):38-46.
8. **Liu Q,** Schlangen E, van de Ven M, García A. Induction healing of asphalt mastic and porous asphalt concrete. Construction and Building Materials 25(2011):3746-3752.
9. **Liu Q,** Schlangen E, van de Ven M, García A. Induction heating of electrically conductive porous asphalt concrete. Construction and Building Materials 24(2010):1207-13.
10. **Liu Q,** Schlangen E, van de Ven M, García A. Healing of porous asphalt concrete via induction heating. Road Materials and Pavement Design 11 (2010):527-542.
11. **Liu Q,** Schlangen E, van de Ven M, Poot M. Optimization of steel fiber used for induction heating in porous asphalt concrete. The 7th International Conference on Traffic and transportation studies 2010 (pp.1320-1330). USA: American society of civil engineers.
12. **Liu Q,** Schlangen E, van de Ven M, Poot M. Mechanical properties of sustainable, self-healing porous asphalt concrete. The 1st international conference on sustainable construction materials: design, performance and application and the 1st annual meeting of the specialized committee of stone materials and aggregates, Chinese ceramic society (pp. 58-65). Wuhan, China, 2010.
13. García A, Schlangen E, van de Ven M, **Liu Q.** Electrical conductivity of asphalt mortar with conductive fibers and fillers. Construction and Building Materials 23(2009):3175-3181.